PACIFIC EARTHQUAKE ENGINEERING
RESEARCH CENTER

Update of the AS08 Ground-Motion Prediction Equations Based on the NGA-West2 Data Set

Norman A. Abrahamson
Pacific Gas & Electric Company
San Francisco, California

Walter J. Silva
Pacific Engineering and Analysis
El Cerrito, California

Ronnie Kamai
Pacific Earthquake Engineering Research Center
University of California, Berkeley

PEER 2013/04
MAY 2013

Update of the AS08 Ground-Motion Prediction Equations Based on the NGA-West2 Data Set

Norman A. Abrahamson
Pacific Gas & Electric Company
San Francisco, California

Walter J. Silva
Pacific Engineering and Analysis
El Cerrito, California

Ronnie Kamai
Pacific Earthquake Engineering Research Center
University of California, Berkeley

PEER Report 2013/04
Pacific Earthquake Engineering Research Center
Headquarters, University of California, Berkeley

May 2013

ABSTRACT

Empirical ground-motion models for the average horizontal component from shallow crustal earthquakes in active tectonic regions are derived using the PEER NGA-West2 database. The model is applicable to magnitudes 3.0–8.5, distances 0–300 km, and spectral periods of 0–10 sec. The model input parameters are the same as used by Abrahamson and Silva (2008) with the following exceptions: the loading level for nonlinear effects is based on the spectral acceleration at the period of interest rather than the PGA; the distance scaling for HW effects off the ends of the rupture includes a dependence on the source-to-site azimuth. Regional differences in large distance attenuation and V_{S30} scaling between California, Japan, China, and Taiwan are included. The scaling for the hanging-wall effect is improved using constraints from numerical simulations. The standard deviation is magnitude dependent with smaller magnitudes leading to larger standard deviations at short periods but smaller standard deviations at long periods. Directivity effects are not included through explicit parameters, but are captured through the variability of the empirical data.

ACKNOWLEDGMENTS

This study was sponsored by the Pacific Earthquake Engineering Research Center (PEER) and funded by the California Earthquake Authority, California Department of Transportation, and the Pacific Gas & Electric Company. Any opinions, findings, and conclusions or recommendations expressed in this material are those of the authors and do not necessarily reflect those of the above mentioned agencies.

ERRATA
PEER Report No 2013-04

Update of the AS08 Ground-Motion Prediction Equations Based on the NGA-West2 Data Set

June 4, 2013

Errors in Section 3:

There is an error Table 3.1 in the range of rakes for normal faults. A normal fault is defined between rakes of -30 and -150.

There is also an error in Table 3.3, in the definition of R_{y0}. R_{y0} can only be zero or positive. For sites located along the rupture, $R_{y0} = 0$, which can be computed from $R_{y0}=R_x$*|tan(Src2SiteA)|.

Errors in Section 4:

There is an error in the last line on page 23, which states that M1 is equal 6.5. Instead, M1 is period dependent, as detailed in Table 5.3(a).

There are a couple of errors in the second line of Equation (4.9). It should read:

$$V_1 = \begin{cases} 1500 & \text{for } T \leq 0.5 \text{ sec} \\ \exp\left(-0.35 \ln\left(\frac{T}{0.5}\right) + \ln(1500)\right) & \text{for } 0.5 \text{ sec} < T < 3 \text{ sec} \\ 800 & \text{for } T \geq 3 \text{ sec} \end{cases} \quad (4.9)$$

Equation (4.22), which defines the regional V_{s30} scaling for Taiwan, China, and Japan, is accidentally re-defining f_{11}. Instead, Equation (4.22) should read:

$$\text{Regional}\left(V_{s30}, R_{rup}\right) = F_{TW}\left(f_{12}(V_{s30}) + a_{25}R_{rup}\right) + F_{CN}\left(a_{28}R_{rup}\right) + F_{JP}\left(f_{13}(V_{s30}) + a_{29}R_{rup}\right) \quad (4.22)$$

Such that Equation (4.23) is defining f_{12} and Equation (4.24) is defining f_{13}.

There is also an error in Equation (4.23). Instead of V_{s30} in the numerator, it should be V_{s30}*. Following the above items, Equations (4.23) and (4.24) should read:

$$f_{12}(V_{s30}) = a_{31} \ln\left(\frac{V_{s30}^*}{V_{Lin}}\right) \quad (4.23)$$

Errors in Section 5:

There is an error in Table 5.3(c) – the coefficient a_{46} at $T = 0.2$ sec should be -0.03 instead of 0.03.

CONTENTS

ABSTRACT iii

ACKNOWLEDGMENTS v

TABLE OF CONTENTS vii

LIST OF FIGURES ix

LIST OF TABLES xv

1 INTRODUCTION 1

2 DATA SET SELECTION 3

2.1 Earthquake Not Considered Applicable to Active Crustal Regions 3

2.2 Censoring at Large Distances 4

2.3 Sites Not Represenative of Free Field 5

2.4 Other Earthquakes Excluded 7

2.5 Questionable Recordings 8

2.6 Missing Metadata 8

2.7 Final Data Set 8

3 MODEL PARAMETERS 19

3.1 Introduction 19

3.2 Source Parameters 19

3.3 Site Classification 20

3.4 Distance Definition 21

3.5 Ground Motion Level 21

4 FUNCTIONAL FORM OF THE MODEL 23

4.1 Base Model 23

4.2 Style-of-Faulting Model 24

4.3 Site Response Model 24

4.4 Hanging-Wall Model 28

4.5 Depth-to-Top of Rupture Model 30

4.6 Soil Depth Model 30
4.7 Aftershock Scaling 31
4.8 Regionalization 31
4.9 Constant Displacement Model 32

5 REGRESSION ANALYSIS 33

6 RESIDUALS 45
6.1 Inter-Event Residuals 45
6.2 Intra-Event Residuals 45
6.2.1 Distance Scaling 45
6.2.2 Site Response 46
6.2.3 Hanging Wall 47
6.3 Correlations of Residuals Across Periods 47
6.4 Dependence on Other Parameters 47

7 EQUATIONS FOR STANDARD DEVIATION 111
7.1 Standard Deviation Model 111
7.1.1 Regionalization of Standard Deviation 111
7.2 Effect of Measurement Errors in the Independent Parameters 112
7.2.1 V_{S30} Uncertainty 112
7.3 Nonlinear Effects on the Standard Deviation 113

8 MODEL RESULTS 119

REFERENCES 135

APPENDIX A: SELECTED EARTHQUAKES 137

LIST OF FIGURES

Figure 2.1(a) Evaluation of censoring distance for earthquakes recorded between 1933 and 1990. 10

Figure 2.1(b) Evaluation of censoring distance for earthquakes recorded between 1991 and 1995. 11

Figure 2.1(c) Evaluation of censoring distance for earthquakes recorded between 1996 and 2000. 12

Figure 2.1(d) Evaluation of censoring distance for earthquakes recorded between 2001 and 2005. 13

Figure 2.1(e) Evaluation of censoring distance for earthquakes recorded between 2006 and 2011. 14

Figure 2.2 Model used for the censoring distance. 15

Figure 2.3 Magnitude-distance distribution for the final subset. 16

Figure 2.4 Number of earthquakes (top) and number of recordings (bottom) in the selected subset by period. The different steps are described in the regression analysis section. 17

Figure 4.1 Example of the V_{S30} scaling terms (from Abrahamson and Silva 2008). 25

Figure 4.2(a) Non-parametric evaluation of the V_{S30} scaling, used to identify the V_1 value. 26

Figure 4.2(b) Non-parametric evaluation of the V_{S30} scaling, used to identify the V_1 value. 27

Figure 4.2(c) Non-parametric evaluation of the V_{S30} scaling, used to identify the V_1 value. 28

Figure 5.1 Smoothing of the quadratic magnitude coefficients. 41

Figure 5.2 Smoothing of the V_{S30} scaling for the linear range. 41

Figure 5.3 Smoothing of the SOF coefficents. 42

Figure 5.4 Smoothing of the earthquake class coefficients. 42

Figure 5.5 Smoothing of the Z_{TOR} coefficients. 43

Figure 5.6 Smoothing of the large distance scaling. 43

Figure 5.7 Smoothing of the Z_1 scaling. 44

Figure 6.1(a) Event terms for PGA. 53

Figure 6.1(b) Event terms for $T = 0.2$ sec....54
Figure 6.1(c) Event terms for $T = 0.5$ sec....55
Figure 6.1(d) Event terms for $T = 1$ sec....56
Figure 6.1(e) Event terms for $T = 3$ sec....57
Figure 6.1(f) Event terms for $T = 6$ sec....58
Figure 6.1(g) Event terms for $T = 10$ sec....59
Figure 6.2(a) Distance dependence of the intra-event residuals, all regions and WUS, PGA....60
Figure 6.2(b) Distance dependence of the intra-event residuals, Taiwan, Japan, and China, PGA....61
Figure 6.2(c) Distance dependence of the intra-event residuals, all regions and WUS, $T = 0.2$ sec....62
Figure 6.2(d) Distance dependence of the intra-event residuals, Taiwan, Japan and China, $T = 0.2$ sec....63
Figure 6.2(e) Distance dependence of the intra-event residuals, all regions and WUS, $T = 0.5$ sec....64
Figure 6.2(f) Distance dependence of the intra-event residuals, Taiwan, Japan, and China, $T = 0.5$ sec....65
Figure 6.2(g) Distance dependence of the intra-event residuals, all regions and WUS, $T = 1$ sec....66
Figure 6.2(h) Distance dependence of the intra-event residuals, Taiwan, Japan, and China, $T = 1$ sec....67
Figure 6.2(i) Distance dependence of the intra-event residuals, all regions and WUS, $T = 3$ sec....68
Figure 6.2(j) Distance dependence of the intra-event residuals, Taiwan, Japan, and China, $T = 3$ sec....69
Figure 6.2(k) Distance dependence of the intra-event residuals, all regions and WUS, $T = 6$ sec....70
Figure 6.2(l) Distance dependence of the intra-event residuals, Taiwan, Japan, and China, $T = 6$ sec....71
Figure 6.2(m) Distance dependence of the intra-event residuals, all regions and WUS, $T = 10$ sec....72
Figure 6.2(n) Distance dependence of the intra-event residuals, Taiwan, Japan, and China, $T = 10$ sec....73
Figure 6.3(a) Distance dependence of the intra-event residuals, WUS only, by Magnitude bins, PGA....74

Figure 6.3(b) Distance dependence of the intra-event residuals, WUS only, by Magnitude bins, $T = 0.2$ sec. 75
Figure 6.3(c) Distance dependence of the intra-event residuals, WUS only, by magnitude bins, $T = 0.5$ sec. 76
Figure 6.3(d) Distance dependence of the intra-event residuals, WUS only, by magnitude bins, $T = 1.0$ sec. 77
Figure 6.3(e) Distance dependence of the intra-event residuals, WUS only, by magnitude bins, $T = 3$ sec. 78
Figure 6.3(f) Distance dependence of the intra-event residuals, WUS only, by magnitude bins, $T = 6$ sec. 79
Figure 6.3(g) Distance dependence of the intra-event residuals, WUS only, by magnitude bins, $T = 10$ sec. 80
Figure 6.4(a) Distance dependence of the intra-event residuals for four WUS events, PGA. 81
Figure 6.4(b) Distance dependence of the intra-event residuals for four WUS events, $T = 1.0$ sec. 82
Figure 6.5(a) V_{s30} dependence of the intra-event residuals, PGA. 83
Figure 6.5(b) V_{s30} dependence of the intra-event residuals, $T = 0.2$ sec. 84
Figure 6.5(c) V_{s30} dependence of the intra-event residuals, $T = 0.5$ sec. 85
Figure 6.5(d) V_{s30} dependence of the intra-event residuals, $T = 1.0$ sec. 86
Figure 6.5e) V_{s30} dependence of the intra-event residuals, $T = 3$ sec. 87
Figure 6.5(f) V_{s30} dependence of the intra-event residuals, $T = 6$ sec. 88
Figure 6.5(g) V_{s30} dependence of the intra-event residuals, $T = 10$ sec. 89
Figure 6.6(a) Sa_{1100} dependence of the intra-event residuals for PGA. 90
Figure 6.6(b) Sa_{1100} dependence of the intra-event residuals for $T = 0.2$ sec. 91
Figure 6.6(c) Sa_{1100} dependence of the intra-event residuals for $T = 0.5$ sec. 92
Figure 6.6(d) Sa_{1100} dependence of the intra-event residuals for $T = 1.0$ sec. 93
Figure 6.7(a) Z_1 dependence of the intra-event residuals for PGA. 94
Figure 6.7(b) Z_1 dependence of the intra-event residuals for $T = 0.2$ sec. 95
Figure 6.7(c) Z_1 dependence of the intra-event residuals for $T = 0.5$ sec. 96
Figure 6.7(d) Z_1 dependence of the intra-event residuals for $T = 1.0$ sec. 97
Figure 6.7(e) Z_1 dependence of the intra-event residuals for $T = 3$ sec. 98
Figure 6.7(f) Z_1 dependence of the intra-event residuals for $T = 6$ sec. 99
Figure 6.7(g) Z_1 dependence of the intra-event residuals for $T = 10$ sec. 100
Figure 6.8(a) HW intra-event residuals (source-to-site azimuth: 85–95) for PGA 101

Figure 6.8(b) HW intra-event residuals (source-to-site azimuth: 85–95) for T = 0.2 sec. 102
Figure 6.8(c) HW intra-event residuals (source-to-site azimuth: 85–95) for T = 0.5 sec. 103
Figure 6.8(d) HW intra-event residuals (source-to-site azimuth: 85–95) for T = 1.0 sec. 104
Figure 6.8(e) HW intra-event residuals (source-to-site azimuth: 85–95) for T = 3 sec. 105
Figure 6.8(f) HW intra-event residuals (source-to-site azimuth: 85–95) for T = 6 sec 106
Figure 6.8(g) HW intra-event residuals (source-to-site azimuth: 85–95) for T =10 sec. 107
Figure 6.9(a) Correlation coefficients for the normalized inter-event residuals across periods. 108
Figure 6.9(b) Correlation coefficients for the normalized intra-event residuals across periods. 108
Figure 6.10 Static stress drop scaling of the inter-event residuals for T = 1, T = 3 and T = 6 sec. 109

Figure 7.1 Smooth coefficients for the standard deviation models. 116
Figure 7.2 Partial derivative of ln(Sa) with respect to ln(V_{S30}) 116
Figure 7.3 Magnitude scaling of $\phi_{A,L}$ and $\tau_{A,L}$ for T = 0.2 and T = 1.0 sec. 117
Figure 7.4 Period dependence of $\phi_{A,L}$ and $\tau_{A,L}$ for magnitudes 5 and 7. 117

Figure 8.1(a) Comparison of the median spectral acceleration: SS, R_{JB} = 30 km, V_{S30} = 760 m/sec. 120
Figure 8.1(b) Comparison of the median spectral acceleration: SS, R_{JB} = 30 km, V_{S30} = 270 m/sec. 121
Figure 8.2(a) Comparison of the median spectral acceleration: SS, R_{JB} = 1 km, V_{S30} = 760 m/sec. 122
Figure 8.2(b) Comparison of the median spectral acceleration: SS, R_{JB} = 1 km, V_{S30} = 270 m/sec. 123
Figure 8.3(a) Comparison of the rupture distance scaling for a vertical strike slip at PGA. 124
Figure 8.3(b) Comparison of the rupture distance scaling for a vertical strike slip at T = 0.2 sec. 125
Figure 8.3(c) Comparison of the rupture distance scaling for a vertical strike slip at T = 1 sec. 126
Figure 8.3(d) Comparison of the rupture distance scaling for a vertical strike slip at T = 3 sec. 127
Figure 8.4(a) Comparison of the magnitude scaling for a vertical strike slip at T = 0.2 sec. 128

Figure 8.4(b) Comparison of the magnitude scaling for a vertical strike slip at T =3 sec. 129
Figure 8.5 HW scaling for a M6.7 reverse fault with 45° dip at T = 0.2 sec. 130
Figure 8.6 Example of V_{S30} scaling for a strike slip M7 at R_{rup}=30 km. 131
Figure 8.7 Example of Z_1 scaling for a strike slip M7 at R_{rup} = 30 km and V_{S30} = 270 m/sec. 132
Figure 8.8 Spectral displacements for a vertical strike slip fault at R_{JB} = 20 km and V_{S30} = 760 m/sec. 133

LIST OF TABLES

Table 2.1 Earthquakes considered not applicable to active crustal regions. 4
Table 2.2. Censor data model parameters. 5
Table 2.3 GMX C1 classification. 6
Table 2.4 Other earthquakes excluded. 7
Table 2.5 Summary of delected dubset by region. 9

Table 3.1 Definition of source parameters used in the regression analysis. 20
Table 3.2 Definition of site parameters used in the regression analysis. 20
Table 3.3 Definition of distance parameters used in the regression analysis. 21

Table 5.1 Constraints on the Model parameters. 34
Table 5.2 Period-independent constants for the median ground motion. 35
Table 5.3(a) Coefficients for the median ground motion. 36
Table 5.3(b) Coefficients for the median ground motion. 37
Table 5.3(c) Coefficients for the Z_1 scaling of the median ground motion. 38
Table 5.4 Coefficients for the median ground motion for other regions. 39
Table 5.5 Coefficients for the V_{s30} scaling of the median ground motion for Japan. 40

Table 6.1(a) Unsmoothed correlation coefficients for inter-event residuals. 49
Table 6.1(b) Unsmoothed correlation coefficients for inter-event residuals (continued). 50
Table 6.2(a) Unsmoothed correlation coefficients for intra-event residuals. 51
Table 6.2(b) Unsmoothed correlation coefficients for intra-event residuals (continued). 52

Table 7.1 Coefficients for the standard deviation. 115

1 Introduction

For engineering applications, the ground motion needs to be computed for a wide range of magnitudes and distances. Although the NGA-West2 data base (Ancheta et. al. 2013) represents a large increase in the data set as compared to the 2008 NGA data base (Ancheta et. al. 2013), the large magnitude (M>7) and short distance (R < 15 km) range is still only sparsely sampled. To develop a ground motion prediction equation (GMPE) that extrapolates to large magnitudes and short distances in a reasonable manner, we rely on seismological and geotechnical models for constraining the extrapolation. Therefore, our approach to the development of our GMPE is not traditional curve fitting (e.g., using the minimum number of parameters needed to explain the observations), but rather, it is a model building exercise that uses analytical results from seismological and geotechnical models to constrain the extrapolation outside the range well represented in the empirical data.

Specifically, we used analytical modeling of site response (Kamai et al. 2013) to constrain the nonlinear site effects as well as analytical modeling of finite-fault effects to constrain the hanging wall (HW) effects (Donahue and Abrahamson 2013). Finally, we used the results of sets of finite-fault simulations (Collins et al. 2006) to evaluate the appropriate large magnitude scaling (scaling from M6.5 to M8).

2 Data Set Selection

The selection of the data set used in the development of the GMPE is a key step. We selected our ground-motion data set from the NGA-West2 data base (January 2013 version). Our general approach for selecting the subset of data for use in the regression analysis was to include all earthquakes, including aftershocks (Class 2 events as defined in Wooddell and Abrahamson 2012) in active crustal regions (ACR) under the assumption that the median ground motions from earthquakes in ACRs at distances less than about 80 km are similar around the world. At distances greater than 80 km, differences in crustal structure can have significant effects on the ground motion leading to a change in the attenuation at large distances (e.g., Q term).

A summary of the criteria for excluding earthquakes and recordings is given below:

- Remove earthquakes not representative of shallow crustal tectonics
- Remove recordings at distances greater than censoring distance
- Remove recordings not representative of free-field ground motion
- Remove earthquakes with questionable hypocentral depths
- Remove the Wenchuan aftershocks
- Remove recordings missing key metadata
- Remove recordings identified as questionable (apparent incorrect gain or spectral shape)
- Remove earthquakes with fewer than three recordings for $M > 5$ and earthquakes with less than ten recordings with good coverage in distance for earthquakes with $M < 5$

2.1 EARTHQUAKE NOT CONSIDERED APPLICABLE TO ACTIVE CRUSTAL REGIONS

We excluded three earthquakes that we considered to be from subduction zones:

1. 1984 Pelekanada, Greece (EQID=93). This earthquake has a focal depth of 81 km, so it is not a shallow crustal earthquake.
2. 1986 eastern Taiwan (EQID=109). This earthquake is located offshore of eastern Taiwan along the subduction zone at latitude 24N.

3. 1979 St. Elias, Alaska (EQID=142). This earthquake is located in the northeast corner of the Yakataga zone defined in the USGS source model (Wesson et al 1999) for the segmentation of Alaska-Aleutian mega-thrust source. The St. Elias earthquake has a low dip angle (12°) and large down dip width (70 km) consistent with interface subduction earthquakes.

The 1992 Cape Mendocino (EQID=123) has been described as a potential subduction zone earthquake in some studies. This earthquake occurred along the southern end of the Cascadia subduction zone, which is a complicated region. Because is it not part of the main Cascadia interface, we have not excluded this event as being representative of subduction earthquakes.

In a previous study of ground motions offshore of northern California, Geomatrix (1995) found that the ground motions from earthquakes in the Gorda plate were significantly different (larger) than typical crustal earthquakes in California. We also excluded five earthquakes from offshore of northern California in the Gorda Plate. These five earthquakes are listed in Table 2.1. Earthquakes along the Mendocino Escarpment and not in the Gorda plate are retained.

Table 2.1 Earthquakes considered not applicable to active crustal regions.

EQID	Location	Magnitude	Reason for Exclusion
3	Offshore N. Cal.	5.8	Gorda Plate earthquake
7	Offshore N. Cal.	6.6	Gorda Plate earthquake
22	Offshore N. Cal.	5.7	Gorda Plate earthquake
26	Offshore N. Cal.	5.6	Gorda Plate earthquake
67	Offshore N. Cal.	7.2	Gorda Plate earthquake
93	Greece	5.0	Deep earthquake
109	Taiwan	7.3	Subduction earthquake
142	St. Elias, Alaska	7.54	Subduction earthquake in the Yakataga source zone

2.2 CENSORING AT LARGE DISTANCES

The ground motions in the NGA-West2 data set are not complete because the very small ground motions are not fully represented, typically due to triggering thresholds in the older instrumentation. At large distances, recordings that are larger than average may exceed the trigger threshold, whereas recordings that are smaller than average may not. This censoring of the smaller ground motions leads to a bias in the data for large distances. Examples of the censoring based on the PGA are shown in Figures 2.1(a) through 2.1(e). The truncation of the small amplitude data (less than about 0.005*g* to 0.02*g*) is clear from these figures. For the more

recent data, the seismic recorders have greater dynamic range and lower trigger thresholds so that the smaller ground motions are recorded. The change in the instrumentation varied by region, so the censoring distance is not the same in all regions. Based on these figures, a censoring model was developed, with different distance limits for different time periods of the observations and for different regions. The censoring model used for the GMPE data set is given below with censoring distance parameters listed in Table 2.2 and presented in Figure 2.2.

$$D_{CENSOR} = \begin{cases} D_5 & for\ M \leq 5 \\ D_5 + (D_6 - D_5)(M-5) & for\ 5 < M \leq 6 \\ D_5 + (D_7 - D_6)(M-6) & for\ 6 < M \leq 7 \\ D_7 & for\ 7 < M \end{cases} \quad (2.1)$$

We used the simple approach of excluding recorded ground motions at distances greater than the censoring distance. An alternative approach would be to use truncated distribution in the regression analysis.

Table 2.2. Censor data model parameters.

Earthquakes	D5	D6	D7
1933–2000	50 km	100 km	200 km
2001–2005	100 km	150 km	250 km
2006–2011	200 km	250 km	350 km
Japanese earthquakes, 2001-2011 (EQID)	200 km	250 km	350 km
L'Aquila Sequence (EQID 274, 275, 276)	200 km	250 km	350 km
Wenchuan (EQID 277)	200 km	250 km	350 km
Wenchuan aftershocks	200 km	250 km	350 km
CA small-moderate mag	200 km	250 km	350 km

2.3 SITES NOT REPRESENATIVE OF FREE FIELD

Previous studies have shown that recordings from strong-motion instruments located in the basements or in structures higher than two stories differ from free-field recordings. We used the GMX C1 classifications to identify stations that are not considered to be representative of the free field. The GMX C1 classifications are listed in Table 2.3.

Table 2.3 GMX C1 classification.

GMX First Letter	Instrument Structure Type
I	Free-field instrument or instrument shelter. Instrument is located at or within several feet of the ground surface, and not adjacent to any structure.
A	One-story structure of lightweight construction. Instrument is located at the lowest level and within several feet of the ground surface.
B	Two- to four-story structure of lightweight construction, or very large (tall) one-story warehouse-type building. Instrument is located at the lowest level and within several feet of the ground surface.
C	One- to four-story structure of lightweight construction. Instrument is located at the lowest level in a basement and below the ground surface.
D	Five or more story structure of heavy construction. Instrument is located at the lowest level and within several feet of the ground surface.
E	Five or more story structure of heavy construction. Instrument is located at the lowest level in a basement and below the ground surface.
F	Structure housing instrument is buried below the ground surface, e.g. tunnel or seismic vault.
G	Structure of light or heavyweight construction, instrument not at lowest level.
H	Earth dam (station at toe of embankment or on abutment).
J	Concrete Dam (none in data base).
K	Near a one-story structure of lightweight construction. Instrument is located outside on the ground surface, within approximately 3 m from the structure.
L	Near a two- to four-story structure. Instrument is located outside on the ground surface, within approximately 6 m of the structure.
M	Near a two- to four-story structure with basement. Instrument is located outside on the ground surface, within approximately 6 m of the structure.
N	Near a five- to eight-story structure. Instrument is located outside on the ground surface, within approximately 10 m of the structure.
O	Near a five- to eight-story structure with basement. Instrument is located outside on the ground surface, within approximately 10 m of the structure.
P	Castle of masonry construction, massive 1-3 stories
Q	Associated with a structure, size of structure is not known
S	Associated with a structure and in the basement, size of structure is not known
T	Associated with a tunnel
U	Il Moro is on an embankment between two roads and retaining walls.

Stations with codes C, D, E, F, and G, P, Q, R, S, T were excluded as not being representative of free-field conditions. In all, there are 423 recordings that were excluded based on the not being representative of the free field. Most of the excluded recordings were for GMX C1 class C. There are 3431 recordings stations without a GMX C1 classification. Even though we don't know if the recordings meet our definition of free field, we have not excluded these recordings.

We have not excluded any stations based on topographic conditions, so our model has some variability due to topography.

2.4 OTHER EARTHQUAKES EXCLUDED

During our preliminary evaluations, we found that the residuals and spectral shape of the Wenchuan aftershocks were very different from other regions, which may reflect unreliable meta data for these events. While we included the Wenchuan mainshock, we removed the aftershocks.

We also excluded earthquakes that had questionable hypocentral depths (less than 1 km) or were deeper than 30 km. As shown in Table 2.4, five earthquakes had hypocentral depths of less than 1 km that we considered to be unreliable. Six earthquakes had hypocentral depths greater than 30 km. Our GMPE is not intended to apply to these deep crustal earthquakes.

Table 2.4 Other earthquakes excluded.

EQID	Mag	Reason
282–345 (Wenchuan Aftershocks)	3.8 to 6.3	unusual spectral shapes and questionable reliability of metadata
1009	4.73	Hypocentral Depth < 1 km
1256	3.19	Hypocentral Depth < 1 km
1244	3.55	Hypocentral Depth < 1 km
242	4.4	Hypocentral Depth < 1 km
1136	3.5	Hypocentral Depth < 1 km
154	5.93	Hypocentral Depth > 30 km
214	4	Hypocentral Depth > 30 km
222	4.8	Hypocentral Depth > 30 km
250	5.4	Hypocentral Depth > 30 km
259	4.6	Hypocentral Depth > 30 km
203	3.7	Hypocentral Depth > 30 km

For the smaller magnitude earthquakes, there is a large number of earthquakes so we used a more selective criteria: only earthquakes with at least ten recordings that covered the distance range of 10 to 100 km were included. This lead to the removal of 157 earthquakes.

We also excluded the four Taiwan earthquakes recorded only by the dense SMART1 array (EQID 71, 86, 95, and 100). These earthquakes have more than three recordings per earthquakes, but the recordings sample a very limited distance range so they do not provide a good estimate of the event term.

Finally, we only included earthquakes that had three or more recordings. This condition only eliminated 70 events from our final dataset.

2.5 QUESTIONABLE RECORDINGS

The large set of recordings from small magnitudes in California was reviewed for reliability of the recordings (Ancheta et. al. 2013). There were some recordings with questionable gains or questionable reliability due to very unusual spectral shapes. These were flagged in the flatfile. We removed all of the recordings that were flagged as questionable. This lead to the removal of 178 recordings from the small magnitude data in California.

The flatfile also flags recordings that are suspected of having a late S-trigger. Thirty-four recordings were removed due to a late S-trigger.

2.6 MISSING METADATA

Recordings missing required metadata such as magnitude, distances, or V_{S30}, were excluded. In all, there were only fifteen recordings removed due to missing metadata.

2.7 FINAL DATA SET

Our final data set consists of 15,750 recordings from 326 earthquakes. The distribution of recordings by region is given in Table 2.5. The magnitude and distance distribution is shown in Figure 2.3. The final set of selected earthquakes and the number of recordings per earthquake are listed in Appendix A.

The response spectral values for the selected recordings are only used in the regression analysis for spectral frequencies greater than 1.25 times the high-pass corner frequency used in the record processing, as defined in the NGA-West2 database. This requirement produces a data set that varies as a function of period. The period dependence of the number of earthquakes and number of recordings used in the regression analysis is shown in Figure 2.4. The steps which Figure 2.4 refers to are regression steps with increasing magnitude and distance ranges, as explained in Section 6.

Table 2.5 Summary of delected dubset by region.

Region No.	Region	No. of Earthquakes	Magnitude Range	Total No. of Recordings
1	California	274	3.1–7.3	12,044
2	Other WUS	2	5.1–7.9	7
3	Taiwan	6	5.9–7.6	1535
4	Italy	25	4.0–6.9	175
5	Middle East	5	6.6–7.5	43
6	Central America	0		0
7	New Zealand	2	6.2–7.0	72
8	Europe (excluding Italy and Greece)	1	7.1	6
9	China	4	4.8–7.9	158
10	Japan	5	6.1–6.9	1700
11	Greece	1	6.4	3
12	Other	1	6.2	5

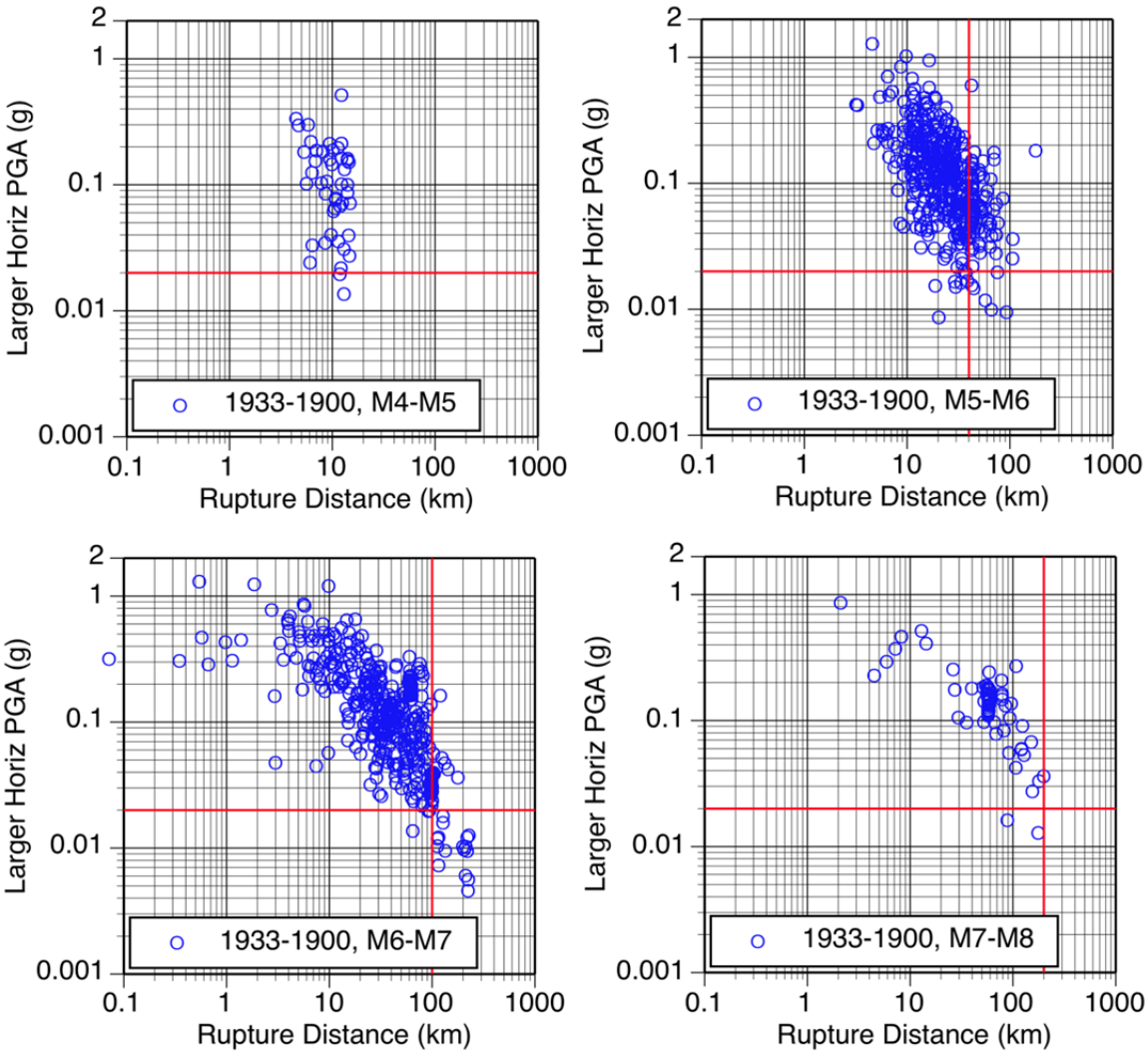

Figure 2.1(a) Evaluation of censoring distance for earthquakes recorded between 1933 and 1990.

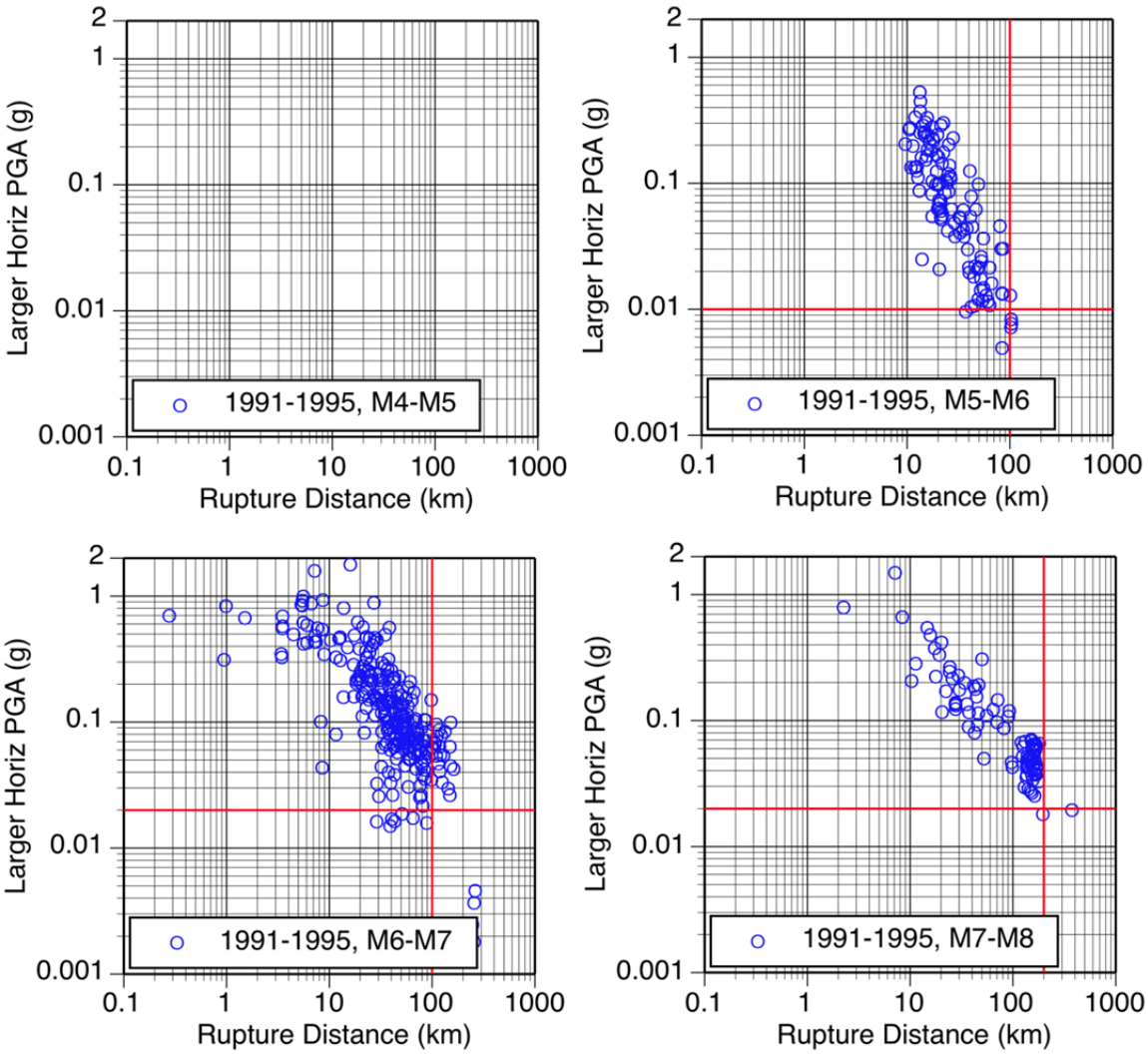

Figure 2.1(b) Evaluation of censoring distance for earthquakes recorded between 1991 and 1995.

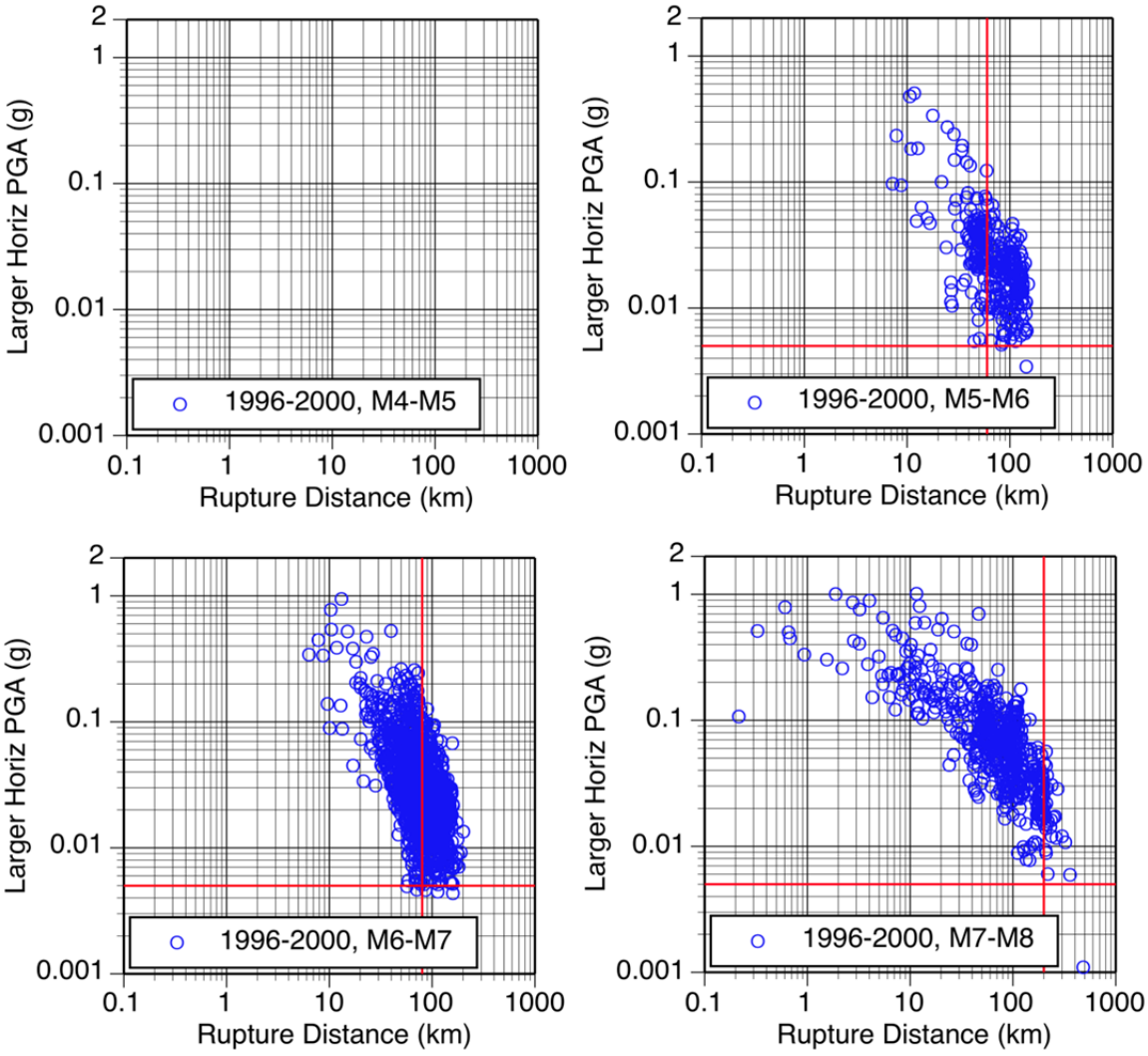

Figure 2.1(c) Evaluation of censoring distance for earthquakes recorded between 1996 and 2000.

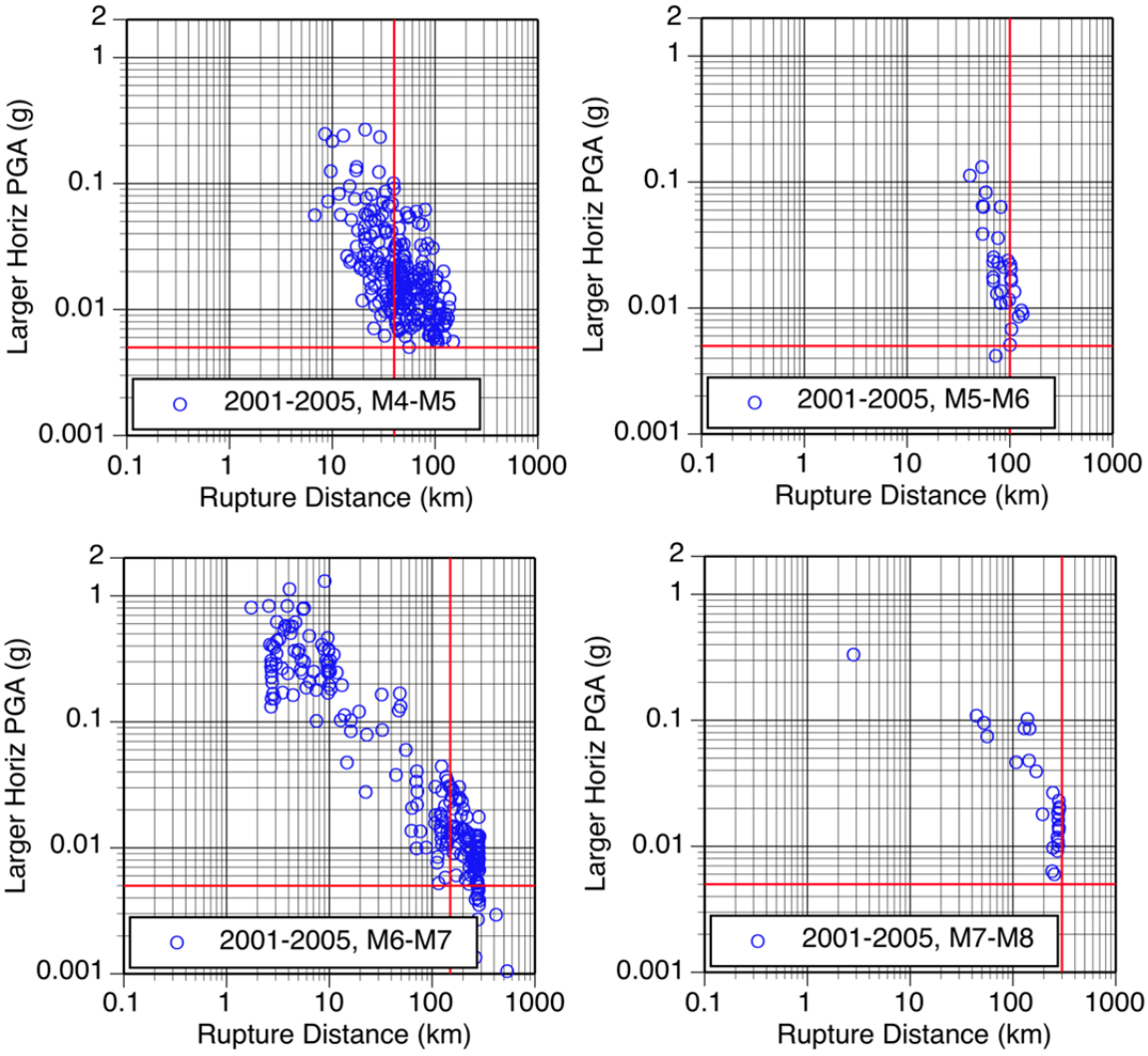

Figure 2.1(d) Evaluation of censoring distance for earthquakes recorded between 2001 and 2005.

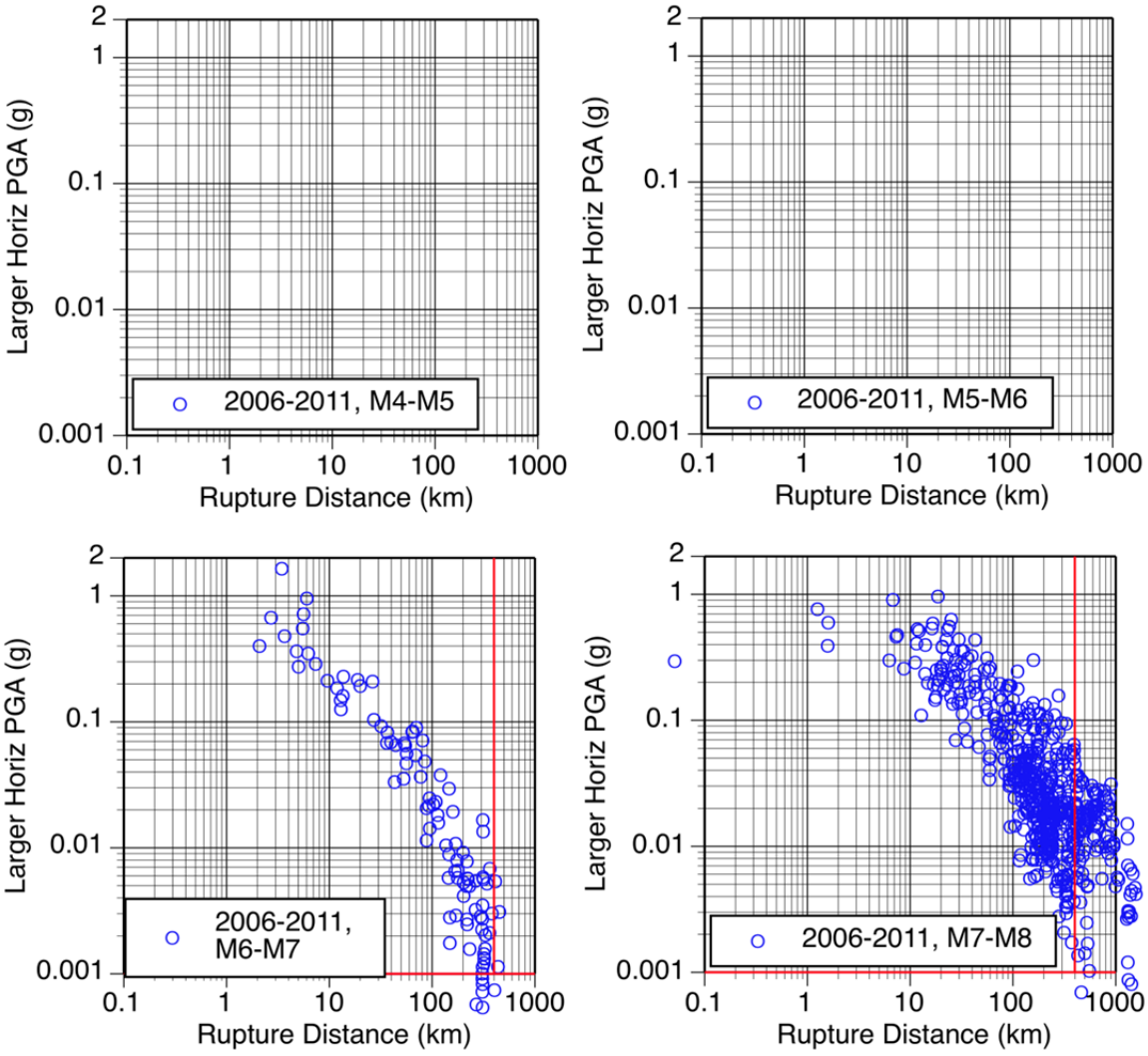

Figure 2.1(e) Evaluation of censoring distance for earthquakes recorded between 2006 and 2011.

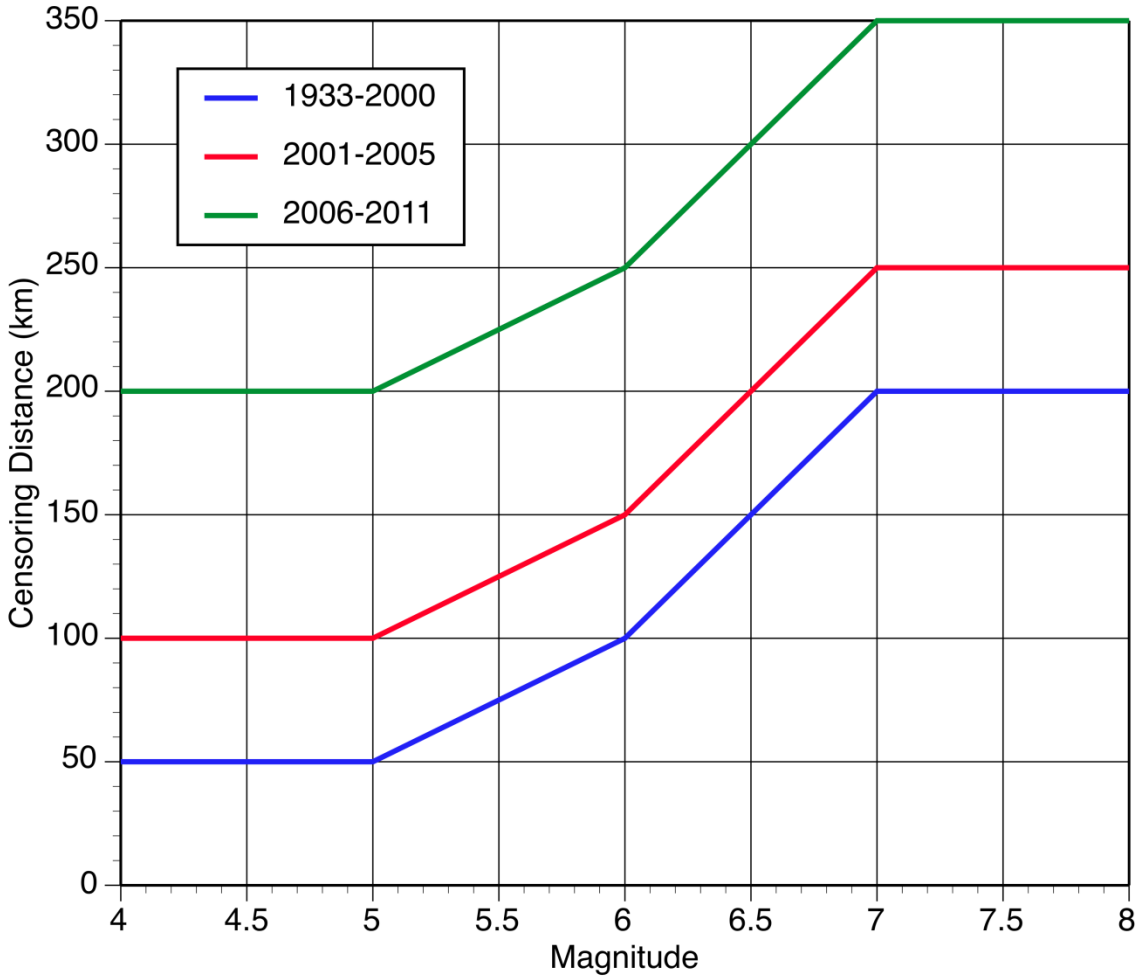

Figure 2.2 Model used for the censoring distance.

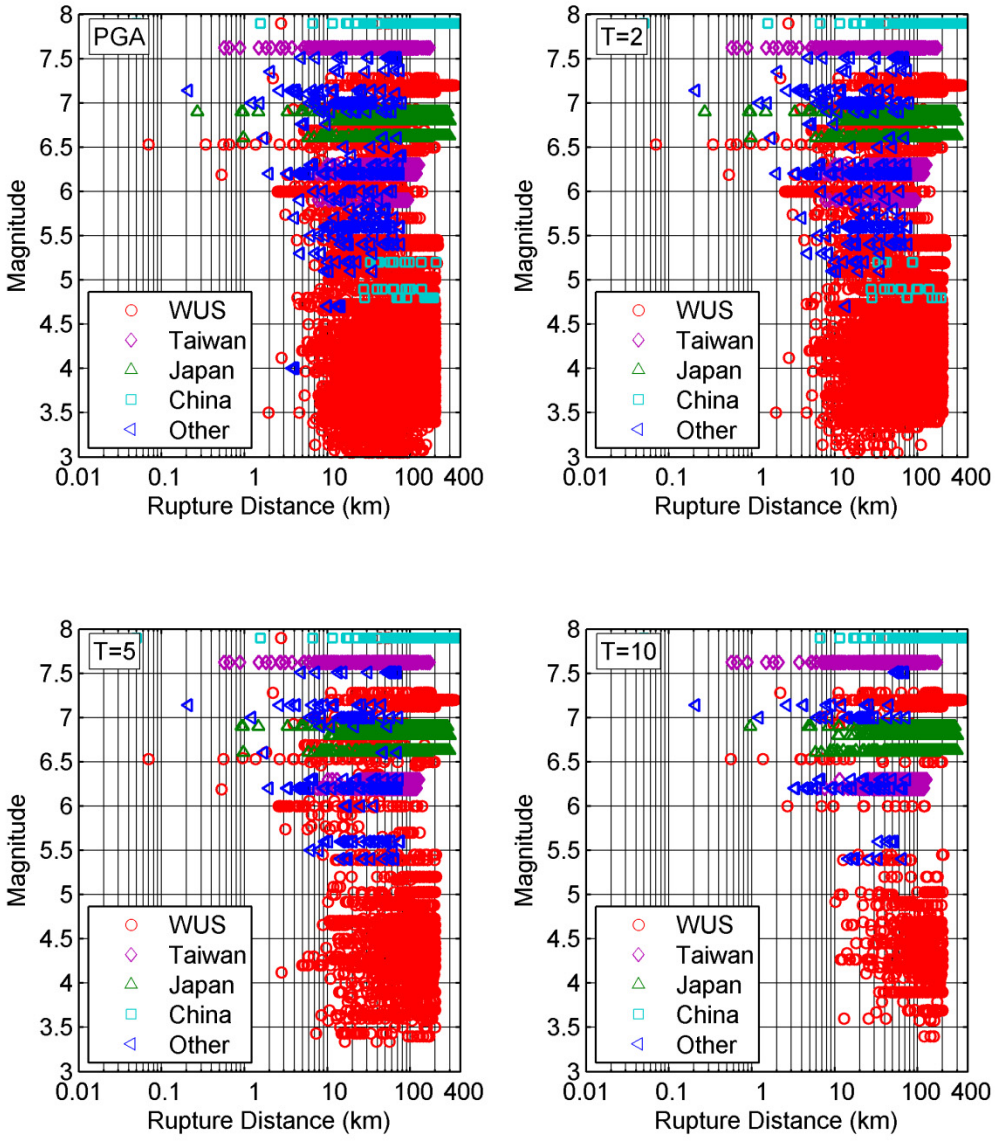

Figure 2.3 Magnitude-distance distribution for the final subset.

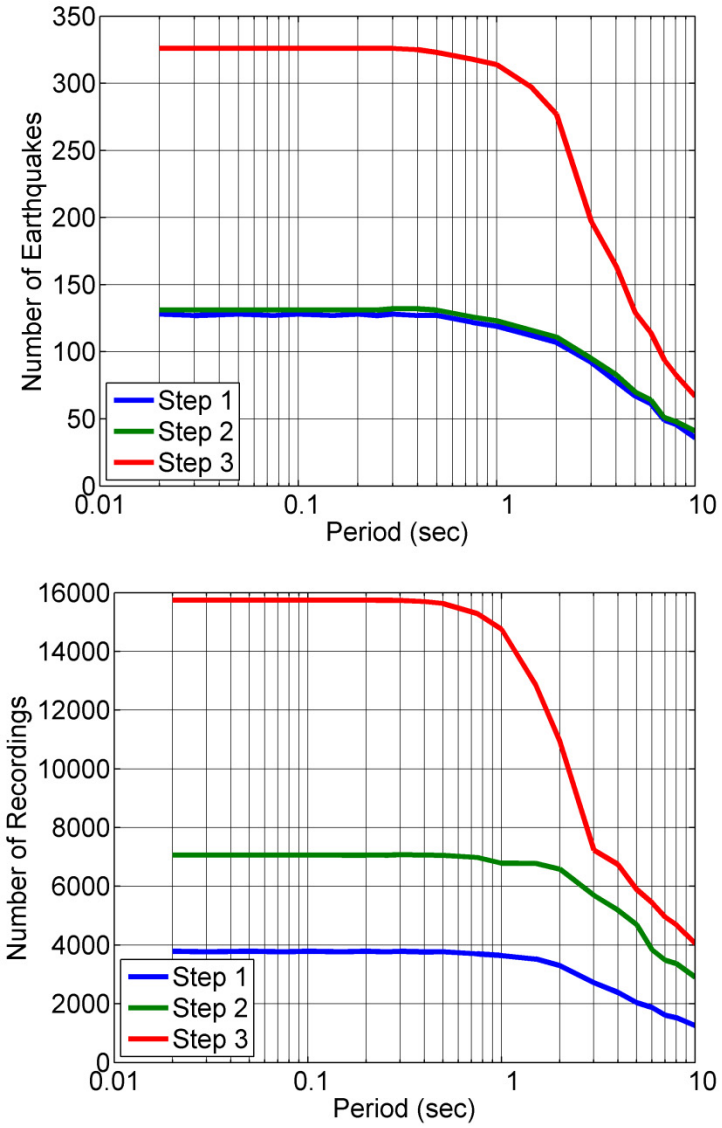

Figure 2.4 **Number of earthquakes (top) and number of recordings (bottom) in the selected subset by period. The different steps are described in the regression analysis section.**

3 Model Parameters

3.1 INTRODUCTION

The independent parameters used in the regression analysis are described in this section. They are separated into source parameters, distance parameters, site parameters, and the ground shaking level parameter.

3.2 SOURCE PARAMETERS

The source parameters are listed in Table 3.1. The scaling of the source is described by five parameters: moment magnitude, depth to the top of rupture, reverse style-of-faulting (SOF), normal SOF, and Class 1−Class 2 (aftershock) flag. The Class 1/Class 2 definition depends on the centroid Joyner-Boore distance, *CRjb*. Two additional source parameters, dip and width, are used only for the hanging-wall (HW) effects.

These parameters are similar to the AS08 model. One difference is that in the current model, the normal oblique earthquakes are grouped into the normal class, whereas in the AS08 model, normal oblique was grouped with strike-slip. There are still not enough normal faulting earthquakes in the data base to clearly define this grouping. The change was made to be consistent with the grouping of reverse oblique earthquakes with the reverse class.

For complex ruptures with variable rake, dip, and width along strike, the parameters for the segment of the rupture closest to the site (in terms of the rupture distance) are used.

Table 3.1 Definition of source parameters used in the regression analysis.

Parameter	Definition	Notes
M	Moment magnitude	
Z_{TOR}	Depth-to -top of rupture (km)	
F_{RV}	Flag for reverse faulting earthquakes	1 for reverse and reverse/oblique earthquakes defined by rake angles between 30 and 150 degrees, 0 otherwise
F_N	Flag for normal faulting earthquakes	1 for normal and normal oblique earthquakes defined by rake angles between -30 and -120 degrees, 0 otherwise
CR_{jb}	Centroid R_{jb} (see Wooddell and Abrahamson (2012)	Class 2 events are those with $CR_{jb} < 15$ km, and within the Gardner-Knopoff (1974) time window
F_{AS}	Flag for aftershocks	1 for class 2, 0 for class 1
dip	Fault dip in degrees	only used for the HW effects
W	Down-dip rupture width (km)	only used for the HW effects

3.3 SITE CLASSIFICATION

The site condition is classified using two parameters: the average shear-wave velocity in the top 30 m (V_{S30}) and the depth to V_S=1.0 km/sec ($Z_{1.0}$). This does not imply that 30 m is the key depth range for the site response, but rather that V_{S30} is correlated with the deeper velocity structure that controls the site amplification. Because the correlation between V_{S30} and the deeper structure may vary from region to region, we allowed the scaling with V_{S30} to be region dependent. Using the soil depth in addition to V_{S30} allows the ground-motion model to distinguish between shallow soil sites, average depth soil sites, and deep soil sites. Although the depth to 2.5 km/sec ($Z_{2.5}$) may be more directly related to the long period site response, we selected $Z_{1.0}$ because it is closer to the traditional geotechnical parameter of "depth to bedrock" and is easier to measure for specific projects.

Table 3.2 Definition of site parameters used in the regression analysis.

Parameter	Definition	Notes
V_{S30}	Shear-wave velocity over the top 30 m (m/s)	
$Z_{1.0}$	Depth to V_S=1.0 km/s at the site (km)	

3.4 DISTANCE DEFINITION

As with the AS08 model, we use the closest distance to the rupture plane, R_{rup}, as the primary distance measure. Four additional distance measures, R_{JB}, R_x, R_1, and R_{y0}, are used to model the attenuation of hanging-wall effects: R_{JB} is the closest horizontal distance to the surface projection of the rupture; R_x is the horizontal distance from the top edge of the rupture, measured perpendicular to the fault strike; R_1 is the value of R_x at the bottom edge of the rupture, and R_{y0} is the horizontal distance off the end of the rupture measured parallel to strike.

Table 3.3 Definition of distance parameters used in the regression analysis.

Parameter	Definition	Notes
R_{rup}	Rupture distance (km)	
R_{jb}	Joyner-Boore distance (km)	
R_x	Horizontal distance (km) from top edge of rupture measured perpendicular to the fault strike	
R_y	Horizontal distance (km) from center of the rupture measured parallel to the fault strike	(Not used in this version)
R_{y0}	Horizontal distance off the end of the rupture measured parallel to strike	For sites located along the rupture, R_{y0}=0. Only used for sites on the HW side. Can be computed from R_{y0}=R_x*tan(Src2SiteA). ** A version of the model without R_{y0} is given, as this a new parameter (see equations 4-15a and 4-15b).

3.5 GROUND MOTION LEVEL

Nonlinear site effects will depend on the level of ground motion. Kamai et al. (2013) developed nonlinear site amplification models for two different measures of the level of shaking: the peak acceleration and the spectral acceleration on rock (V_{S30}=1100 m/sec) at the period of interest. Kamai et al. (2013) showed that both parameters work about equally well. We selected the spectral acceleration on rock because it simplifies the models as the correlation of peak acceleration and spectral acceleration is no longer needed.

4 Functional Form of the Model

The functional form for our ground-motion model is similar to the AS08 model form with the following changes: (1) the nonlinear site term is based on the spectral acceleration on rock; (2) there is an additional break in the magnitude scaling for M<5; (3) the HW scaling with magnitude, dip, and distance is modified; (4) the SOF factor is magnitude dependent; and (5) the form of the Z_1 scaling is modified. The model for the median ground motion is given by:

$$\begin{aligned} lnSa(g) = {} & f_1(M, R_{rup}) + F_{RV} f_7(M) + F_N f_8(M) + F_{AS} f_{11}(CR_{jb}) + \\ & f_5(\widehat{Sa}_{1100}, V_{s30}) + F_{HW} f_4(R_{jb}, R_{rup}, R_x, R_{y0}, W, dip, Z_{TOR}, M) + f_6(Z_{TOR}) + \\ & f_{10}(Z_{1.0}, V_{s30}) + Regional(V_{s30}, R_{rup}) \end{aligned} \quad (4.1)$$

The parameters in Equation (4.1) are defined in Section 3. The functional forms for f_1, f_4, f_5, f_6, f_7, f_8, and f_{10} are given below.

4.1 BASE MODEL

The base form of the magnitude and distance dependence for strike-slip earthquakes is similar to our 2008 model, with additional breaks in the magnitude scaling for small magnitudes:

$$f_1 = \begin{cases} a_1 + a_5(M - M_1) + a_8(8.5 - M)^2 + [a_2 + a_3(M - M_1)]\ln(R) + a_{17}R_{rup} & for\ M > M_1 \\ a_1 + a_4(M - M_1) + a_8(8.5 - M)^2 + [a_2 + a_3(M - M_1)]\ln(R) + a_{17}R_{rup} & for\ M_2 \le M < M_1 \\ a_1 + a_4(M_2 - M_1) + a_8(8.5 - M_2)^2 + a_6(M - M_2) + a_7(M - M_2)^2 & \\ \quad + [a_2 + a_3(M_2 - M_1)]\ln(R) + a_{17}R_{rup} & for\ M < M_2 \end{cases} \quad (4.2)$$

where

$$R = \sqrt{R_{rup}^2 + c_{4M}^2} \quad (4.3)$$

Based on preliminary regression results, the breaks in the magnitude scaling in Equation (4.2) are set at M_1=6.75 and M_2 = 5.0.

The fictitious depth term is modified to reduce to 1 km at small magnitudes. The c_{4M} term is given by:

$$c_{4M}(M) = \begin{cases} c_4 & for\ M > 5 \\ c_4 - (c_4 - 1)(5 - M) & for\ 4 < M \leq 5 \\ 1 & for\ M \leq 4 \end{cases} \quad (4.4)$$

4.2 STYLE-OF-FAULTING MODEL

A preliminary evaluation of the SOF factor found that the difference between ground motions for different faulting style was not seen for the large set of small magnitude data from California. Therefore, a magnitude dependent SOF factor was used for both RV (f_7) and NML (f_8) earthquakes in which the full scaling is only applied for magnitudes greater than 5 and is tapered to zero effect for magnitude 4 or smaller. The style-of-faulting scaling is shown below in Equations (4.5) and (4.6):

$$f_7(M) = \begin{cases} a_{11} & for\ M > 5.0 \\ a_{11}(M - 4) & for\ 4 \leq M \leq 5 \\ 0 & for\ M < 4.0 \end{cases} \quad (4.5)$$

$$f_8(M) = \begin{cases} a_{12} & for\ M > 5.0 \\ a_{12}(M - 4) & for\ 4 \leq M \leq 5 \\ 0 & for\ M < 4.0 \end{cases} \quad (4.6)$$

4.3 SITE RESPONSE MODEL

Our model for the V_{S30} dependence of the site amplification is the same as the AS08 form, but uses the median spectral acceleration on hard rock ($\widehat{Sa}_{1100}$) instead of the peak acceleration to define the strength of shaking. We adopted the nonlinear site response developed by Kamai et al. (2013) using the Peninsular Range soil model:

$$f_5\left(\hat{S}a_{1100}, V_{S30}^*\right) = \begin{cases} (a_{10})ln\left(\frac{V_{S30}^*}{V_{Lin}}\right) - b\ ln\left(\hat{S}a_{1100} + c\right) + b\ ln\left(\hat{S}a_{1100} + c\left(\frac{V_{S30}^*}{V_{Lin}}\right)^n\right) & for\ V_{s30} < V_{Lin} \\ (a_{10} + bn)ln\left(\frac{V_{S30}^*}{V_{Lin}}\right) & for\ V_{s30} \geq V_{Lin} \end{cases} \quad (4.7)$$

where

$$V_{S30}^* = \begin{cases} V_{s30} & for\ V_{s30} < V_1 \\ V_1 & for\ V_{s30} \geq V_1 \end{cases} \quad (4.8)$$

The model for the nonlinear site response was selected so that it becomes proportional to ln(V_{S30}) as the input motion ($\widehat{Sa}_{1100}$) becomes small and as the V_{S30} approaches V_{LIN}. We define a second shear-wave velocity, V_1, above which there is no scaling with V_{S30}. An example of the relation of

the V_{LIN} and V_1 parameters to the site response scaling is shown in Figure 4.1. For $V_{S30}>V_{LIN}$, there is no dependence on the $\widehat{Sa}_{1100}$, for $V_{S30}>V_1$, there is no dependence on V_{S30}.

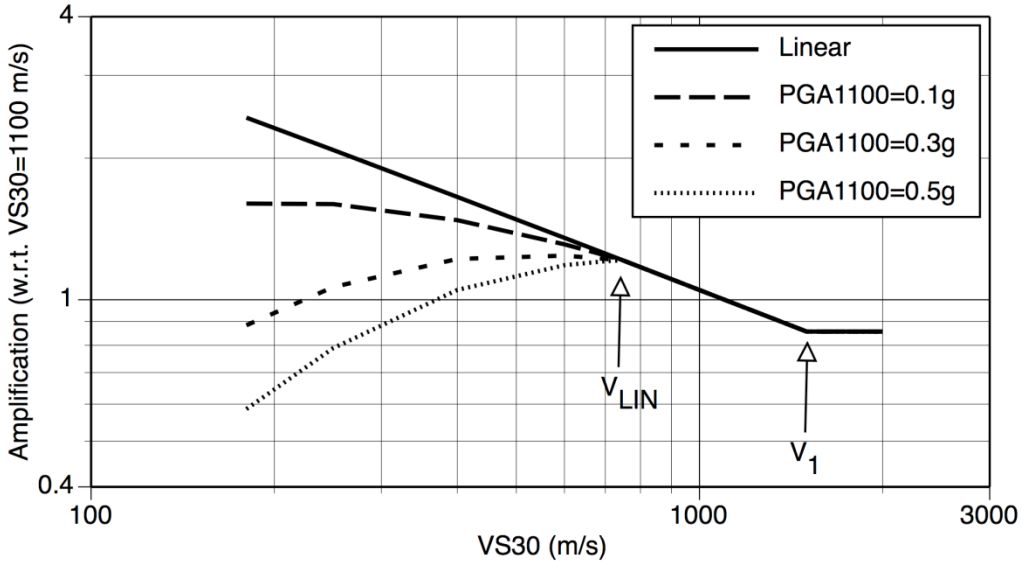

Figure 4.1 Example of the V_{S30} scaling terms (from Abrahamson and Silva 2008).

To constrain the V_1 term, non-parametric models of the V_{S30} scaling are used [Figure 4.2(a-c)]. These plots show that at long periods, the scaling with V_{S30} becomes weaker for higher V_{S30} values. This indicates that for rock sites, the V_{S30} is not well correlated with deeper structure that controls the long-period amplification. Based on Figures 4.2(a-c), the following model is used for the V_1 scaling:

$$V_1 = \begin{cases} 1500 & for\ T \le 0.5sec \\ \exp(-0.35 \ln\left(\frac{T}{0.5}\right) + \ln(1500)) & for\ 0.5sec > T > 3sec \\ 800 & for\ T \ge 3sec \end{cases} \quad (4.9)$$

The nonlinear site response terms (*b, c, n, V_{LIN}*) were constrained by the results of the one-dimensional (1D) analytical site response model using the Peninsula Range soil model (Kamai et al. 2013), with one exception: although the *b* parameter was allowed to become positive at long periods in the Kamai et al. model, we constrain it to be smaller or equal to zero herein. Finally, note that the Kamai et al. model is constrained for $190 \le V_{s30} \le 900$ and should not be used for softer sites.

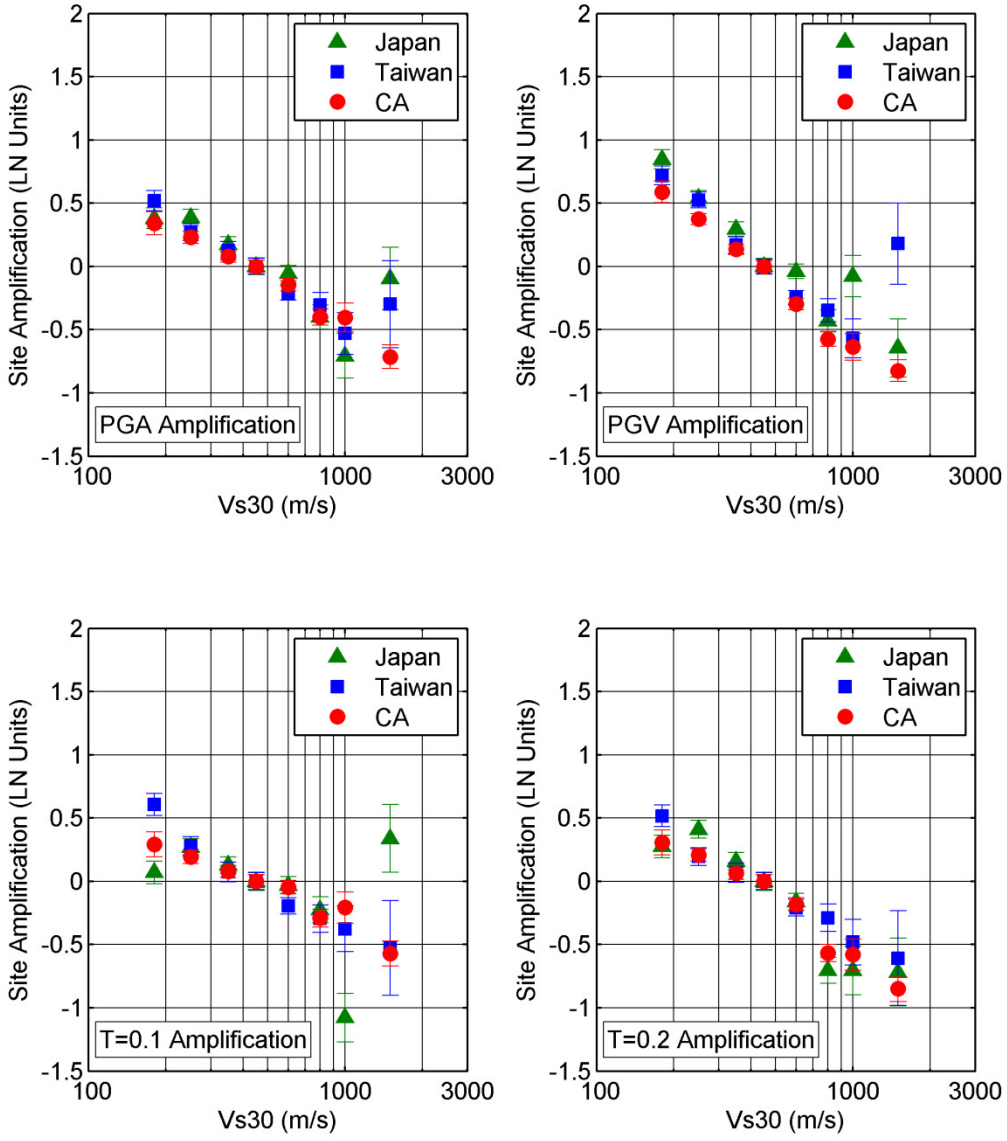

Figure 4.2(a) **Non-parametric evaluation of the V_{S30} scaling, used to identify the V_1 value.**

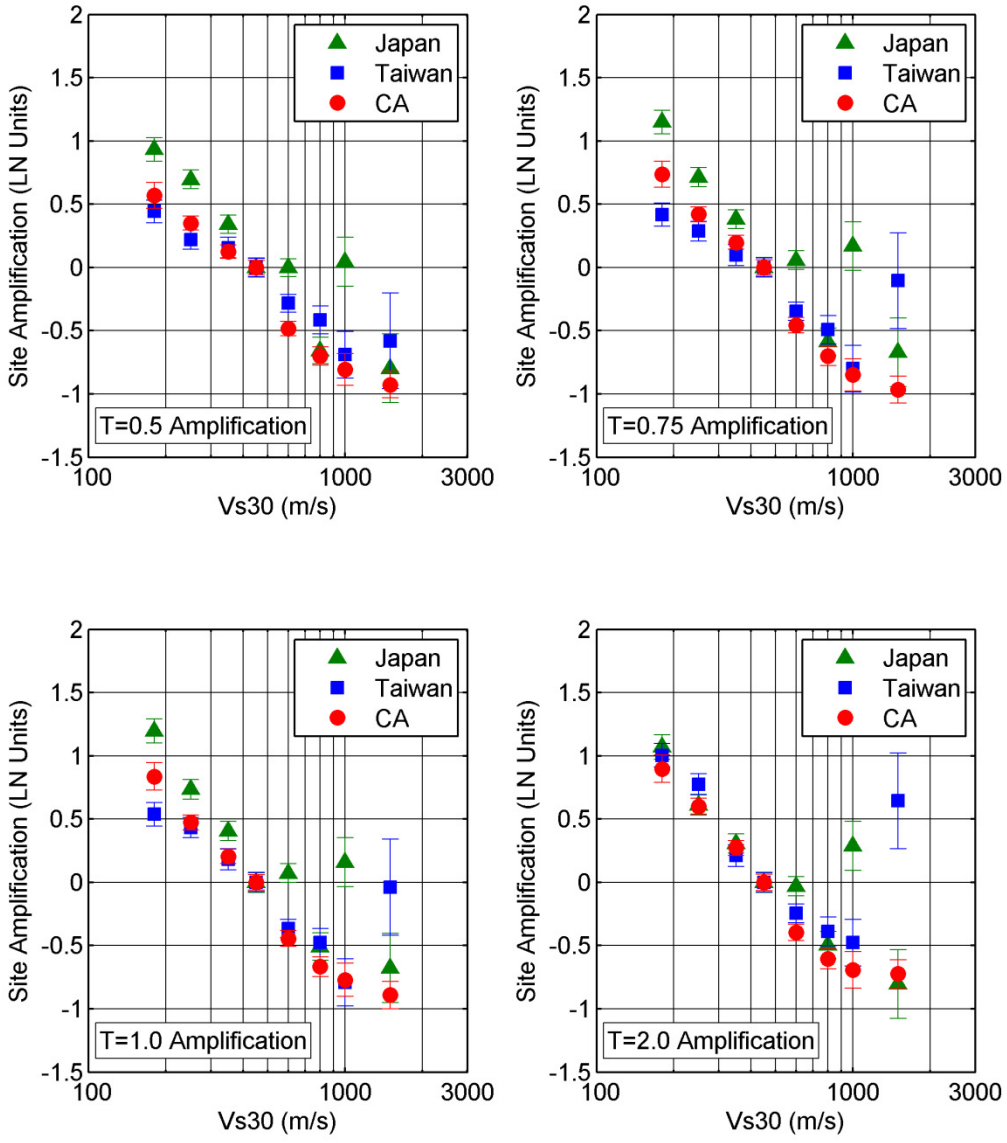

Figure 4.2(b) Non-parametric evaluation of the V_{S30} scaling, used to identify the V_1 value.

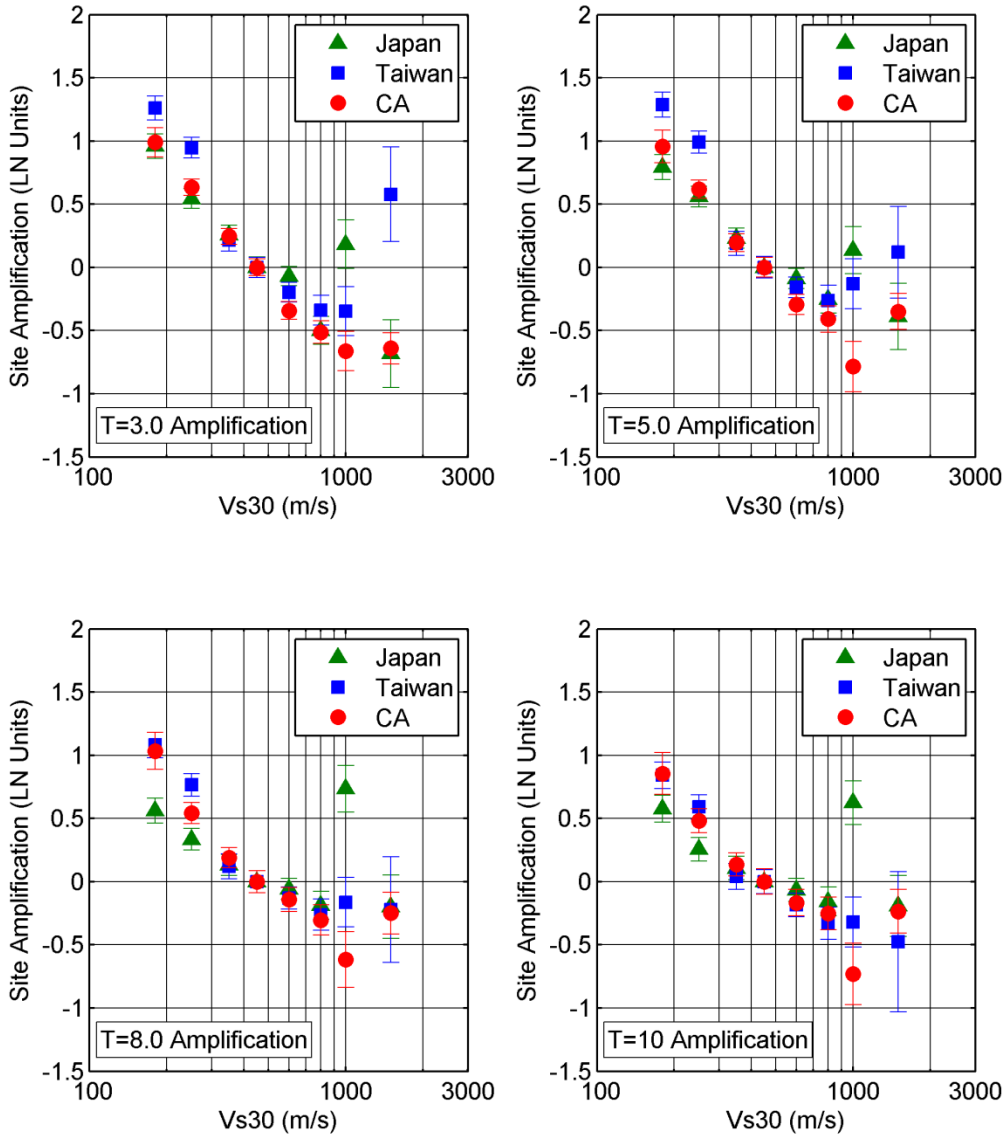

Figure 4.2(c) Non-parametric evaluation of the V_{S30} scaling, used to identify the V_1 value.

4.4 HANGING-WALL MODEL

Our 2008 model included a HW factor, but the scaling with magnitude and distance were not well constrained. Donahue and Abrahamson (2013) used results from finite-fault simulations to constrain the dependence of the HW effects on magnitude, dip, and distance (over the rupture). The HW model includes five tapers to produce a smoothly varying HW effect as a function of the dip, magnitude, location over the rupture, depth, and distance off of the ends of the rupture.

$$f_4\left(R_{jb}, R_{rup}, R_x, R_{y0}, dip, Z_{tor}, M\right) = a_{13} T_1(dip) T_2(M) T_3(R_x, W, dip) T_4(Z_{tor}) T_5(R_x, R_{y0})$$

(4.10)

where

$$T_1(dip) = \begin{cases} (90 - dip)/45 & for\ dip > 30 \\ 60/45 & for\ dip < 30 \end{cases} \quad (4.11)$$

$$T_2(M) = \begin{cases} 1 + \mathrm{a_{2HW}}(M - 6.5) & for\ M \geq 6.5 \\ 1 + \mathrm{a_{2HW}}(M - 6.5) - (1 - \mathrm{a_{2HW}})(M - 6.5)^2 & for\ 5.5 < M < 6.5 \\ 0 & for\ M \leq 5.5 \end{cases} \quad (4.12)$$

$$T_3(R_x) = \begin{cases} h_1 + h_2(R_x/R_1) + h_3(R_x/R_1)^2 & for\ R_x < R_1 \\ 1 - \left(\frac{R_x - R_1}{R_2 - R_1}\right) & for\ R_1 \leq R_x \leq R_2 \\ 0 & for\ R_x > R_2 \end{cases} \quad (4.13)$$

$$T_4(Z_{TOR}) = \begin{cases} 1 - \frac{Z_{TOR}^2}{100} & for\ Z_{TOR} \leq 10\ km \\ 0 & for\ Z_{TOR} \geq 10\ km \end{cases} \quad (4.14)$$

$$T_5(R_x, R_{y0}) = \begin{cases} 1 & for\ R_{y0} < R_{y1} \\ 1 - \frac{R_{y0} - R_{y1}}{5} & for\ R_{y0} - R_{y1} < 5 \\ 0 & for\ R_{y0} - R_{y1} \geq 5 \end{cases} \quad (4.15a)$$

where $R_1 = Wcos(dip)$, $R_2 = 3R_1$, $R_{y1} = R_x \tan(20)$, $h_1 = 0.25$, $h_2 = 1.5$ and $h_3 = -0.75$.

If the R_{y0} distance metric is not available, the T_5 taper can be replaced using the following model:

$$T_5(R_{jb}) = \begin{cases} 1 & for\ R_{jb} = 0 \\ 1 - \frac{R_{jb}}{30} & for\ R_{jb} < 30 \\ 0 & for\ R_{jb} \geq 30 \end{cases} \quad (4.15b)$$

The first three tapers (T_1, T_2, and T_3) are constrained by the Donahue and Abrahamson (2013) HW model (called DA13), but include some modifications. For the magnitude taper (T_2), we smoothed the a_{2HW} term in the DA13 model to be 0.2 for all periods. For the distance tapers (T_3 and T_5), the values of h_1, h_2, and h_3 are set by DA13 while the models for R_2 and R_{y1} were set based on an evaluation of the HW residuals from the Chi-Chi data. . There were only two Z_{TOR} values considered in the DA13 model (Z_{TOR} = 0 and Z_{TOR} = 5 km) so this model did not provide constraints on the HW scaling with Z_{TOR} for depths greater than 5 km. We assumed that the HW effect reduced to zero at Z_{TOR} = 10 km. Finally, the scaling off the end of the rupture (T_5) found in the Donahue and Abrahamson (2013) model showed the HW effect remaining for much larger R_x distances than seen in the empirical data. Although the empirical data is sparse, we relied on the empirical data from the Chi-Chi, Taiwan earthquake to set this scaling.

Although a complex form is used such that the HW effect scales in a reasonable manner with magnitude, dip, depth, and distance, only the a_{13} term (e.g. maximum amplitude of HW effect for M = 6.5, dip =45, Z_{TOR} = 0) was estimated in regression analysis.

4.5 DEPTH-TO-TOP OF RUPTURE MODEL

Based on preliminary evaluations, we simplified the AS08 model to use the same depth scaling for all styles of faulting. Although there is some evidence for a reduction of the depth dependence at shallow depths, we used a linear scaling at all depths for simplicity. To avoid having the small magnitude data control the scaling for the large magnitudes, the scaling was constrained for the larger magnitudes (see Table 5.1). There is still sparse data at large Z_{TOR} values (greater than 20 km). To avoid an unconstrained extrapolation, the depth scaling is capped at 20 km depth.

$$f_6(Z_{TOR}) = \begin{cases} a_{15}\frac{Z_{TOR}}{20} & for\ Z_{TOR} < 20\ km \\ a_{15} & for\ Z_{TOR} \geq 20\ km \end{cases} \tag{4.16}$$

4.6 SOIL DEPTH MODEL

In the AS08 model, we used results from analytical modeling [both three-dimensional (3D) basin modeling and 1D shallow site response modeling] to constrain the soil depth scaling due to the sparse and sometimes inconsistent Z_1 values in the 2008 NGA data set. In the NGA-West2 data set, there are many more sites with Z_1 values. Therefore, we used the empirical data to set the Z_1 scaling. Of the 15750 recordings in our selected data set, 9668 have estimates of Z_1. For the remaining 6082 recordings without Z_1 estimates, we set $Z_1 = Z_{1,ref}(V_{S30})$, where $Z_{1,ref}$ is the average Z_1 for the given V_{s30} value.

Preliminary evaluations showed that the Z_1 scaling is dependent on the V_{S30} value. We used a non-parametric approach to model this dependence by using V_{S30} bins:

$$f_{10}(Z_1, V_{s30}) = \begin{cases} a_{43} ln\left(\frac{Z_1+0.01}{Z_{1,ref}+0.01}\right) & for\ V_{s30} \leq 200 \\ a_{44} ln\left(\frac{Z_1+0.01}{Z_{1,ref}+0.01}\right) & for\ 200 < V_{s30} \leq 300 \\ a_{45} ln\left(\frac{Z_1+0.01}{Z_{1,ref}+0.01}\right) & for\ 300 < V_{s30} \leq 500 \\ a_{46} ln\left(\frac{Z_1+0.01}{Z_{1,ref}+0.01}\right) & for\ 500 < V_{s30} \end{cases} \tag{4.17}$$

For the reference Z_1 value, we adopted the relationships developed by Chiou and Youngs (2013) for Z_1 (in km) as a function of V_{s30}. The relationships for California and Japan are shown in Equations (4.18) and (4.19), respectively:

$$Z_{1,ref} = \frac{1}{1000} exp\left(-\frac{7.67}{4} ln\left(\frac{V_{s30}^4+610^4}{1360^4+610^4}\right)\right) \tag{4.18}$$

$$Z_{1,ref} = \frac{1}{1000} exp\left(-\frac{5.23}{2} ln\left(\frac{V_{S30}^2+412^2}{1360^2+412^2}\right)\right) \quad (4.19)$$

4.7 AFTERSHOCK SCALING

Previous studies, such as AS08, have found that the median short-period ground motions from aftershocks are smaller than the median ground motions from mainshocks. The definition for aftershocks has been modified in this project using the definition of Class 1 and Class 2 events as described in Wooddell and Abrahamson (2012). According to this new terminology, we define Class 2 events as those events that have a CR_{jb} < 15 km and that fall within the Gardner and Knopoff (1974) time window. Following the hypothesis that the stress drops are lower for earthquakes that re-rupture the Class 1 mainshock rupture plane, the ground motions from Class 2 events are scaled using the following expression:

$$f_{11}(CR_{jb}) = \begin{cases} a_{14} & for\ CR_{jb} \leq 5 \\ a_{14}\left[1 - \frac{CR_{jb}-5}{10}\right] & for\ 5 < CR_{jb} < 15 \\ 0 & for\ CR_{jb} > 15 \end{cases} \quad (4.21)$$

4.8 REGIONALIZATION

We allowed for regionalization of the V_{S30} scaling and the Q term for the data from Taiwan, Japan, and China. In all cases, the additional coefficient is added to the base model (all other regions, dominated by California), which is used as a reference. For all three regions, we allow for a difference in the large distance (linear R) terms, such that the linear R coefficients a_{25} for Taiwan, a_{28} for China, and a_{29} for Japan, are added to the base model coefficient, a_{17}. The regionalization is given by:

$$Regional(V_{s30}, R_{rup}) = F_{TW}(f_{11}(V_{s30}) + a_{25}R_{rup}) + F_{CN}(a_{28}R_{rup}) + F_{JP}(f_{12}(V_{s30}) + a_{29}R_{rup}) \quad (4.22)$$

where F_{TW} equals 1.0 for Taiwan and 0 for all other regions, F_{CN} equals 1.0 for China and 0 for all other regions, and F_{JP} equals 1.0 for Japan and 0 for all other regions.

The linear V_{S30} scaling in the base model is described by the coefficients a_{10}+bn. For Taiwan, the change in the ln(V_{S30}) slope is included, using the coefficient a_{31}.

$$f_{11}(V_{s30}) = a_{31} ln\left(\frac{V_{S30}}{V_{Lin}}\right) \quad (4.23)$$

For Japan, the preliminary analyses showed a break in the V_{S30} scaling, such that there isn't a constant slope for all V_{s30} values and rather the scaling seems to be bi-linear. Therefore, for the Japanese data, we allowed for a non-parametric deviation from the base $ln(V_{S30})$ scaling using V_{S30} bins, expressed by the coefficients a_{36} through a_{42} for the different V_{s30} bins, as follows:

$$f_{12}(V_{s30}) = \begin{cases} a_{36} & for\ V_{s30} < 200\ m/sec \\ a_{37} & for\ 200 \le V_{s30} < 300\ m/sec \\ a_{38} & for\ 300 \le V_{s30} < 400\ m/sec \\ a_{39} & for\ 400 \le V_{s30} < 500\ m/sec \\ a_{40} & for\ 500 \le V_{s30} < 700\ m/sec \\ a_{41} & for\ 700 \le V_{s30} < 1000\ m/sec \\ a_{42} & for\ V_{s30} \ge 1000\ m/sec \end{cases} \quad (4.24)$$

The middle V_{s30} bin 400< V_{s30}<500 m/sec was set as a reference value and its coefficient (a_{39}) was set to zero to normalize the site amplification relative to the base model. A regionalized V_{S30} scaling for China was not included due to the smaller amount of data available.

4.9 CONSTANT DISPLACEMENT MODEL

In the AS08 model, the spectral displacement was constrained to reach a constant value at long periods. In the new model, this constraint is not applied, but the regression led to reasonably constant displacement spectra without the additional constraint.

5 Regression Analysis

The random-effects model was used for the regression analysis following the procedure described by Abrahamson and Youngs (1992) with modifications for the effects of the nonlinear site response on the standard deviations described in Al Atik and Abrahamson (2010). The random-effects method leads to two types of residuals: inter-event residuals and intra-event residuals. The effects of nonlinear site response on τ and ϕ are included in the likelihood function.

Our model includes a large number of coefficients; a recurring issue raised regarding our model is the model complexity. There has been a concern that the model is over-parameterized such that the parameters cannot be reliably estimated from the empirical data. Much of the model complexity is associated with nonlinear site response and HW scaling which are partly or fully constrained outside of the regression analysis.

The regression is performed in a number of steps, starting with a more limited data set and then proceeding to the full range, including M>3, R_{rup}<300. Table 5.1 lists the parameters that were regressed in each step and those which were smoothed and fixed following each step. The step numbers are consistent with Figure 2.4, which shows the number of events and number of recordings for each step.

A key issue we faced was the large magnitude scaling at long periods (T=1 to 3 sec). In this range, the Wenchuan earthquake (M7.9) has very weak ground motions. Including the data from the Wenchuan earthquake led to large magnitude (M6.5 to M8) scaling that was about 1/2 of the scaling seen from finite-fault numerical simulations (Collins et al, 2006). In contrast, excluding the data from the Wenchuan earthquake led to large magnitude scaling that was consistent with the scaling seen in the numerical simulations. With only a few large magnitude earthquakes (M>7.5) in our data set, we chose to remove the Wenchuan earthquake from the early regression steps (step 1 and 2). Once the magnitude scaling was fixed, the Wenchuan earthquake was then included in the regression. This allows the Wenchaun data to affect the standard deviation, but not the median in terms of the magnitude scaling.

To arrive at a smooth model, the coefficients were smoothed in a series of steps (Table 5-1). Smoothing could be performed for a number of reasons, including (1) to assure a smooth spectra, and (2) to constrain the model to a more physical behavior where the data is sparse. For example – smoothing of the parameters $a8$, $a10$, $a11$, $a12$, $a14$, and $a15$ (shown in Figures 5-1, 5-2, 5-3, 5-4, and 5-5, respectively) were performed to assure that the final model spectra will be smooth across the application range, including where it is extrapolated outside of the range well constrained by the data. Smoothing of the long distance scaling parameters (see Figure 5-6) was

Table 5.1 Constraints on the Model parameters.

Step	Data Set	Estimated Parameters	Parameters Smoothed after run
1a	M>5.5, *Rrup*< 80 km (PGA only)	*a*1, *a*2, *a*3, *a*4, *a*5, *a*10, *a*11, *a*12, *a*13, *a*14, *a*15	*a*4 (linear mag, M5-M6.75) *a*5 (linear mag, M>7.75)
1b	M>5.5, *Rrup* < 80 km (HW data only)	*a*1, *a*2, *a*3, *a*10, *a*11, *a*12, *a*13, *a*14, *a*15	*a*13 (HW)
1c	M>5.5, *Rrup* < 80 km	*a*1, *a*2, *a*3, *a*6, *a*8, *a*10, *a*11, *a*12, *a*14, *a*15	*c*4 (ficticious depth) *a*3 (mag dep GS)
1d	M>4.5, *Rrup* < 80 km	*a*1, *a*2, a6, a8, *a*10, *a*11, *a*12, *a*14, *a*15, *a*31	a15 (Z_{TOR}), *a*8 (quadratic magnitude)
1e	M>4.5, *Rrup* < 80 km	*a*1, *a*2, *a*6, *a*10, *a*11, *a*12, *a*14,, *a*31	*a*11 (RV SOF) *a*12 (NML SOF) *a*14 (eqk class)
1f	M>4.5, *Rrup* < 80 km	*a*1, *a*2, a6, *a*10, *a*25, *a*29, *a*31, *a*36, *a*37, *a*38,, *a*40, *a*41, *a*42	*a*10 (linear site)
2a	M>4.5 *Rrup* <300 (CA, Japan, Taiwan) *Rrup* <80 (other)	*a*1, *a*2, *a*6, *a*17, *a*25, *a*29, *a*31, *a*36, *a*37, *a*38,, *a*40, *a*41, *a*42, *a*43, *a*44, *a*45, *a*46	*a*17 (linear R)
2b	M>4.5 *Rrup* <300 (CA, Japan, Taiwan) Rrup<80 (other)	*a*1, *a*2, *a*6, *a*25, *a*29, *a*31, *a*36, *a*37, *a*38, *a*40, *a*41, *a*42, *a*43, *a*44, *a*45, *a*46	*a*2, *a*43, *a*44, *a*45, *a*46 (*Z1* for vs30 bins)
3a	M>3.0 *Rrup* <300 (CA, Japan, Taiwan) *Rrup* <80 (other)	*a*1, *a*6, *a*25, *a*29, *a*31, *a*36, *a*37, *a*38, *a*40, *a*41, *a*42	*a*6 (small mag linear)
3b	M>3.0 *Rrup* <300 (CA, Japan, Taiwan) *Rrup* <80 (other)	*a*1, *a*25, *a*29, *a*31, *a*36, *a*37, *a*38, *a*40, *a*41, *a*42	*a*1

constrained to be negative across all periods to assure that the ground motion will continue to attenuate at long distances and not curve upwards, as some of the regressed coefficients suggest. The smoothing of the Z_1 scaling is shown in Figure 5-7. The values of the smoothed coefficients for the median ground motion are listed in Tables 5-2 to 5-5.

The $a14$ term had an unexpected trend with period. Previous studies have noted that there is a reduction in the short-period ground motions from aftershocks as compared to mainshocks (e.g. AS08 model). Figure 5-4 shows the expected reduction at short periods, but it also shows a large increase in the long-period ground motion from aftershocks. Currently, we do not have an explanation for this increase, but we included it in our model to avoid biasing the ground motions from mainshocks.

Table 5.2 Period-independent constants for the median ground motion.

M_2	a_4	a_5	a_7	N	c
5.0	-0.10	-0.49	0.0	1.5	2.4 (2400 for PGV)

Table 5.3(a) Coefficients for the median ground motion.

Parameter	V_{LIN}	b	c_4	M_1	a_1	a_2	a_3	a_6	a_8
PGA	660	-1.47	6	6.75	0.464	-0.790	0.281	2.28	0
PGV	330	-2.02	3	6.75	6.168	-0.950	0.281	2.30	-0.120
T=0.010	660	-1.47	6	6.75	0.464	-0.790	0.281	2.28	0
T=0.020	680	-1.46	6	6.75	0.473	-0.790	0.281	2.28	0
T=0.030	770	-1.39	6	6.75	0.457	-0.790	0.281	2.25	0
T=0.050	800	-1.22	6	6.75	0.652	-0.790	0.281	2.18	0
T=0.075	800	-1.15	6	6.75	0.950	-0.790	0.278	2.13	0
T=0.100	800	-1.23	5.9	6.75	1.160	-0.790	0.27	2.14	0
T=0.150	740	-1.59	5.8	6.75	1.487	-0.790	0.258	2.19	-0.029
T=0.200	590	-2.01	5.7	6.75	1.712	-0.790	0.25	2.25	-0.050
T=0.250	495	-2.41	5.6	6.75	1.796	-0.790	0.242	2.30	-0.066
T=0.300	430	-2.76	5.5	6.75	1.849	-0.790	0.239	2.35	-0.079
T=0.400	360	-3.28	5.2	6.75	1.825	-0.790	0.231	2.45	-0.099
T=0.500	340	-3.6	4.8	6.75	1.768	-0.790	0.23	2.55	-0.115
T=0.750	330	-3.8	4.4	6.75	1.543	-0.790	0.23	2.65	-0.144
T=1.000	330	-3.5	4	6.75	1.292	-0.790	0.23	2.70	-0.165
T=1.500	330	-2.4	3.75	6.75	0.855	-0.790	0.23	2.75	-0.194
T=2.000	330	-1	3.5	6.75	0.521	-0.790	0.23	2.75	-0.214
T=3.000	330	0	3.25	6.82	0.160	-0.790	0.23	2.75	-0.243
T=4.000	330	0	3	6.92	-0.070	-0.790	0.23	2.75	-0.264
T=5.000	330	0	3	7	-0.410	-0.756	0.23	2.75	-0.270
T=6.000	330	0	3	7.06	-0.838	-0.700	0.23	2.75	-0.270
T=7.500	330	0	3	7.15	-1.433	-0.620	0.23	2.75	-0.270
T=10.000	330	0	3	7.25	-2.368	-0.515	0.23	2.75	-0.270

Table 5.3(b) Coefficients for the median ground motion.

Parameter	a_{10}	a_{11}	a_{12}	a_{13}	a_{14}	a_{15}	a_{17}
PGA	1.735	0	-0.1	0.60	-0.30	1.10	-0.0066
PGV	2.360	0	-0.1	0.25	0.22	0.90	-0.0010
T=0.010	1.735	0	-0.1	0.60	-0.30	1.10	-0.0066
T=0.020	1.718	0	-0.1	0.60	-0.30	1.10	-0.0066
T=0.030	1.615	0	-0.1	0.60	-0.30	1.10	-0.0066
T=0.050	1.358	0	-0.1	0.60	-0.30	1.10	-0.0075
T=0.075	1.258	0	-0.1	0.60	-0.30	1.10	-0.0092
T=0.100	1.310	0	-0.1	0.60	-0.30	1.10	-0.0101
T=0.150	1.660	0	-0.1	0.60	-0.30	1.10	-0.0097
T=0.200	2.220	0	-0.1	0.60	-0.30	1.10	-0.0084
T=0.250	2.770	0	-0.1	0.60	-0.24	1.10	-0.0074
T=0.300	3.250	0	-0.1	0.60	-0.19	1.03	-0.0064
T=0.400	3.990	0	-0.1	0.58	-0.11	0.92	-0.0043
T=0.500	4.450	0	-0.1	0.56	-0.04	0.84	-0.0032
T=0.750	4.750	0	-0.1	0.53	0.07	0.68	-0.0025
T=1.000	4.300	0	-0.1	0.50	0.15	0.57	-0.0022
T=1.500	2.650	0	-0.1	0.42	0.27	0.42	-0.0016
T=2.000	0.550	0	-0.1	0.35	0.35	0.31	-0.0013
T=3.000	-0.950	0	-0.1	0.20	0.46	0.16	-0.0010
T=4.000	-0.950	0	-0.1	0	0.54	0.05	-0.0010
T=5.000	-0.930	0	-0.1	0	0.61	-0.04	-0.0010
T=6.000	-0.910	0	-0.1	0	0.65	-0.11	-0.0010
T=7.500	-0.875	0	-0.1	0	0.72	-0.19	-0.0010
T=10.000	-0.800	0	-0.1	0	0.80	-0.30	-0.0010

Table 5.3(c) Coefficients for the Z_1 scaling of the median ground motion.

Parameter	a_{43}	a_{44}	a_{45}	a_{46}
PGA	0.10	0.05	0.00	-0.05
PGV	0.28	0.15	0.09	0.07
T=0.010	0.10	0.05	0.00	-0.05
T=0.020	0.10	0.05	0.00	-0.05
T=0.030	0.10	0.05	0.00	-0.05
T=0.050	0.10	0.05	0.00	-0.05
T=0.075	0.10	0.05	0.00	-0.05
T=0.100	0.10	0.05	0.00	-0.05
T=0.150	0.10	0.05	0.00	-0.05
T=0.200	0.10	0.05	0.00	0.03
T=0.250	0.10	0.05	0.00	0.00
T=0.300	0.10	0.05	0.03	0.03
T=0.400	0.10	0.07	0.06	0.06
T=0.500	0.10	0.10	0.10	0.09
T=0.750	0.14	0.14	0.14	0.13
T=1.000	0.17	0.17	0.17	0.14
T=1.500	0.22	0.21	0.20	0.16
T=2.000	0.26	0.25	0.22	0.16
T=3.000	0.34	0.30	0.23	0.16
T=4.000	0.41	0.32	0.23	0.14
T=5.000	0.51	0.32	0.22	0.13
T=6.000	0.55	0.32	0.20	0.10
T=7.500	0.55	0.29	0.17	0.08
T=10.000	0.42	0.22	0.14	0.08

Table 5.4 Coefficients for the median ground motion for other regions.

Parameter	a_{25}	a_{28}	a_{29}	a_{31}
PGA	-0.0015	0.0025	-0.0034	-0.1503
PGV	-0.0001	0.0005	-0.0037	-0.1462
T=0.010	-0.0015	0.0025	-0.0034	-0.1503
T=0.020	-0.0015	0.0024	-0.0033	-0.1479
T=0.030	-0.0016	0.0023	-0.0034	-0.1447
T=0.050	-0.0020	0.0027	-0.0033	-0.1326
T=0.075	-0.0027	0.0032	-0.0029	-0.1353
T=0.100	-0.0033	0.0036	-0.0025	-0.1128
T=0.150	-0.0035	0.0033	-0.0025	0.0383
T=0.200	-0.0033	0.0027	-0.0031	0.0775
T=0.250	-0.0029	0.0024	-0.0036	0.0741
T=0.300	-0.0027	0.0020	-0.0039	0.2548
T=0.400	-0.0023	0.0010	-0.0048	0.2136
T=0.500	-0.0020	0.0008	-0.0050	0.1542
T=0.750	-0.0010	0.0007	-0.0041	0.0787
T=1.000	-0.0005	0.0007	-0.0032	0.0476
T=1.500	-0.0004	0.0006	-0.0020	-0.0163
T=2.000	-0.0002	0.0003	-0.0017	-0.1203
T=3.000	0	0	-0.0020	-0.2719
T=4.000	0	0	-0.0020	-0.2958
T=5.000	0	0	-0.0020	-0.2718
T=6.000	0	0	-0.0020	-0.2517
T=7.500	0	0	-0.0020	-0.1337
T=10.000	0	0	-0.0020	-0.0216

Table 5.5 **Coefficients for the V_{s30} scaling of the median ground motion for Japan.**

Parameter	a_{36}	a_{37}	a_{38}	a_{40}	a_{41}	a_{42}
PGA	0.265	0.337	0.188	0.088	-0.196	0.044
PGV	0.377	0.212	0.157	0.095	-0.038	0.065
T=0.010	0.265	0.337	0.188	0.088	-0.196	0.044
T=0.020	0.255	0.328	0.184	0.088	-0.194	0.061
T=0.030	0.249	0.320	0.180	0.093	-0.175	0.162
T=0.050	0.202	0.289	0.167	0.133	-0.090	0.451
T=0.075	0.126	0.275	0.173	0.186	0.090	0.506
T=0.100	0.022	0.256	0.189	0.160	0.006	0.335
T=0.150	-0.136	0.162	0.108	0.068	-0.156	-0.084
T=0.200	-0.078	0.224	0.115	0.048	-0.274	-0.178
T=0.250	0.037	0.248	0.122	0.055	-0.248	-0.187
T=0.300	-0.091	0.203	0.096	0.073	-0.203	-0.159
T=0.400	0.129	0.232	0.123	0.143	-0.154	-0.023
T=0.500	0.310	0.252	0.134	0.160	-0.159	-0.029
T=0.750	0.505	0.208	0.129	0.158	-0.141	0.061
T=1.000	0.358	0.208	0.152	0.145	-0.144	0.062
T=1.500	0.131	0.108	0.118	0.131	-0.126	0.037
T=2.000	0.123	0.068	0.119	0.083	-0.075	-0.143
T=3.000	0.109	-0.023	0.093	0.070	-0.021	-0.028
T=4.000	0.135	0.028	0.084	0.101	0.072	-0.097
T=5.000	0.189	0.031	0.058	0.095	0.205	0.015
T=6.000	0.215	0.024	0.065	0.133	0.285	0.104
T=7.500	0.166	-0.061	0.009	0.151	0.329	0.299
T=10.000	0.092	-0.159	-0.050	0.124	0.301	0.243

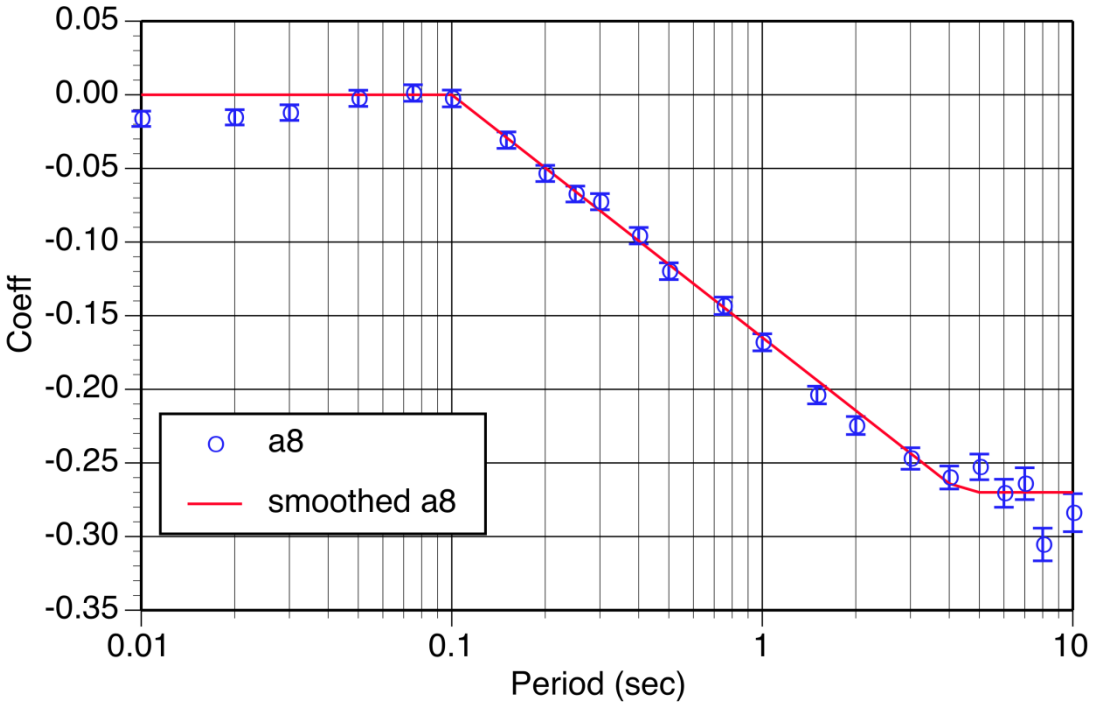

Figure 5.1 **Smoothing of the quadratic magnitude coefficients.**

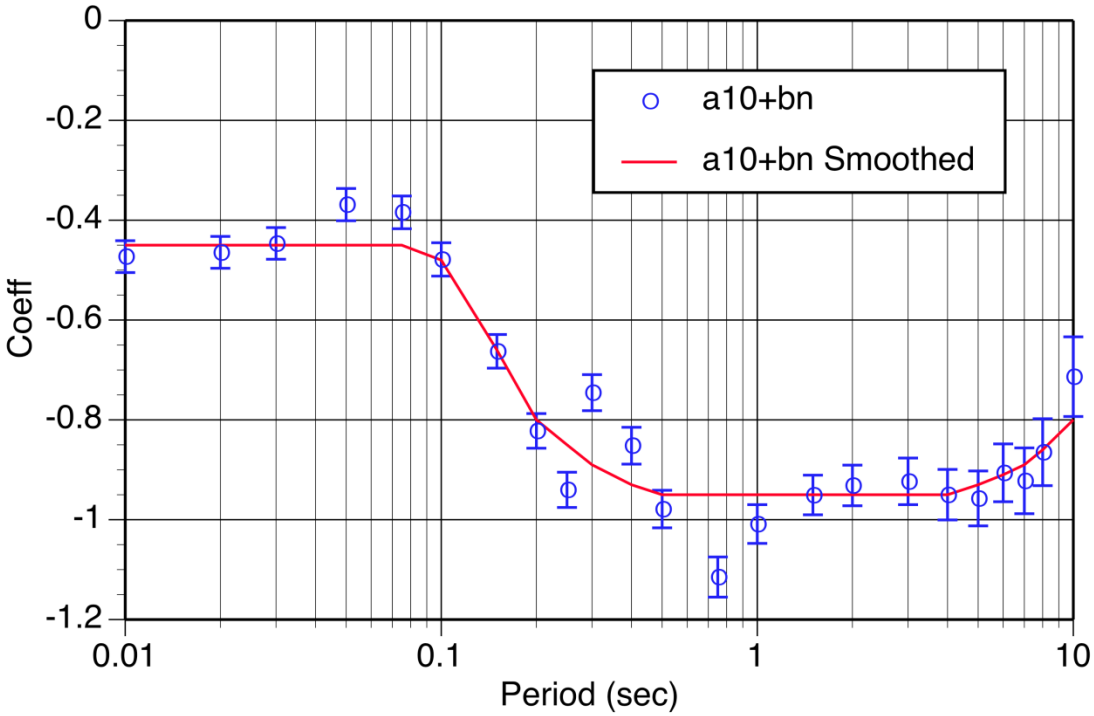

Figure 5.2 **Smoothing of the V_{S30} scaling for the linear range.**

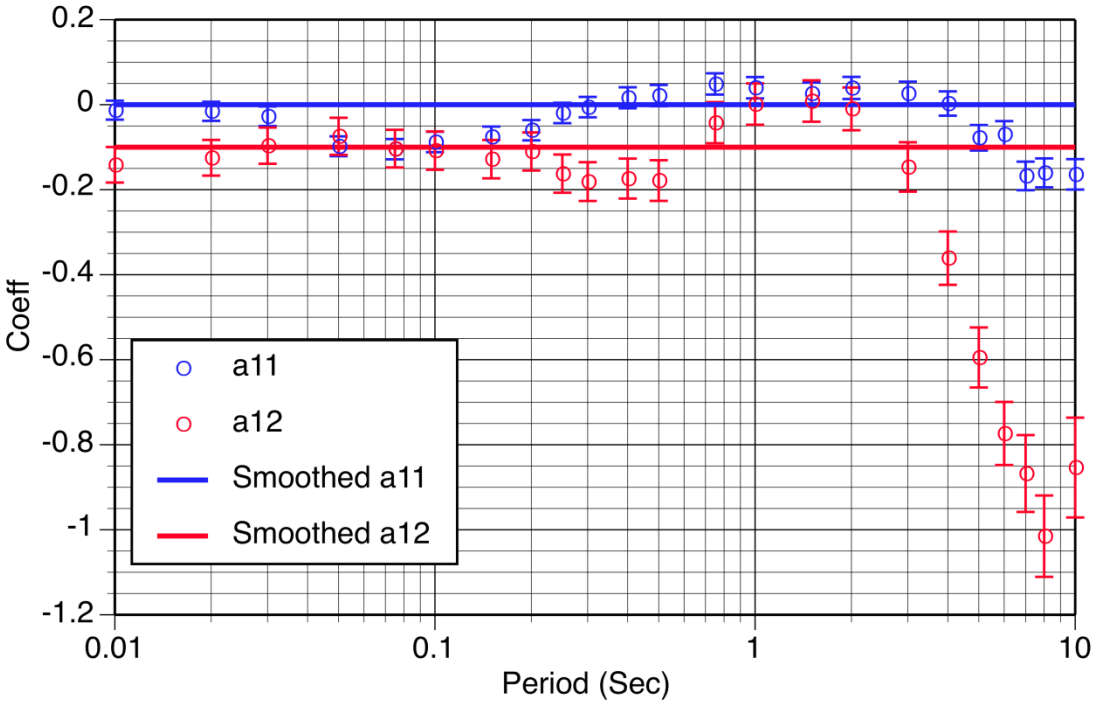

Figure 5.3 **Smoothing of the SOF coefficents.**

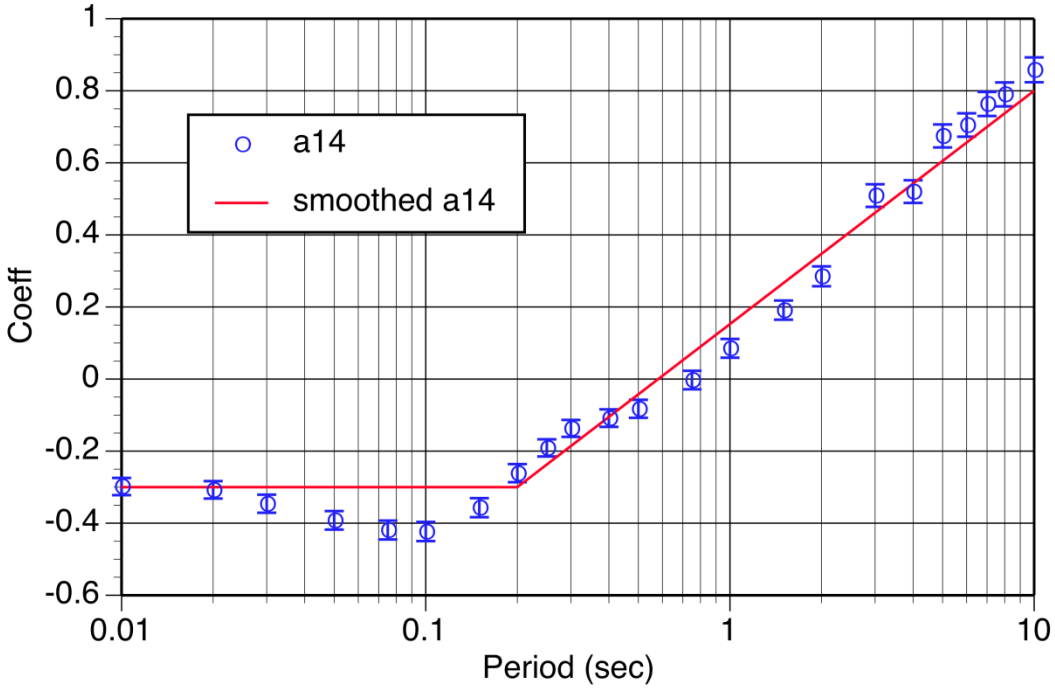

Figure 5.4 **Smoothing of the earthquake class coefficients.**

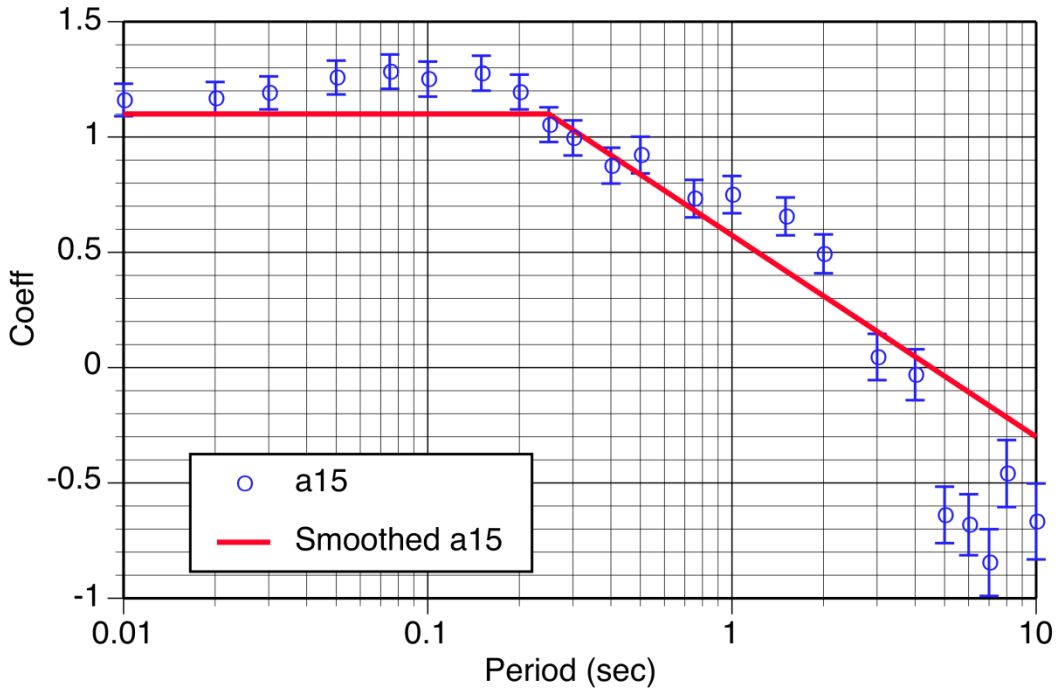

Figure 5.5 Smoothing of the Z_{TOR} coefficients.

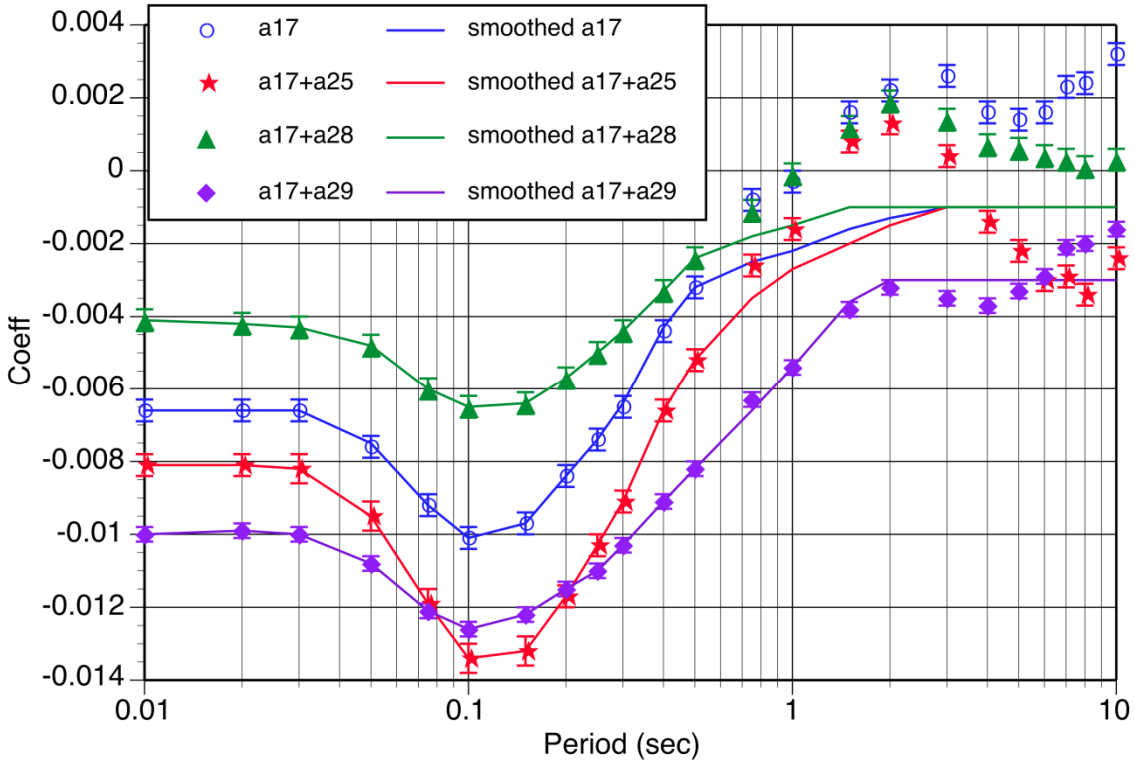

Figure 5.6 Smoothing of the large distance scaling.

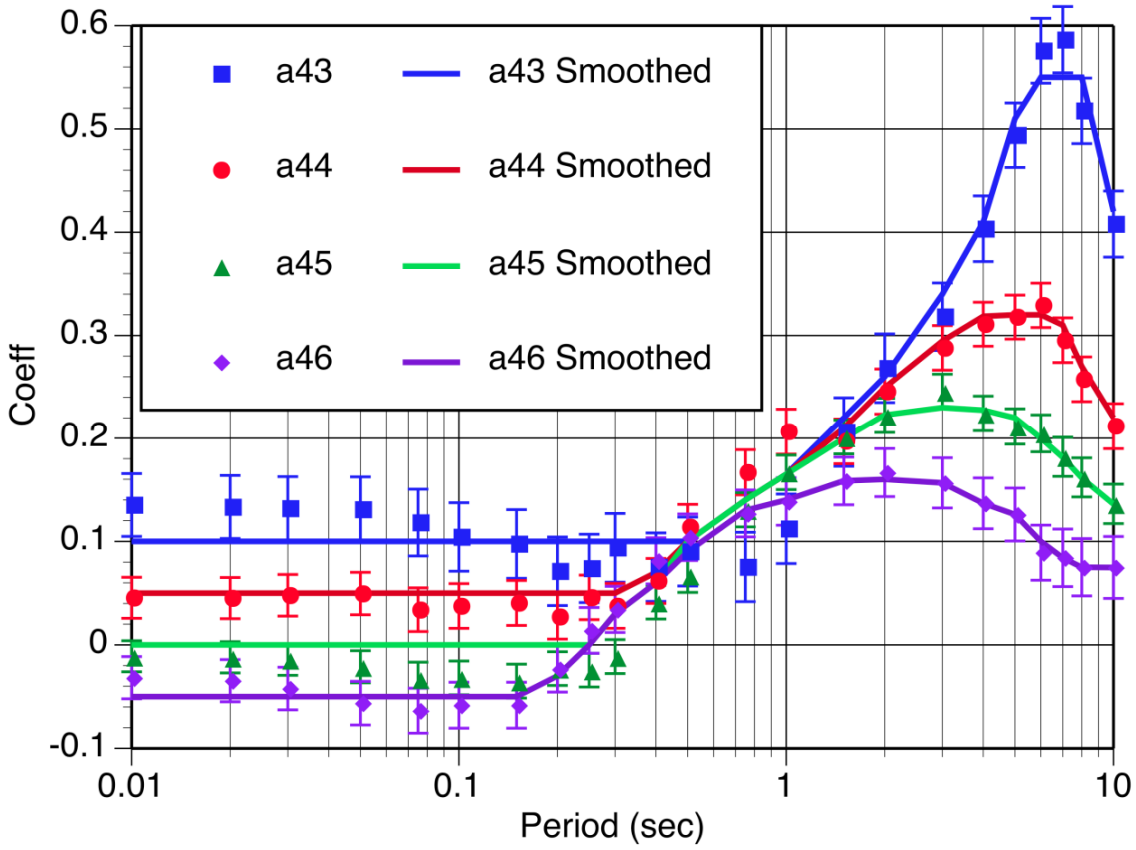

Figure 5.7 Smoothing of the Z_1 scaling.

6 Residuals

In this section, residuals from the regression analysis are shown as functions of all the main independent parameters to allow an evaluation of the model. The residuals are shown for PGA and spectral periods of 0.2, 0.5, 1.0, 3.0, 6.0 and 10.0 sec.

6.1 INTER-EVENT RESIDUALS

The inter-event residuals are plotted as functions of magnitude, depth-to-top of rupture, and rake in Figures 6-1a-g for PGA and spectral periods of 0.2, 0.5, 1.0, 3.0, 6.0 and 10.0 sec, respectively. The open circles represent the Western U.S (WUS) data while the open squares represent all other regions. For all periods, there is not a strong magnitude or rake dependence. For Z_{TOR}, there is no trend up to 15 km but the average residual beyond 15 km is slightly negative. Given the sparse data at that range (only nine events) we consider the model scaling of Z_{TOR} to be acceptable, but note that it is poorly constrained for $Z_{TOR} > 15$ km.

6.2 INTRA-EVENT RESIDUALS

6.2.1 Distance Scaling

The basic model is evaluated through the distance dependence of the intra-event residuals. The distance dependence is evaluated by region, by magnitude bins for WUS data only and for a selected number of well-recorded events.

The distance dependence of the intra-event residuals are shown in Figures 6.2(a) through 6.2(n), separated by region (All regions, WUS, Taiwan, Japan, and China). Overall, there is no trend seen in the residuals up to distances greater than $R_{rup} = 200$ km. For those larger distances, the WUS data is generally over-estimated at periods between PGA and 1 sec, while the Chinese data is generally under-estimated.

The distance scaling by magnitude bins, for the WUS data only, is presented in Figures 6.3(a) through 6.3(g). The magnitude bins 3, 4, 5, 6, and 7 correspond to magnitude ranges of: $3 \le M < 3.5$, $3.5 \le M < 4.5$, $4.5 \le M < 5.5$, $5.5 \le M < 6.5$ and $6.5 \le M < 8$, respectively. There are no apparent trends in the residuals up to a distance of about 100 km at longer distance and periods of 0.5 sec and longer, the magnitude-bin 6 data is under-predicted while the magnitude-bin 7

data is over-predicted at distance of R_{rup} >200 and periods of 0.2 to 0.5 sec. The magnitude-bin 7 data is clearly fit by the model out to distances of 300 km for all periods.

Comparisons of our preliminary model with the preliminary models of the other NGA-West2 developers showed that our model was producing much larger ground motions at large magnitudes (M>7) and large distances (R_{rup}> 100 km) for T=1 sec. For the large magnitudes at T=1 sec, the other models attenuated much faster with distance. To evaluate the distance attenuation in our final model, we examined the residuals from four well-recorded California events - the 1989 M6.9 Loma Prieta, the 1994 M6.7 Northridge, the 1992 M7.3 Landers, and the 2010 M7.2 El-Mayor Cucapah. Figures 6-4a and 6-4b present the residuals for these four events for periods of PGA and 1 sec, respectively. At PGA, the residuals show no trend with distance for all four events. At 1 sec, though, there are contradicting distance trends. For example, the El Mayor Cucapah earthquake, which is the best recorded large earthquake in California, has a faster attenuation than our model. As most of the data were at large distances, the event term centered the model on the values near 200 km. The steeper attenuation at large distances is reflected in the positive residuals at short distances. The Northridge data also have a steeper attenuation than our model, but the Loma-Prieta data have weaker distance attenuation and the Landers data have an attenuation rate that is consistent with our model. This suggests that these events have different long-period attenuation attributes but that they are all captured, on average, by the model as seen in Figure 6-3d.

6.2.2 Site Response

The linear site response model is evaluated through the V_{S30} dependence of the intra-event residuals, shown in Figures 6.5(a) through 6.5(f). Overall, there is no trend in the residuals as a function of V_{S30}, but the three WUS recordings with V_{S30} = 2000 m/sec are high for all spectral periods. This could be related to lower kappa which is not accounted for in this model.

The nonlinear site response model is evaluated through the Sa_{1100} dependence of the intra-event residuals for soil sites, shown in Figures 6.6(a) through 6.6(d) for sites with $180<V_{s30}<360$ m/sec only. Overall, for the WUS and other regions, there is no trend in the residuals as a function of the Sa_{1100} (apart for where the data is very sparse), indicating that for this range of V_{s30}, the nonlinear site response constrained by the PEN analytical model is consistent with the observations. Our model over-predicts the short-period ground motions from soil sites in Japan for high input rock motions, indicating that there is less non-linearity for the Japanese soil sites than given in the PEN model.

The residuals for $V_{s30} \leq 180$ m/sec are not plotted since there are very few data points, but based on the sparse available data, nonlinearity seems to be over-predicted by the analytical model. We note that the model is not applicable at these low velocities and should not be used.

Finally, the $Z_{1.0}$ scaling is evaluated by examining the residuals for five different V_{s30} bins in Figure 6.7(a) through 6.7(g). The intra-event residuals are plotted as a function of $Z_{1.0.}$ No trends are observed in the results.

6.2.3 Hanging Wall

The Hanging Wall (HW) scaling is evaluated by examining the residuals for sites on the HW side of the rupture. Figure 6.8(a) through 6.8(g) show the dependence of the intra-event residuals for sites with source-to-site azimuths of 85–95° (Using 85–95° rather than 90° includes sites located just off the edge of the rupture). The residuals are plotted as a function of R_{JB} and as functions of magnitude and dip for R_{JB}< 2 km (sites either over the rupture or within 2 km of the edge of the surface projection of the rupture). No trend is observed with distance or dip, but the residuals below magnitude 6 are positive for short periods, indicating that the HW effects may extend to smaller magnitudes than assumed in developing the small magnitude part of the T_2(M) taper.

6.3 CORRELATIONS OF RESIDUALS ACROSS PERIODS

The correlation of the residuals across periods is needed to develop mean conditional spectra (Baker and Cornell 2006) and for vector hazard calculations for multiple spectra periods that can be used to better predict structural response (Watson-Lamprey 2007). Contour plots of the correlation coefficient for the normalized inter-event and intra-event residuals are shown in Figures 6.9(a) and 6.9(b), respectively. For a subset of spectral periods, the digital values of the unsmoothed correlation coefficients for the normalized inter-event and intra-event residuals are listed in Tables 6.1 and 6.2, respectively.

As discussed in Carlton and Abrahamson (2013), the correlation of the total residuals is given by the following equation:

$$\rho_{total}\,(T_i, T^*) = \frac{\tau(T_i)\cdot\tau(T^*)}{\sigma(T_i)\cdot\sigma(T^*)}\rho_\tau(T_i, T^*) + \frac{\phi(T_i)\cdot\phi(T^*)}{\sigma(T_i)\cdot\sigma(T^*)}\rho_\phi(T_i, T^*) \quad (6.1)$$

where T^* is the conditioning period, T_i is the other period of interest, ρ_ϕ is the correlation of the intra-event residuals and ρ_τ is the correlation of inter-event residuals.

6.4 DEPENDENCE ON OTHER PARAMETERS

A measure of the static stress-drop was also considered as a source parameter. We used the difference between the magnitude and [Log(Area) + 4] as a proxy for the scaling with static stress-drop: above average stress-drops will have positive values of [M-(log(A)+4)] and below average stress drops will have negative values of [M-(log(A)+4)]. Figure 6-10 shows the event terms from large magnitude (M>6.5) earthquakes for periods of T=1 sec, T=3 sec and T=6 sec. If we were simply scaling the slip and keeping all other parameters the same, we would expect that the ground motions would be larger (positive residual) for above average slip (positive M-LOG(A)-4) and smaller for below average slip (negative M-LOG(A)-4); however, these figures show there is no trend in the residuals with static stress drop. We note that this result is not consistent with the finite-fault simulations which show a strong dependence on static stress drop. The implication is that there are correlations between static stress drop and other source parameters that are currently not account for in the finite-fault simulations.

We also evaluated the dependence of the inter-event residuals on the fault slip-rate. There are only 16 events in our selected data set that have a slip-rate associated with the event. These 16 slip-rates range from 0.2 mm/yr to 35 mm/yr. Our residuals do not show a trend with slip-rate for the 16 available events. The small subset of events that were assigned slip-rates in the NGA-West2 data set have larger slip-rates, so this comparison does not address the potential impact of slip-rate on ground motions for faults with very low slip-rates (e.g. < 0.1 mm/yr).

Finally, we evaluated the residuals for an indication of kappa scaling for rock sites. The version of the flatfile that was available to the NGA-West2 developers did not include kappa estimates for the stations. For this evaluation, we used a proxy for kappa based on the response spectral shape (Sa/PGA): we used the smallest period at which the spectral shape reaches a value of 1.5 (called $T_{amp1.5}$). For M>5 and R_{rup}< 50 km, there is little change in the high frequency spectral shape for a given V_{s30}. Therefore, we used a subset of data with M>5, R_{rup} < 50 km, and V_{s30} > 600 m/s to evaluate the potential for kappa scaling. For this subset, there is a significant trend in the 0.02 sec to 0.1 sec intra-event residuals with larger residuals at smaller $T_{amp1.5}$ values. This suggests that kappa should be considered as a potential additional parameter in updates of the GMPE for short-period ground motions on rock sites

Table 6.1(a) Unsmoothed correlation coefficients for inter-event residuals.

	PGA	T=0.02	T=0.03	T=0.05	T=0.075	T=0.1	T=0.15	T=0.2	T=0.25	T=0.3	T=0.4
PGA	1.000	0.998	0.991	0.960	0.941	0.939	0.935	0.908	0.828	0.727	0.602
T=0.02	0.998	1.000	0.995	0.969	0.948	0.942	0.929	0.895	0.810	0.705	0.578
T=0.03	0.991	0.995	1.000	0.984	0.959	0.944	0.915	0.866	0.768	0.655	0.524
T=0.05	0.960	0.969	0.984	1.000	0.981	0.954	0.897	0.812	0.684	0.560	0.413
T=0.075	0.941	0.948	0.959	0.981	1.000	0.981	0.918	0.811	0.669	0.542	0.378
T=0.1	0.939	0.942	0.944	0.954	0.981	1.000	0.950	0.848	0.710	0.585	0.414
T=0.15	0.935	0.929	0.915	0.897	0.918	0.950	1.000	0.946	0.840	0.740	0.575
T=0.2	0.908	0.895	0.866	0.812	0.811	0.848	0.946	1.000	0.956	0.880	0.745
T=0.25	0.828	0.810	0.768	0.684	0.669	0.710	0.840	0.956	1.000	0.963	0.867
T=0.3	0.727	0.705	0.655	0.560	0.542	0.585	0.740	0.880	0.963	1.000	0.940
T=0.4	0.602	0.578	0.524	0.413	0.378	0.414	0.575	0.745	0.867	0.940	1.000
T=0.5	0.479	0.454	0.397	0.283	0.243	0.275	0.441	0.623	0.762	0.857	0.963
T=0.75	0.273	0.247	0.192	0.073	0.021	0.055	0.220	0.423	0.585	0.699	0.847
T=1	0.165	0.142	0.088	-0.024	-0.072	-0.043	0.107	0.308	0.478	0.613	0.774
T=1.5	0.162	0.139	0.085	-0.028	-0.083	-0.055	0.098	0.295	0.456	0.582	0.731
T=2	0.148	0.126	0.078	-0.029	-0.086	-0.061	0.076	0.264	0.413	0.530	0.677
T=3	0.205	0.184	0.142	0.037	-0.026	-0.010	0.125	0.310	0.438	0.519	0.645
T=4	0.154	0.141	0.107	0.023	-0.030	-0.028	0.075	0.236	0.349	0.431	0.533
T=5	0.241	0.230	0.198	0.117	0.064	0.063	0.152	0.279	0.377	0.443	0.521
T=6	0.248	0.237	0.207	0.124	0.069	0.073	0.141	0.260	0.343	0.388	0.450
T=7	0.284	0.274	0.250	0.169	0.118	0.116	0.164	0.277	0.336	0.340	0.379
T=8	0.331	0.322	0.301	0.221	0.169	0.161	0.193	0.302	0.361	0.345	0.382
T=10	0.316	0.307	0.289	0.199	0.136	0.133	0.133	0.247	0.308	0.268	0.291

Table 6.1(b) Unsmoothed correlation coefficients for inter-event residuals (continued).

	T=0.5	T=0.75	T=1	T=1.5	T=2	T=3	T=4	T=5	T=6	T=7	T=8	T=10
PGA	0.479	0.273	0.165	0.162	0.148	0.205	0.154	0.241	0.248	0.284	0.331	0.316
T=0.02	0.454	0.247	0.142	0.139	0.126	0.184	0.141	0.230	0.237	0.274	0.322	0.307
T=0.03	0.397	0.192	0.088	0.085	0.078	0.142	0.107	0.198	0.207	0.250	0.301	0.289
T=0.05	0.283	0.073	-0.024	-0.028	-0.029	0.037	0.023	0.117	0.124	0.169	0.221	0.199
T=0.075	0.243	0.021	-0.072	-0.083	-0.086	-0.026	-0.030	0.064	0.069	0.118	0.169	0.136
T=0.1	0.275	0.055	-0.043	-0.055	-0.061	-0.010	-0.028	0.063	0.073	0.116	0.161	0.133
T=0.15	0.441	0.220	0.107	0.098	0.076	0.125	0.075	0.152	0.141	0.164	0.193	0.133
T=0.2	0.623	0.423	0.308	0.295	0.264	0.310	0.236	0.279	0.260	0.277	0.302	0.247
T=0.25	0.762	0.585	0.478	0.456	0.413	0.438	0.349	0.377	0.343	0.336	0.361	0.308
T=0.3	0.857	0.699	0.613	0.582	0.530	0.519	0.431	0.443	0.388	0.340	0.345	0.268
T=0.4	0.963	0.847	0.774	0.731	0.677	0.645	0.533	0.521	0.450	0.379	0.382	0.291
T=0.5	1.000	0.933	0.873	0.822	0.772	0.736	0.629	0.599	0.517	0.433	0.421	0.324
T=0.75	0.933	1.000	0.971	0.920	0.876	0.829	0.739	0.693	0.632	0.554	0.526	0.444
T=1	0.873	0.971	1.000	0.965	0.926	0.861	0.788	0.720	0.649	0.556	0.513	0.427
T=1.5	0.822	0.920	0.965	1.000	0.970	0.918	0.856	0.788	0.709	0.610	0.563	0.491
T=2	0.772	0.876	0.926	0.970	1.000	0.950	0.891	0.832	0.754	0.655	0.604	0.555
T=3	0.736	0.829	0.861	0.918	0.950	1.000	0.953	0.898	0.830	0.723	0.671	0.634
T=4	0.629	0.739	0.788	0.856	0.891	0.953	1.000	0.964	0.908	0.816	0.762	0.715
T=5	0.599	0.693	0.720	0.788	0.832	0.898	0.964	1.000	0.962	0.893	0.853	0.806
T=6	0.517	0.632	0.649	0.709	0.754	0.830	0.908	0.962	1.000	0.964	0.925	0.885
T=7	0.433	0.554	0.556	0.610	0.655	0.723	0.816	0.893	0.964	1.000	0.977	0.935
T=8	0.421	0.526	0.513	0.563	0.604	0.671	0.762	0.853	0.925	0.977	1.000	0.958
T=10	0.324	0.444	0.427	0.491	0.555	0.634	0.715	0.806	0.885	0.935	0.958	1.000

Table 6.2(a) Unsmoothed correlation coefficients for intra-event residuals.

	PGA	T=0.02	T=0.03	T=0.05	T=0.075	T=0.1	T=0.15	T=0.2	T=0.25	T=0.3	T=0.4
PGA	1.000	0.999	0.989	0.956	0.930	0.913	0.891	0.871	0.842	0.806	0.737
T=0.02	0.999	1.000	0.993	0.963	0.933	0.913	0.885	0.863	0.833	0.795	0.725
T=0.03	0.989	0.993	1.000	0.975	0.937	0.906	0.866	0.839	0.804	0.764	0.694
T=0.05	0.956	0.963	0.975	1.000	0.959	0.908	0.838	0.791	0.741	0.694	0.618
T=0.075	0.930	0.933	0.937	0.959	1.000	0.949	0.858	0.792	0.730	0.676	0.587
T=0.1	0.913	0.913	0.906	0.908	0.949	1.000	0.906	0.831	0.763	0.705	0.608
T=0.15	0.891	0.885	0.866	0.838	0.858	0.906	1.000	0.919	0.842	0.779	0.674
T=0.2	0.871	0.863	0.839	0.791	0.792	0.831	0.919	1.000	0.928	0.858	0.753
T=0.25	0.842	0.833	0.804	0.741	0.730	0.763	0.842	0.928	1.000	0.939	0.838
T=0.3	0.806	0.795	0.764	0.694	0.676	0.705	0.779	0.858	0.939	1.000	0.904
T=0.4	0.737	0.725	0.694	0.618	0.587	0.608	0.674	0.753	0.838	0.904	1.000
T=0.5	0.675	0.663	0.632	0.551	0.516	0.534	0.595	0.674	0.760	0.822	0.926
T=0.75	0.557	0.546	0.515	0.433	0.394	0.414	0.468	0.547	0.634	0.694	0.796
T=1	0.487	0.475	0.445	0.367	0.329	0.348	0.396	0.467	0.548	0.611	0.709
T=1.5	0.415	0.404	0.376	0.302	0.261	0.274	0.319	0.384	0.456	0.517	0.606
T=2	0.386	0.377	0.352	0.284	0.241	0.246	0.280	0.338	0.405	0.459	0.538
T=3	0.370	0.364	0.346	0.290	0.249	0.244	0.264	0.300	0.352	0.398	0.459
T=4	0.340	0.336	0.323	0.276	0.238	0.228	0.241	0.274	0.314	0.352	0.403
T=5	0.311	0.307	0.297	0.254	0.218	0.206	0.220	0.248	0.282	0.317	0.364
T=6	0.270	0.267	0.256	0.216	0.181	0.172	0.182	0.207	0.240	0.274	0.322
T=7	0.255	0.253	0.242	0.203	0.170	0.164	0.173	0.193	0.220	0.253	0.297
T=8	0.247	0.244	0.235	0.196	0.163	0.159	0.169	0.187	0.215	0.248	0.287
T=10	0.254	0.252	0.243	0.207	0.173	0.167	0.174	0.190	0.218	0.252	0.284

Table 6.2(b) Unsmoothed correlation coefficients for intra-event residuals (continued).

	T=0.5	T=0.75	T=1	T=1.5	T=2	T=3	T=4	T=5	T=6	T=7	T=8	T=10
PGA	0.675	0.557	0.487	0.415	0.386	0.370	0.340	0.311	0.270	0.255	0.247	0.254
T=0.02	0.663	0.546	0.475	0.404	0.377	0.364	0.336	0.307	0.267	0.253	0.244	0.252
T=0.03	0.632	0.515	0.445	0.376	0.352	0.346	0.323	0.297	0.256	0.242	0.235	0.243
T=0.05	0.551	0.433	0.367	0.302	0.284	0.290	0.276	0.254	0.216	0.203	0.196	0.207
T=0.075	0.516	0.394	0.329	0.261	0.241	0.249	0.238	0.218	0.181	0.170	0.163	0.173
T=0.1	0.534	0.414	0.348	0.274	0.246	0.244	0.228	0.206	0.172	0.164	0.159	0.167
T=0.15	0.595	0.468	0.396	0.319	0.280	0.264	0.241	0.220	0.182	0.173	0.169	0.174
T=0.2	0.674	0.547	0.467	0.384	0.338	0.300	0.274	0.248	0.207	0.193	0.187	0.190
T=0.25	0.760	0.634	0.548	0.456	0.405	0.352	0.314	0.282	0.240	0.220	0.215	0.218
T=0.3	0.822	0.694	0.611	0.517	0.459	0.398	0.352	0.317	0.274	0.253	0.248	0.252
T=0.4	0.926	0.796	0.709	0.606	0.538	0.459	0.403	0.364	0.322	0.297	0.287	0.284
T=0.5	1.000	0.874	0.787	0.678	0.606	0.517	0.451	0.403	0.362	0.340	0.326	0.317
T=0.75	0.874	1.000	0.911	0.801	0.726	0.618	0.543	0.483	0.431	0.405	0.387	0.376
T=1	0.787	0.911	1.000	0.886	0.810	0.701	0.609	0.535	0.471	0.437	0.420	0.405
T=1.5	0.678	0.801	0.886	1.000	0.916	0.801	0.709	0.632	0.562	0.526	0.506	0.494
T=2	0.606	0.726	0.810	0.916	1.000	0.877	0.787	0.709	0.635	0.588	0.562	0.546
T=3	0.517	0.618	0.701	0.801	0.877	1.000	0.902	0.814	0.742	0.693	0.670	0.661
T=4	0.451	0.543	0.609	0.709	0.787	0.902	1.000	0.914	0.830	0.765	0.729	0.704
T=5	0.403	0.483	0.535	0.632	0.709	0.814	0.914	1.000	0.926	0.852	0.810	0.778
T=6	0.362	0.431	0.471	0.562	0.635	0.742	0.830	0.926	1.000	0.941	0.888	0.835
T=7	0.340	0.405	0.437	0.526	0.588	0.693	0.765	0.852	0.941	1.000	0.956	0.886
T=8	0.326	0.387	0.420	0.506	0.562	0.670	0.729	0.810	0.888	0.956	1.000	0.930
T=10	0.317	0.376	0.405	0.494	0.546	0.661	0.704	0.778	0.835	0.886	0.930	1.000

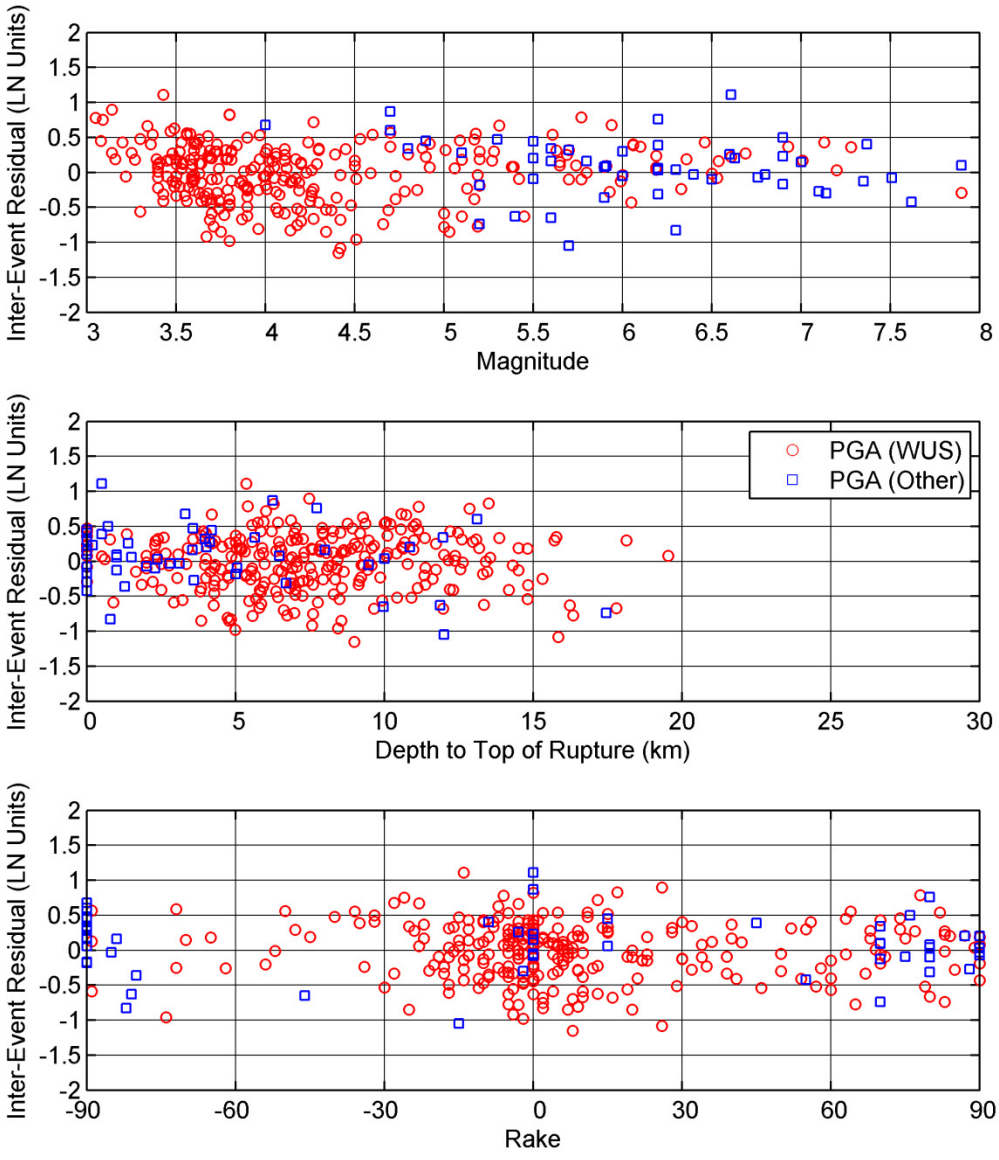

Figure 6.1(a) Event terms for PGA.

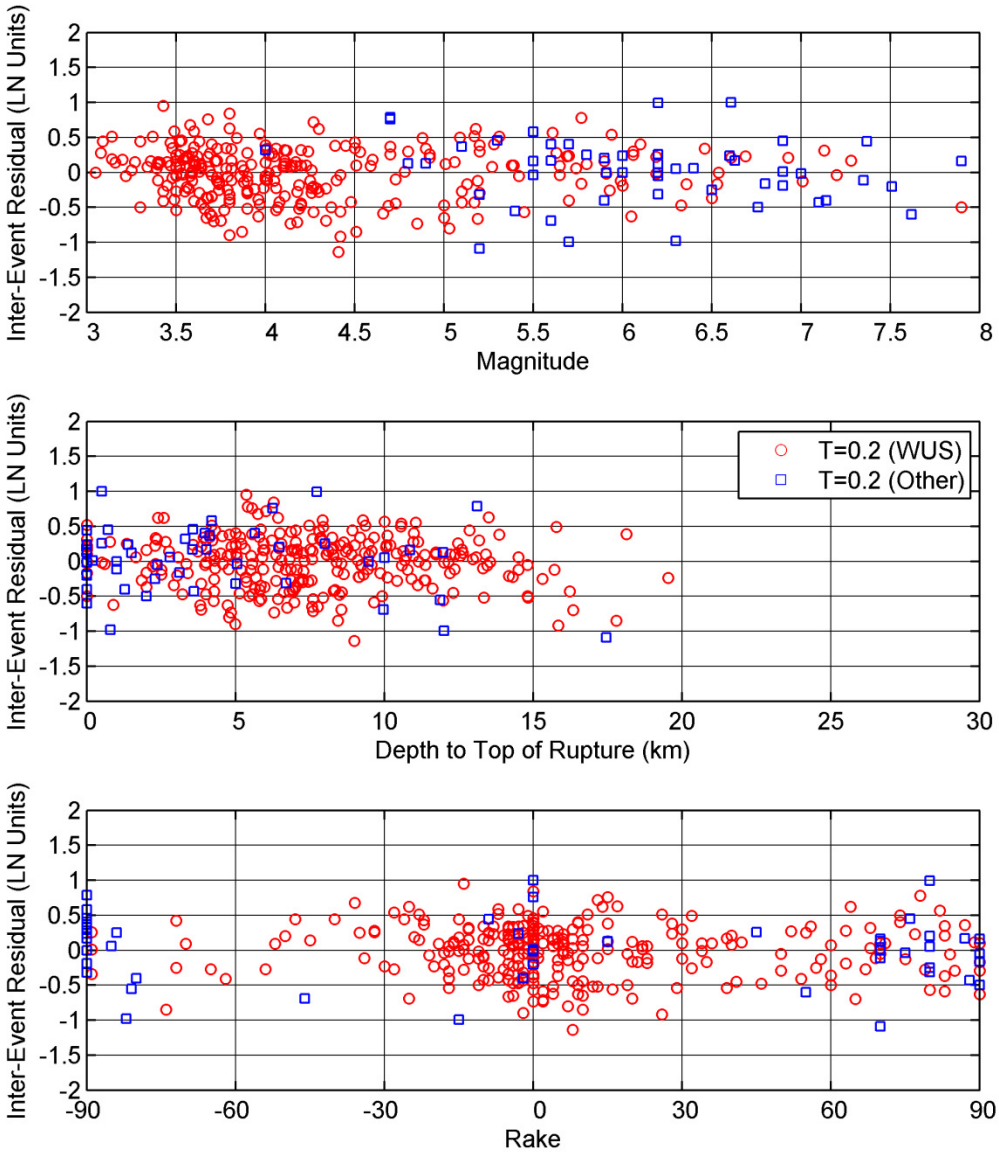

Figure 6.1(b) Event terms for T = 0.2 sec.

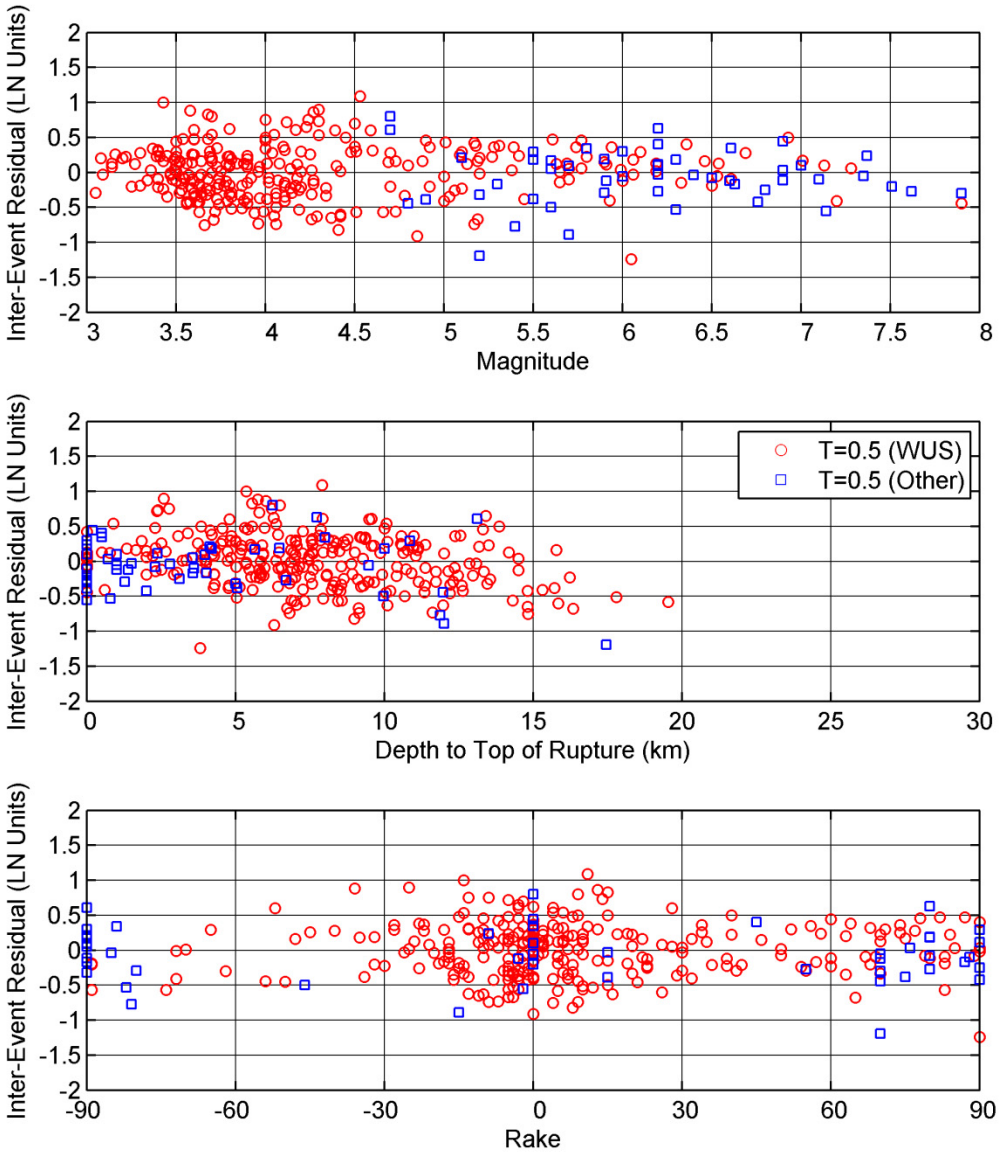

Figure 6.1(c) Event terms for T = 0.5 sec.

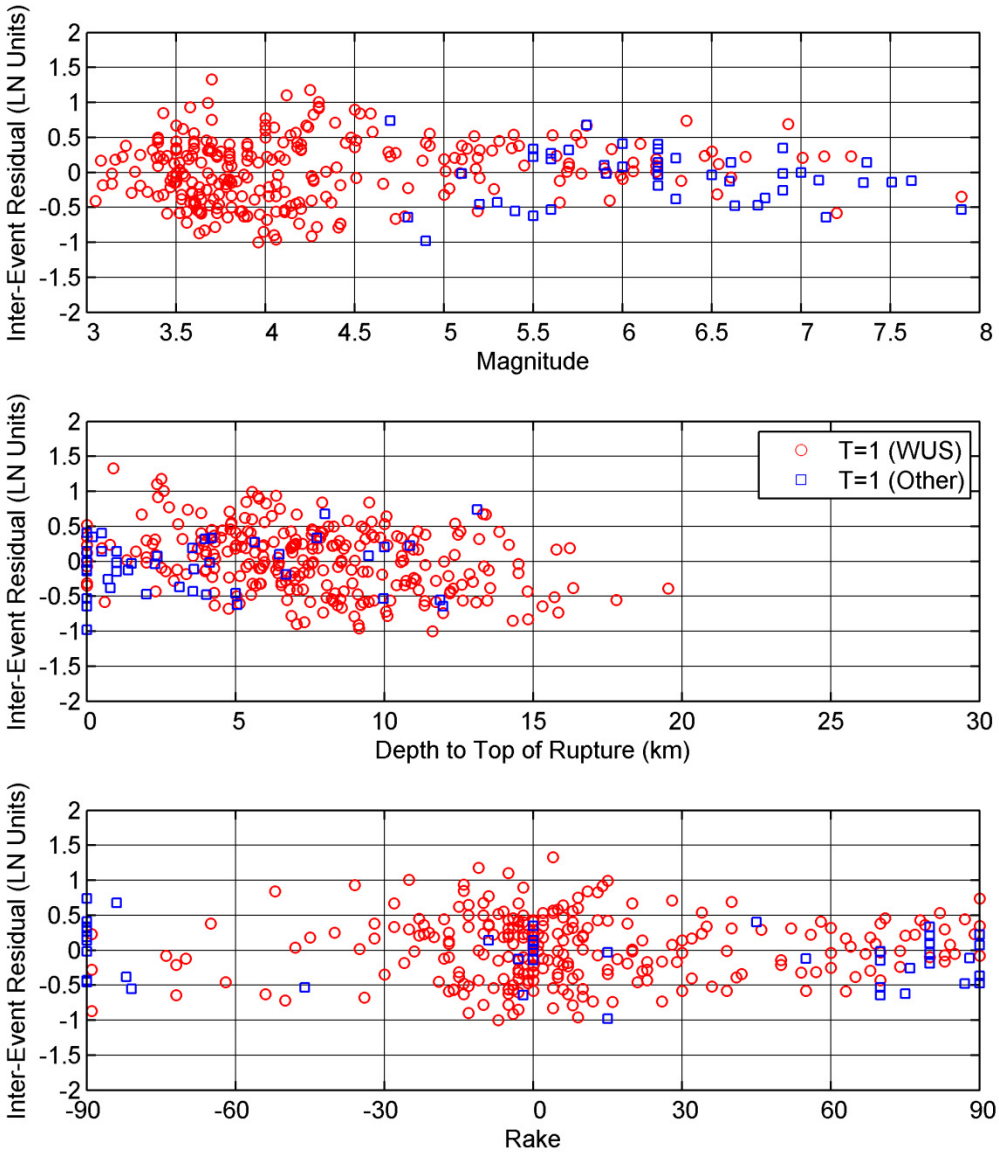

Figure 6.1(d) Event terms for T = 1 sec.

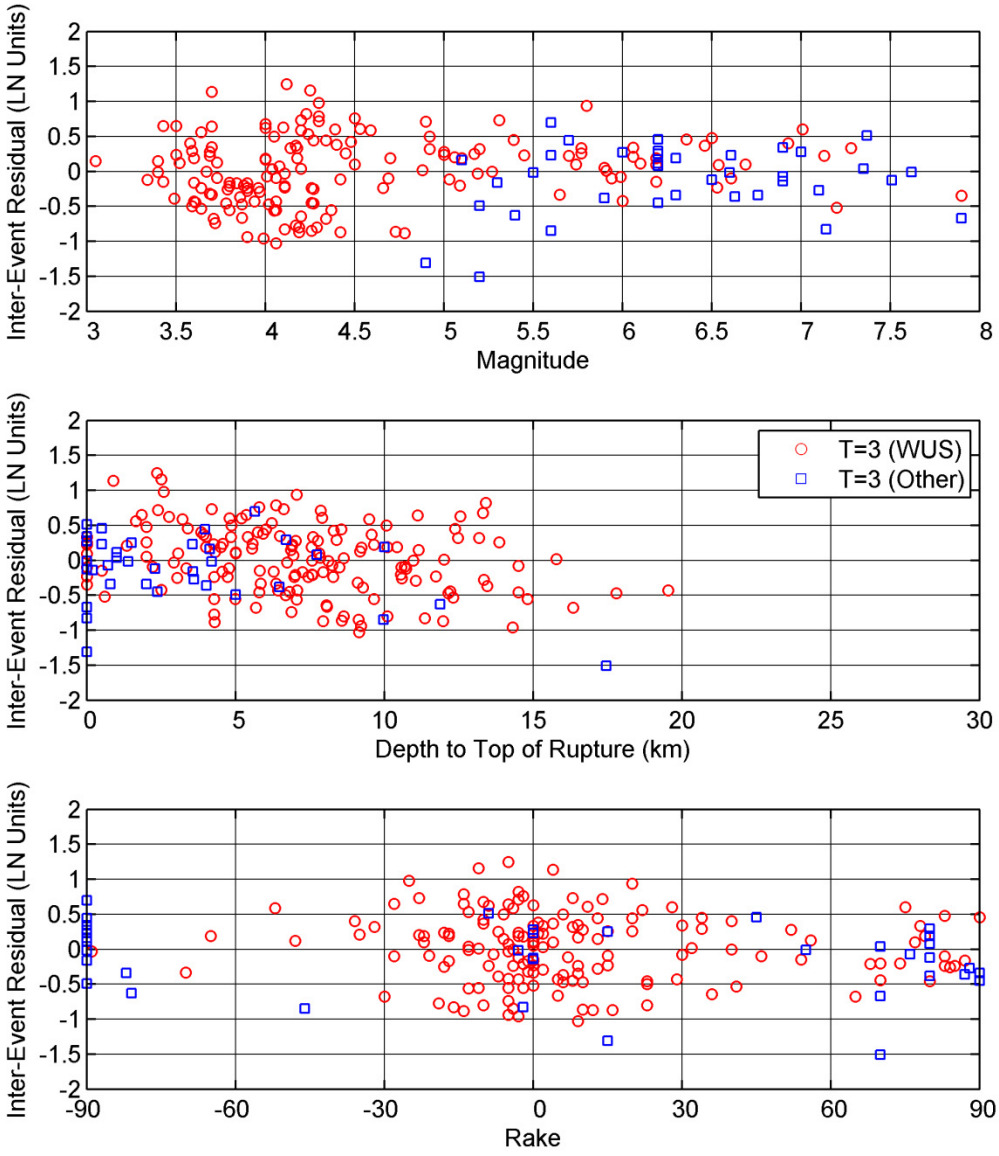

Figure 6.1(e) Event terms for T = 3 sec.

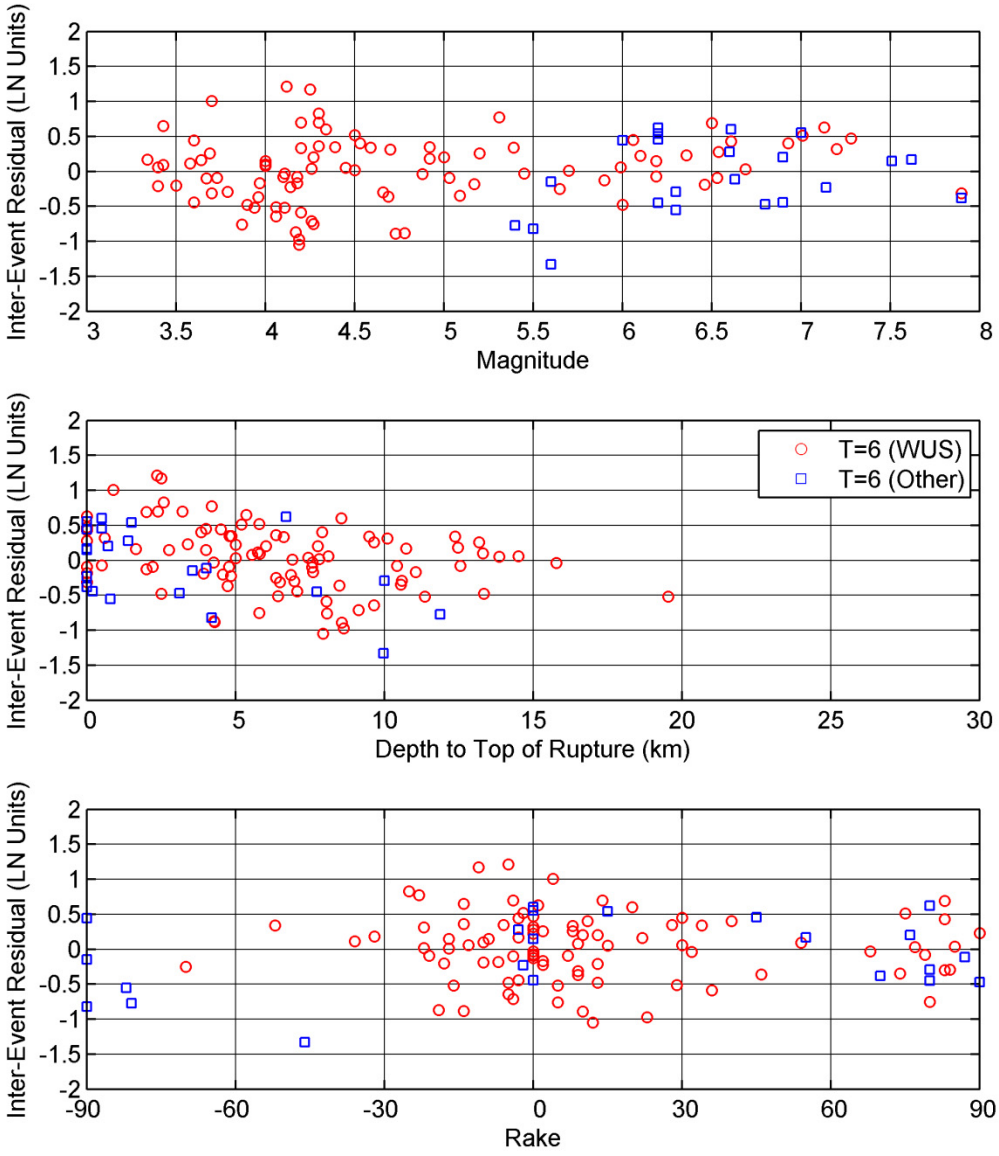

Figure 6.1(f) Event terms for T = 6 sec.

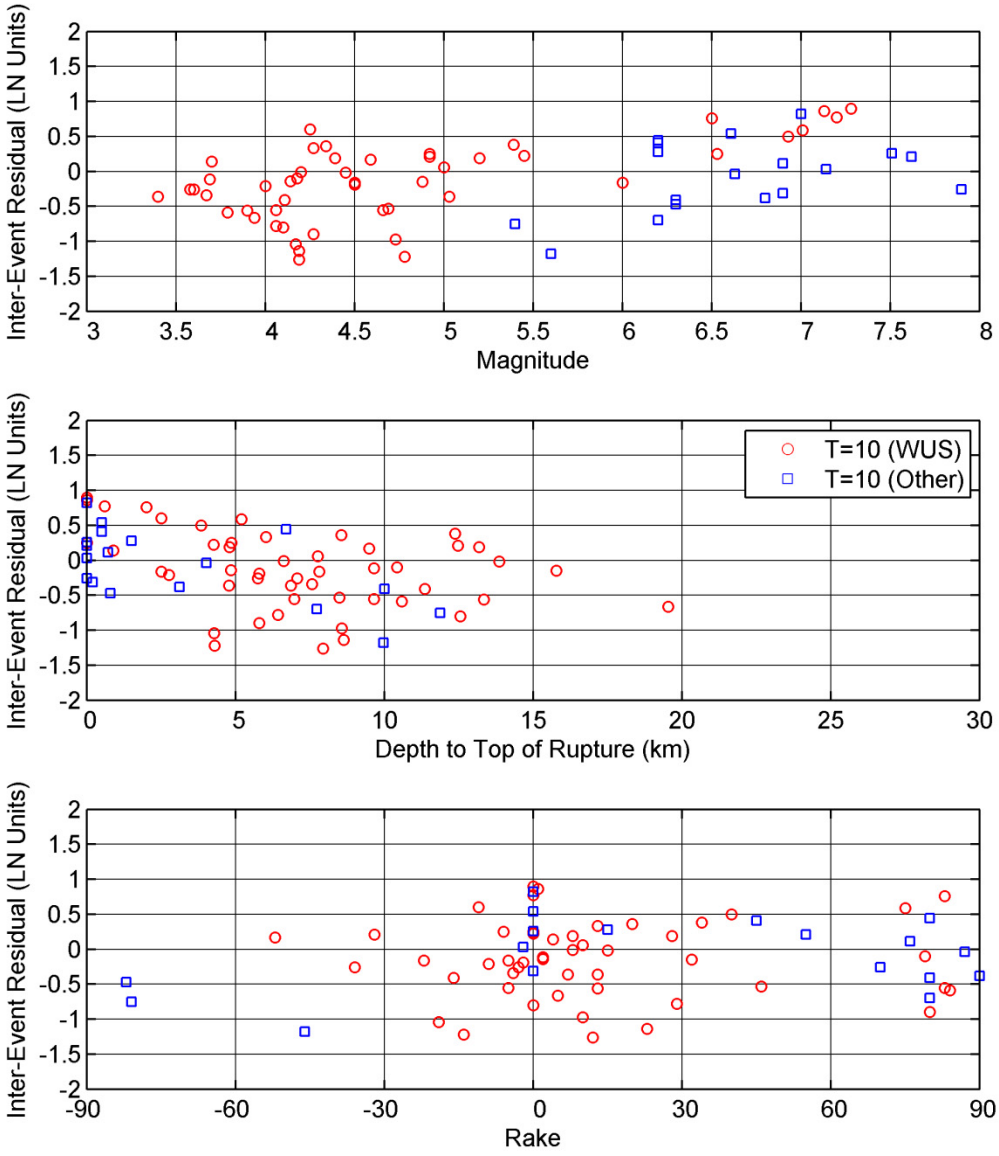

Figure 6.1(g) Event terms for *T*= 10 sec.

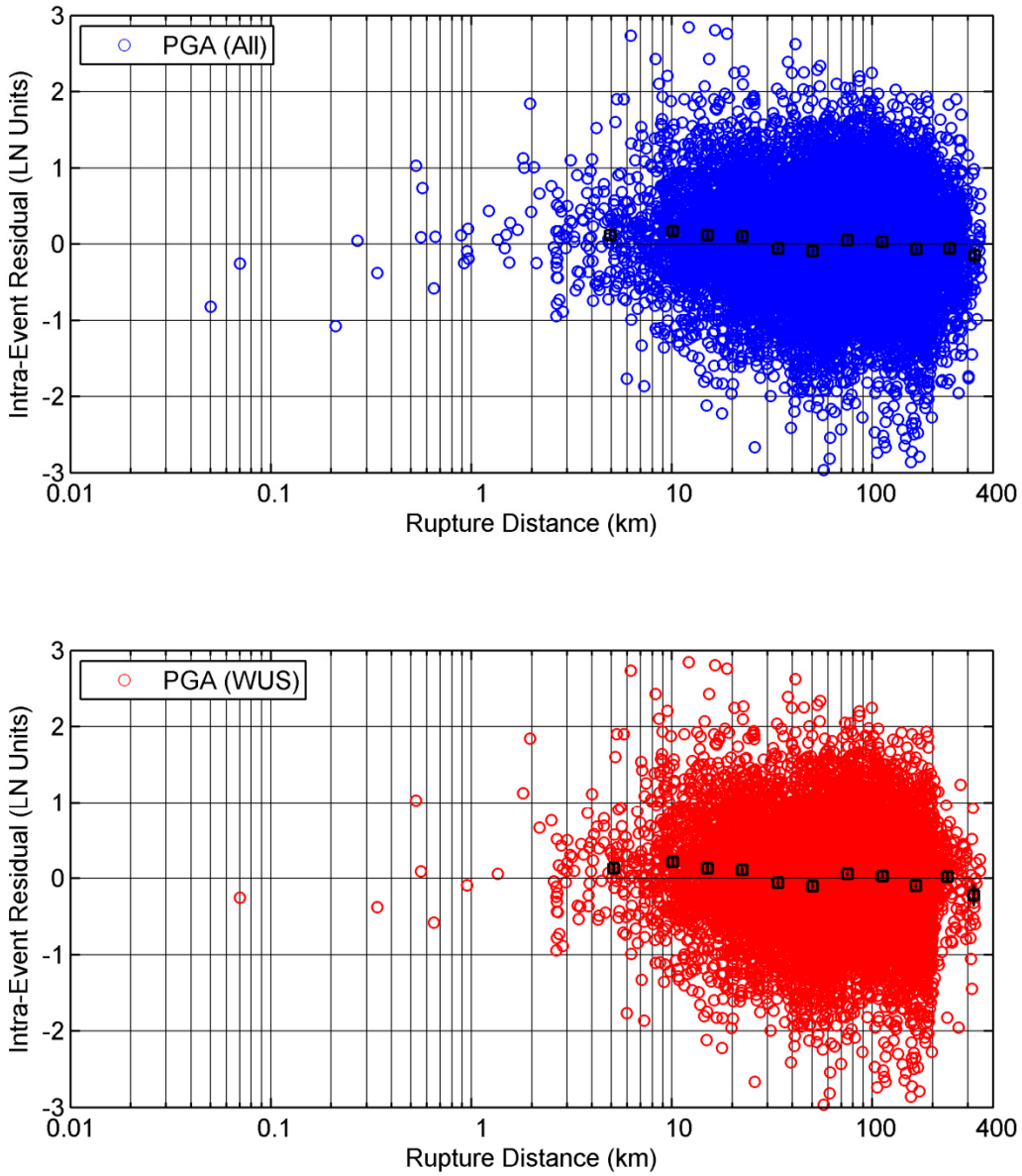

Figure 6.2(a) Distance dependence of the intra-event residuals, all regions and WUS, PGA.

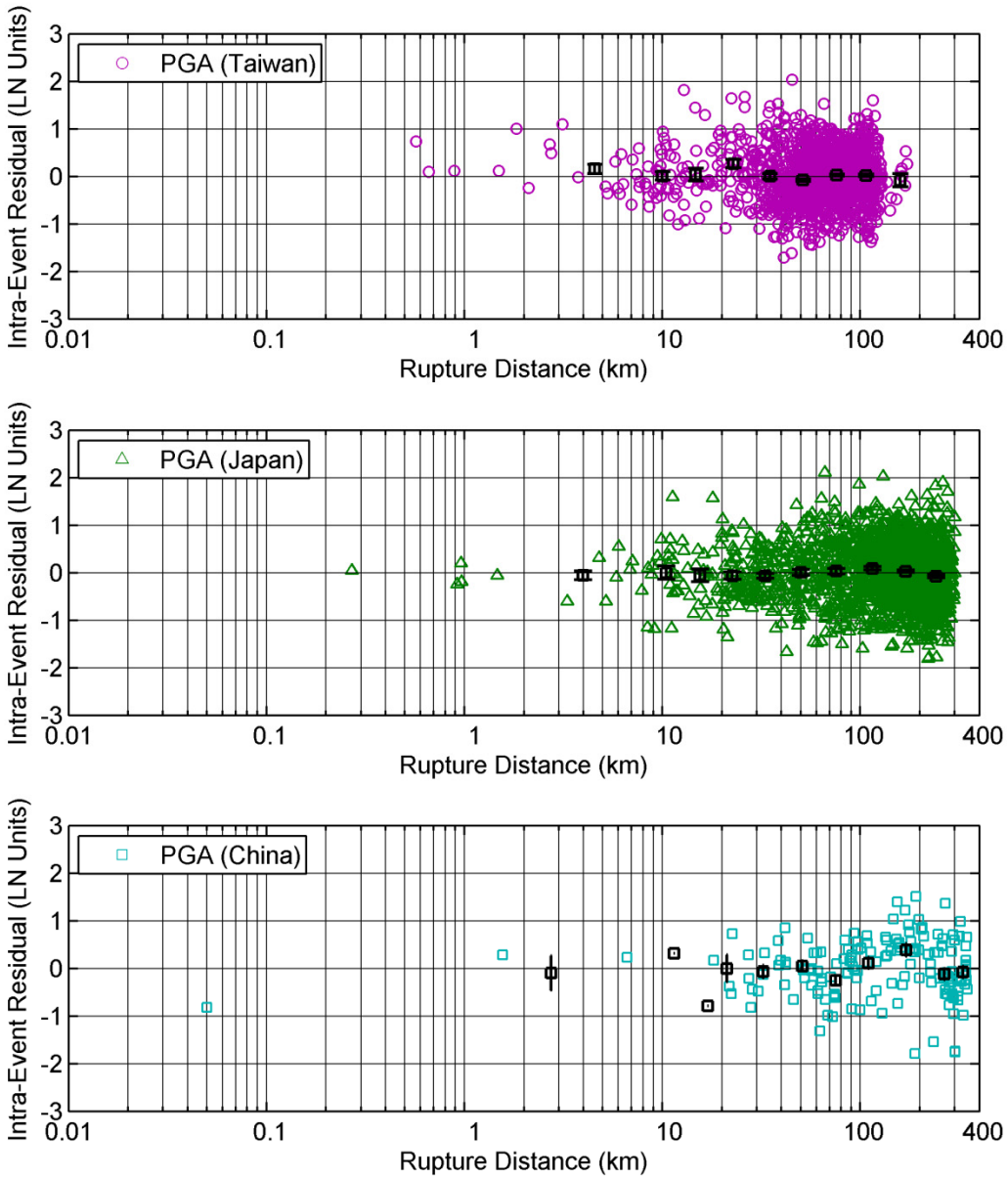

Figure 6.2(b) Distance dependence of the intra-event residuals, Taiwan, Japan, and China, PGA.

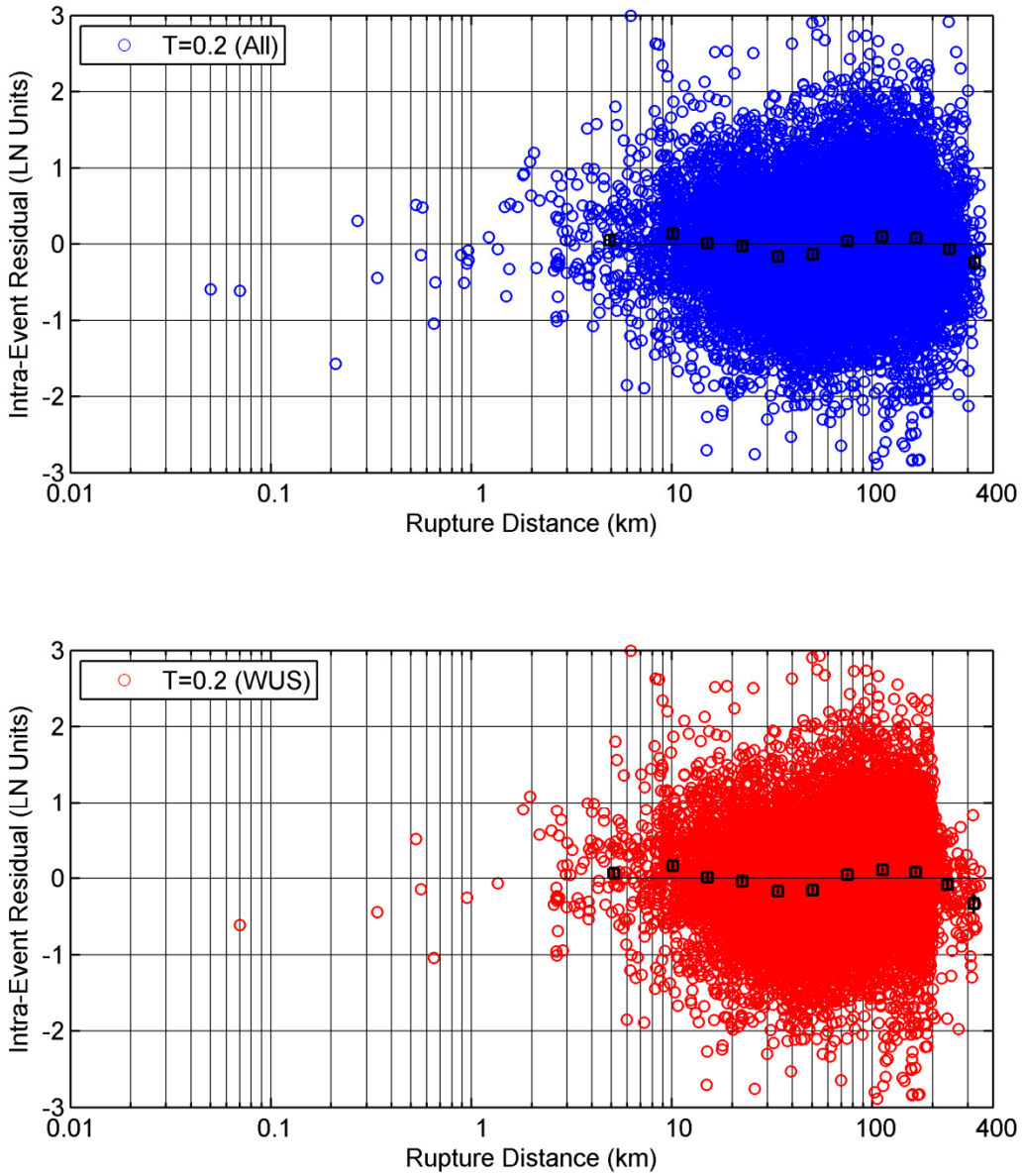

Figure 6.2(c) Distance dependence of the intra-event residuals, all regions and WUS, *T*= 0.2 sec.

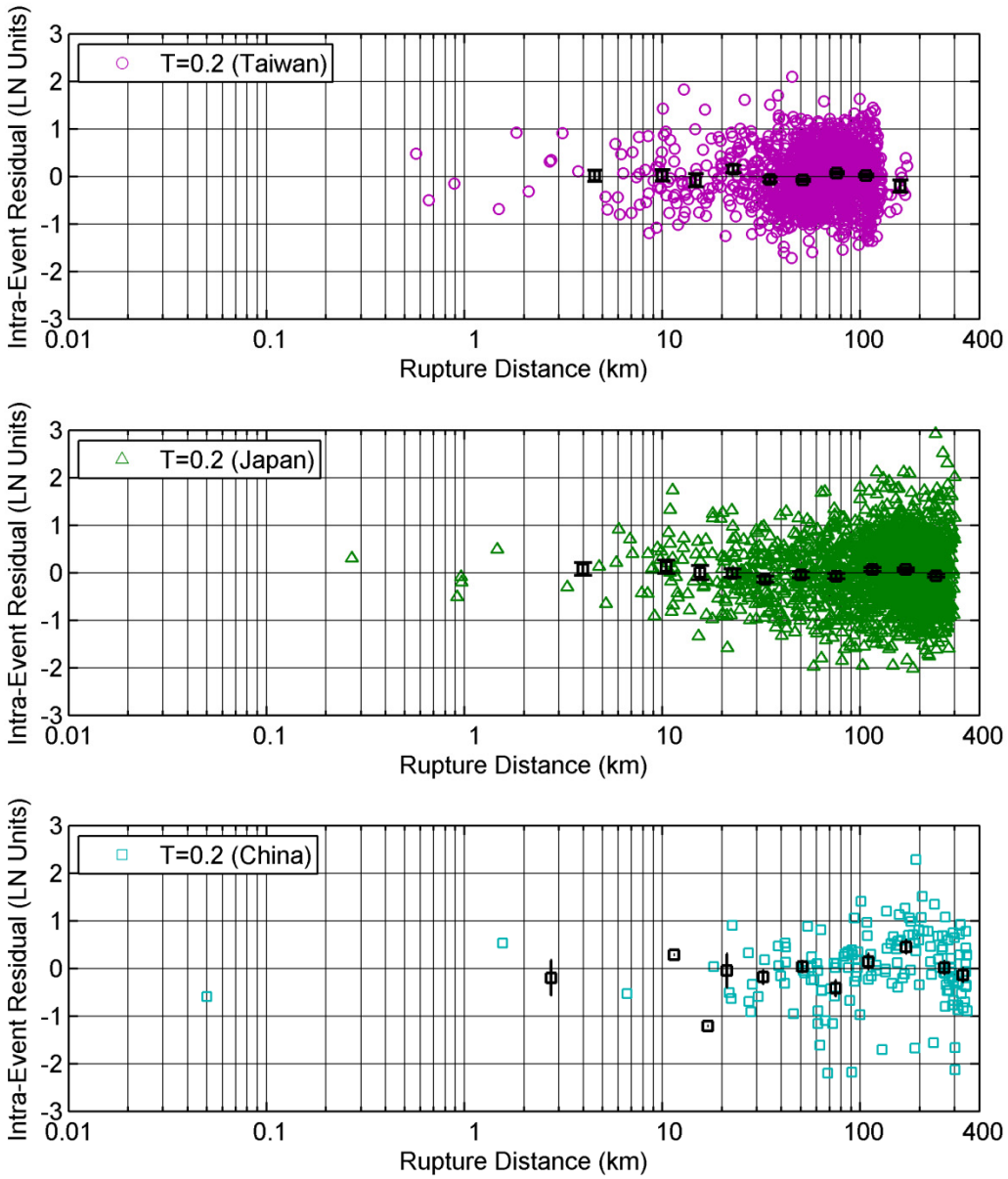

Figure 6.2(d) Distance dependence of the intra-event residuals, Taiwan, Japan and China, T = 0.2 sec

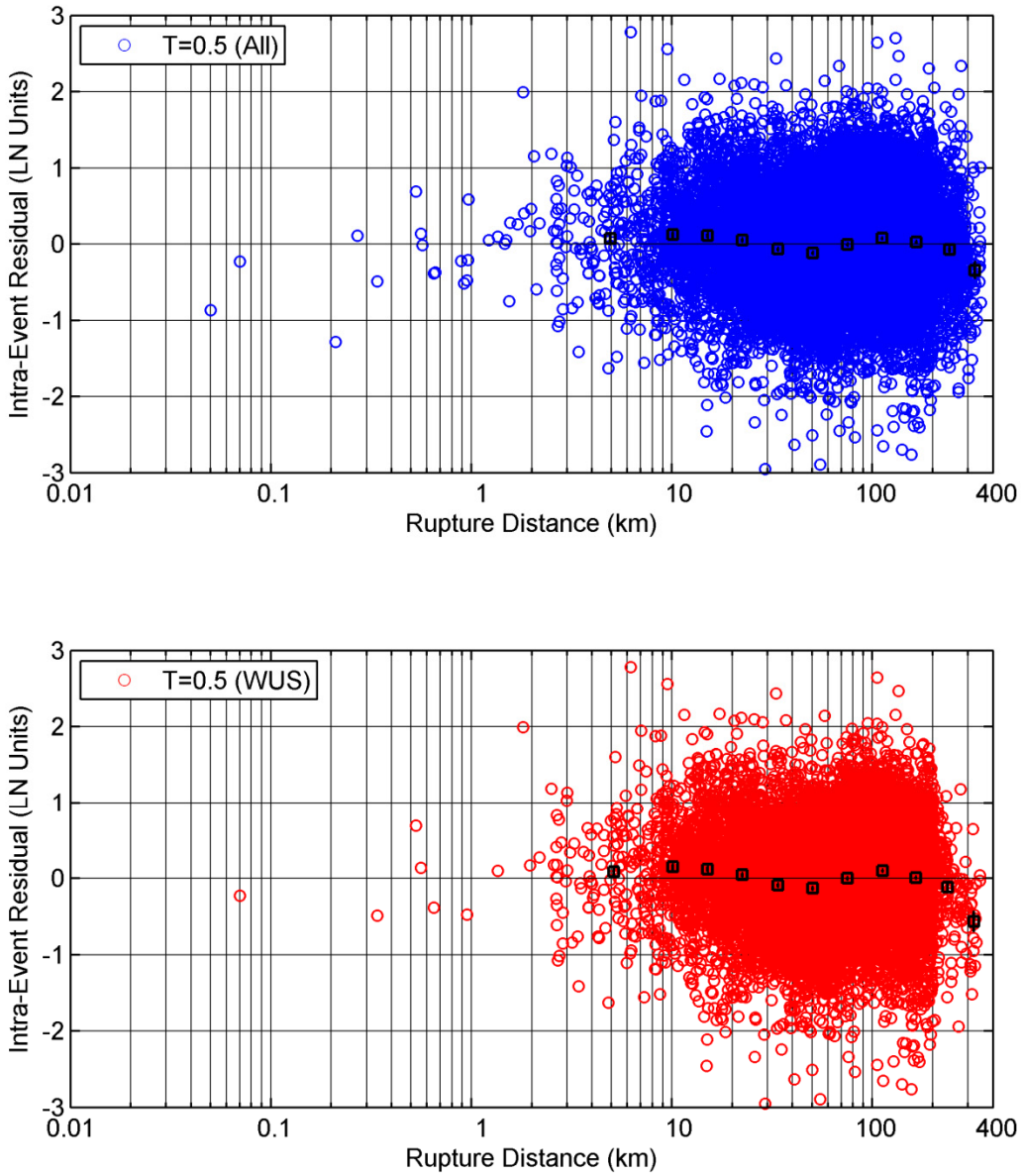

Figure 6.2(e) Distance dependence of the intra-event residuals, all regions and WUS, *T* = 0.5 sec.

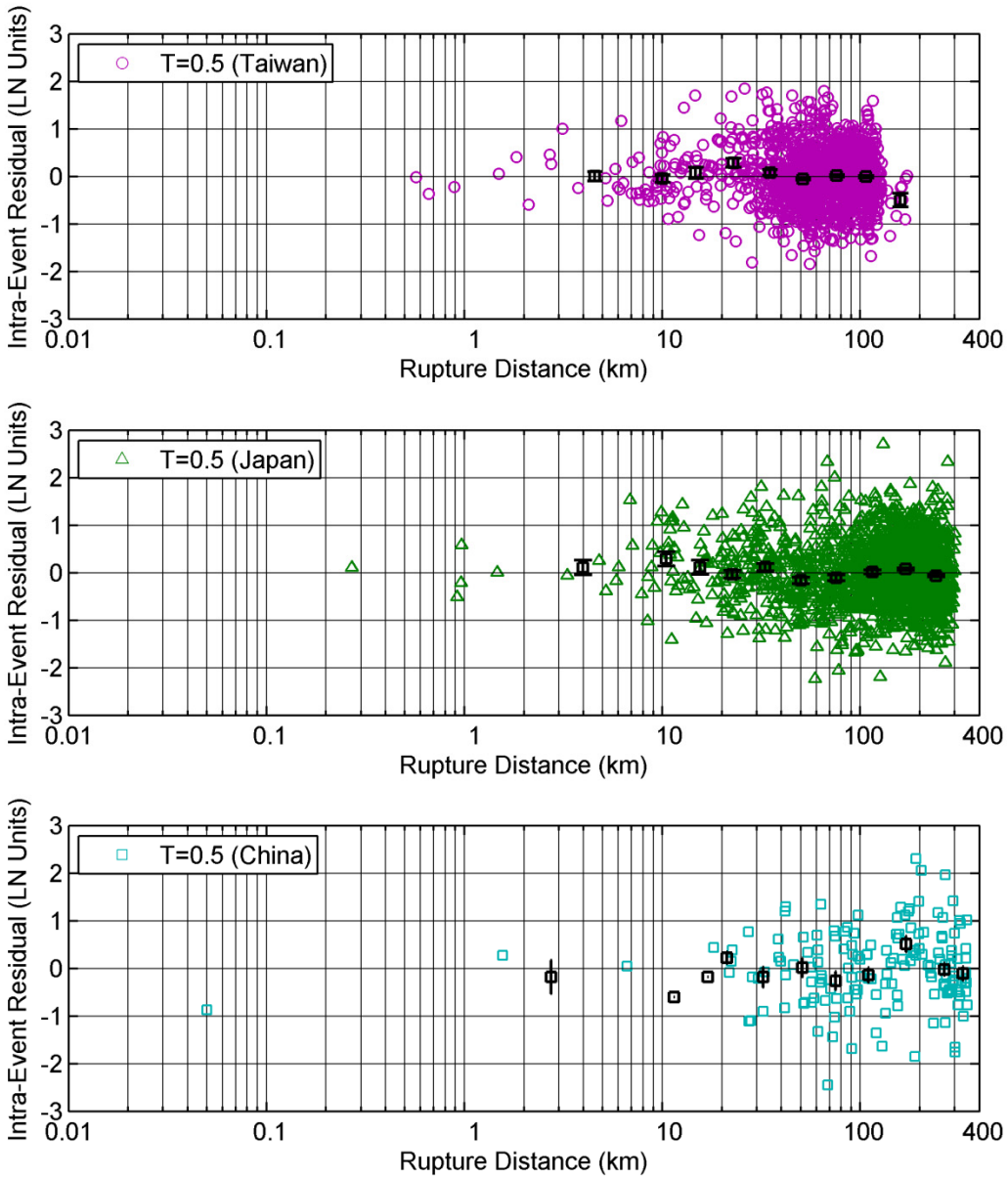

Figure 6.2(f) Distance dependence of the intra-event residuals, Taiwan, Japan, and China, T = 0.5 sec.

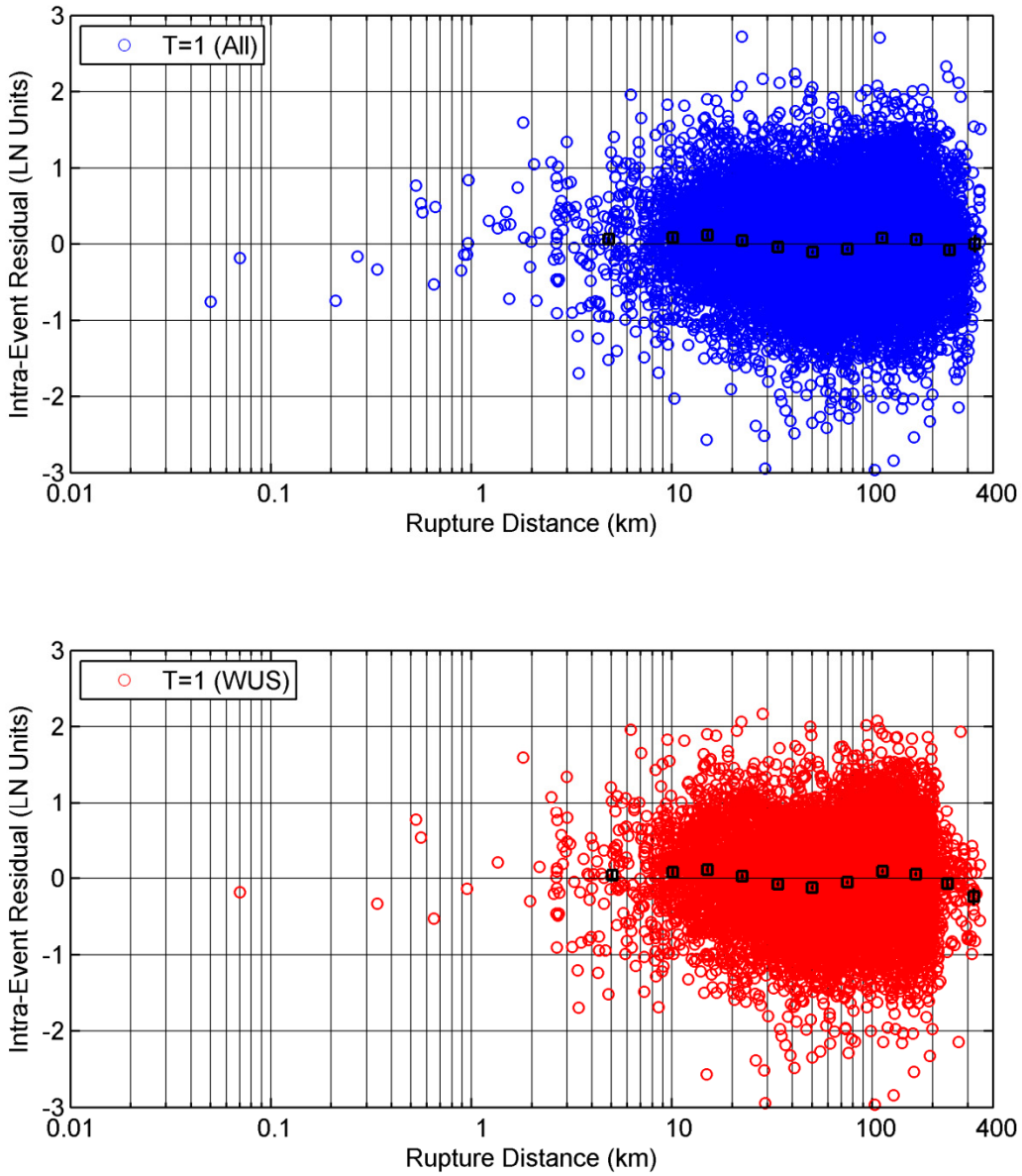

Figure 6.2(g) Distance dependence of the intra-event residuals, all regions and WUS, *T* = 1 sec.

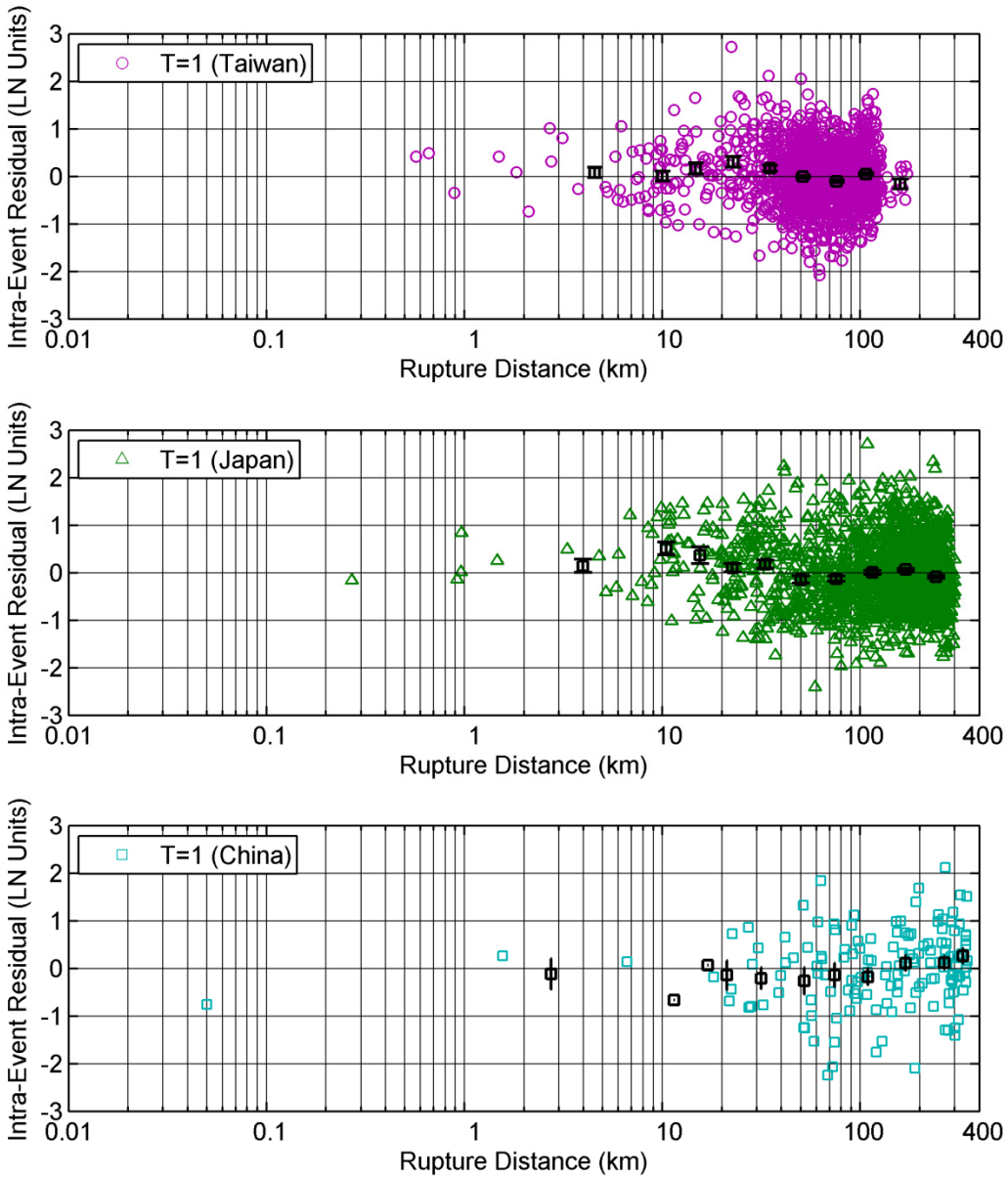

Figure 6.2(h) Distance dependence of the intra-event residuals, Taiwan, Japan, and China, T = 1 sec.

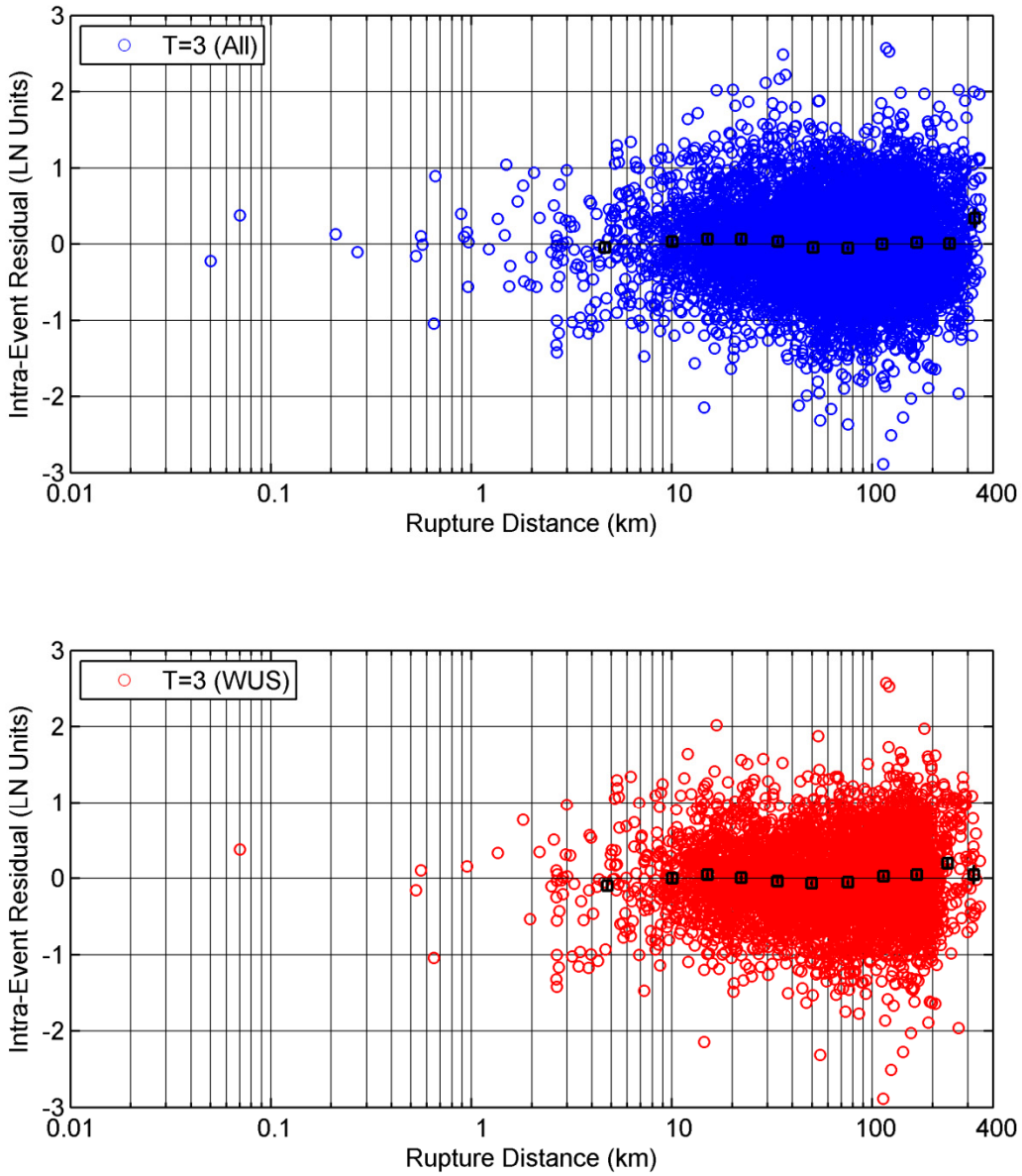

Figure 6.2(i) **Distance dependence of the intra-event residuals, all regions and WUS, *T* = 3 sec.**

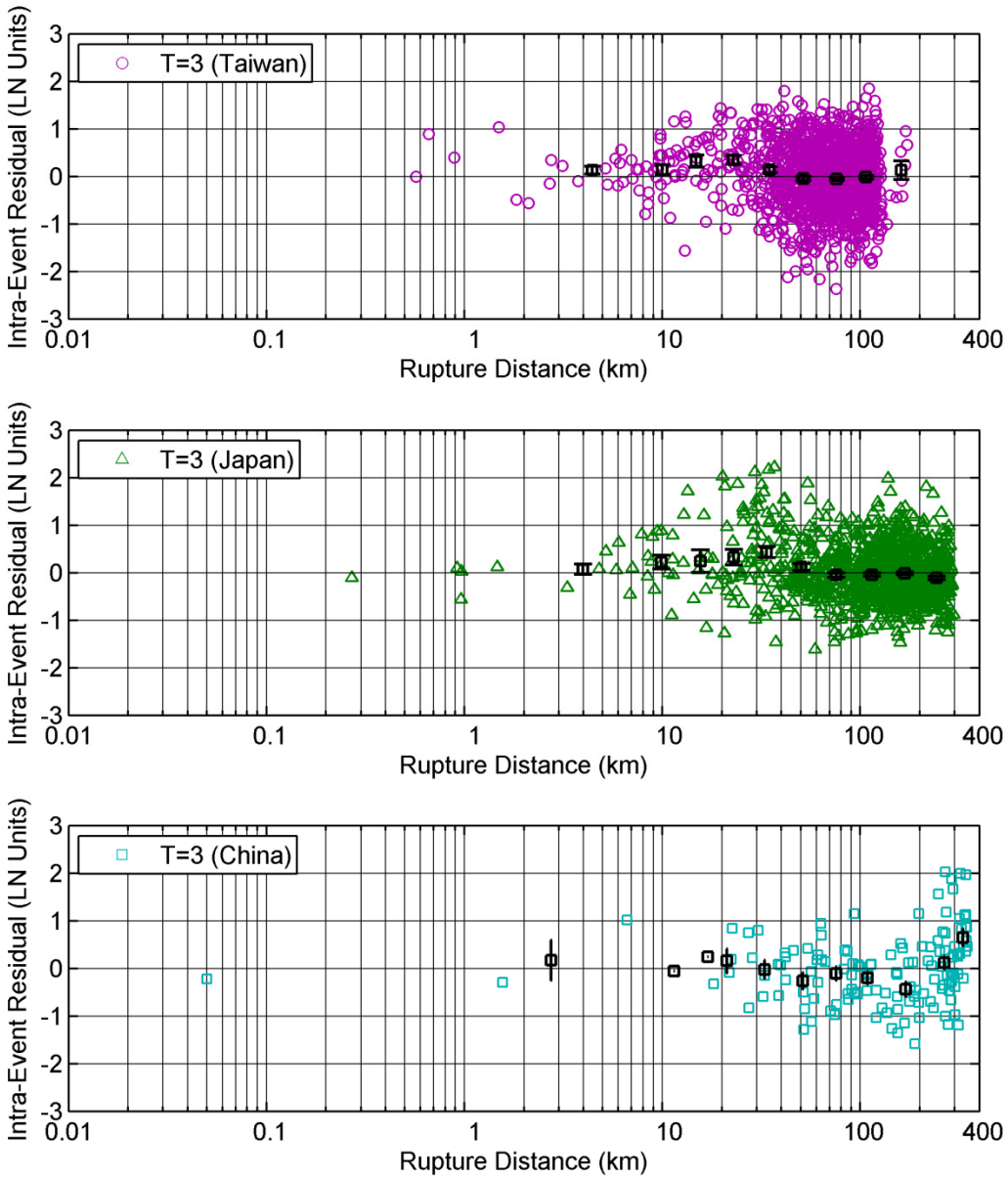

Figure 6.2(j) **Distance dependence of the intra-event residuals, Taiwan, Japan, and China, T = 3 sec.**

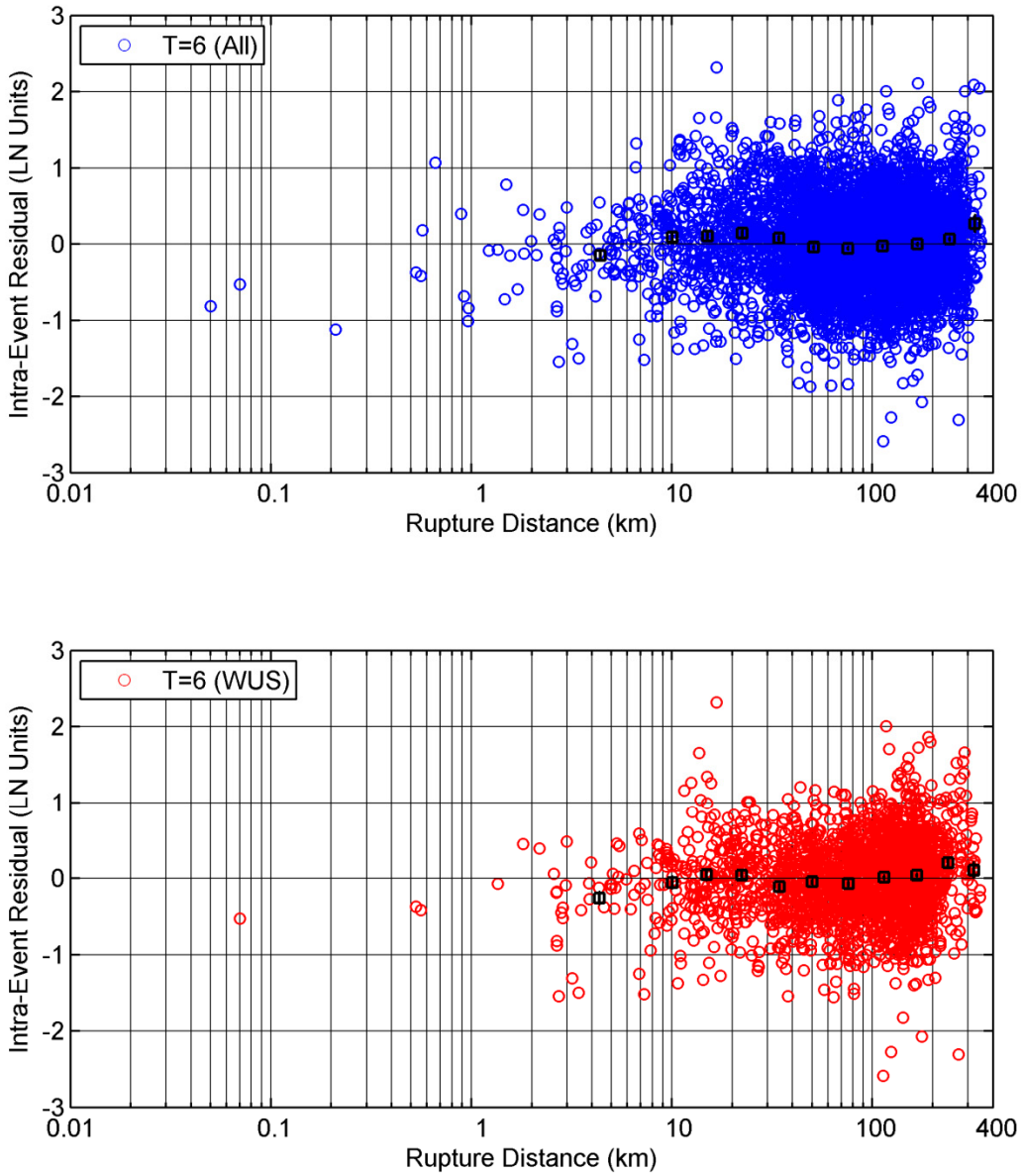

Figure 6.2(k) Distance dependence of the intra-event residuals, all regions and WUS, *T*= 6 sec.

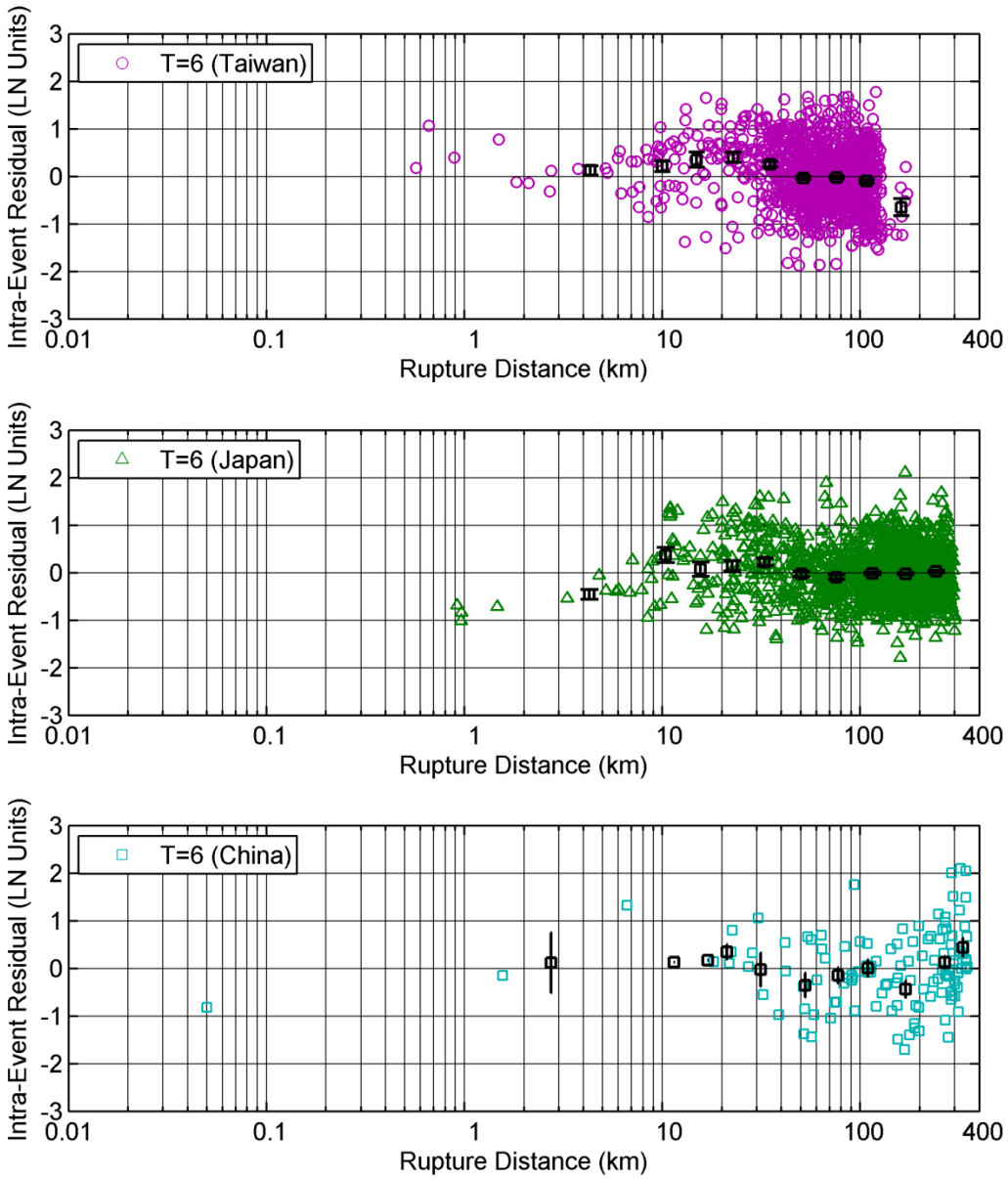

Figure 6.2(l) Distance dependence of the intra-event residuals, Taiwan, Japan, and China, T = 6 sec.

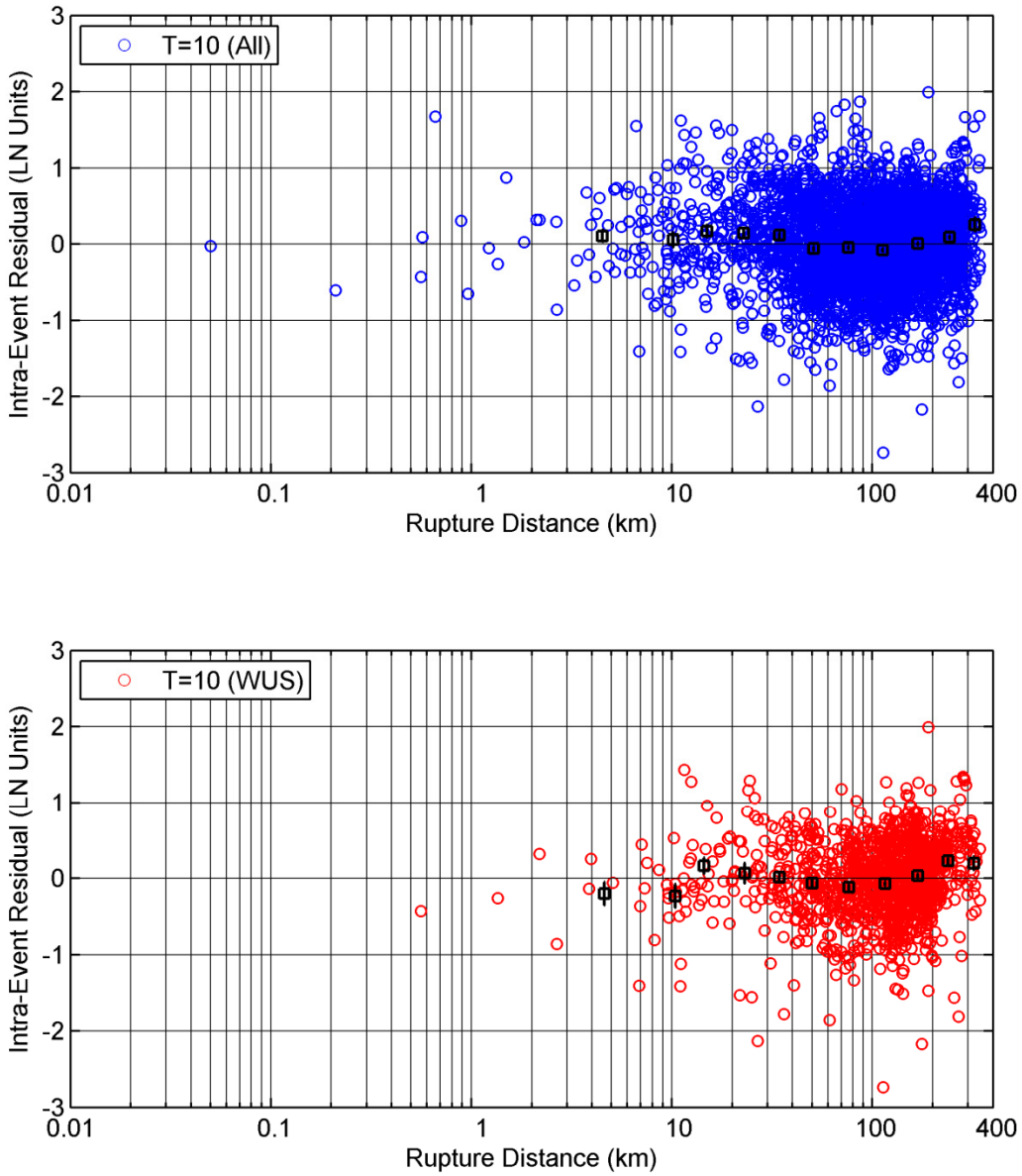

Figure 6.2(m) Distance dependence of the intra-event residuals, all regions and WUS, *T* = 10 sec.

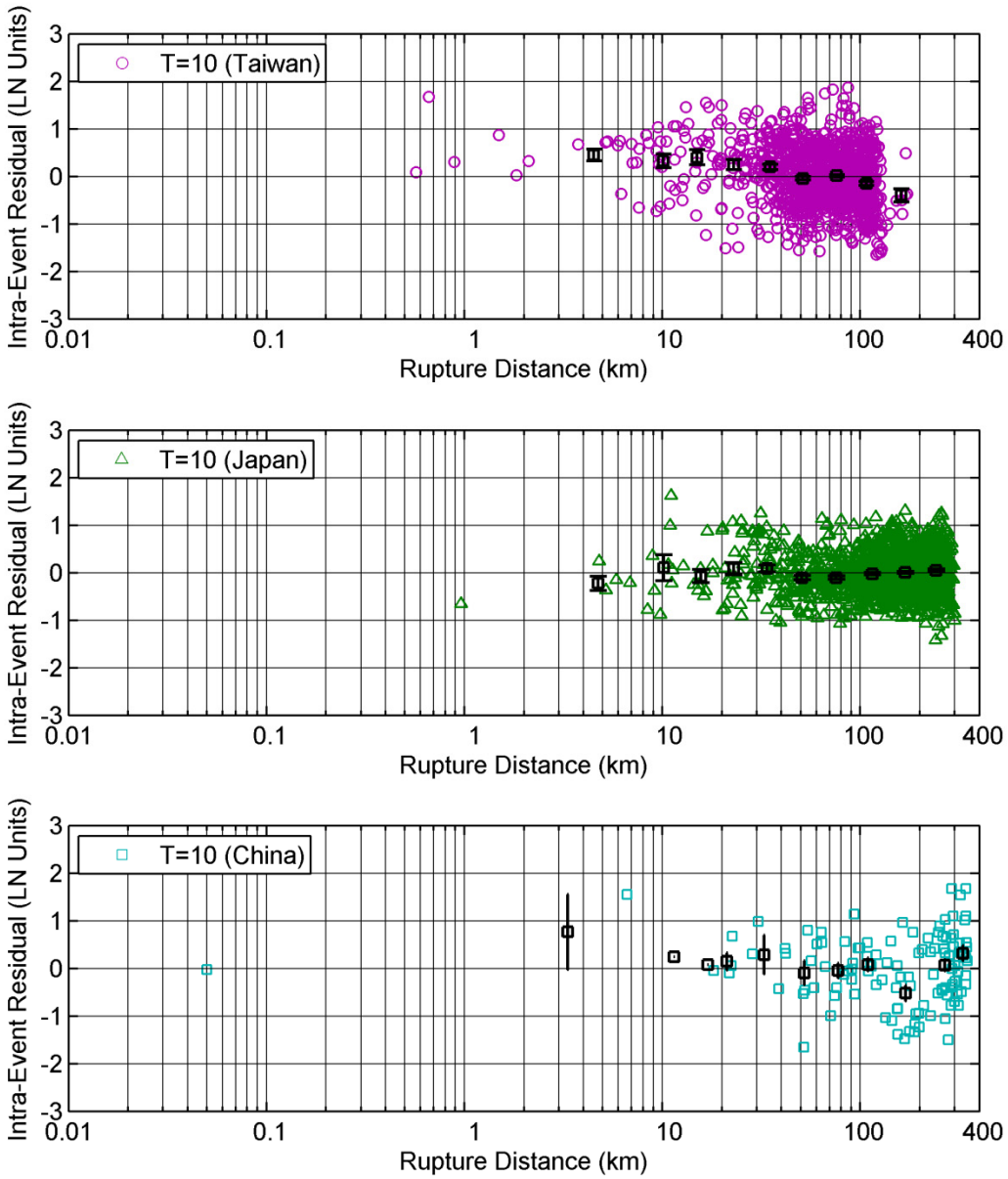

Figure 6.2(n) Distance dependence of the intra-event residuals, Taiwan, Japan, and China, T = 10 sec.

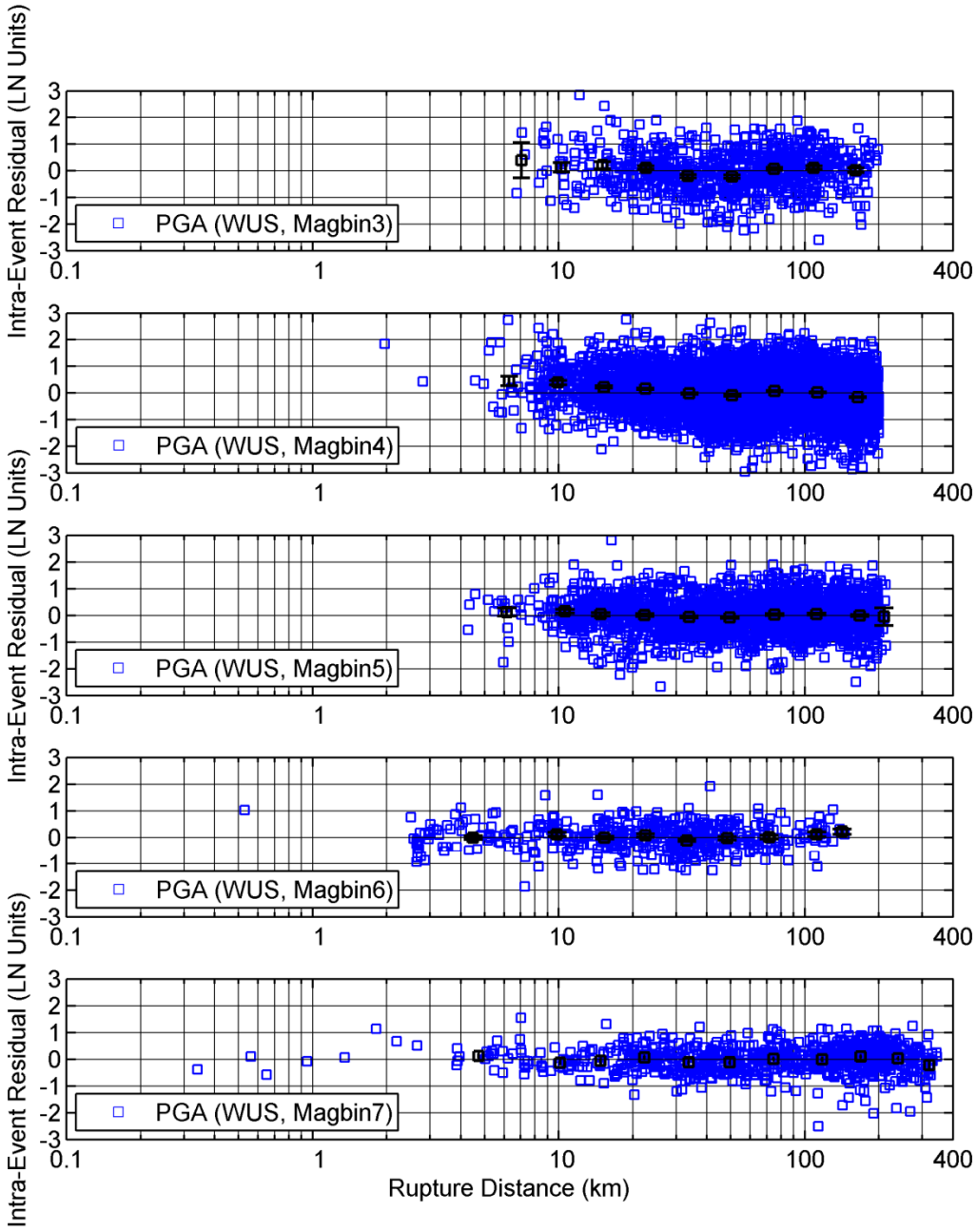

Figure 6.3(a) Distance dependence of the intra-event residuals, WUS only, by Magnitude bins, PGA.

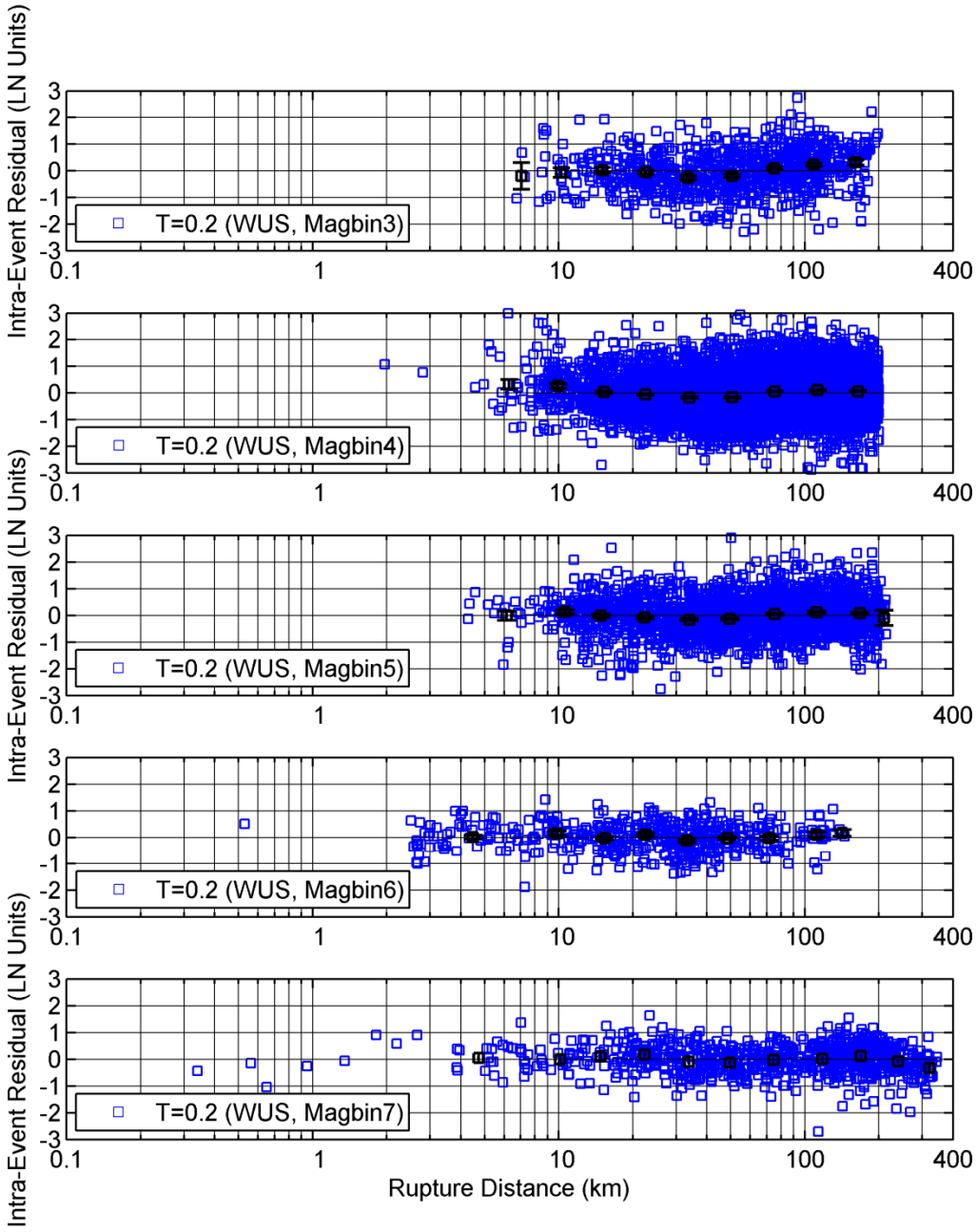

Figure 6.3(b) Distance dependence of the intra-event residuals, WUS only, by Magnitude bins, T = 0.2 sec.

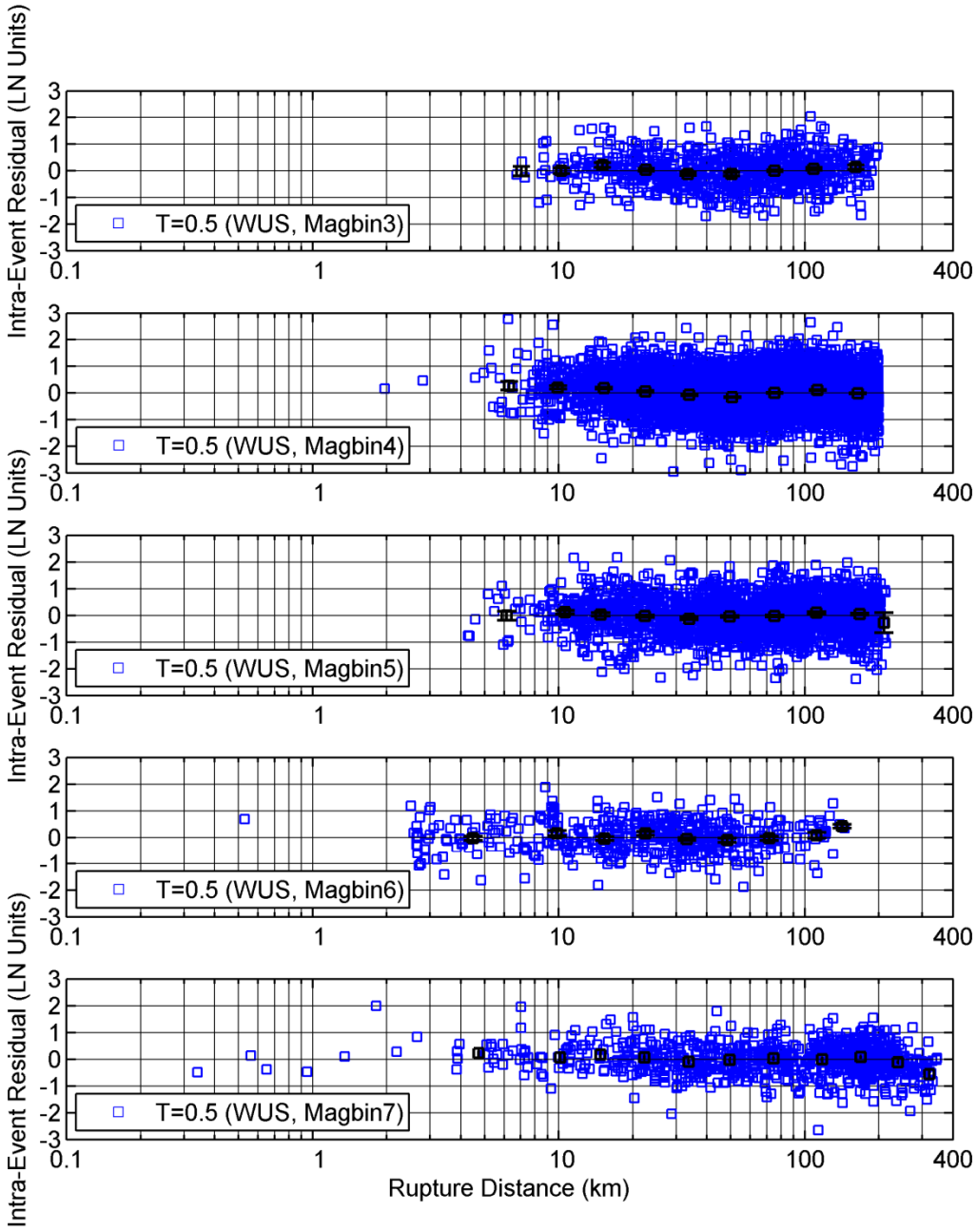

Figure 6.3(c) Distance dependence of the intra-event residuals, WUS only, by magnitude bins, T = 0.5 sec.

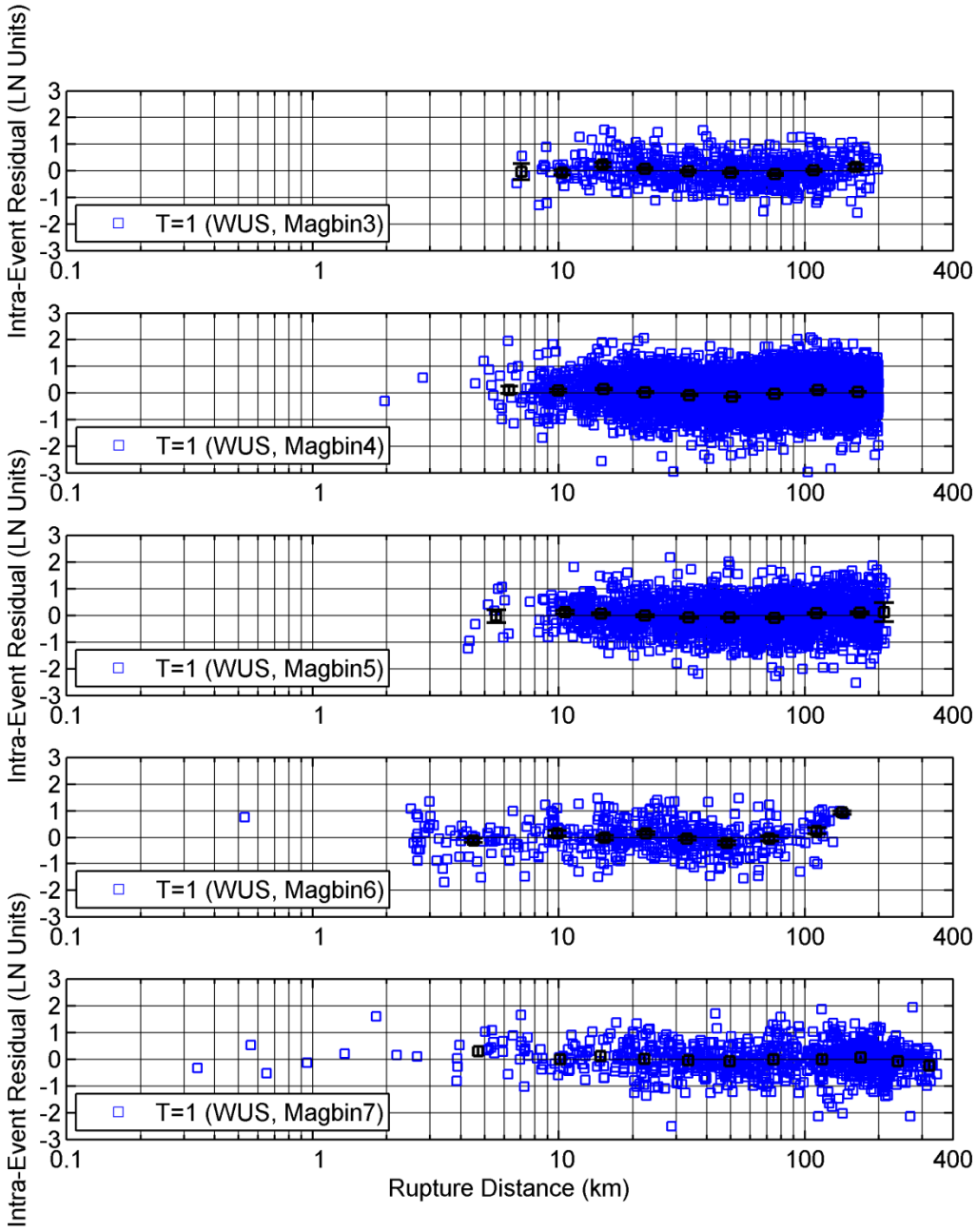

Figure 6.3(d) Distance dependence of the intra-event residuals, WUS only, by magnitude bins, T = 1.0 sec.

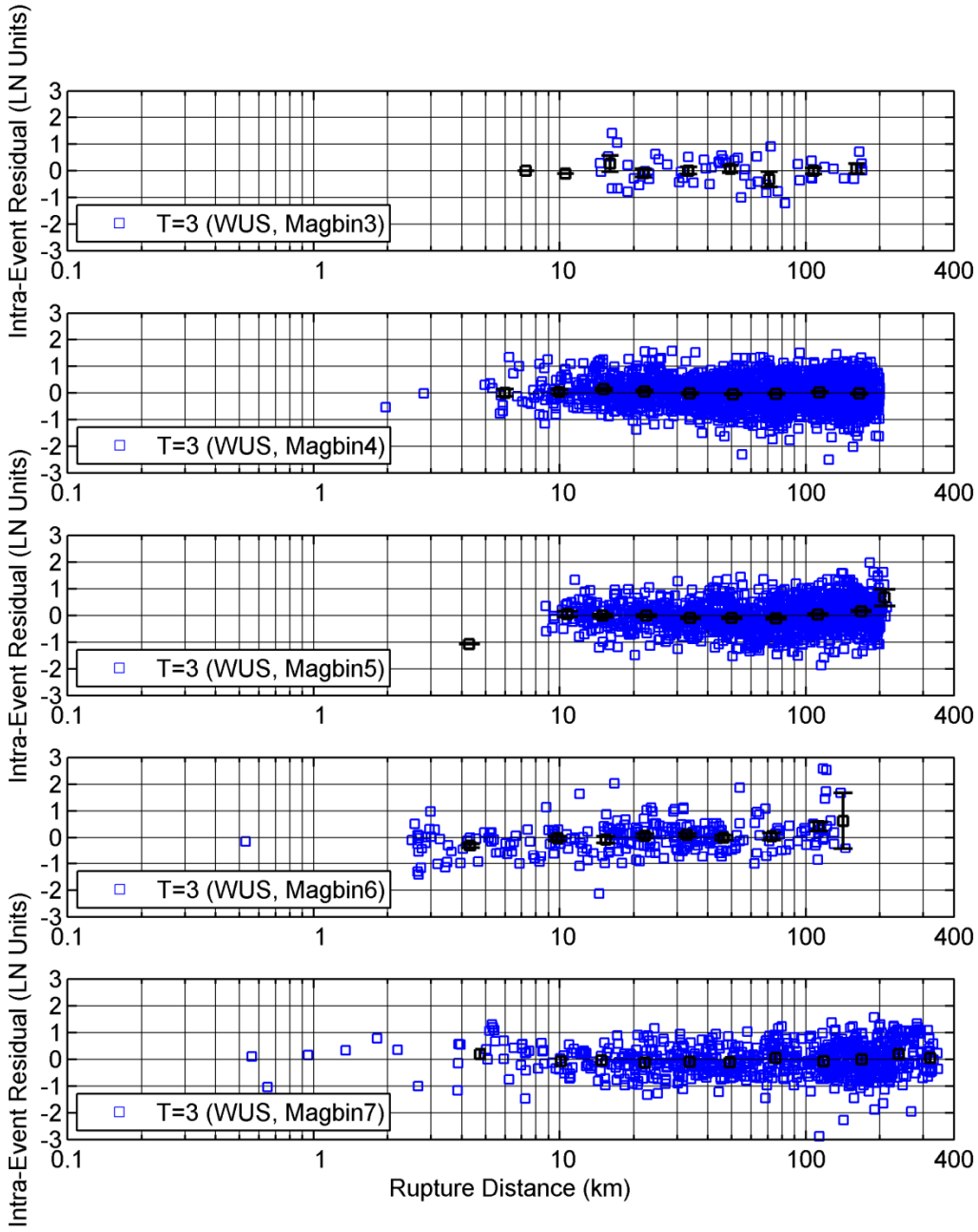

Figure 6.3(e) Distance dependence of the intra-event residuals, WUS only, by magnitude bins, T = 3 sec.

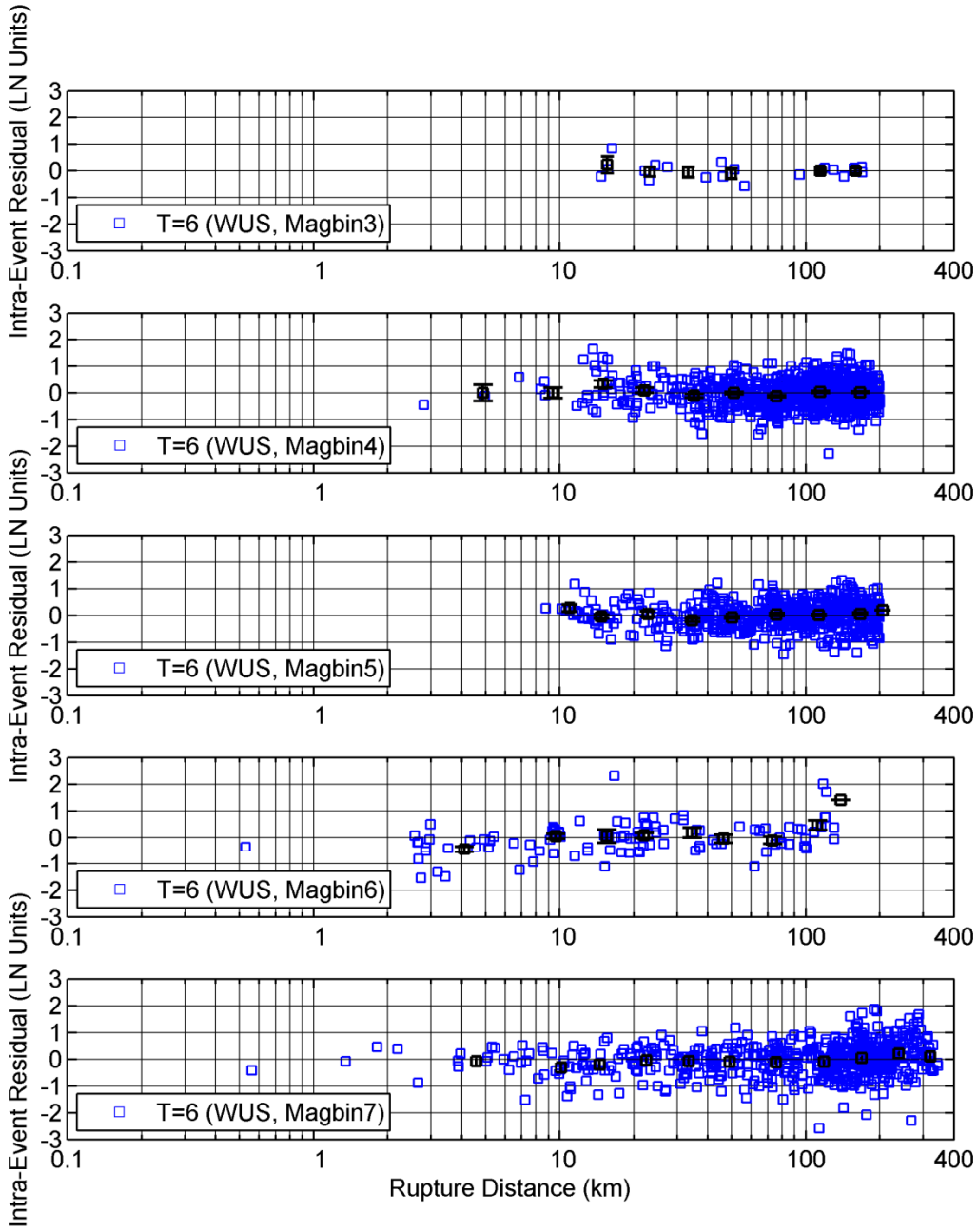

Figure 6.3(f) Distance dependence of the intra-event residuals, WUS only, by magnitude bins, T = 6 sec.

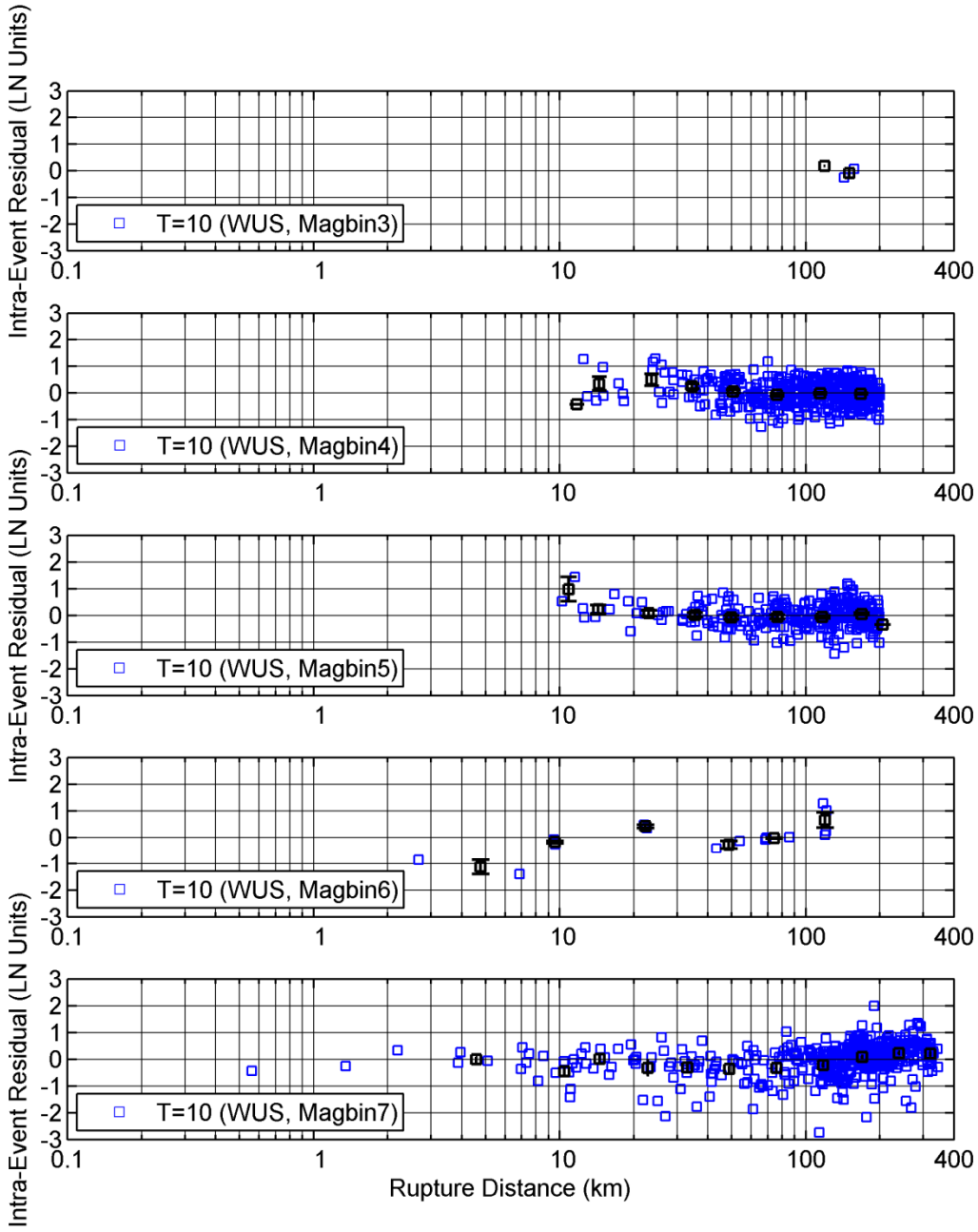

Figure 6.3(g) Distance dependence of the intra-event residuals, WUS only, by magnitude bins, T=10 sec.

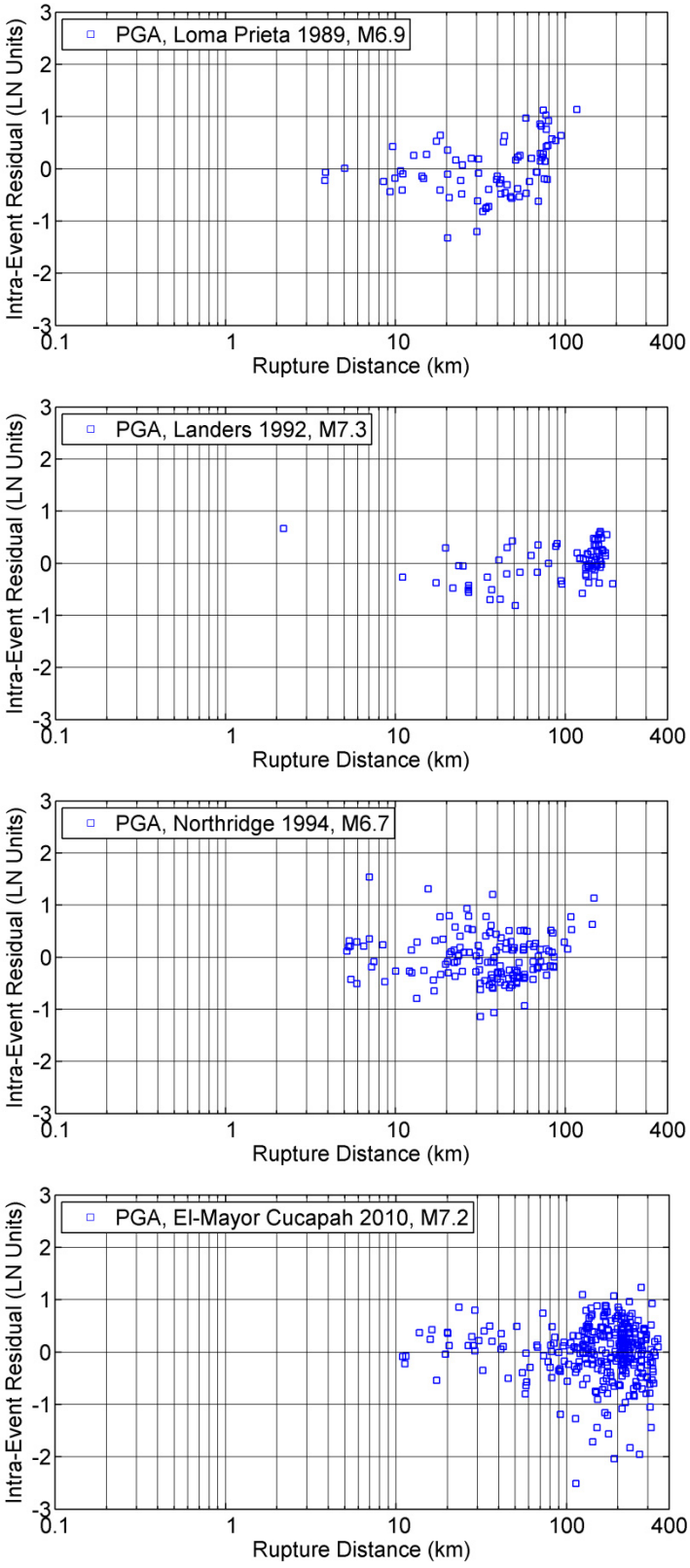

Figure 6.4(a) Distance dependence of the intra-event residuals for four WUS events, PGA.

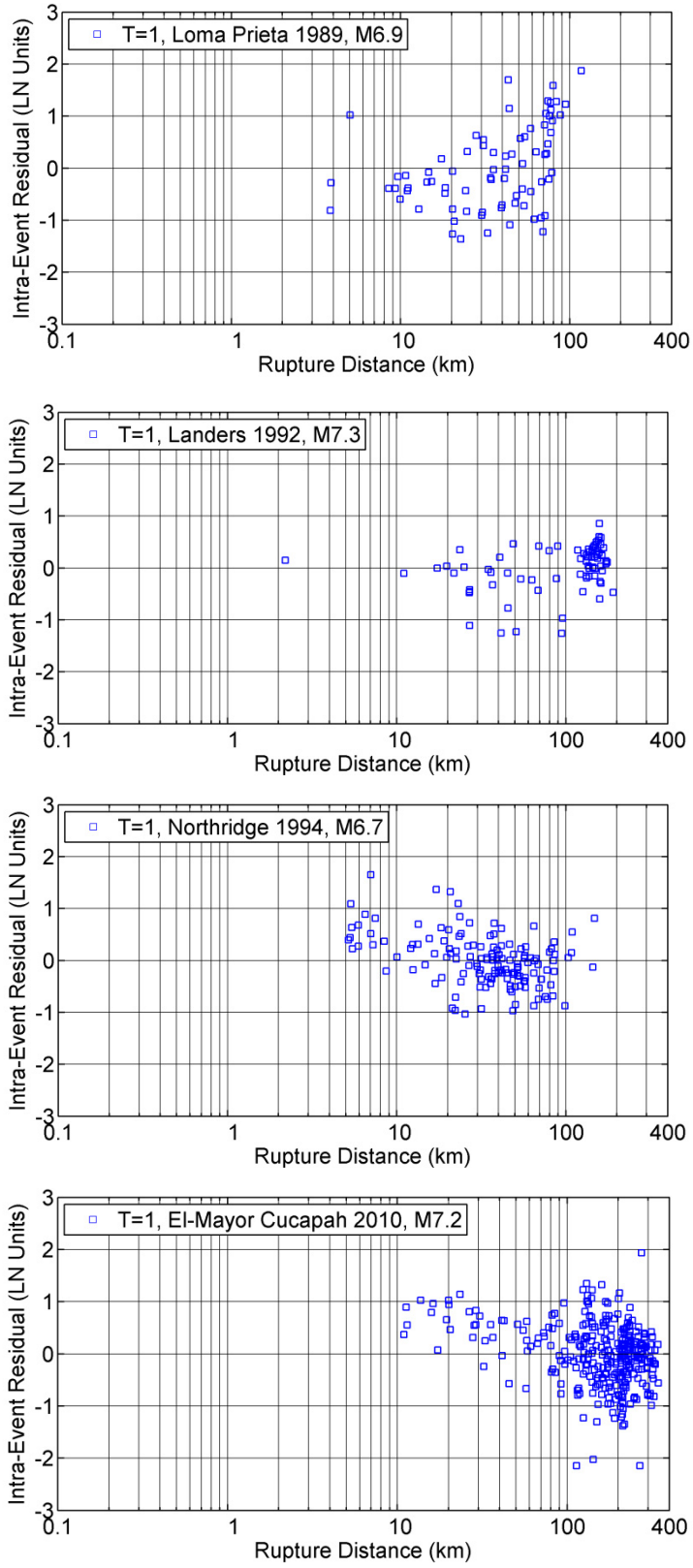

Figure 6.4(b) Distance dependence of the intra-event residuals for four WUS events, T=1.0 sec.

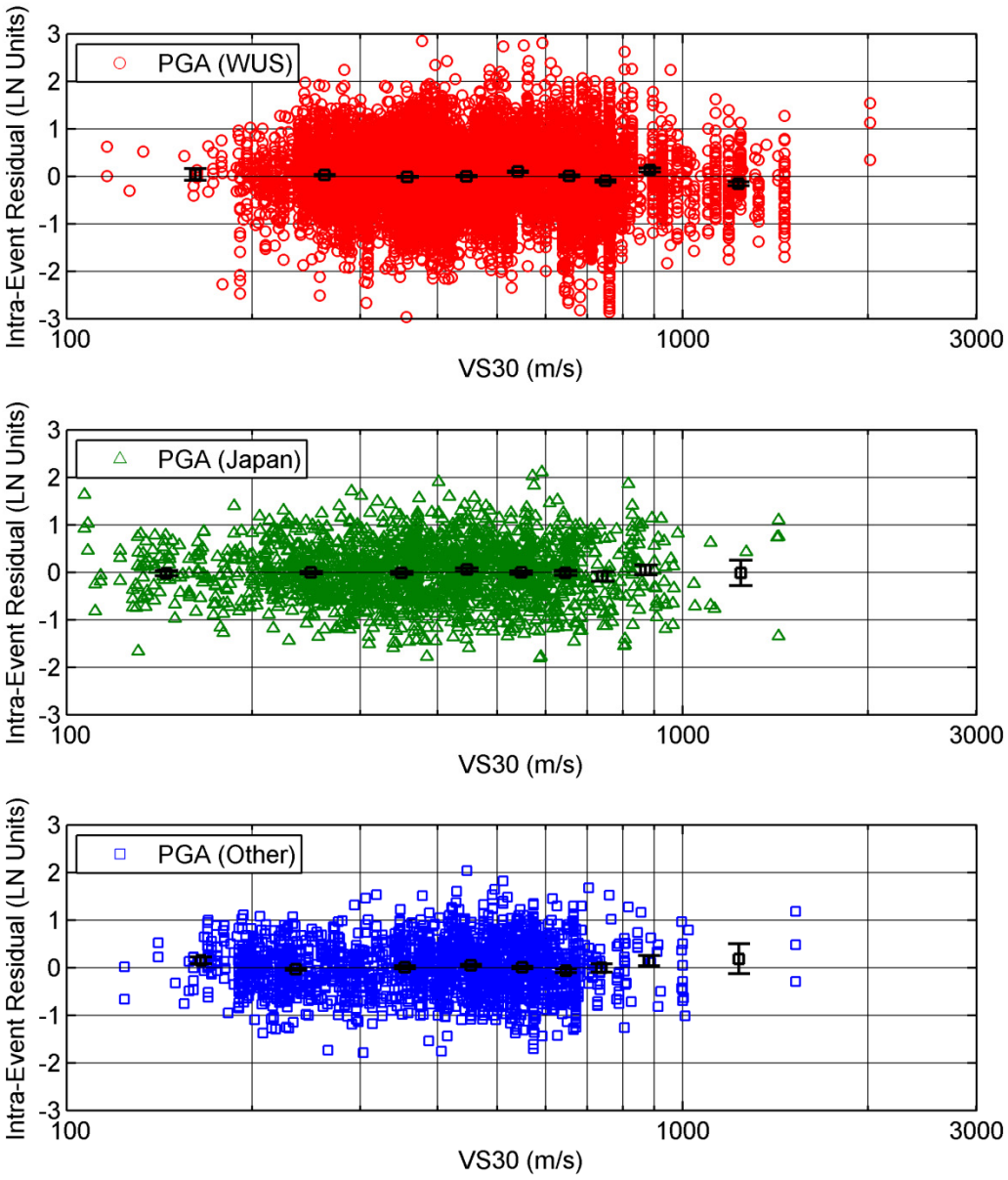

Figure 6.5(a) V_{s30} **dependence of the intra-event residuals, PGA.**

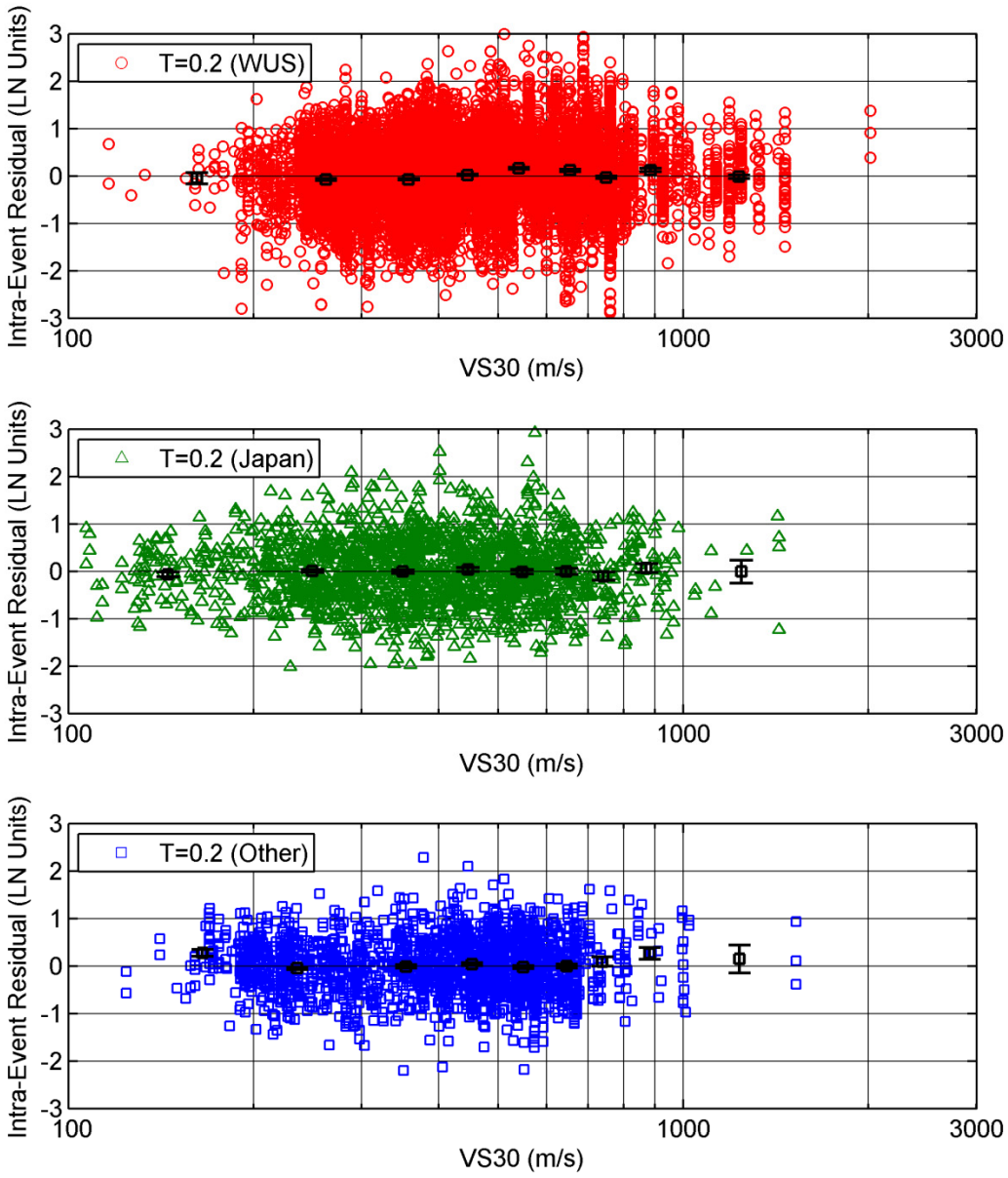

Figure 6.5(b) V_{s30} **dependence of the intra-event residuals, T = 0.2 sec.**

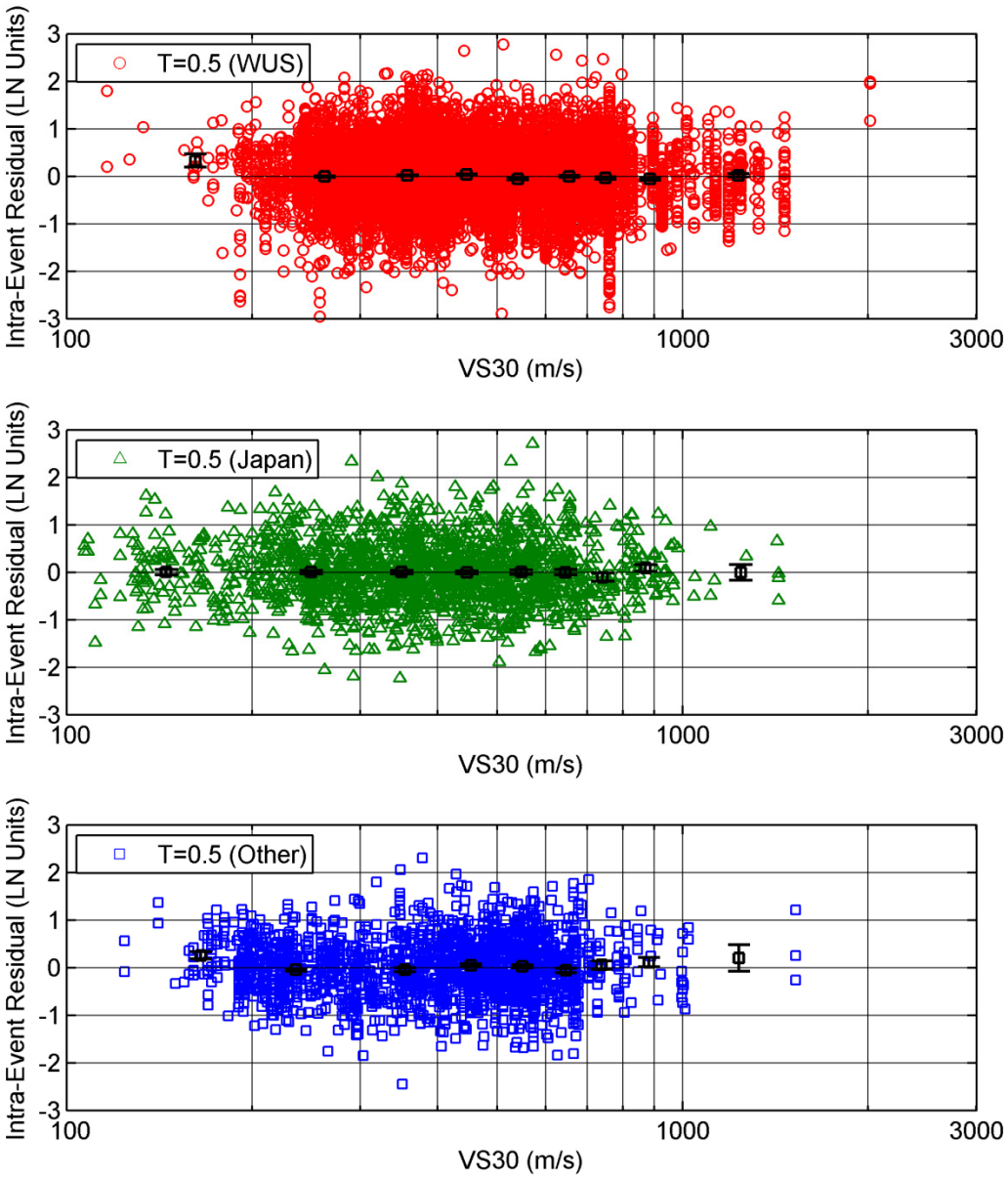

Figure 6.5(c) V_{s30} **dependence of the intra-event residuals,** T **= 0.5 sec.**

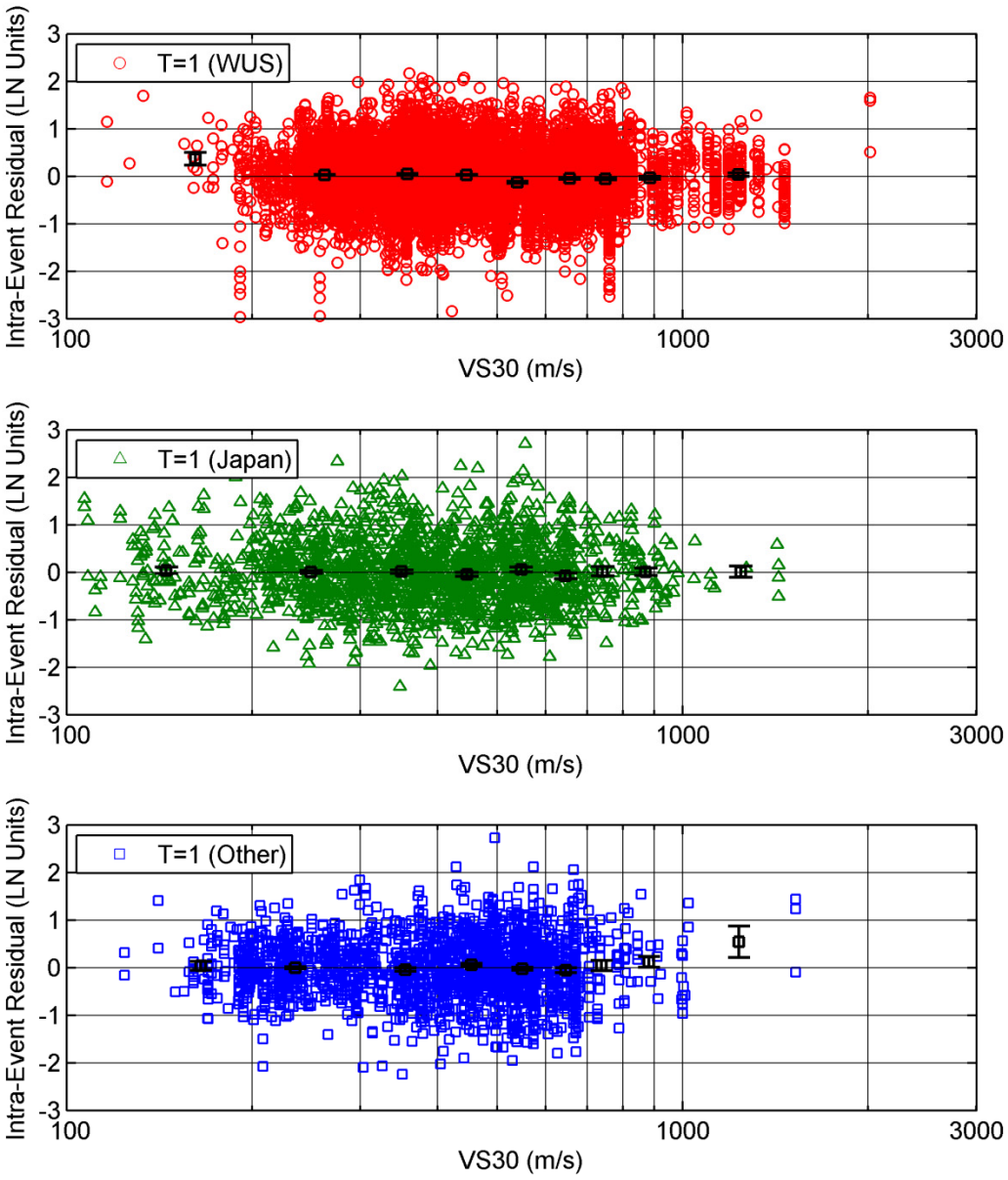

Figure 6.5(d) V_{s30} **dependence of the intra-event residuals,** T **= 1.0 sec.**

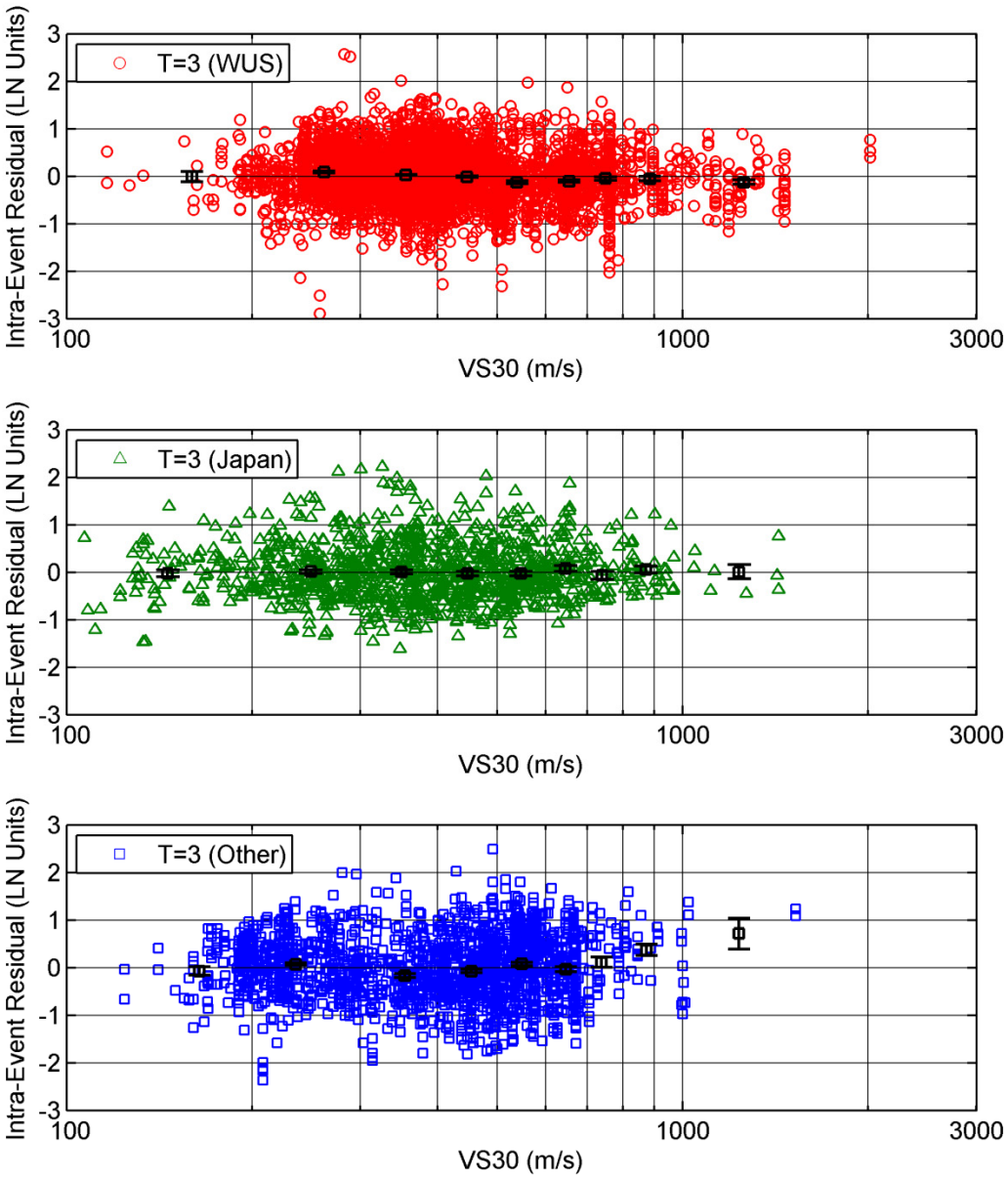

Figure 6.5e) V_{s30} **dependence of the intra-event residuals,** T **= 3 sec.**

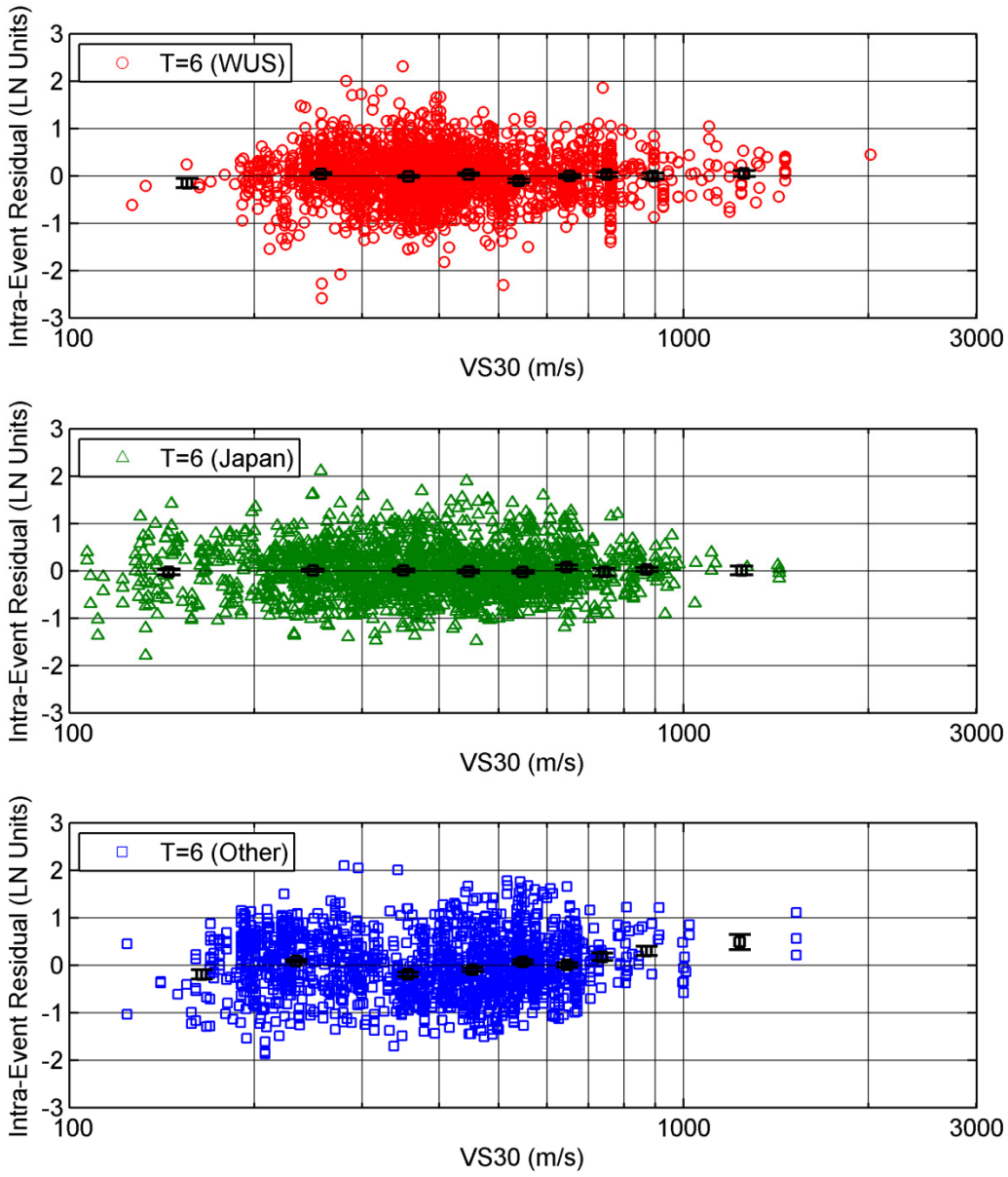

Figure 6.5(f) V_{s30} **dependence of the intra-event residuals, T = 6 sec.**

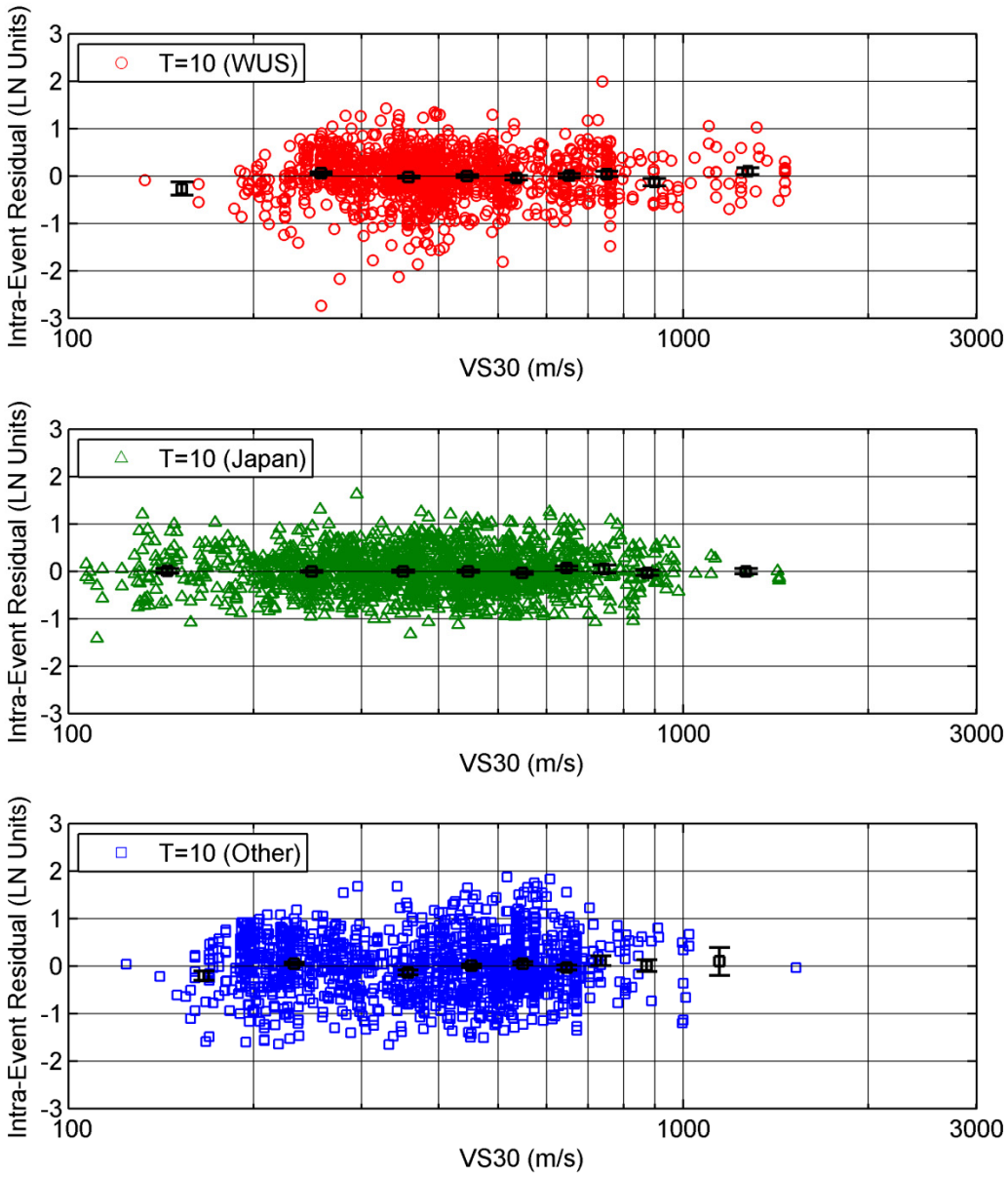

Figure 6.5(g) ***Vs30*** **dependence of the intra-event residuals,** ***T*** **=10 sec.**

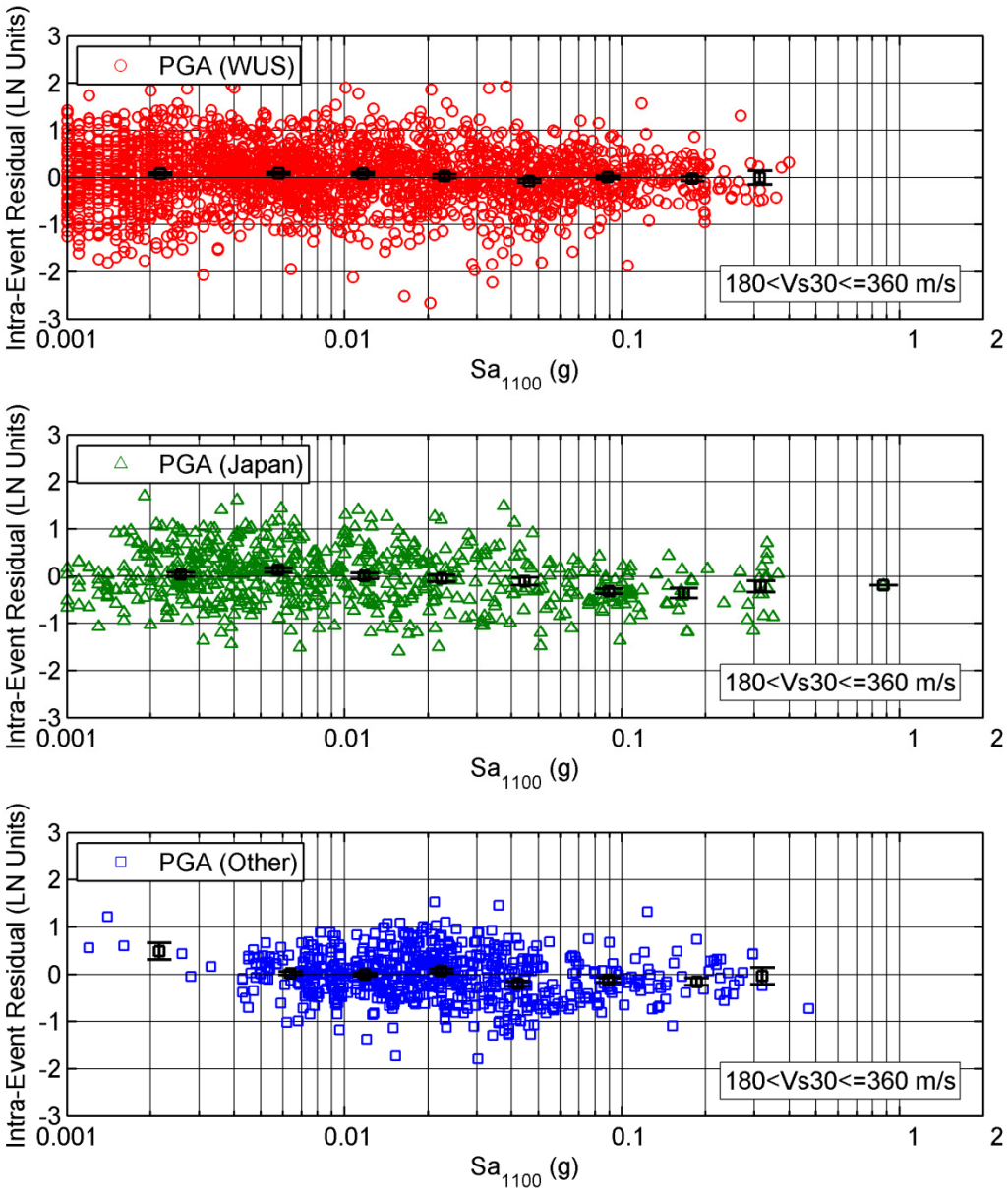

Figure 6.6(a) Sa_{1100} dependence of the Intra-event residuals for PGA.

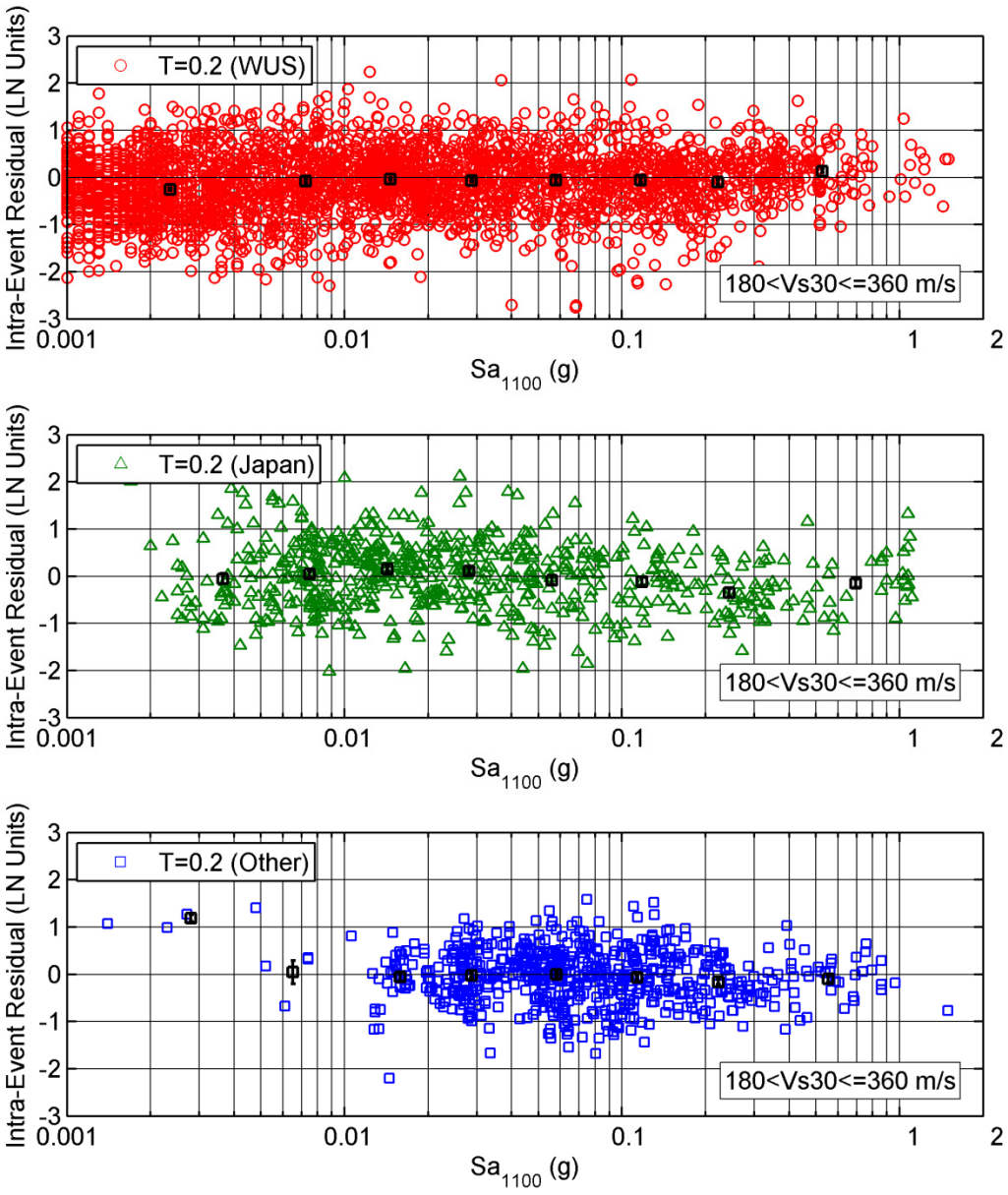

Figure 6.6(b) Sa_{1100} **dependence of the Intra-event residuals for** T **= 0.2 sec.**

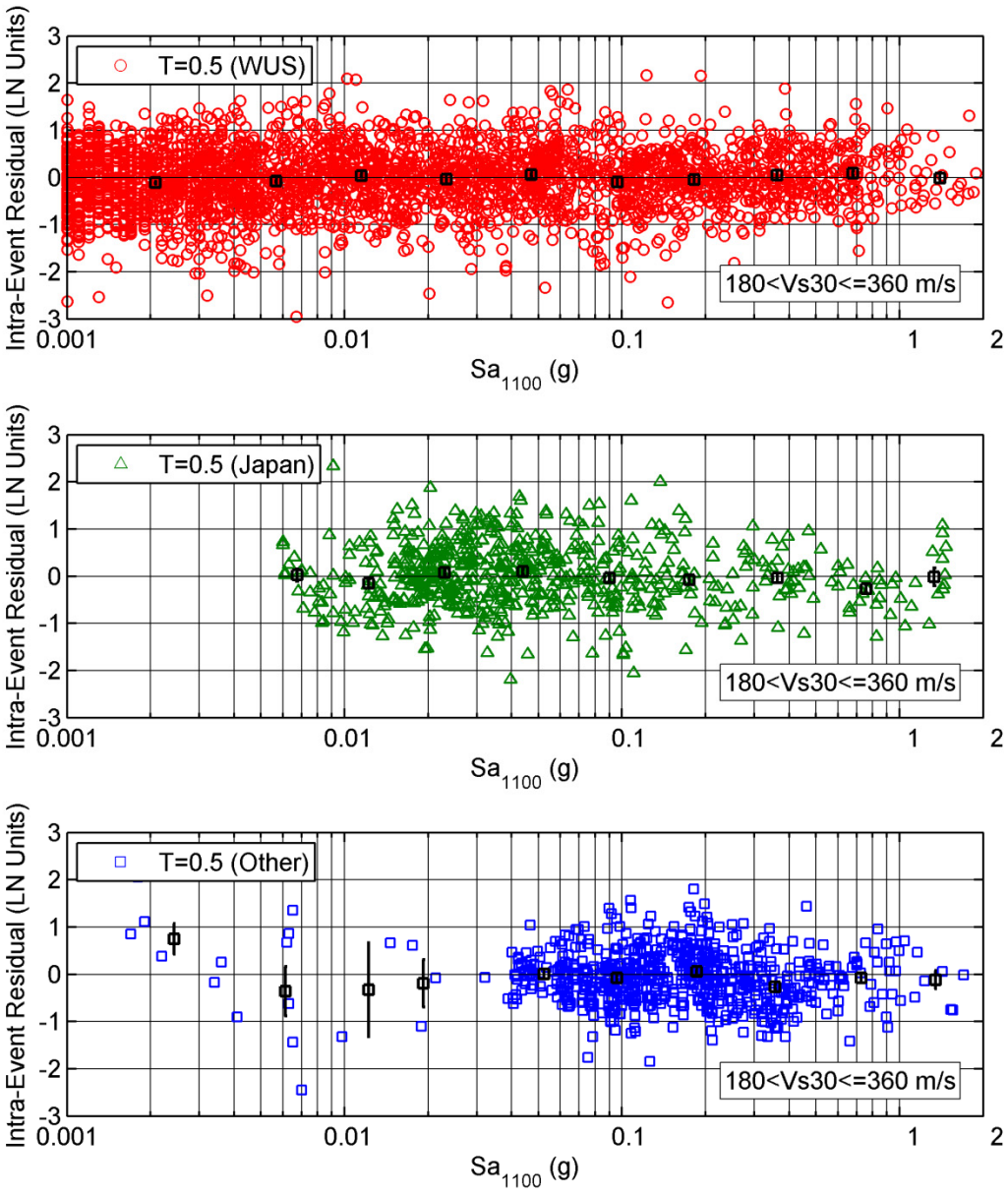

Figure 6.6(c) Sa_{1100} **dependence of the Intra-event residuals for** T **= 0.5 sec.**

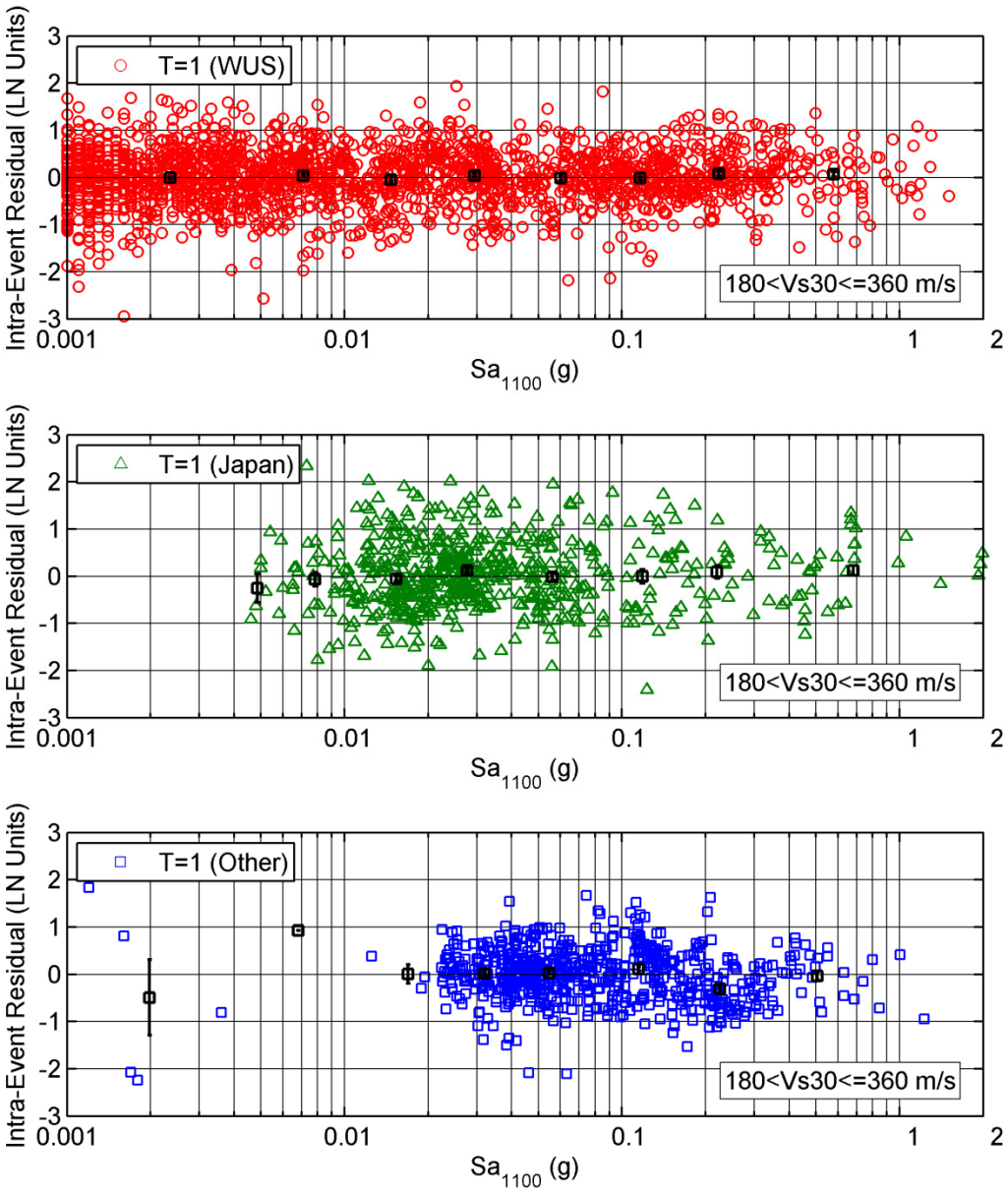

Figure 6.6(d) Sa_{1100} **dependence of the Intra-event residuals for** T **= 1.0 sec.**

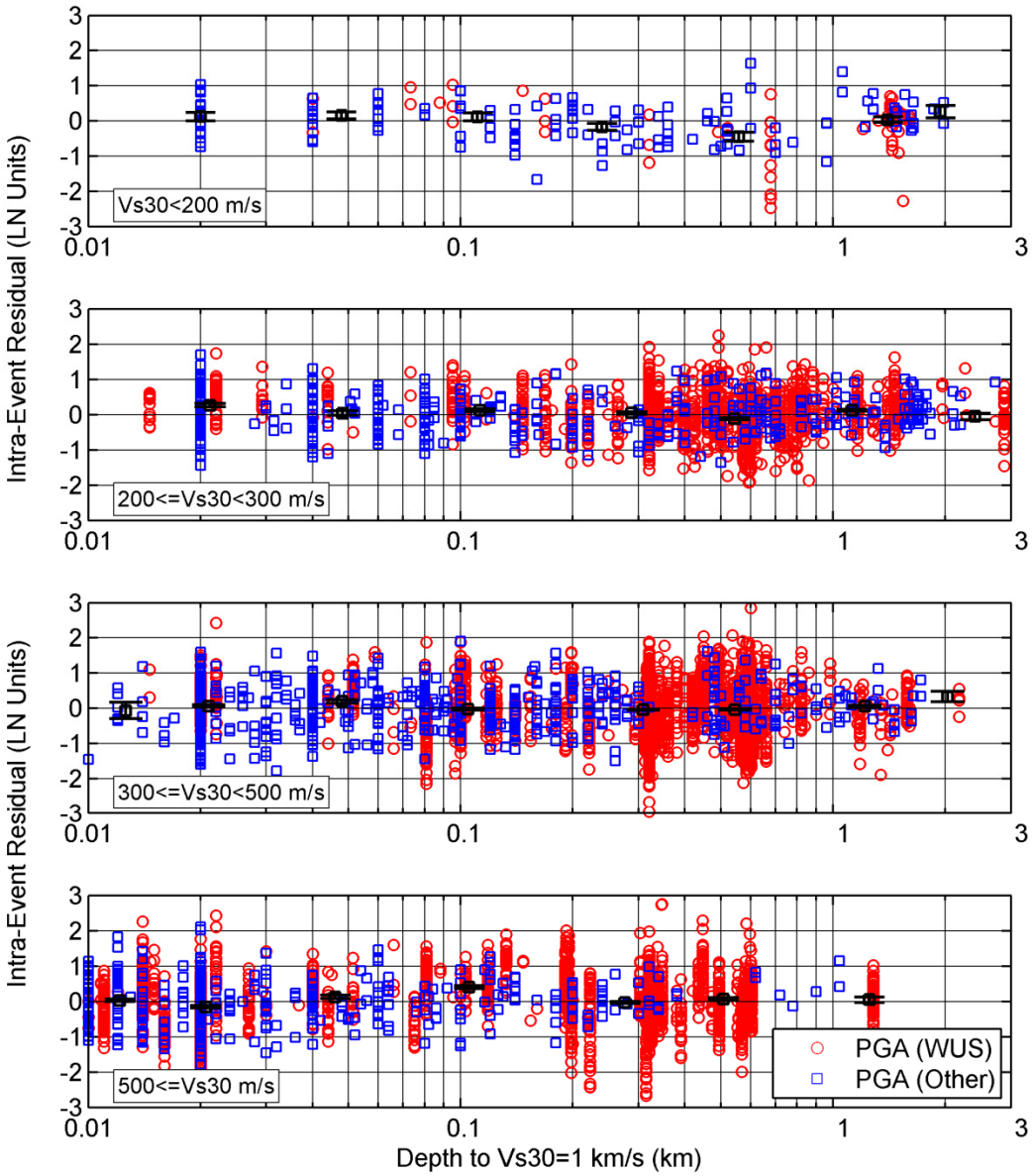

Figure 6.7(a) Z_1 **dependence of the intra-event residuals for PGA.**

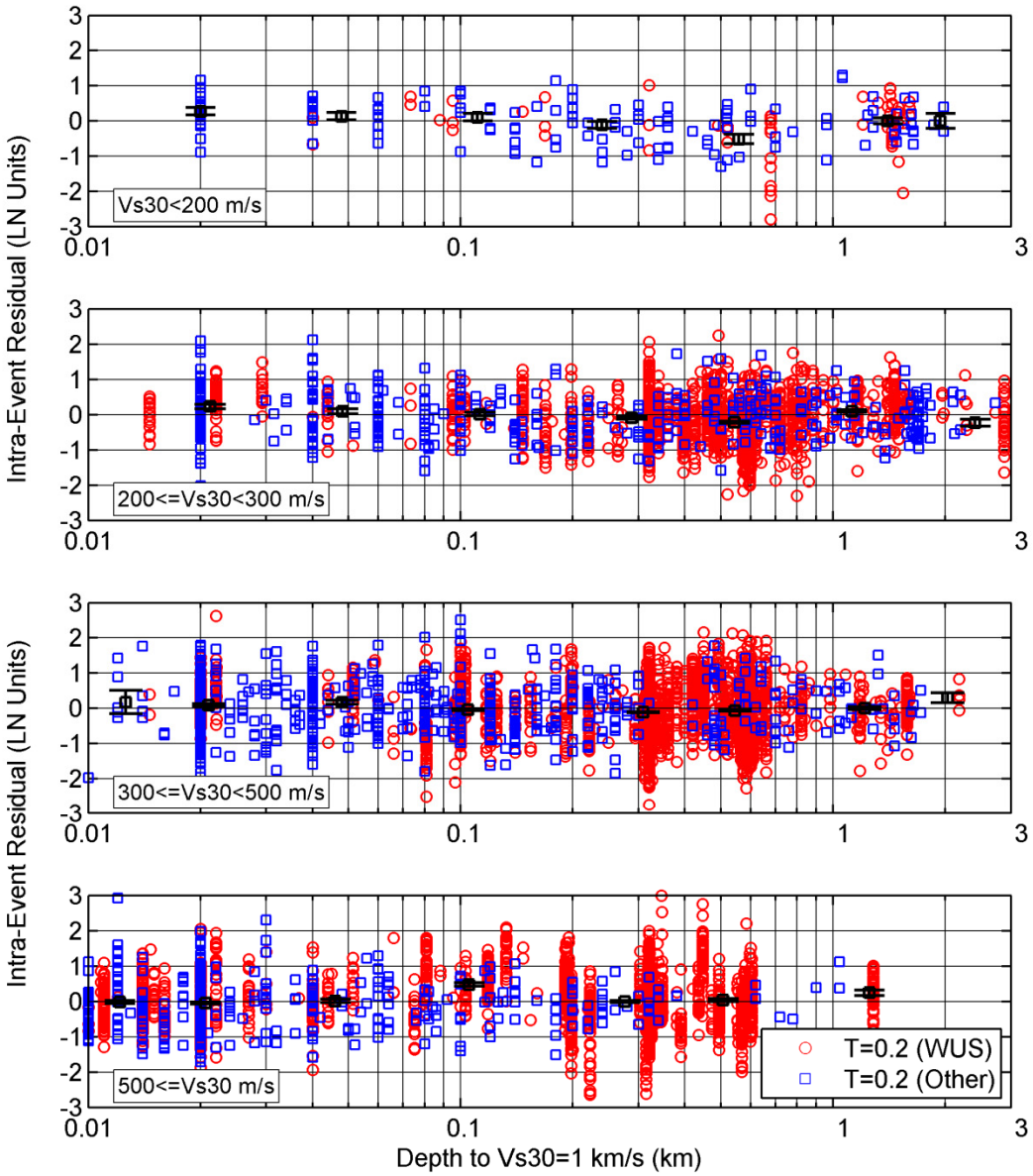

Figure 6.7(b) Z_1 **dependence of the Intra-event residuals for** T **= 0.2 sec.**

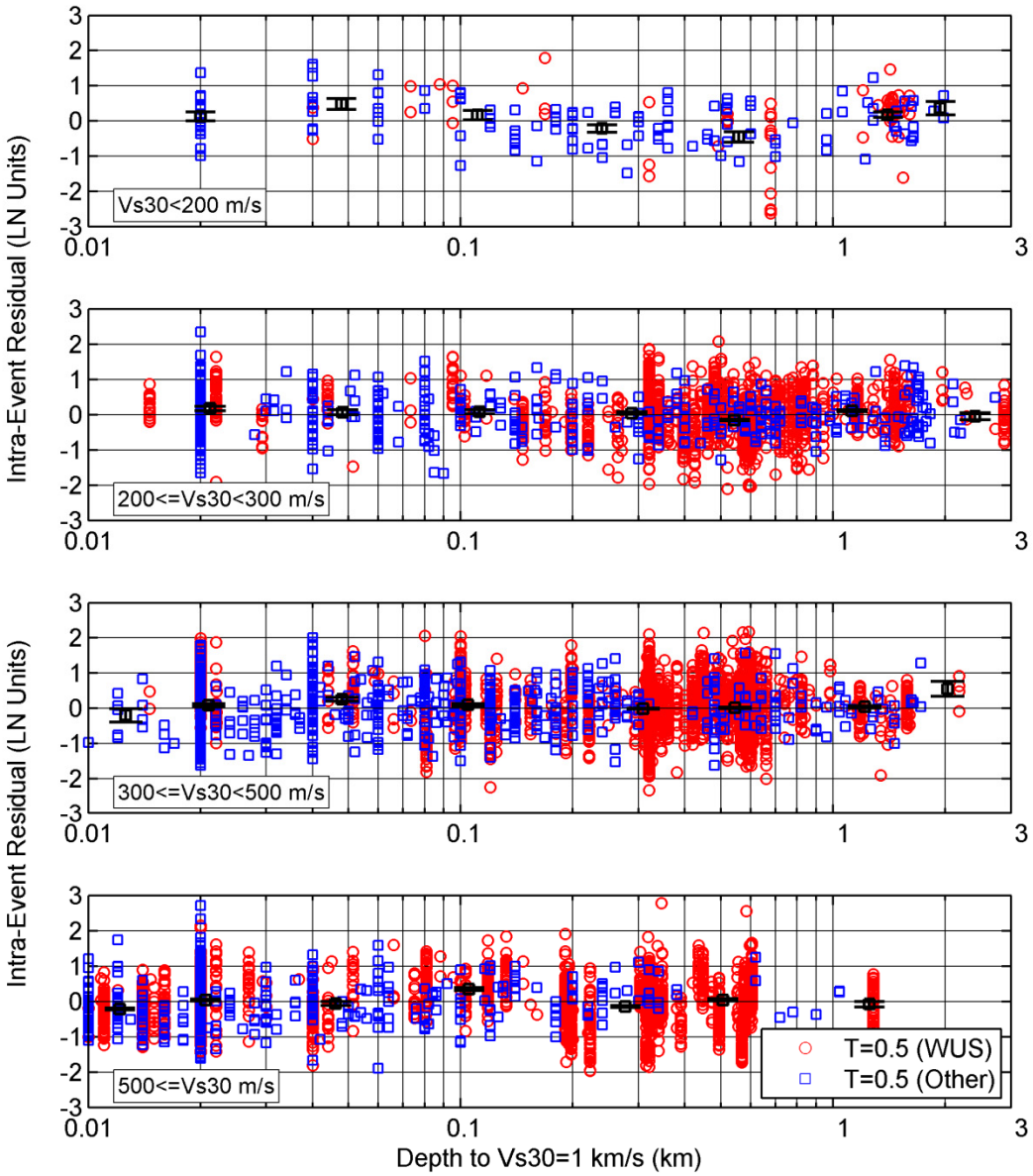

Figure 6.7(c) Z_1 **dependence of the Intra-event residuals for** T **= 0.5 sec.**

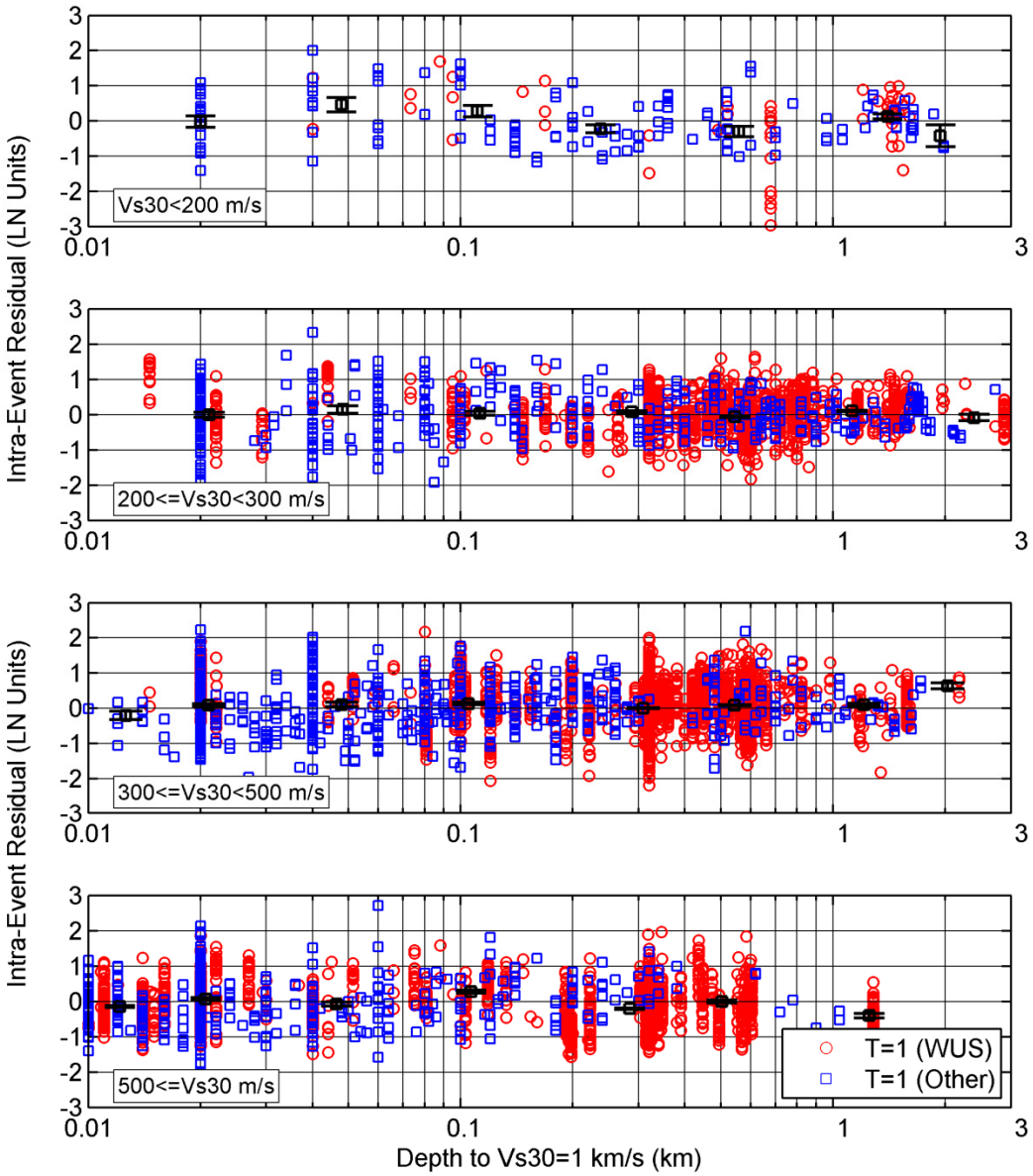

Figure 6.7(d) Z_1 **dependence of the Intra-event residuals for** T **= 1.0 sec.**

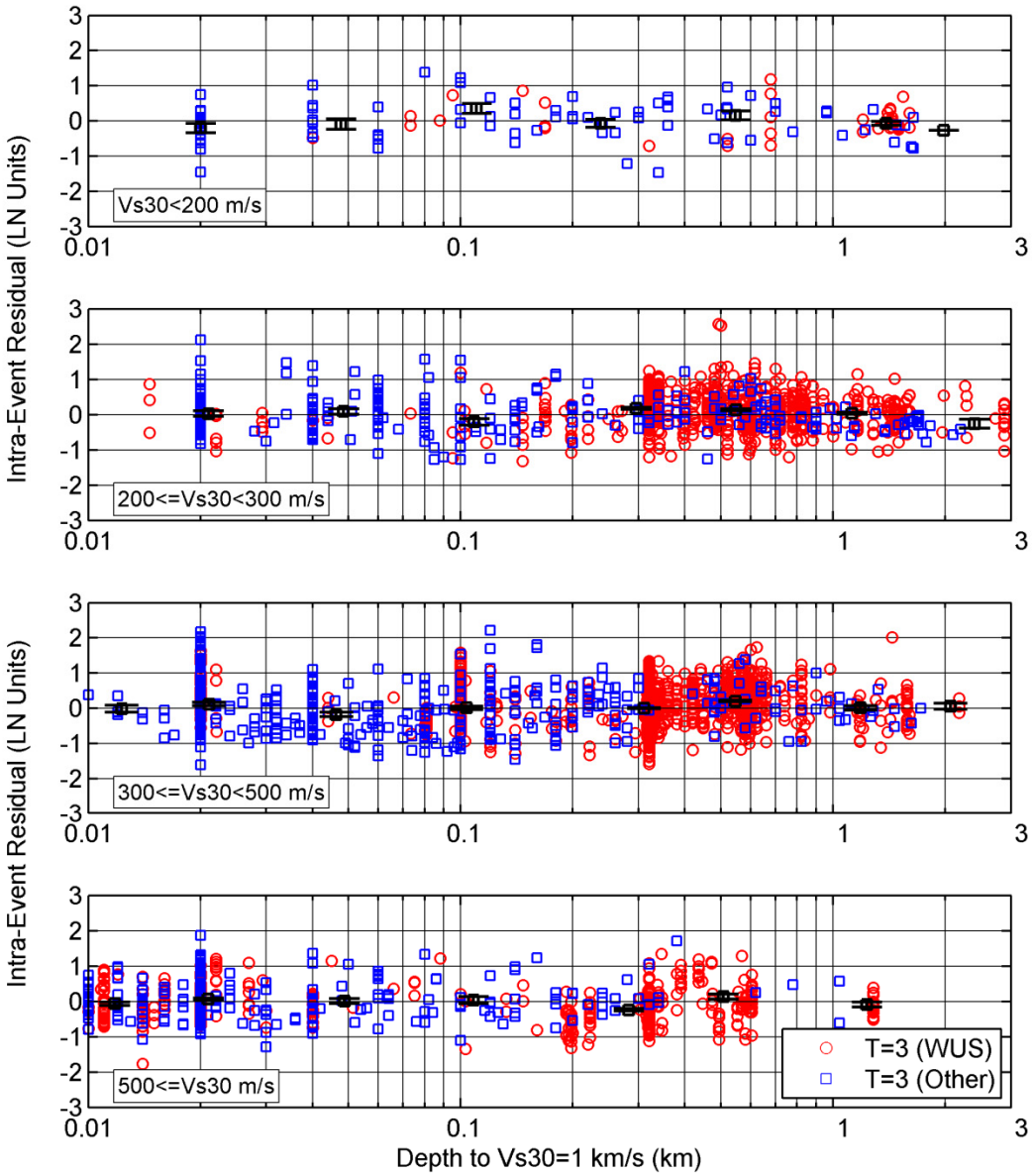

Figure 6.7(e) Z_1 **dependence of the intra-event residuals for** T **= 3 sec.**

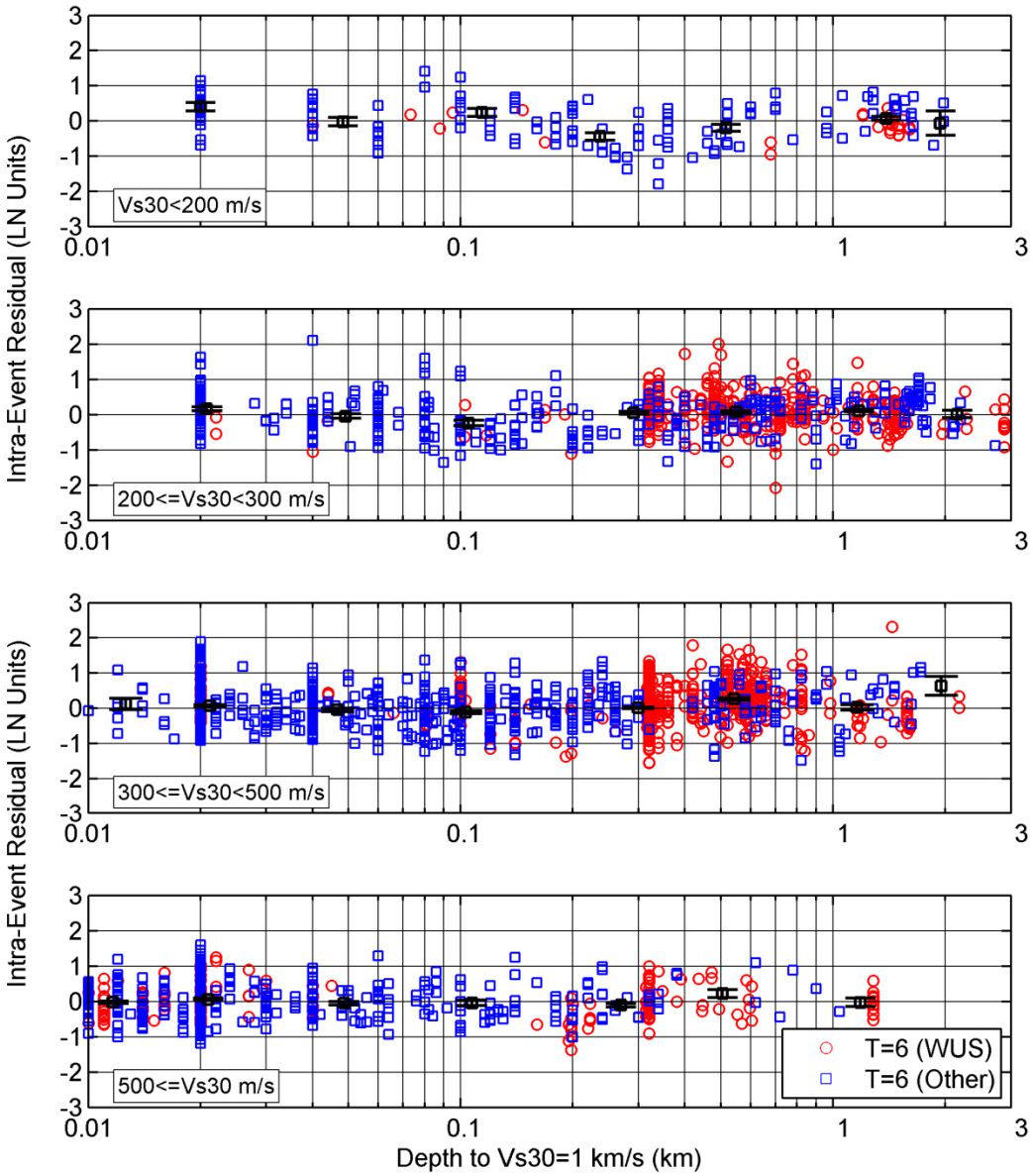

Figure 6.7(f) Z_1 **dependence of the intra-event residuals for** T **= 6 sec.**

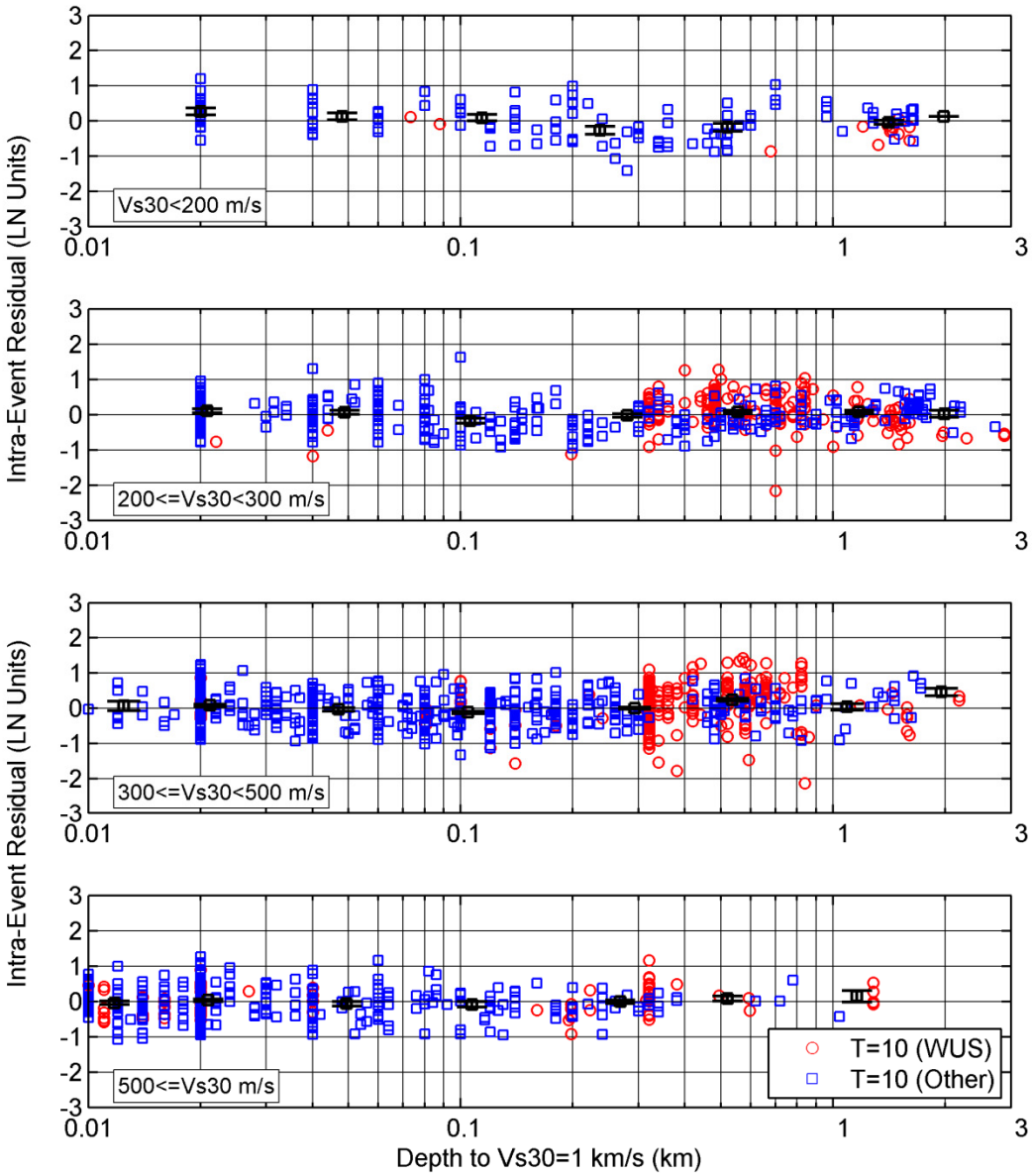

Figure 6.7(g) Z_1 **dependence of the intra-event residuals for** T **= 10 sec.**

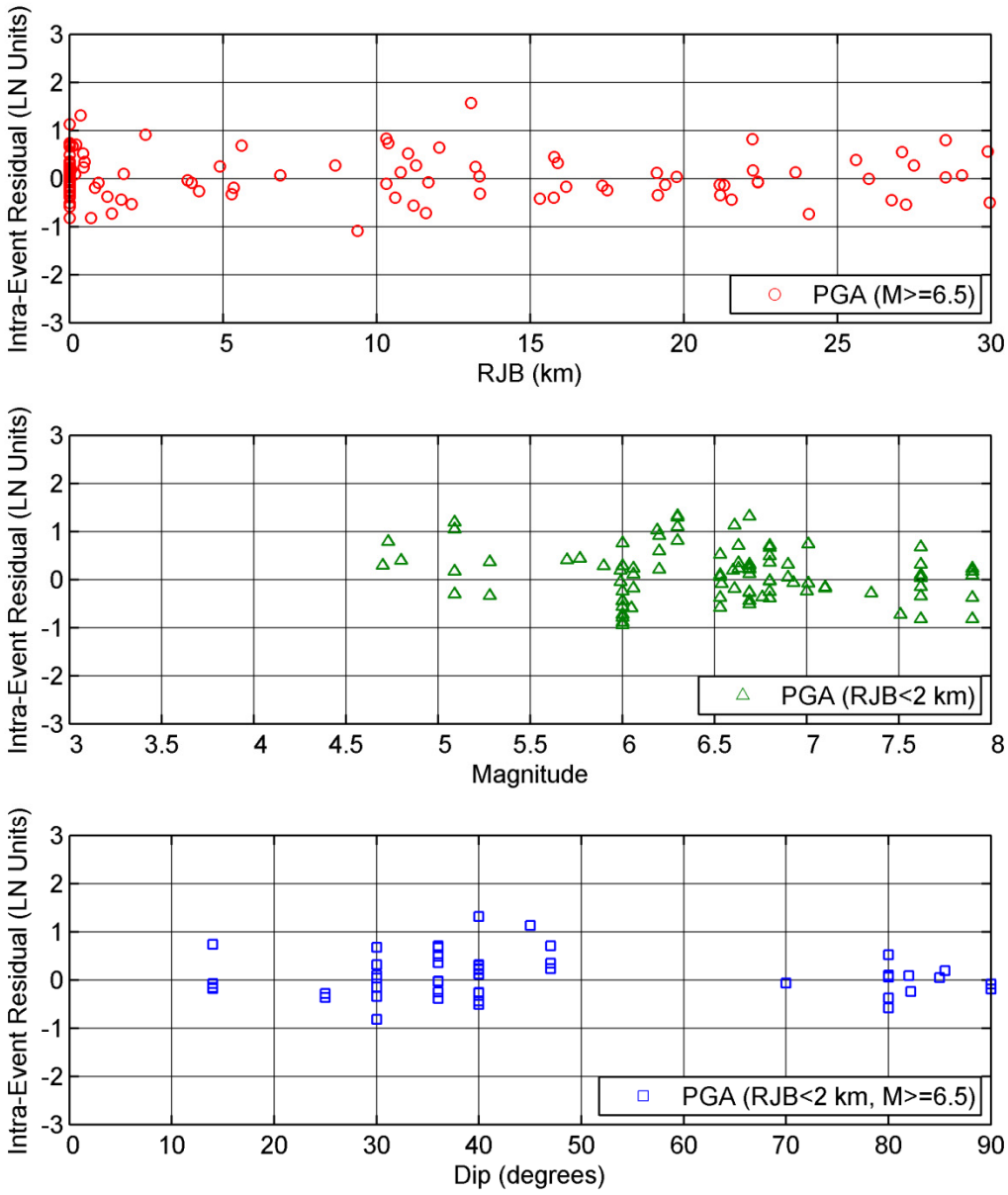

Figure 6.8(a) HW intra-event residuals (source-to-site azimuth: 85–95) for PGA.

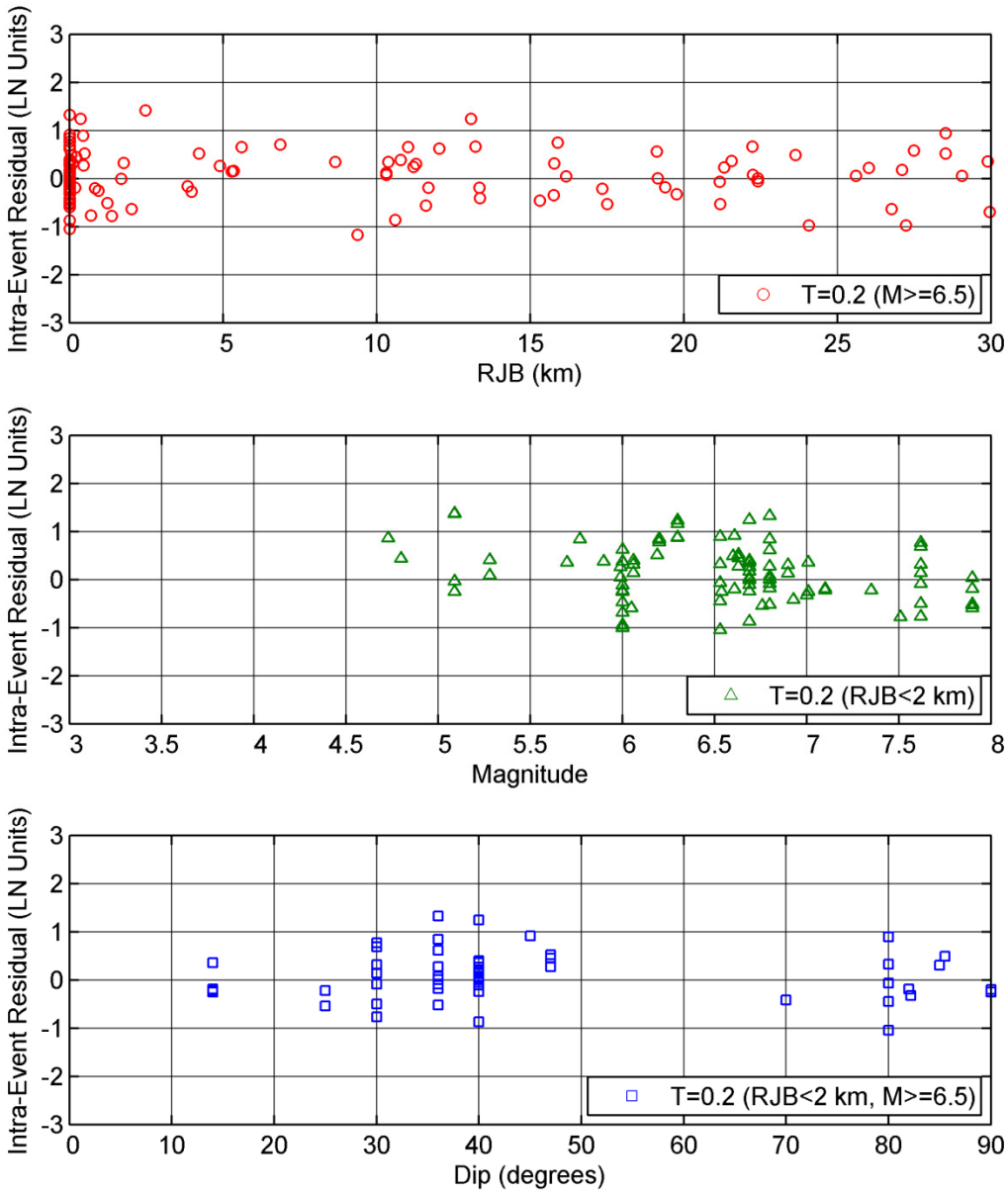

Figure 6.8(b) **HW intra-event residuals (source-to-site azimuth: 85–95) for T = 0.2 sec.**

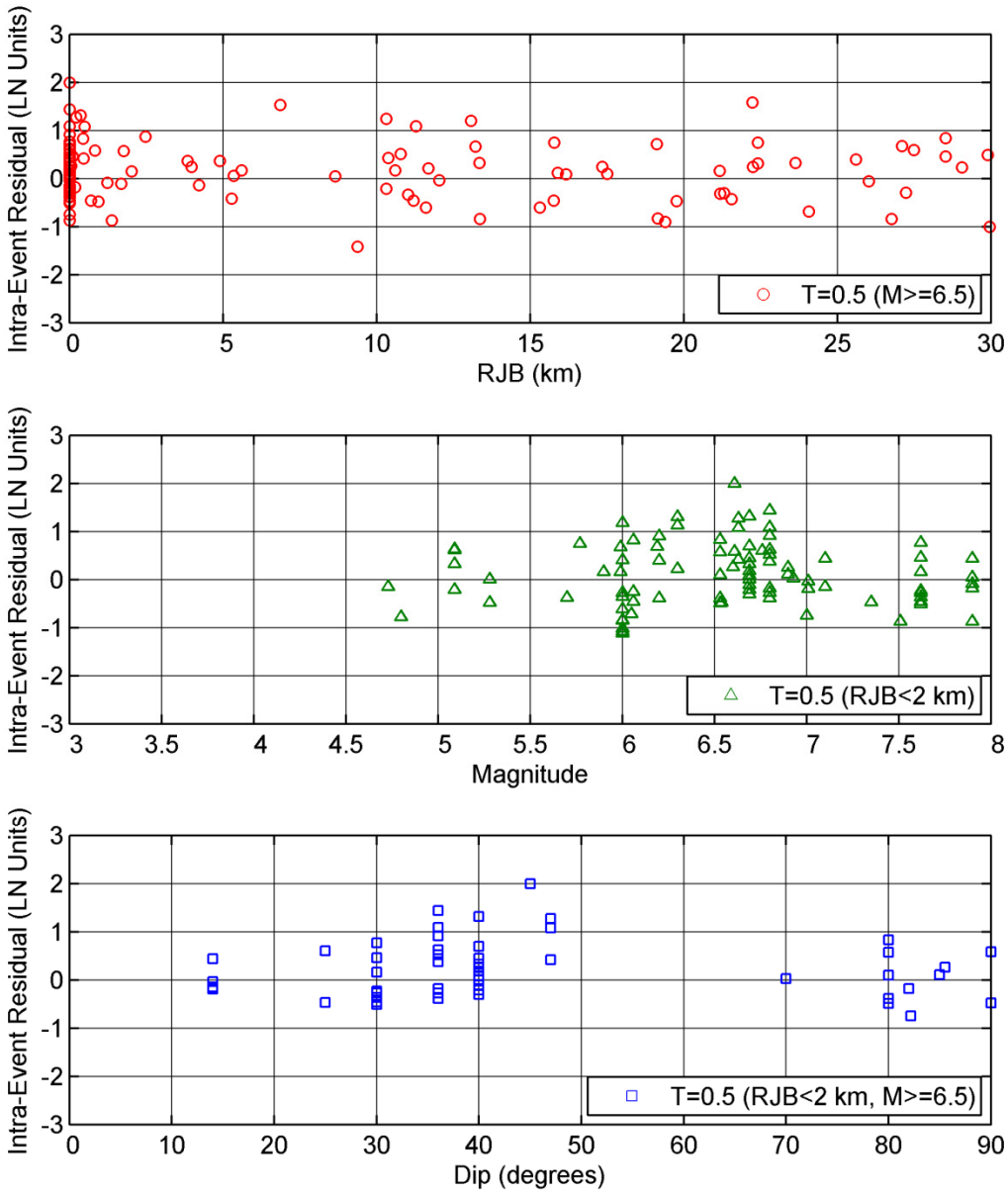

Figure 6.8(c) **HW intra-event residuals (source-to-site azimuth: 85–95) for T = 0.5 sec.**

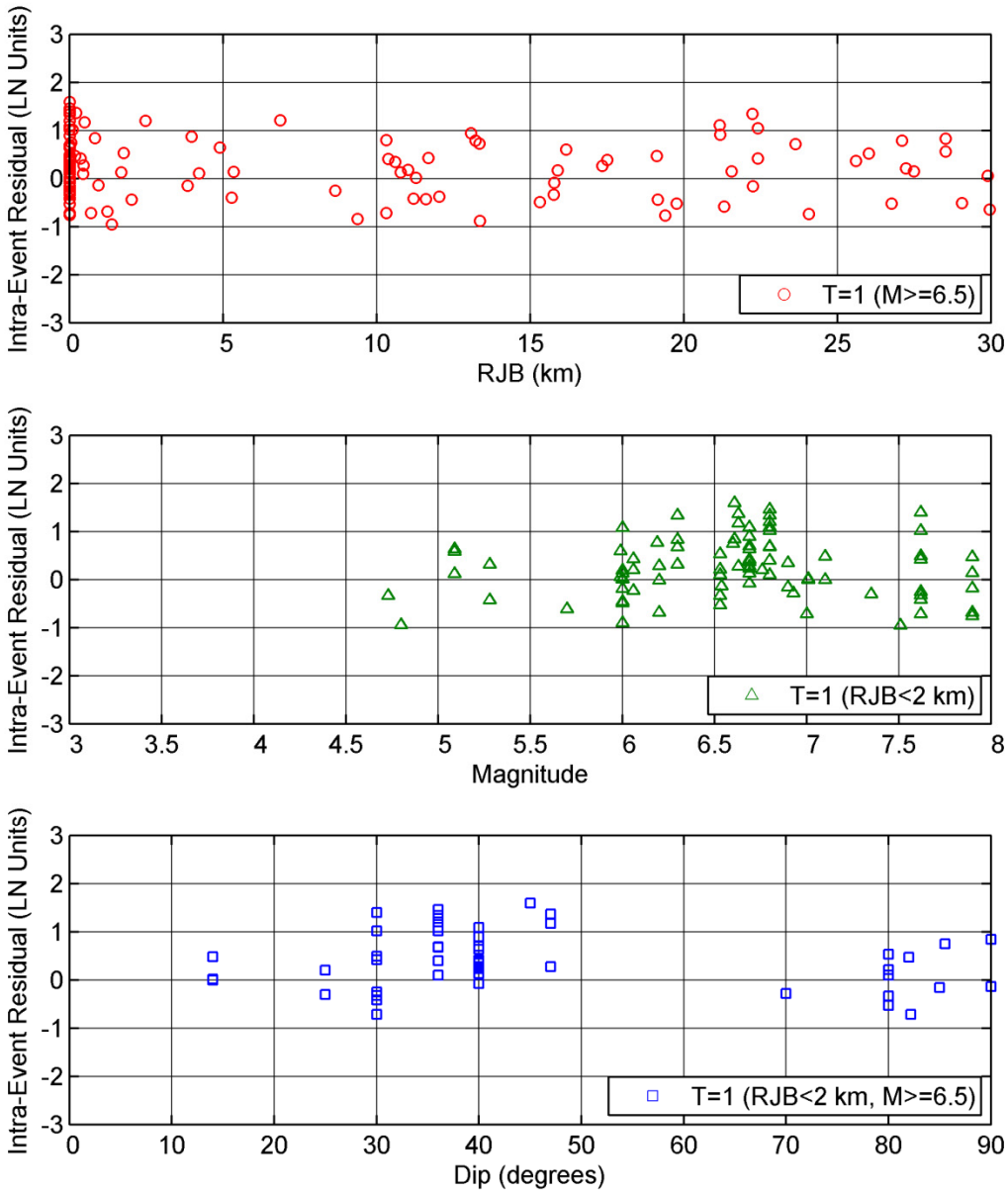

Figure 6.8(d) **HW intra-event residuals (source-to-site azimuth: 85–95) for T = 1.0 sec.**

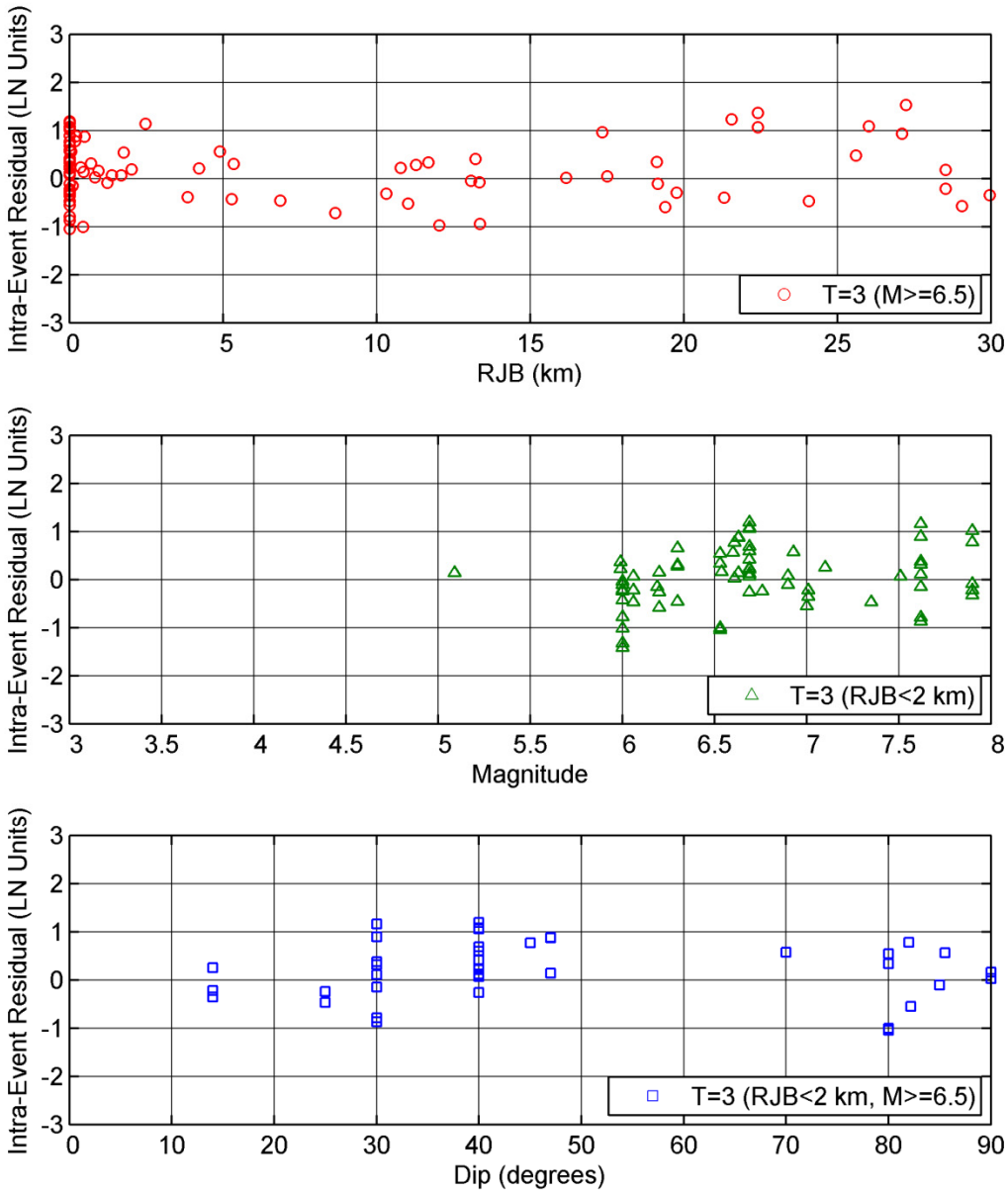

Figure 6.8(e) **HW intra-event residuals (source-to-site azimuth: 85–95) for $T = 3$ sec.**

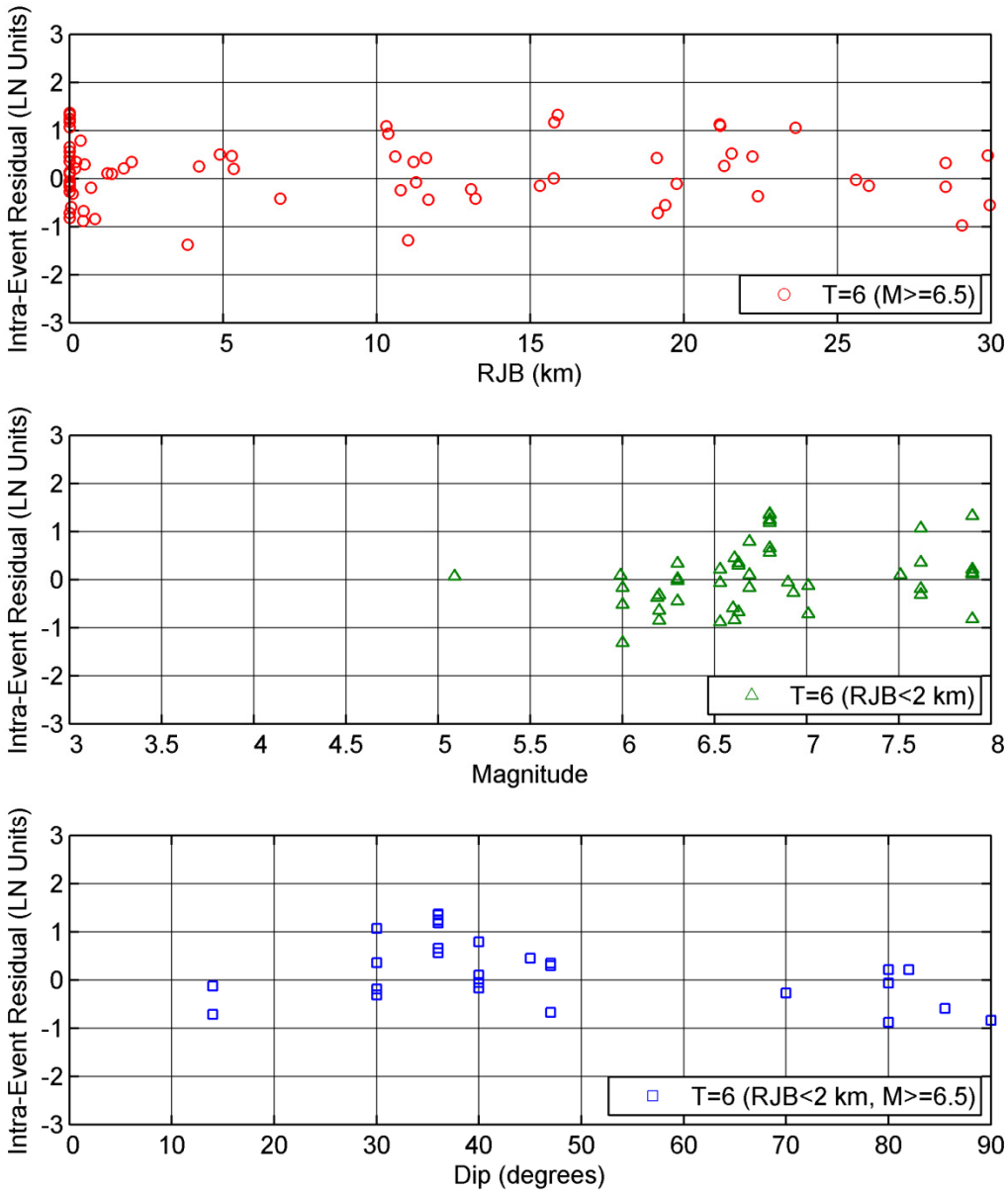

Figure 6.8(f) **HW intra-event residuals (source-to-site azimuth: 85–95) for $T = 6$ sec**

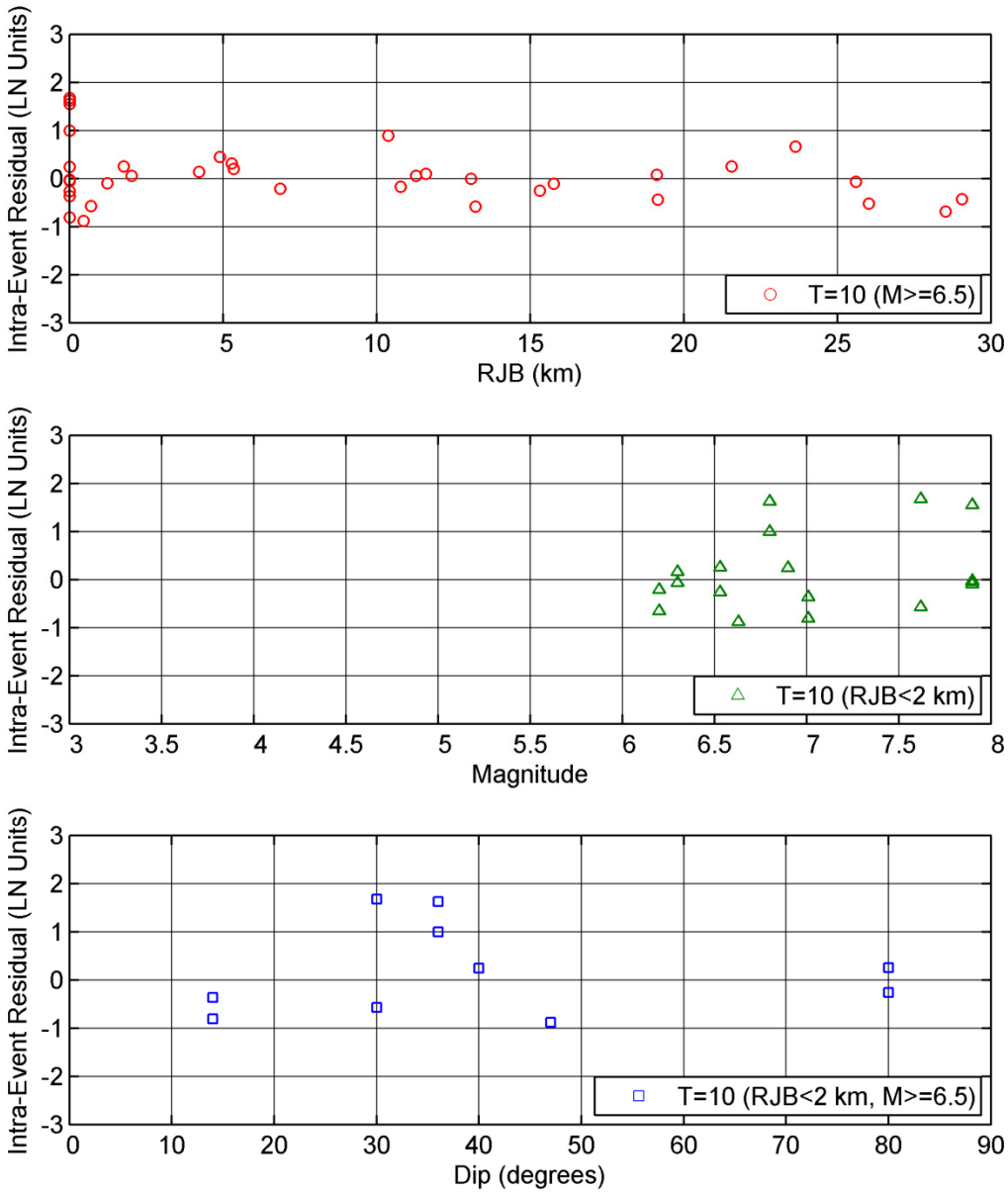

Figure 6.8(g) HW intra-event residuals (source-to-site azimuth: 85–95) for T=10 sec.

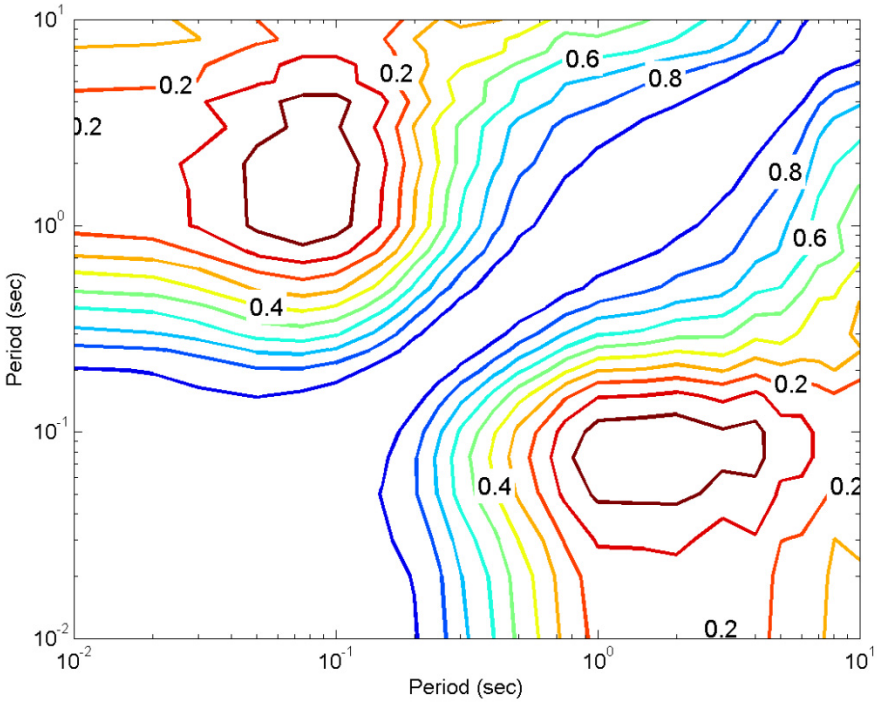

Figure 6.9(a) Correlation coefficients for the normalized inter-event residuals across periods.

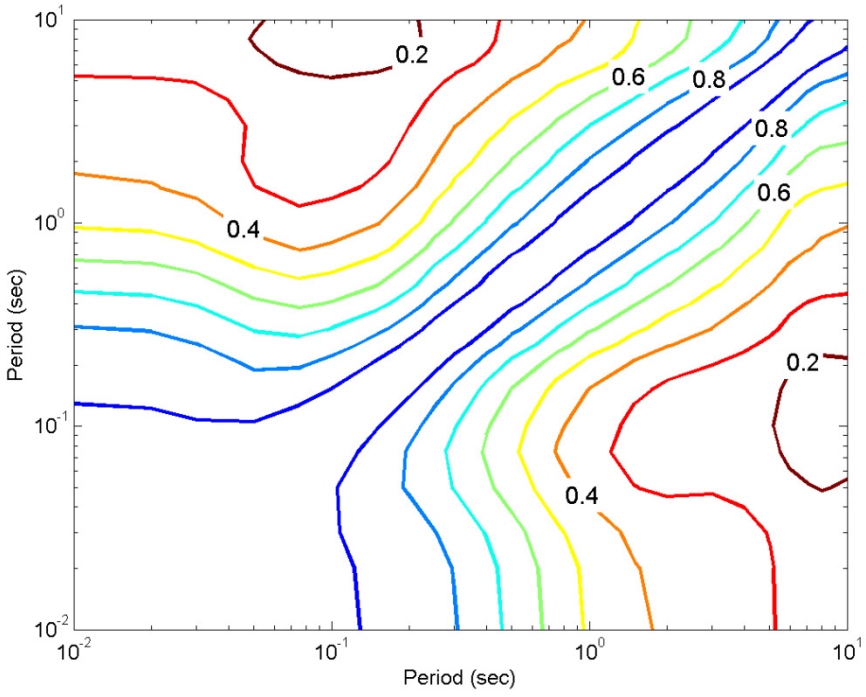

Figure 6.9(b) Correlation coefficients for the normalized intra-event residuals across periods.

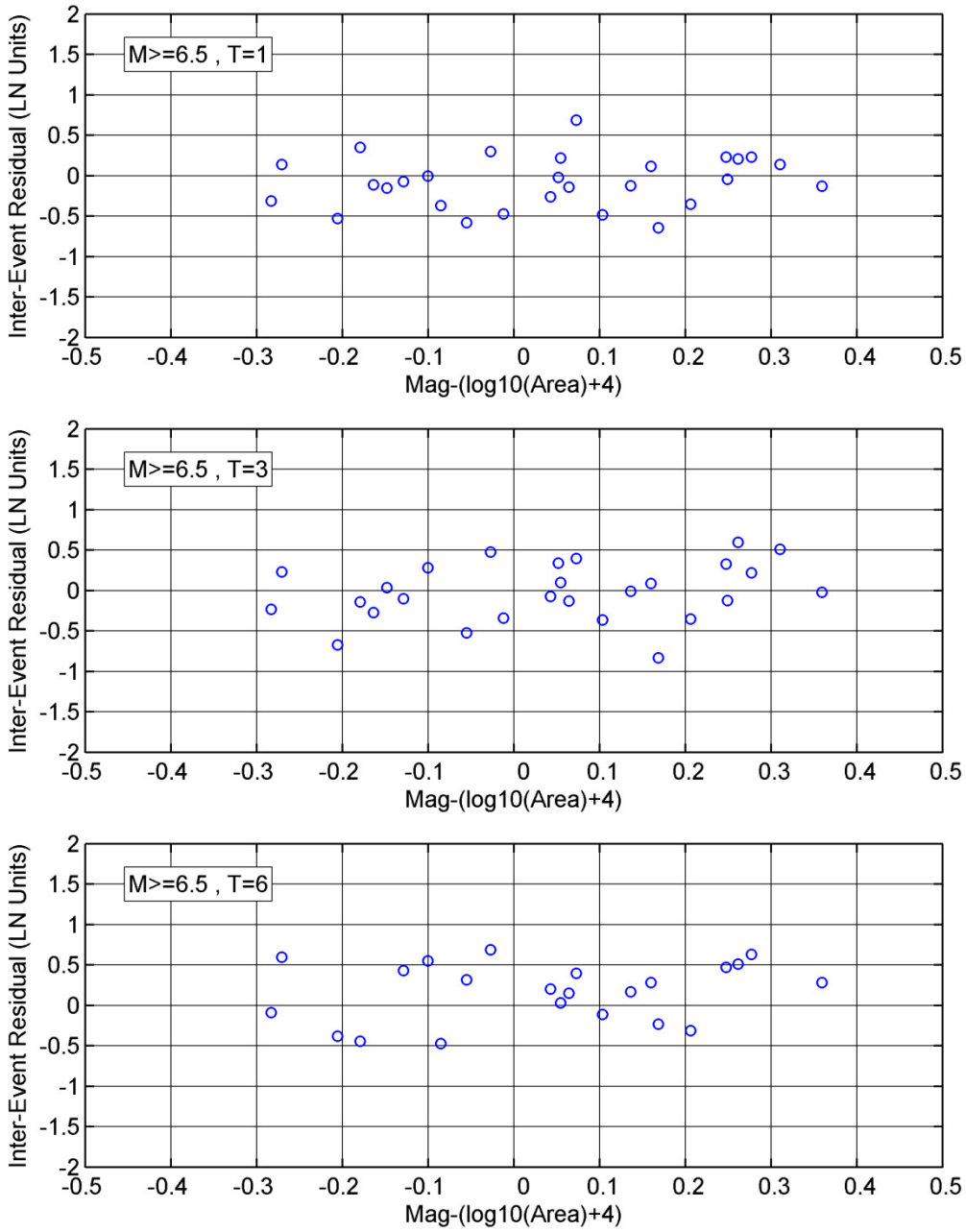

Figure 6.10 **Static stress drop scaling of the inter-event residuals for $T = 1$, $T = 3$ and $T = 6$ sec.**

7 Equations for Standard Deviation

7.1 STANDARD DEVIATION MODEL

The intra-event and inter-event standard deviations are magnitude dependent, as follows:

$$\phi_{A,L}(M) = \begin{cases} s_1 & for\ M < 4 \\ s_1 + \frac{s_2 - s_1}{2}(M-4) & for\ 4 \le M \le 6 \\ s_2 & for\ M > 6 \end{cases} \quad (7.1)$$

and

$$\tau_{A,L}(M) = \begin{cases} s_3 & for\ M < 5 \\ s_3 + \frac{s_4 - s_3}{2}(M-5) & for\ 5 \le M \le 7 \\ s_4 & for\ M > 7 \end{cases} \quad (7.2)$$

where $\phi_{A,L}$ is the linear intra-event standard deviation and $\tau_{A,L}$ is the linear inter-event standard deviation. The smoothed s_1 through s_4 parameters are provided in Table 7.1 and presented in Figure 7.1.

7.1.1 Regionalization of Standard Deviation

The intra-event standard deviation of the Japanese data is significantly higher than that from California and Taiwan. Therefore, we created a separate model for the Japanese intra-event standard deviation so that it would not affect the results of the other regions. Since our dataset includes only five Japanese events, all with magnitudes between 6.0 and 7.0, we cannot determine the magnitude scaling for this data. On the other hand, we see a clear distance scaling for the Japanese standard deviation, which is not apparent for the other regions. Hence, the intra-event standard deviation model for Japan has the following form:

$$\phi_{A-JP}(R_{rup}) = \begin{cases} s_5 & for\ R_{rup} < 30 \\ s_5 + \frac{s_6 - s_5}{50}(R_{rup} - 30) & for\ 30 \le R_{rup} \le 80 \\ s_6 & for\ R_{rup} > 80 \end{cases} \quad (7.3)$$

7.2 EFFECT OF MEASUREMENT ERRORS IN THE INDEPENDENT PARAMETERS

Some of the variability in the observed ground motions can be attributed to measurement errors in the independent parameters for our subset of the data. The standard deviation of the ground motion due to measurement error in a single parameter can be estimated by:

$$\sigma^2_{lnSa}(\Delta P_i) \approx \left(\frac{\partial ln(Sa)}{\partial P_i}\right)^2 \sigma^2_{\Delta P_i} \tag{7.4}$$

where P_i is the i^{th} independent parameter (e.g., M, R_{rup}, ….) and $\sigma_{\Delta P_i}$ is the standard deviation of measurement error in parameter P_i. If the model functional form is correct, then the standard deviation calculated from the regression, which assumed no errors in the independent parameters, can be reduced. For multiple parameters, the general form is

$$\sigma^2_{lnSa}(P) \approx$$

$$\left(\frac{\partial \ln(Sa)}{\partial P_1}\right)^2 \sigma^2_{\Delta P_1} + 2\frac{\partial \ln(Sa)}{\partial P_1}\frac{\partial \ln(Sa)}{\partial P_2} COV(\Delta P_1, \Delta P_2) + \left(\frac{\partial \ln(Sa)}{\partial P_2}\right)^2 \sigma^2_{\Delta P_2} + \ldots \tag{7.5}$$

where COV(ΔP_1,ΔP_2) is the covariance of the measurement errors in P_1 and P_2.

In the Abrahamson and Silva (2008) model, measurement errors were evaluated explicitly for magnitude, distance, depth to top-of-rupture, style-of-faulting, distance, V_{s30} estimate, and HW location. Most of these parameters had a minor effect on reducing the total standard deviation. The only parameter that had a significant impact on the standard deviation was the uncertainty associated with an estimated V_{s30} value. Therefore, we will only take into account that effect. Since the standard deviations from the regression are dominated by data in the near linear site response range, we assume linear site response in evaluating the impact of the measurement errors of the independent parameters.

The effect of measurement errors in Z_1 can also be significant but has not yet been evaluated. This effect on the standard deviation will be considered in updates of the GMPE.

7.2.1 V_{S30} Uncertainty

For linear site response, the partial derivative of the ln(Sa) with respect to the ln(V_{S30}) is given by

$$\frac{\partial ln(Sa)}{\partial ln(V_{s30})} = a_{10} + bn \tag{7.6}$$

The partial derivative is shown in Figure 7.2 as a function of period. In the new NGA-West2 database, nearly all stations have a V_{s30} value associated with them, but only 22% of those are from direct measurements. The rest of the V_{s30} values are estimations based on correlations of V_{s30} with the local surface geology or the slope (see Ancheta et al. 2013 for a full description of the available V_{s30} values in the database). The average standard deviation of the estimated V_{S30} given in the flat-file is 0.31 natural log units, while the average standard deviation of the

measured V_{s30} sites is 0.1. Hence, the measurement error we should account for is the difference between the two (in RSS) which results in a standard deviation due to use of proxy value for V_{s30} of 0.29 natural log units. .

The uncertainty in the V_{S30} depends how it is estimated for a specific application. If the V_{S30} is estimated from the surface geology or from a broad site class (such as NEHRP class), then it is not appropriate to reduce the intra-event standard deviation for V_{S30} measurement uncertainty since this same level of uncertainty applies to the V_{S30} for the projects. On the other hand, if the V_{S30} is measured at the site or is specified (for example, for reference rock site conditions), then the effect of measurement errors in the V_{S30} should be removed from the total intra-event standard deviation. Therefore, two separate models for the total intra-event standard deviation are developed: one for V_{S30} estimated from site geology and one for V_{S30} measured or specified.

The intra-event standard deviation for a site with a measured V_{s30} can be computed using Equation (7.1) and the modified parameters for a measured V_{s30}, which are provided in Table 7.1. The magnitude dependence of the inter- and intra- event standard deviation models for periods of $T = 0.2$ and $T = 1$ sec is presented in Figure 7.3. The period dependence of the inter- and intra-event standard deviation models for magnitudes 5 and 7 is presented in Figure 7.4. Both also show the intra-event standard deviation for a measured V_{s30}, displaying the effect of such reduction.

7.3 NONLINEAR EFFECTS ON THE STANDARD DEVIATION

The standard deviation in the linear site response range is dependent on the earthquake magnitude. The non-linear site effects also affect the standard deviation and the same approach as used in AS08 is used here with the difference being that the level of shaking is parameterized by the $\widehat{Sa}_{1100}$ instead of the $\widehat{PGA}_{1100}$.

As discussed in Al Atik and Abrahamson (2010), the nonlinear effects on the standard deviation are influenced by the variability of the rock motion. If the rock motion is above average, the amplification will have more nonlinearity and hence will be below average. Similarly, if the rock motion is below average, the amplification will have less nonlinearity and hence will be above average. That effect leads to a reduction in the variability in the short-period soil motion.

Because the NL effect depends on the variability of the rock motion, we need to estimate the standard deviation of the rock motion. We can estimate the standard deviation of the rock motion by removing the site amplification variability from the surface motion:

$$\phi_{\mathrm{B}}(\mathrm{M},\mathrm{T}) = \sqrt{\phi_{\mathrm{A,L}}^2(\mathrm{M},\mathrm{T}) - \phi_{\mathrm{Amp}}^2(\mathrm{T})} \tag{7.7}$$

where $\phi_{A,L}$ is the linear intra-event standard deviation for soil which is derived from the regression, ϕ_{Amp} is the standard deviation of the site amplification, and ϕ_B is the standard deviation of the rock motion. . We assume that $\phi_{Amp}(T) = 0.4$ for all periods based on the site response simulation results described in Kamai et al (2013). For the inter-event variability, the

standard deviation of the rock motion is the the observed inter-event variability for the linear range, so $\tau_B(M,T) = \tau_{A,L}(M,T)$.

To account for the effects of nonlinearity on the soil ground motion, the variability of the soil motion is computed using propagation of errors. The intra-event standard deviation is given by:

$$\phi\left(T,M,\hat{S}a_{1100},V_{s30}\right) = \left[\phi_B^2(M,T)\left(1+\frac{\partial\, ln\, Amp(T,\hat{S}a_{1100},V_{S30})}{\partial\, ln\, Sa_{1100}}\right)^2 + \phi_{Amp}^2(T)\right]^{1/2} \tag{7.8}$$

and the inter-event standard deviation is given by

$$\tau\left(T,M,\hat{S}a_{1100},V_{s30}\right) = \tau_B(M,T)\left(1+\frac{\partial\, ln\, Amp(T,\hat{S}a_{1100},V_{S30})}{\partial\, ln\, Sa_{1100}}\right) \tag{7.9}$$

where

$$\frac{\partial\, ln\, Amp(T,\hat{S}a_{1100},V_{S30})}{\partial\, ln\, Sa_{1100}} = \begin{cases} 0 & for\ V_{s30} \geq V_{Lin} \\ \frac{-b(T)\hat{S}a_{1100}}{\hat{S}a_{1100}+c} + \frac{b(T)\hat{S}a_{1100}}{\hat{S}a_{1100}+c\left(\frac{V_{S30}}{V_{Lin}}\right)^n} & for\ V_{s30} < V_{Lin} \end{cases} \tag{7.10}$$

Table 7.1 Coefficients for the standard deviation.

	V_{s30} Estimated		V_{s30} Measured				Japan	
T (sec)	s_1	s_2	s_1	s_2	s_3	s_4	s_5	s_6
PGA	0.754	0.520	0.741	0.501	0.47	0.36	0.54	0.63
PGV	0.662	0.510	0.660	0.510	0.38	0.38	0.58	0.53
0.010	0.754	0.520	0.741	0.501	0.47	0.36	0.54	0.63
0.020	0.760	0.520	0.747	0.501	0.47	0.36	0.54	0.63
0.030	0.781	0.520	0.769	0.501	0.47	0.36	0.55	0.63
0.050	0.810	0.530	0.798	0.512	0.47	0.36	0.56	0.65
0.075	0.810	0.540	0.798	0.522	0.47	0.36	0.57	0.69
0.100	0.810	0.550	0.795	0.527	0.47	0.36	0.57	0.7
0.150	0.801	0.560	0.773	0.519	0.47	0.36	0.58	0.7
0.200	0.789	0.565	0.753	0.514	0.47	0.36	0.59	0.7
0.250	0.770	0.570	0.729	0.513	0.47	0.36	0.61	0.7
0.300	0.740	0.580	0.693	0.519	0.47	0.36	0.63	0.7
0.400	0.699	0.590	0.644	0.524	0.47	0.36	0.66	0.7
0.500	0.676	0.600	0.616	0.532	0.47	0.36	0.69	0.7
0.750	0.631	0.615	0.566	0.548	0.47	0.36	0.73	0.69
1.000	0.609	0.630	0.541	0.565	0.47	0.36	0.77	0.68
1.500	0.578	0.640	0.506	0.576	0.47	0.36	0.80	0.66
2.000	0.555	0.650	0.480	0.587	0.47	0.36	0.80	0.62
3.000	0.548	0.640	0.472	0.576	0.47	0.36	0.80	0.55
4.000	0.527	0.630	0.447	0.565	0.47	0.36	0.76	0.52
5.000	0.505	0.630	0.425	0.568	0.47	0.36	0.72	0.5
6.000	0.477	0.630	0.395	0.571	0.47	0.36	0.70	0.5
7.500	0.457	0.630	0.378	0.575	0.47	0.36	0.67	0.5
10.000	0.429	0.630	0.359	0.585	0.47	0.36	0.64	0.5

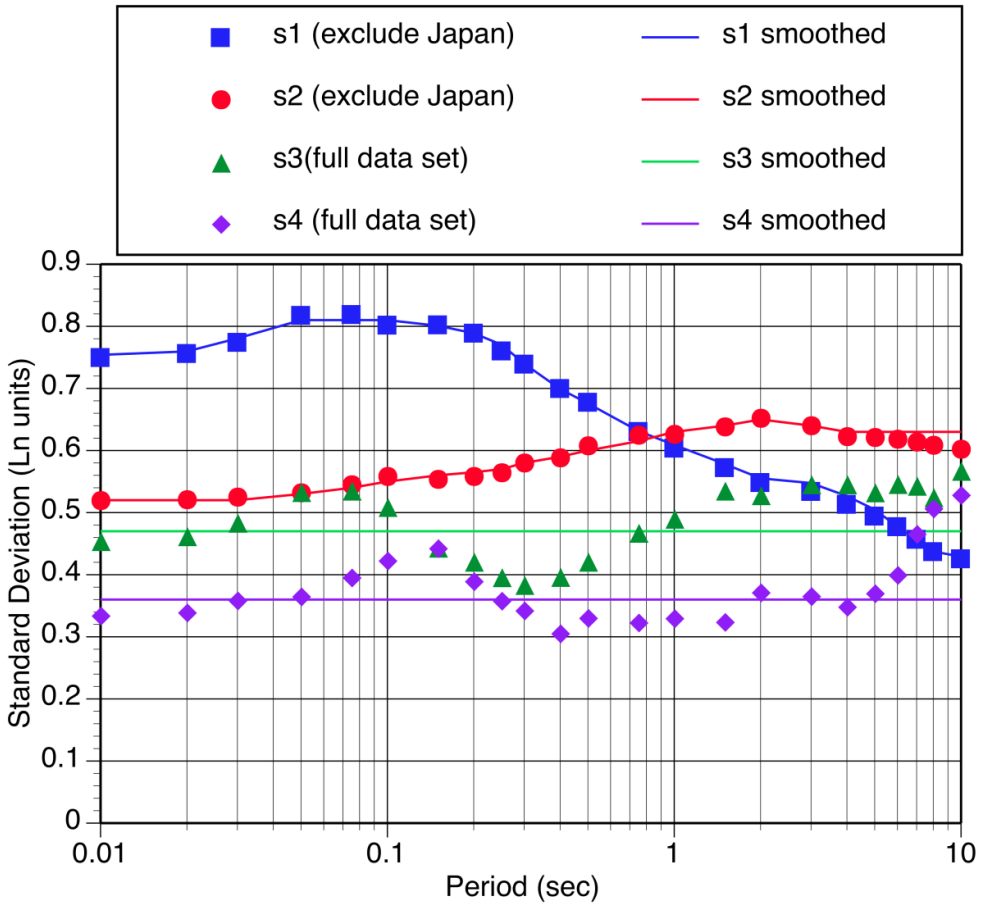

Figure 7.1 **Smooth coefficients for the standard deviation models.**

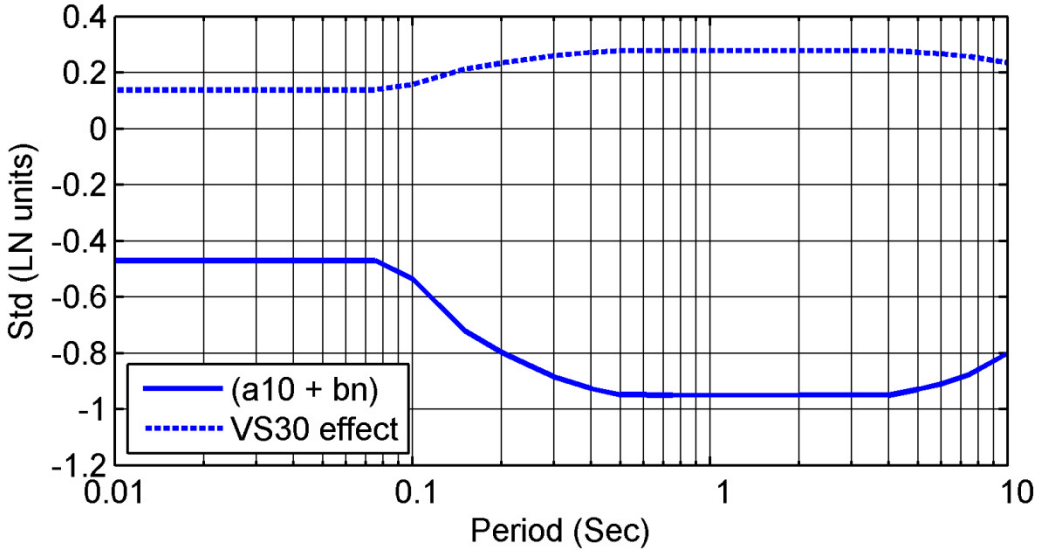

Figure 7.2 **Partial derivative of ln(Sa) with respect to ln(V_{S30})**

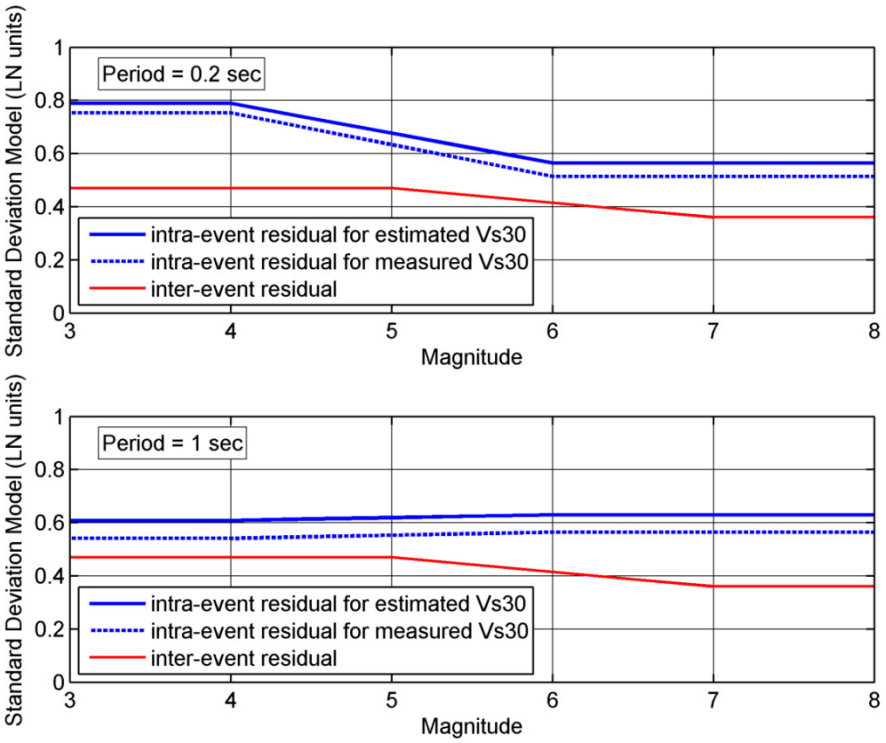

Figure 7.3 Magnitude scaling of $\phi_{A,L}$ and $\tau_{A,L}$ for T = 0.2 and T = 1.0 sec.

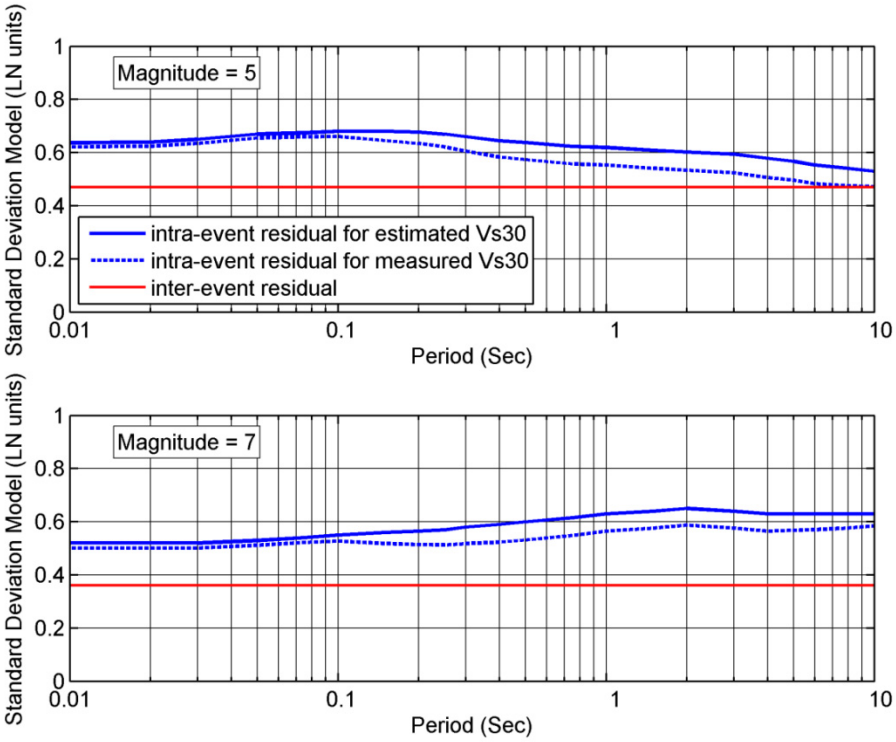

Figure 7.4 Period dependence of $\phi_{A,L}$ and $\tau_{A,L}$ for magnitudes 5 and 7.

8 Model Results

The median response spectra for the ASK13 model are compared to the AS08 model in Figures 8.1(a) and (b) for a vertical strike-slip scenario at an R_{JB} distance of 30 km and V_{s30} values of 760 m/sec and 270 m/sec, respectively. For this case, the Z_{TOR} values are 8, 6.5, 3, and 0 for magnitudes 5, 6, 7, and 8, respectively. The $Z_{1.0}$ values are set at the Z_{ref} value (Chiou and Youngs 2013) for the given V_{S30}. Figure 8.1 shows that the medial spectra from the current model are generally lower than those from AS08, especially for lower magnitudes (e.g., M5.0). The difference between the two models is larger for rock sites [Figure 8.1(a)] than for soil sites [Figure 8.1(b)]. A similar comparison of the medians at a R_{JB} distance of 1 km is shown in Figure 8.2(a-b) for V_{S30} values of 760 m/sec and 270 m/sec. Here, the decrease in median PGA is more significant.

The distance scaling is shown in Figure 8.3 for PGA and spectral periods of 0.2, 1.0, and 3.0 sec In this figure, the median ground motion from vertical strike-slip earthquakes on rock site conditions (V_{S30} = 760 m/sec) is shown for four different magnitudes.

The magnitude scaling of the current model is shown in Figures 8.4 for vertical strike-slip earthquakes on rock site conditions (V_{S30}=760 m/sec) for T =0.2 and T =3.0 sec. Note that the break in the magnitude scaling at M5.0 is driven by the additional small magnitude dataset which was not available at 2008, hence the large difference between the models for small magnitudes. The weak scaling of the short-period motion at short distances reflects the saturation with magnitude.

The HW scaling for a reverse M6.7 rupture with 45° dip is shown in Figure 8.5 for PGA on rock site conditions (V_{S30} = 760 m/sec). While the AS08 model had a step in the ground motion from the Foot Wall (FW) to the HW for surface ruptures only, such a step is now current for both surface and buried ruptures but it is smoother. The HW term is more smoothly tapering now back to the base-line FW value, at a distance away from the down-dip fault edge that depends on the fault dip and width (see Section 4.4). The short-period ground motion for buried ruptures is larger than the short-period ground motion for surface ruptures at most locations even though the rupture distances are larger for the buried rupture. This is due to the scaling with Z_{TOR}.

The site response scaling for **M**7 vertical strike-slip earthquakes at a rupture distance of 30 km is shown in Figures 8.6 and 8.7: Figure 8.6 shows the dependence of the spectra on the V_{S30} and Figure 8.7 shows that dependence of the spectra on the $Z_{1.0}$ for a soil site with V_{S30}=270 m/sec.

The spectral displacements of a vertical strike slip at a R_{JB} distance of 20 km is shown in Figure 8.8 for a range of magnitudes. Although the spectral displacement was not constrained to a constant value at long periods for this model, the regression leads to this condition without additional constraint.

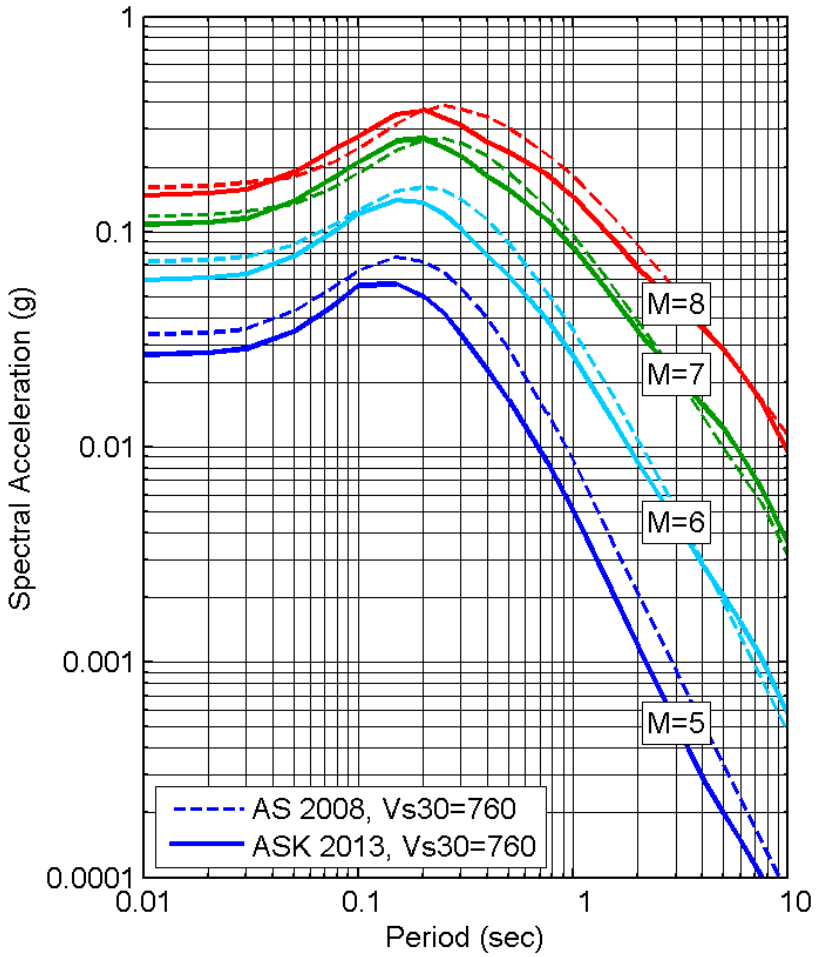

Figure 8.1(a) Comparison of the median spectral acceleration: SS, R_{JB}= 30 km, V_{S30}= 760 m/sec.

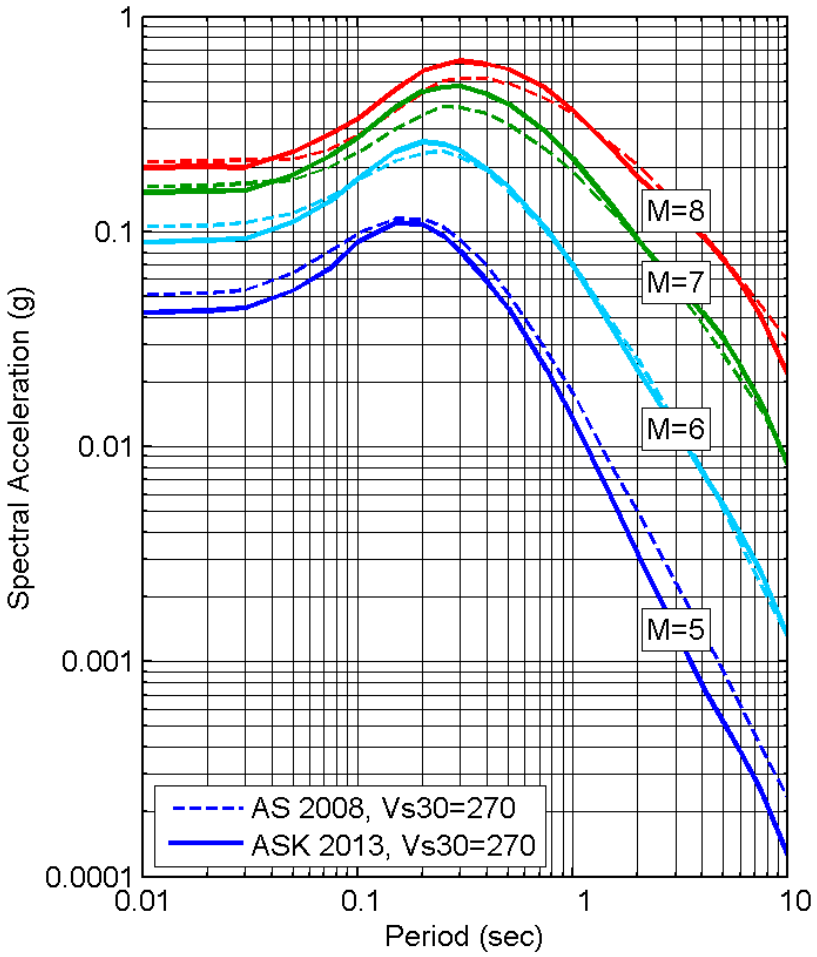

Figure 8.1(b) Comparison of the median spectral acceleration: SS, R_{JB} = 30 km, V_{S30} = 270 m/sec.

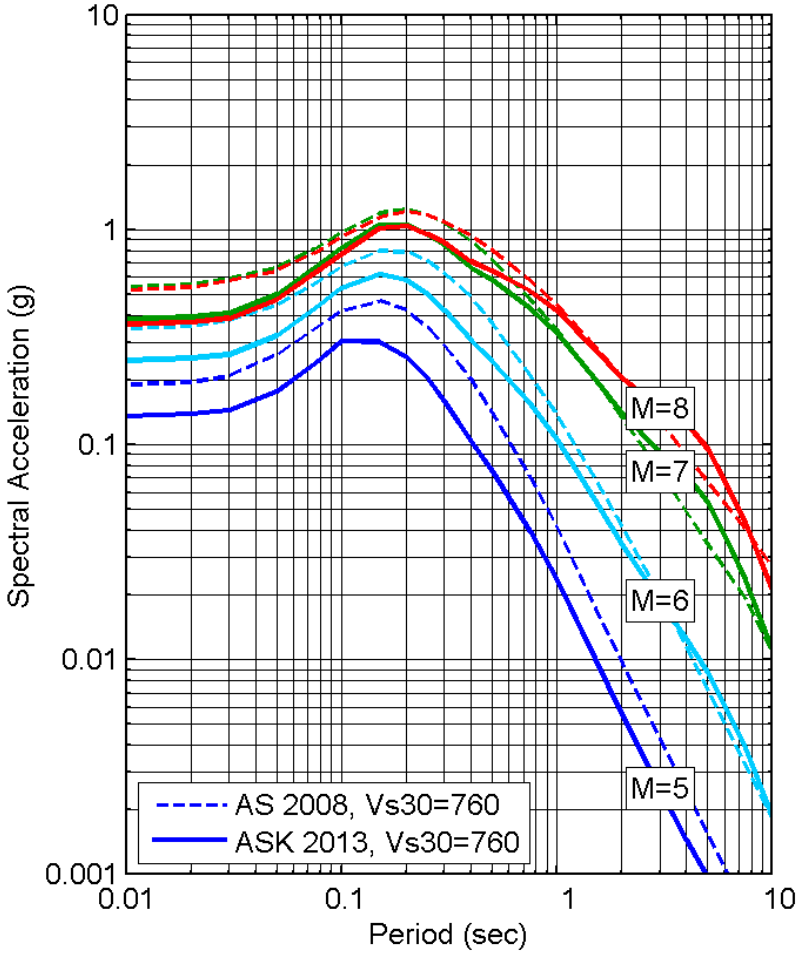

Figure 8.2(a) Comparison of the median spectral acceleration: SS, R_{JB} = 1 km, V_{S30} = 760 m/sec.

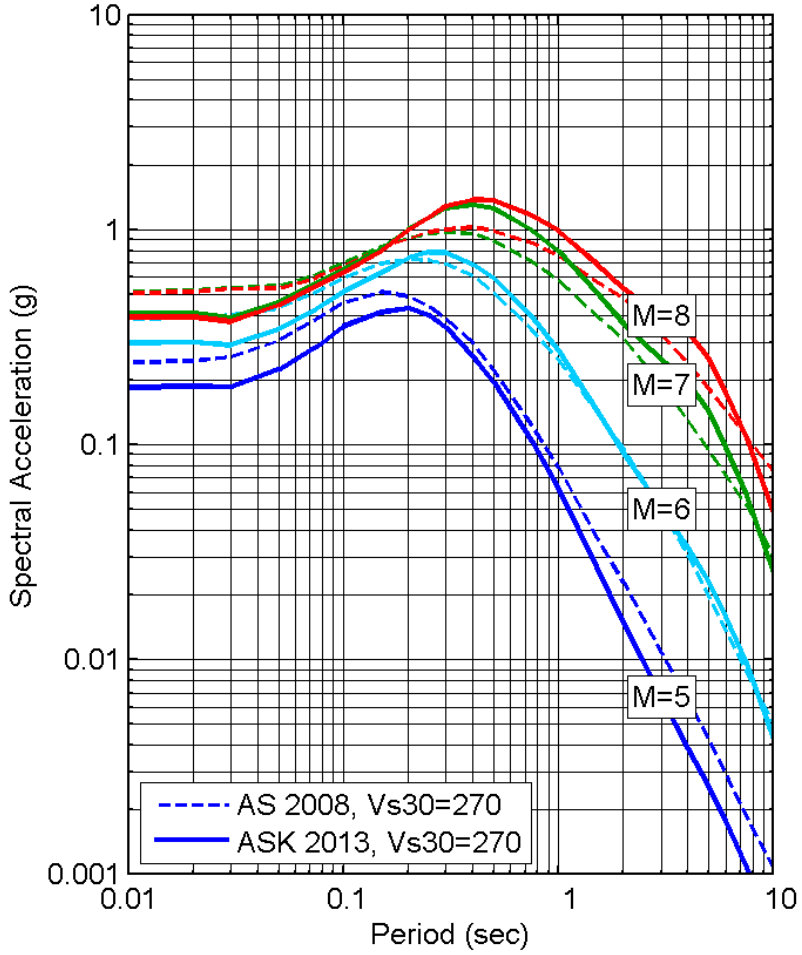

Figure 8.2(b) Comparison of the median spectral acceleration: SS, R_{JB} = 1 km, V_{S30} = 270 m/sec.

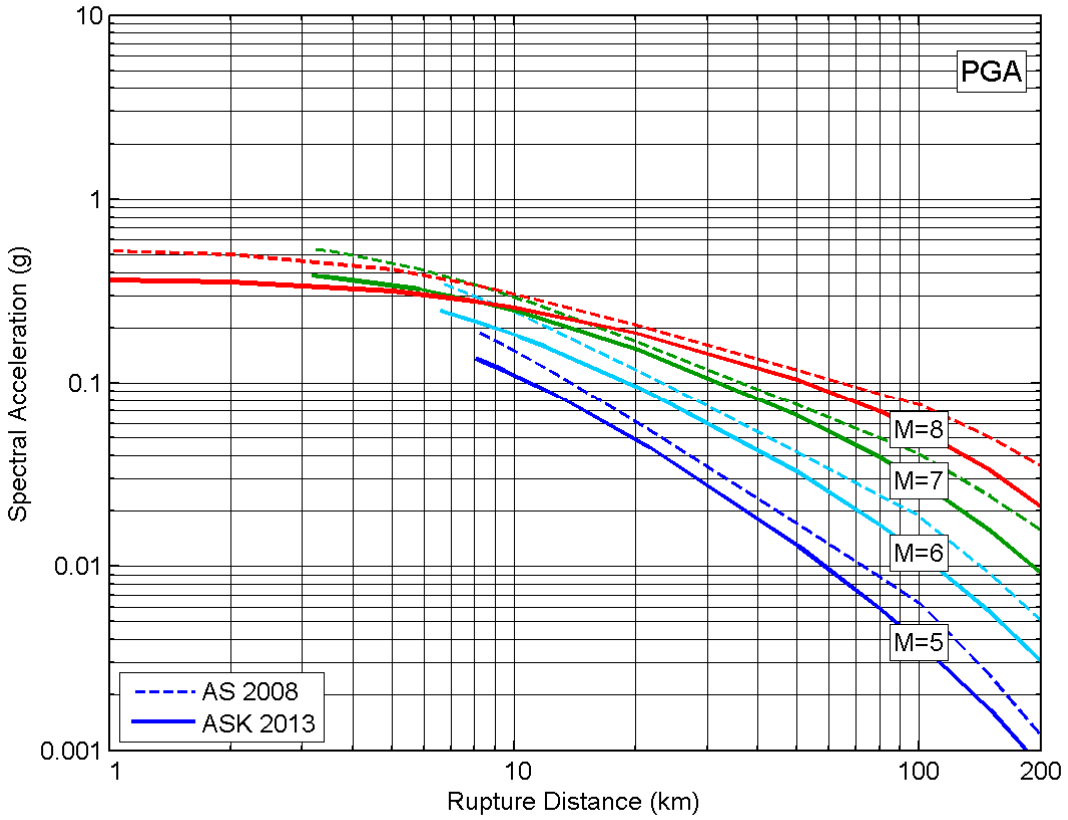

Figure 8.3(a) Comparison of the rupture distance scaling for a vertical strike slip at PGA.

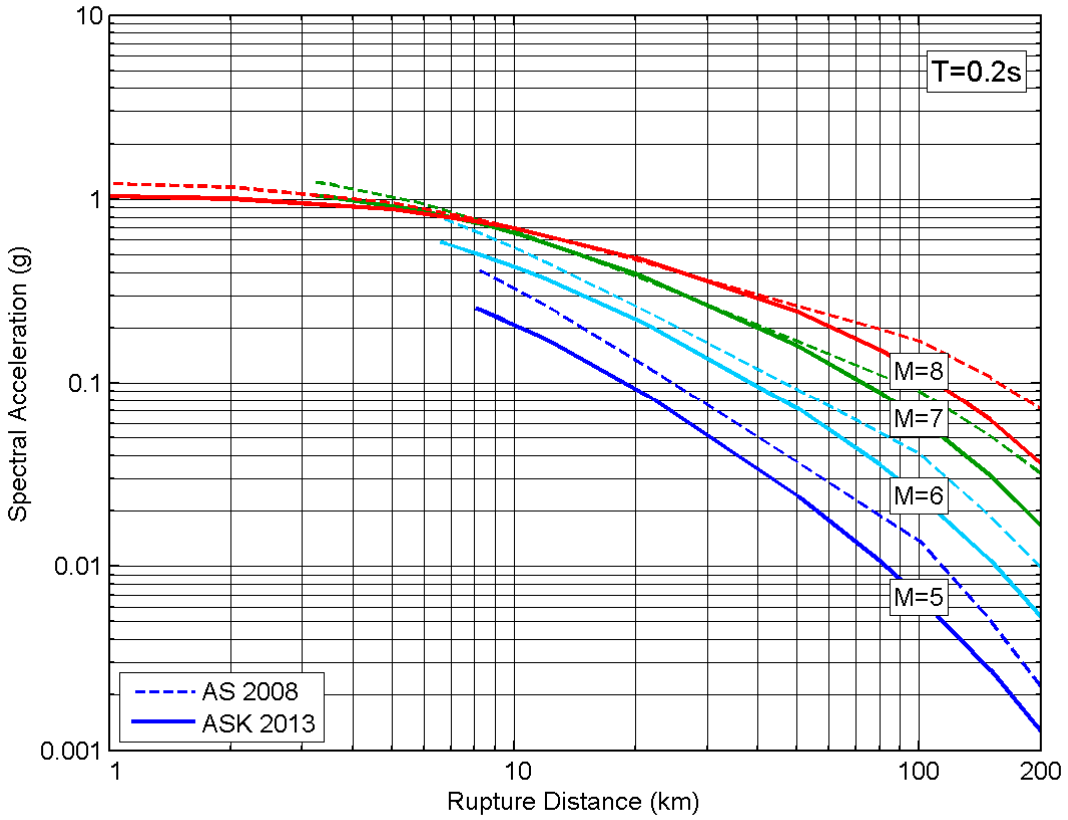

Figure 8.3(b) **Comparison of the rupture distance scaling for a vertical strike slip at T = 0.2 sec.**

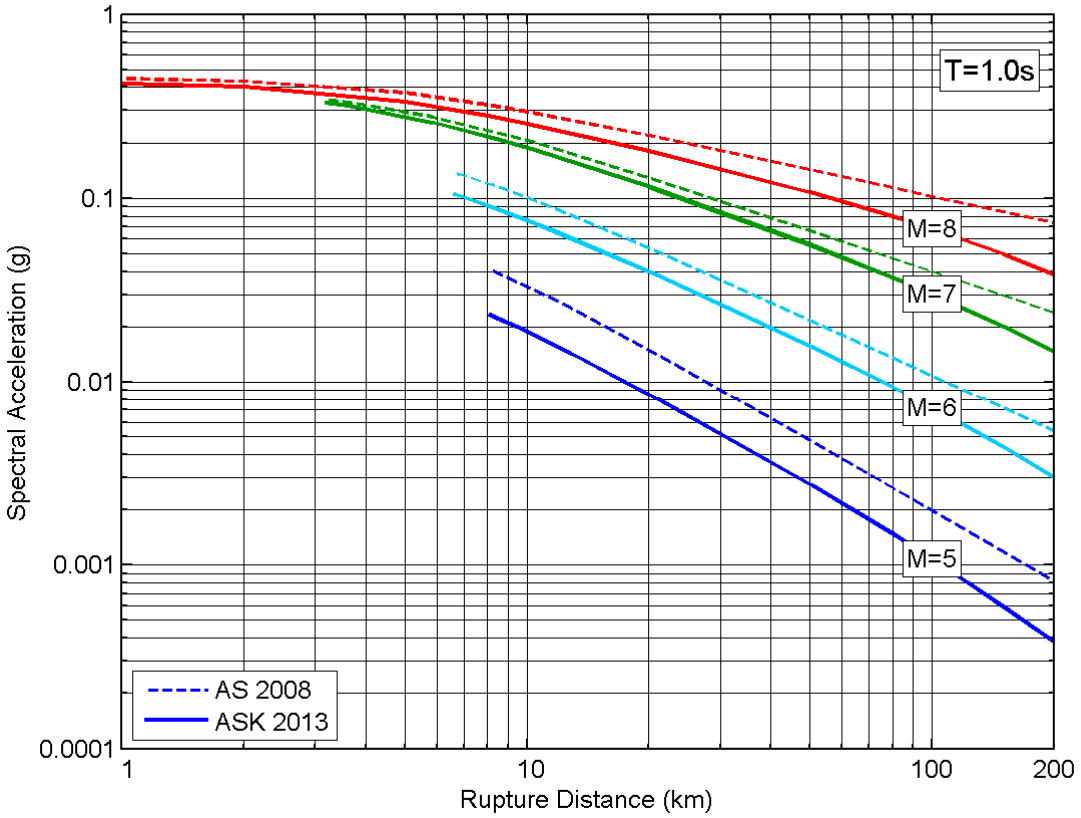

Figure 8.3(c) Comparison of the rupture distance scaling for a vertical strike slip at T = 1 sec.

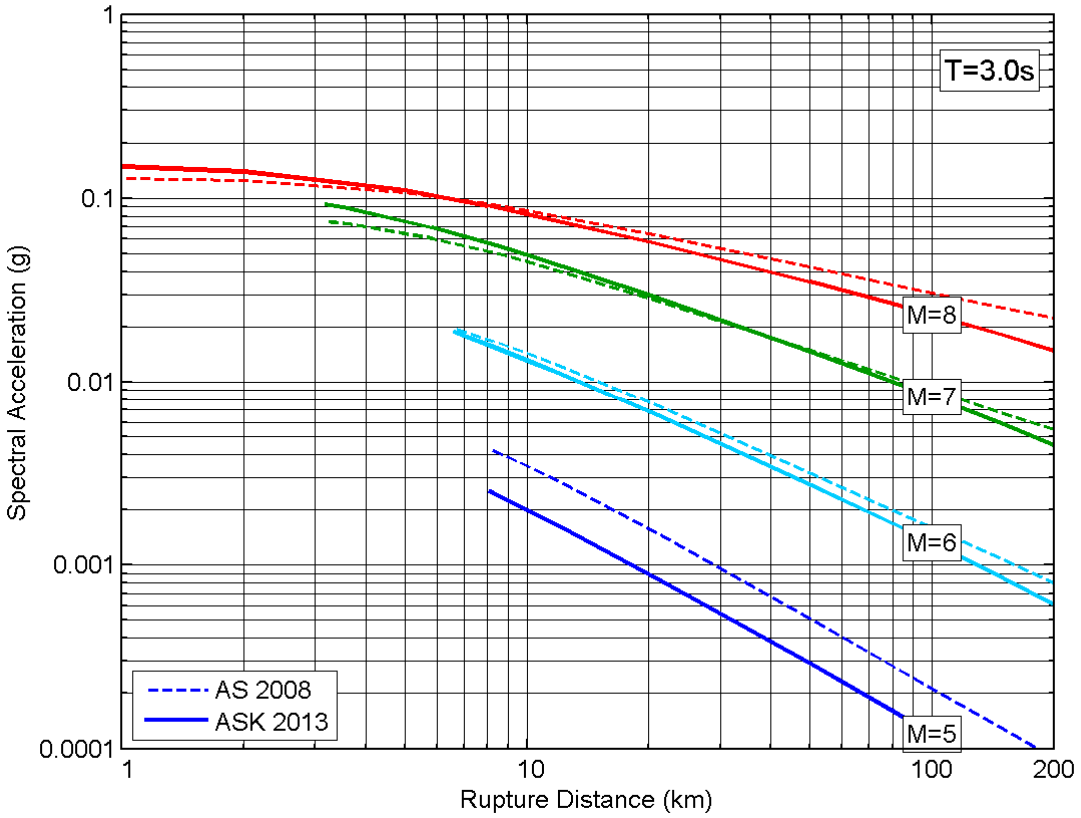

Figure 8.3(d) Comparison of the rupture distance scaling for a vertical strike slip at T = 3 sec.

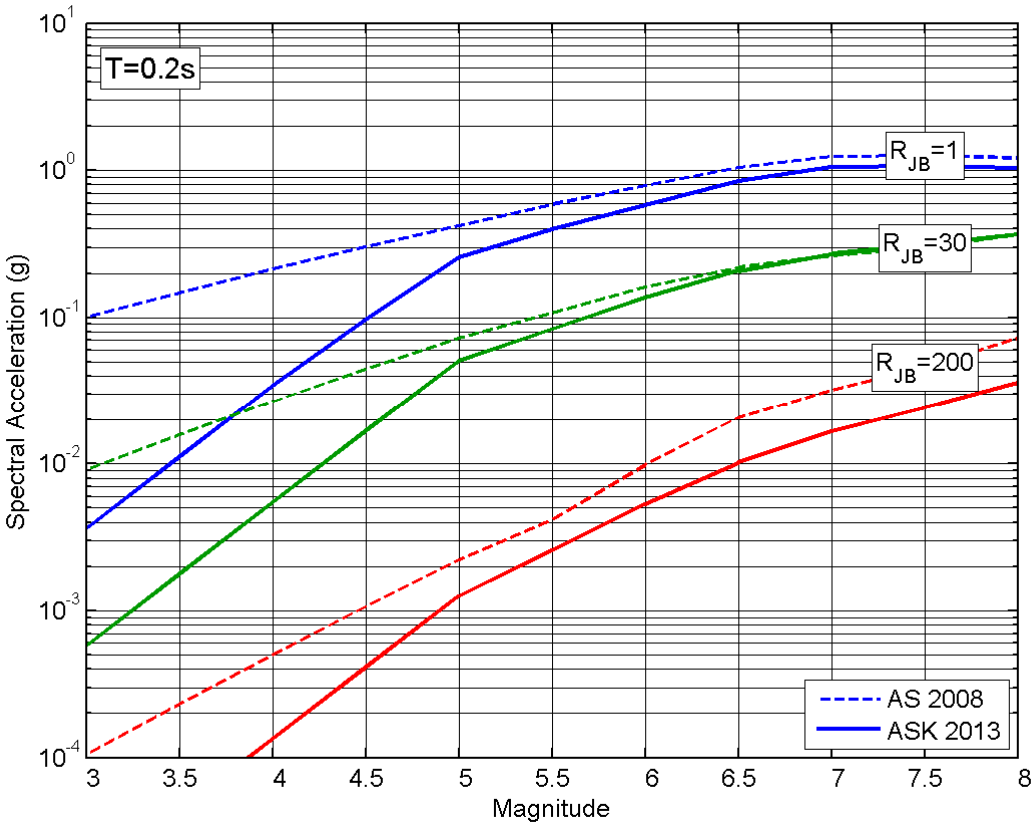

Figure 8.4(a) Comparison of the magnitude scaling for a vertical strike slip at T = 0.2 sec.

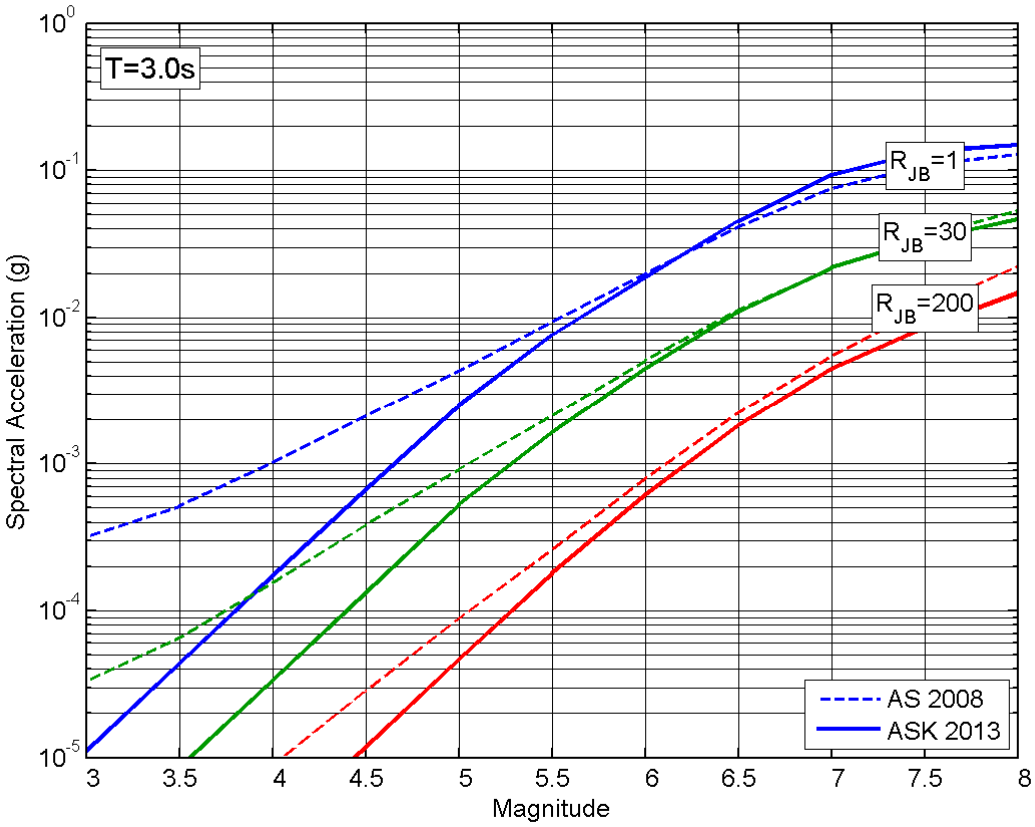

Figure 8.4(b) Comparison of the magnitude scaling for a vertical strike slip at *T* =3 sec.

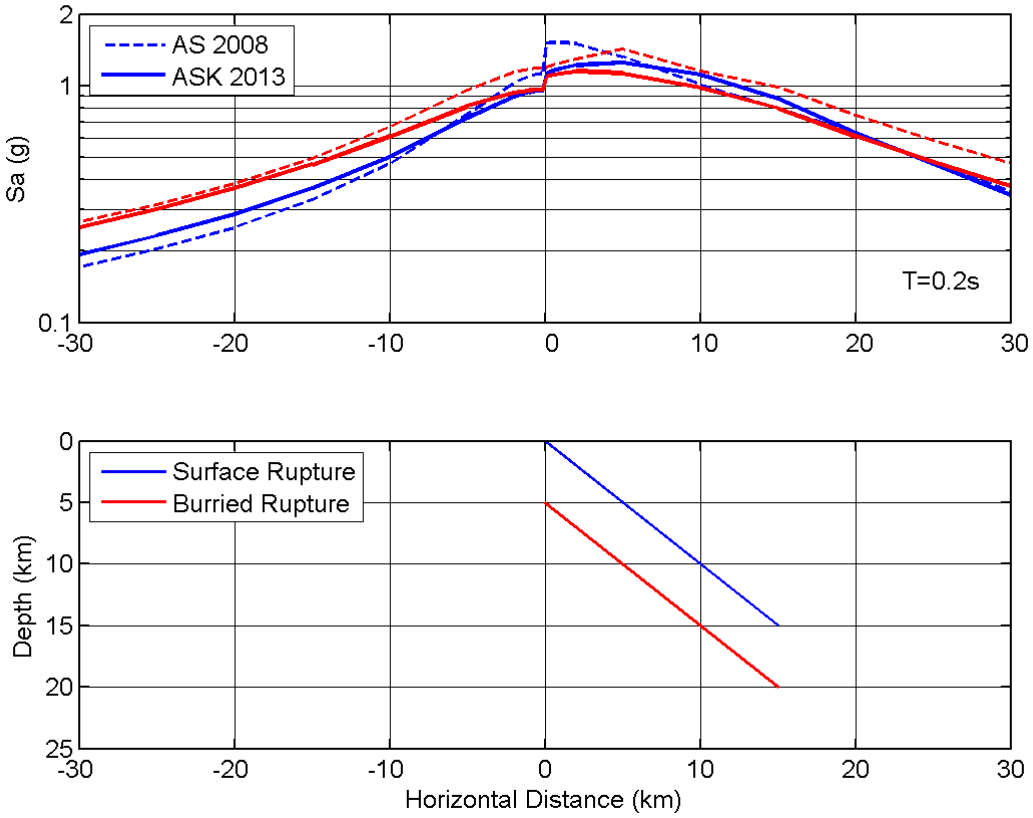

Figure 8.5 HW scaling for a M6.7 reverse fault with 45° dip at T= 0.2 sec.

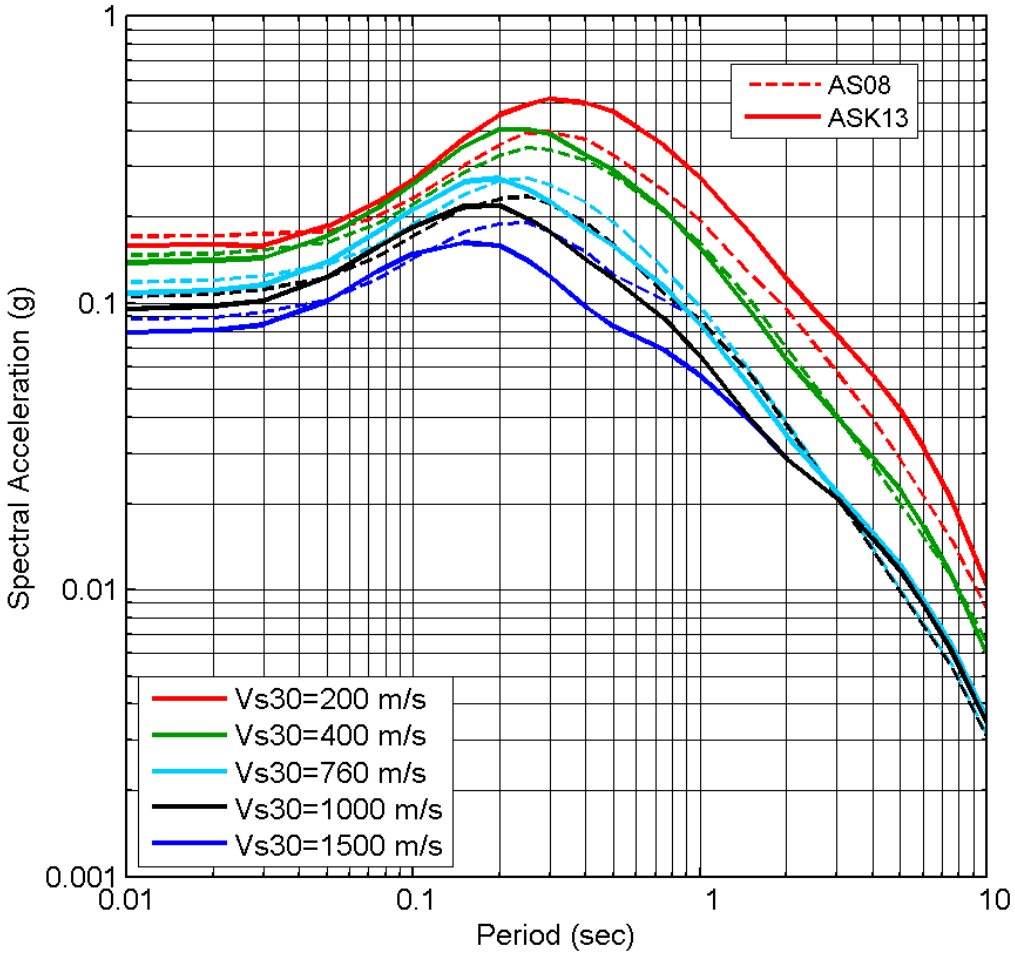

Figure 8.6 Example of V_{S30} scaling for a strike slip M7 at R_{rup}=30 km.

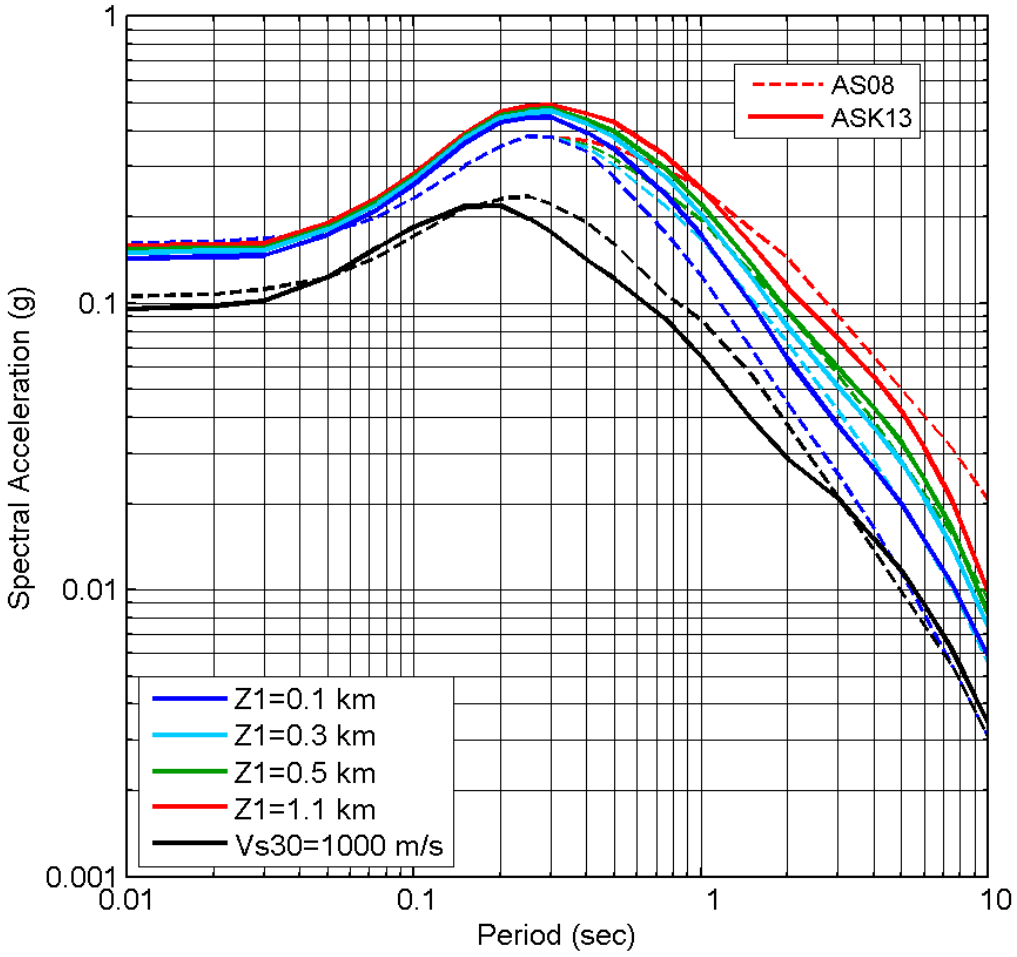

Figure 8.7 **Example of Z_1 scaling for a strike slip M7 at R_{rup} = 30 km and V_{S30} = 270 m/sec.**

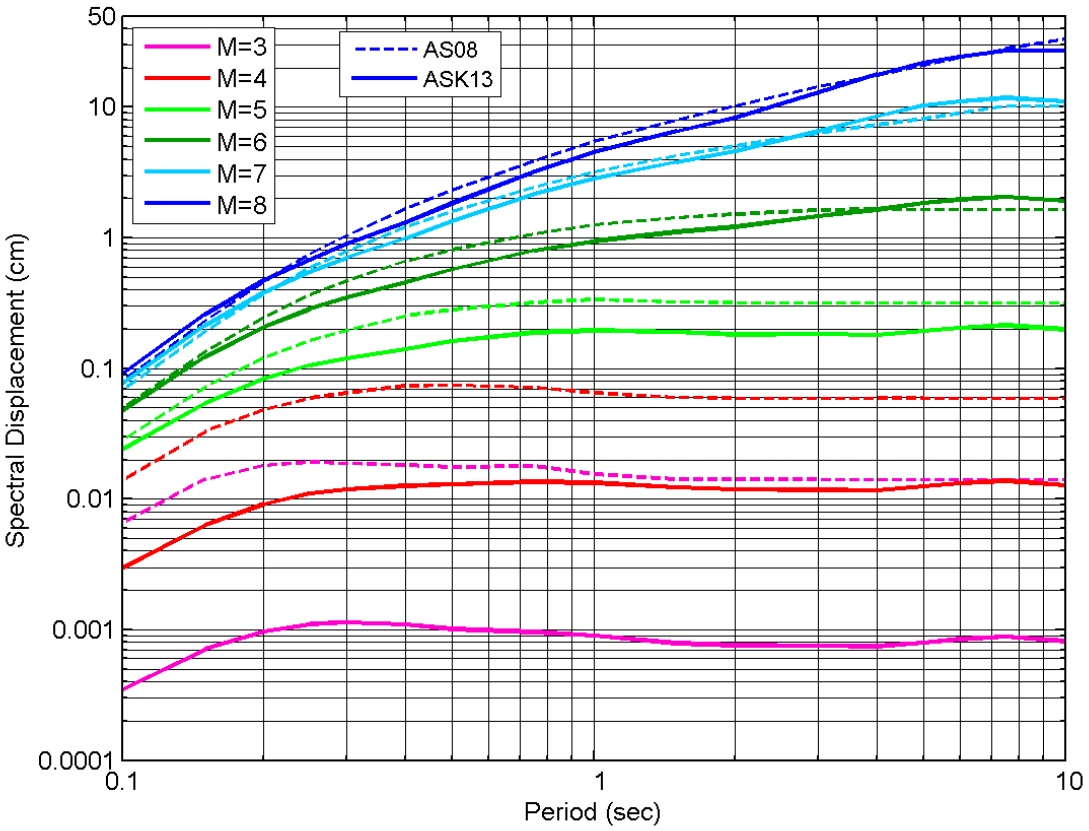

Figure 8.8 **Spectral displacements for a vertical strike slip fault at R_{JB} = 20 km and V_{S30} = 760 m/sec.**

REFERENCES

Abrahamson N.A., Youngs R.R. (1992). A stable algorithm for regression analyses using the random effects model, *Bull. Seismol. Soc. Am*., 82: 505−510.

Abrahamson N.A., Silva W.J. (2007). Abrahamson and Silva NGA ground motion relations for the geometric mean horizontal component of peak and spectral ground motion parameters, Final Report, Pacific Earthquake Engineering Research Center, University of California, Berkeley, CA.

Al Atik L., Abrahamson N.A. (2010). Nonlinear site response effects on the standard deviations of predicted ground motions*, Bull. Seismol. Soc. Am*., 100: 1288−1292.

Ancheta T.D., Darragh R.B., Stewart J.P., Seyhan E., Silva W.J., Chiou B., Wooddell K.E., Graves R.W., Kottke A.R., Boore D.M., Kishida T., Donahue J.L. (2013). PEER NGA-West2 database, *PEER Report No. 2013/03*, Pacific Earthquake Engineering Research Center, University of California, Berkeley, CA.

Baker J., Cornell C.A. (2006). Correlation of response spectral values for multi-component ground motions, *Bull. Seismol. Soc. Am.,* 96: 215−227.

Carlton B., Abrahamson N.A. (2013). Issues and approaches for implementing conditional mean spectra in practice. *Bull. Seismol. Soc. Am.,* submitted for publication.

Chiou B., Youngs R.R. (2013). Update to the Chiou and Youngs 2008 GMPE, *PEER Report No. 2013/07*, Pacific Earthquake Engineering Research Center, University of California, Berkeley, CA.

Collins N., Graves R.W., Somerville P. (2006). Revised analysis of 1D rock simulations for the NGA-E project, *Final Report*, Pacific Earthquake Engineering Research Center, University of California, Berkeley, CA.

Donahue J.L., Abrahamson N.A. (2013). Hanging-wall scaling using finite-fault simulations, PEER NGA-West2 database, *PEER Report No. 2013/14*, Pacific Earthquake Engineering Research Center, University of California, Berkeley, CA.

Geomatrix (1995). Seismic Design Mapping State of Oregon, Report for Oregon Department of Transportation, Salem, Oregon, January, 1995.

Kamai R., Abrahamson N.A., Silva W.J. (2013). Nonlinear horizontal site response for the NGA-West2 project, *PEER Report No. 2013/12*, Pacific Earthquake Engineering Research Center, University of California, Berkeley, CA.

Watson-Lamprey J. (2007). *Selection and Scaling of Ground Motion Time Series*, PhD Thesis, University of California, Berkeley, CA.

Wesson R. L, Frankel A. D., Mueller C. S., Harmsen S. C. (1999). Probabilistic seismic hazard maps of Alaska, USGS OFR 99-36.

Wooddell K.E., Abrahamson N.A. (2012). New earthquake classification scheme for mainshocks and aftershocks in the NGA-West2 ground motion prediction equations (GMPEs), *Proceedings, 15th World Conference on Earthquake Engineering*, Lisbon, Portugal.

Appendix A: Selected Earthquakes

EQID	Region	Mag	Class	CRJB (km)	Rake	Z_{TOR} (km)	Depth (km)	Dip	Number of Stations
25	1	6.19	1	0	0	0	10	90	4
30	1	6.61	1	0	83	0	13	45	22
35	1	5.2	1	0	0	18.13	21	72	3
39	1	4.7	2	1.81	-89	5.95	7.6	46	9
40	4	6.5	1	0	80	2.3	5.1	11.8	3
42	4	5.5	2	0.2	75	5.06	6	16	4
43	4	5.91	2	8.79	70	1	3.69	18.9	4
46	5	7.35	1	0	70	1	5.75	25	3
48	1	5.74	1	0	4	3.08	8	80	10
49	4	5.9	1	0	-80	1.28	6	64	3
50	1	6.53	1	0	0	0	9.96	80	32
51	1	5.01	2	0	0	7.26	9.5	90	16
53	1	5.8	1	0	20	7.06	12	85	6
54	1	5.42	2	10.75	19	11.38	14.5	70	7
55	1	5.19	1	0	10	10.79	13.6	70	5
56	1	6.06	1	0	-35	1.34	9	50	3
57	1	5.69	2	1.08	0	9	14	90	3
58	1	5.91	2	2.34	-11	12	16	50	4
59	1	5.7	2	0	28	3.57	5	50	4
61	1	5.94	2	5.24	-28	10.58	14	50	5
62	1	4.73	2	5	0	4.32	6	75	6
63	1	4.8	2	5.52	0	4.22	6	75	7
64	1	6.33	1	0	0	4	11	90	4
65	1	4.85	2	0	0	6.3	7.63	67.5	7
68	4	6.9	1	0	-90	0	9.5	60	12
69	4	6.2	2	2.41	-90	1	7	70	10
70	4	4.7	2	0	-90	13.12	15	65	6
73	1	5.9	2	21.03	0	2	2.3	90	6
76	1	6.36	1	0	90	3.4	4.6	30	45
77	1	5.09	2	0	74	10.55	12	44	19
78	1	5.38	2	3.62	90	0	2.4	50	3
79	1	5.18	2	0.15	64	6.43	9	41	11
80	1	5.77	2	0	78	5.41	7.4	38	11
88	2	5.1	2	0	-65	7.56	10	51	3
90	1	6.19	1	0	0	0.5	8.5	90	23
91	4	5.8	1	0	-84	8	14	48	8
97	4	6.76	1	0	90	2	8	25	3

101	1	6.06	1	0	30	4	11	46	33
102	1	5.77	-1	0	20	2	6.7	90	5
103	1	6.19	1	0	-17	4	10	55	11
104	1	5.65	2	4.01	0	2.32	5	90	3
113	1	5.99	1	0	30	14.5	14.6	30	111
114	1	5.27	2	0	40	10.98	13.3	70	69
116	1	6.54	1	0	0	0	9	90	11
118	1	6.93	1	0	40	3.85	17.48	70	77
120	12	6.2	1	0	90	2.38	6	30	5
123	1	7.01	1	0	75	5.2	9.5	14	13
125	1	7.28	1	0	0	0	7	90	76
126	1	6.46	2	35.4	-10	3.93	13	85	43
127	1	6.69	1	0	77	5	17.5	40	149
129	10	6.9	1	0	0	0.2	17.9	85	22
130	11	6.4	1	0	-85	2.8	12.64	43	3
136	5	7.51	1	0	0	0	16	-80	17
137	3	7.62	1	0	55	0	8	30	394
138	5	7.14	2	15.68	-2	0	14	65	15
143	1	5.63	1	0	5	0.79	4.49	77	3
144	5	7.37	1	0	-9	0	16	88	4
145	1	5.61	1	0	82	10	12	50	9
146	1	6.1	-1	23.31	0	5	12.4	90	5
147	1	6.05	2	0	90	3.82	6	40	19
148	1	5.2	2	0	90	5.37	6	40	7
149	1	5.93	2	4.28	32	7.26	9.83	40	8
150	1	5.13	-1	7.21	35	9.86	11.34	54	7
151	1	5.28	2	0.73	74	10.99	13.09	40	59
152	1	5.65	1	0	-70	6.36	12	70	5
157	1	5.17	1	0	-9	6.82	9.13	85	3
158	1	7.13	1	0	1	0	14.8	82	107
160	1	5	1	0	10	7.76	10.12	90	15
161	1	4.53	1	0	11	7.91	9.1	90	42
162	1	5.17	1	0	-7	0.01	3.95	81	10
163	1	4.92	1	0	-32	12.48	15.2	78	94
164	1	5.7	1	0	-17	6.91	10	59	11
165	1	5.31	1	0	-23	4.2	7	74	8
166	1	4.9	1	0	-3	7.86	10.12	84	29
167	1	4.27	1	0	13	6.02	7	88.3	101
169	2	7.9	1	0	9	0	8.9	82	4
170	1	4.92	1	0	-6	4.86	6.3	72	39
171	3	5.9	2	0	80	6.47	8	50	182
172	3	6.2	2	0	80	6.7	7.8	10	227
173	3	6.2	2	0	15	1.5	18	89	234
174	3	6.2	2	4.99	80	7.74	10	70	228
175	3	6.3	2	0	80	10	16	30	270
176	10	6.61	1	0	0	0.5	12.5	90	169
177	1	6.5	1	0	83	2	8.5	52	28
178	5	6.6	1	0	-3	1.4	6	85.5	4
179	1	6	1	0	-5	2.5	8.1	89	90
180	10	6.63	1	0	87	4.02	10.6	47	530
189	4	4.7	1	0	0	6.25	8	90	3
191	4	4	2	9.82	-90	3.32	4	55	3
199	4	5.5	2	0.49	90	10.86	12	40	3

202	4	6	1	0	0	9.47	15	90	4
224	4	5.6	1	0	-90	5.65	9	55	6
233	4	5.7	-1	0	-90	3.98	7	55	7
234	4	6	1	0	-90	0	6	55	9
235	4	5.3	2	0	-90	3.58	6	55	4
237	4	5.5	2	0	-90	4.2	7	55	9
241	4	5.2	2	10.59	-90	5.01	6	55	5
243	4	5.6	2	8.84	-90	3.55	7	55	11
251	4	5.1	2	16.31	-90	4.14	6	55	4
254	4	5.7	1	0	-15	12	21.4	86	3
262	8	7.1	1	0	88	3.61	7	14	6
274	4	6.3	1	0	-82	0.8	9.27	48	16
275	4	5.6	2	0	-46	9.98	15.1	53	19
276	4	5.4	2	6.88	-81	11.88	15.4	46	16
277	9	7.9	1	0	70	0	10.04	-35	124
278	10	6.8	1	0	90	3.12	9	36	613
279	10	6.9	1	0	76	0.71	6.5	40	367
280	1	7.2	1	0	0	0.61	5.5	50	324
281	7	7	1	0	0	0	10.9	82.2	36
309	9	4.8	2	0	70	11.97	13	35	11
319	9	5.2	2	11.44	70	17.46	19.1	35	12
329	9	4.9	2	0.88	15	0	1.8	65	11
346	7	6.2	2	23.68	45	0.5	6	67	36
1001	1	5.45	1	0	0	4.26	7.49	87	141
1002	1	5.39	1	0	34	12.38	14.89	66	193
1003	1	5.2	1	0	8	13.18	15.48	58	112
1004	1	5.1	-1	0.78	-5	16.23	18.65	66	5
1005	1	5.06	1	0	-23	6.89	9.33	79	14
1006	1	5.03	1	0	7	4.79	7.3	82	96
1007	1	4.88	1	0	32	15.79	17.5	64	109
1011	1	4.7	1	0	-22	10.11	11.59	83	168
1012	1	4.69	1	0	46	8.49	9.25	28	99
1013	1	4.6	1	0	5	8.77	10.22	76	12
1014	1	4.59	1	0	-52	9.49	10.66	35	108
1015	1	4.18	1	0	79	10.43	11.15	55	101
1016	1	4.34	1	0	20	8.55	9.56	56	95
1018	1	4.45	-1	34.82	15	13.86	14.8	60	235
1019	1	4.66	1	0	83	6.97	8.04	42	170
1020	1	4.26	1	0	-4	9.13	10.06	83	82
1021	1	4.3	1	0	-25	2.59	3.36	78	130
1023	1	4.5	1	0	-2	5.8	6.99	69	94
1024	1	4.4	1	0	1	5.93	6.96	74	29
1025	1	4.42	1	0	16	11.98	12.83	60	86
1026	1	4.39	1	0	28	4.8	5.9	86	28
1027	1	4.78	1	0	-14	4.3	5.97	81	46
1028	1	4.73	1	0	10	8.58	10.02	68	189
1029	1	4.51	1	0	-74	8.45	9.4	30	16
1030	1	4.3	1	0	-14	6.36	7.26	83	62
1031	1	4.25	1	0	-11	2.5	3.69	80	73
1032	1	4.2	1	0	8	6.62	7.51	89	66
1033	1	4.3	1	0	14	2.4	3.44	89	48
1034	1	4.5	1	0	-22	7.81	8.94	89	47
1035	1	4.26	1	0	85	7.45	8.03	35	97

1036	1	4.24	1	0	-13	6.22	7.29	83	12
1038	1	4.27	1	0	80	5.8	6.22	23	74
1039	1	4.37	-1	36.69	-11	14.81	15.83	83	37
1040	1	4.42	1	0	7	3.35	4.57	72	21
1042	1	4.42	1	0	26	15.84	16.97	87	36
1043	1	4.12	1	0	-5	2.37	3.46	84	70
1044	1	4.14	1	0	2	4.85	5.73	77	66
1045	1	4.2	1	0	-4	3.22	4.13	82	150
1046	1	4.23	1	0	-3	13.41	14.38	90	95
1048	1	4.27	1	0	-18	3.04	4.06	87	30
1049	1	4	-1	34	-10	13.32	14.03	72	60
1050	1	4.18	2	31.72	2	7.61	8.48	84	104
1051	1	4.1	1	0	0	12.56	13.32	86	116
1052	1	4.11	1	0	-16	11.37	12.27	87	66
1053	1	4.34	1	0	-30	5.68	6.86	51	42
1054	1	4.26	1	0	8	6.82	7.7	87	74
1055	1	3.81	2	39.96	-4	2.32	2.88	85	18
1056	1	4.02	1	0	6	12.15	12.81	54	44
1057	1	4.11	1	0	-89	2.93	4.03	82	32
1058	1	4.41	1	0	8	8.99	10.16	77	24
1059	1	4	1	0	-9	2.77	3.48	89	92
1060	1	4	1	0	-2	9.23	10.02	77	100
1061	1	4.11	1	0	68	7.59	8.33	44	40
1062	1	4.06	1	0	-5	9.65	10.53	83	58
1063	1	4.11	1	0	15	11.74	12.56	68	23
1064	1	4.19	2	26.1	23	8.64	9.49	74	94
1065	1	4.2	1	0	36	8.05	8.93	63	45
1066	1	3.9	1	0	13	13.35	13.61	23	91
1067	1	4.29	1	0	-10	10.1	10.89	71	19
1068	1	4.06	1	0	29	6.43	7.17	89	48
1069	1	3.9	1	0	-17	7.25	7.86	87	77
1070	1	3.96	1	0	9	4.73	5.49	84	81
1071	1	3.9	1	0	-32	10.97	11.87	83	10
1072	1	3.97	1	0	2	11.05	11.87	82	36
1073	1	3.88	1	0	70	7.58	7.9	25	20
1074	1	4.06	1	0	15	10.69	11.36	80	33
1075	1	4.17	1	0	-19	4.28	4.96	85	91
1076	1	3.79	1	0	84	10.59	11.02	40	66
1077	1	4.15	2	32.11	30	11.74	12.65	80	19
1079	1	3.7	-1	8.46	-5	11.12	11.55	89	92
1080	1	3.8	2	3.39	0	6.28	6.78	85	19
1081	1	3.8	-1	11.34	-2	4.99	5.57	66	42
1082	1	3.81	1	0	-3	9.45	10.08	87	31
1083	1	3.69	1	0	2	9.65	10.11	77	21
1084	1	4.02	2	34.78	-2	6.54	7	40	10
1085	1	3.94	1	0	5	19.54	20.24	85	50
1086	1	4.19	1	0	12	7.94	8.88	65	69
1087	1	3.75	1	0	-25	3.84	4.26	53	36
1088	1	4.14	1	0	-14	5.52	6.47	85	40
1089	1	4.05	1	0	-13	7.05	7.82	69	41
1090	1	4.01	1	0	-34	4.77	5.76	86	31
1091	1	3.78	1	0	23	14.5	14.93	59	48
1093	1	4.11	1	0	4	8.24	9.05	87	32

1094	1	3.9	2	5.91	-5	9.22	9.91	80	60
1095	1	3.84	1	0	-1	7.95	8.59	90	73
1096	1	3.58	1	0	-36	5.75	6.48	84	90
1097	1	3.67	1	0	-4	7.58	8.08	60	49
1098	1	3.68	-1	37.34	15	5.56	6.07	87	79
1100	1	3.7	2	27.43	4	0.9	1.33	67	31
1101	1	3.7	1	0	9	6.49	6.97	51	112
1102	1	3.7	1	0	0	5.85	6.53	84	19
1103	1	3.74	1	0	5	7.29	7.88	75	73
1104	1	3.52	1	0	6	4.74	5.22	88	18
1105	1	3.56	1	0	0	14.19	14.52	45	14
1106	1	3.97	1	0	-3	5.14	5.84	67	9
1107	1	3.78	1	0	0	5.16	5.86	68	48
1108	1	3.9	1	0	-54	11.35	11.86	36	82
1110	1	3.86	2	37.37	6	13.46	14.18	74	69
1111	1	3.74	1	0	57	10.91	11.07	17	26
1112	1	3.87	1	0	10	17.8	18.5	60	34
1113	1	3.99	1	0	-3	14.31	15	63	89
1114	1	3.88	1	0	7	8.42	9.01	74	18
1115	1	3.77	1	0	-17	5.87	6.32	50	16
1116	1	3.68	1	0	-5	2.3	2.73	65	14
1118	1	4.06	1	0	9	9.16	9.76	71	37
1119	1	3.87	1	0	5	8.07	8.76	89	40
1120	1	3.59	1	0	34	8.39	8.88	83	25
1121	1	3.81	1	0	-1	12.6	13.18	72	32
1122	1	3.81	1	0	-4	5.04	5.73	77	27
1123	1	3.6	1	0	-62	8.35	8.93	61	73
1124	1	3.57	1	0	-20	5.34	5.85	90	45
1125	1	3.6	1	0	-3	4.51	5.01	64	109
1126	1	3.6	2	6.24	87	4.55	4.91	55	19
1127	1	3.96	1	0	-7	11.62	12.34	79	34
1128	1	3.64	1	0	22	1.65	2.16	71	75
1129	1	3.73	1	0	-21	2.21	2.69	88	30
1130	1	3.71	2	29.75	65	16.34	16.7	39	85
1131	1	3.58	-1	33.38	-1	14.82	15.13	45	54
1132	1	3.64	1	0	41	12.31	12.78	59	66
1133	1	3.63	1	0	-16	12.63	13.11	80	32
1134	1	3.64	1	0	-4	8.29	8.69	89	68
1135	1	3.74	1	0	21	12.2	12.93	88	61
1137	1	3.5	1	0	-28	1.84	2.39	86	75
1138	1	3.5	1	0	-18	4.57	5.08	84	106
1139	1	3.61	1	0	70	12.21	12.48	32	60
1140	1	3.69	1	0	-1	9.1	9.69	58	84
1141	1	3.79	1	0	-72	15.32	15.93	44	33
1142	1	3.73	1	0	-13	15.71	16.28	81	44
1143	1	3.72	-1	26.44	-5	6.88	7.49	64	44
1145	1	3.49	1	0	-7	9.29	9.68	79	51
1146	1	3.6	1	0	-3	7.07	7.54	84	66
1147	1	3.63	1	0	-15	8.92	9.56	86	42
1148	1	3.59	1	0	23	6.68	7.01	41	27
1149	1	3.45	1	0	63	9.3	9.54	37	26
1150	1	3.43	1	0	54	5.81	6.09	44	31
1151	1	3.52	2	27.89	-48	4.32	4.64	27	46

1152	1	3.53	-1	2.92	-15	13.55	13.86	50	90
1153	1	3.55	-1	1.28	67	11.38	11.64	39	24
1154	1	3.53	1	0	0	5.84	6.28	72	69
1156	1	3.56	2	7.13	-50	10.06	10.56	53	49
1157	1	3.56	-1	39.9	-5	10.2	10.84	88	43
1158	1	3.66	1	0	4	14.83	15.28	67	10
1159	1	3.73	1	0	39	7.5	7.92	74	27
1160	1	3.4	1	0	13	6.87	7.21	71	64
1161	1	3.4	1	0	-13	8.12	8.47	75	45
1162	1	3.59	-1	16.24	3	2.66	3.02	74	15
1163	1	3.62	-1	2.36	-8	8.53	9.07	87	55
1166	1	3.4	1	0	42	10.41	10.65	44	45
1167	1	3.52	1	0	55	9.48	9.73	41	37
1168	1	3.47	1	0	-72	6.87	7.37	74	47
1169	1	3.59	1	0	22	6.54	7	83	12
1170	1	3.41	1	0	-5	8.7	9.08	90	103
1171	1	3.63	-1	25.84	-89	7.31	7.89	57	34
1172	1	3.08	-1	21.99	63	11.14	11.33	43	22
1174	1	3.25	1	0	68	12.98	13.12	25	25
1175	1	3.14	1	0	26	7.47	7.73	74	25
1176	1	3.14	1	0	-24	6.46	6.77	80	33
1178	1	4.04	-1	0.22	2	8.64	9.44	76	28
1182	1	5	-1	0.62	-3	5.58	7.41	86	25
1186	1	5.19	1	0	-5	6.73	9.42	82	37
1188	1	4.08	-1	0.74	-5	6.95	7.66	74	19
1190	1	4.2	1	0	-13	7.85	8.83	78	30
1193	1	3.47	1	0	2	8.89	9.15	35	10
1194	1	3.05	-1	3.53	-6	11.16	11.46	82	22
1195	1	3.34	1	0	-3	10.73	11.15	68	27
1202	1	4.17	1	0	4	9.58	10.38	87	17
1203	1	3.54	2	0.66	1	8.55	9.13	84	4
1204	1	3.68	1	0	5	5.97	6.53	82	4
1205	1	3.45	-1	3.93	0	7.59	8.05	89	6
1206	1	4.48	1	0	-10	8.3	9.52	88	7
1207	1	3.27	2	0	10	10.63	10.96	80	6
1208	1	4.01	2	11.35	-8	8.25	9.13	85	26
1209	1	3.4	1	0	69	12.36	12.65	45	4
1210	1	3.48	1	0	-10	6.45	6.94	85	8
1211	1	3.3	2	15.23	19	9.92	10.32	86	5
1212	1	3.43	1	0	-6	6.86	7.18	86	5
1213	1	3.4	1	0	6	9.34	9.77	87	7
1214	1	3.3	2	21.67	-40	7.03	7.53	80	26
1215	1	3.5	1	0	6	5.92	6.36	67	40
1216	1	3.69	1	0	52	7.02	7.42	77	40
1217	1	3.2	-1	6.52	-1	8.29	8.64	83	29
1218	1	3.49	1	0	0	5.65	6.13	80	13
1219	1	3.5	1	0	39	7.61	7.93	52	33
1220	1	3.39	2	13.33	10	5.89	6.27	70	20
1221	1	4.05	1	0	6	10.08	11.01	76	143
1222	1	3.73	2	0.48	56	9.19	9.63	55	34
1223	1	3.37	-1	38.69	11	9.36	9.78	87	22
1224	1	3.22	2	17.72	70	9.57	9.86	55	19
1226	1	4.51	1	0	71	4.83	5.56	49	7

1228	1	3.92	2	0.61	89	5.03	5.44	49	4
1230	1	4.07	1	0	60	5.46	6.03	45	7
1231	1	3.5	2	28.72	50	3.98	4.38	60	6
1233	1	3.48	2	1.77	83	4.13	4.38	45	3
1234	1	3.9	2	0.32	58	5.5	5.81	27	5
1235	1	3.63	2	5.1	50	7.14	7.32	20	6
1236	1	3.67	2	5.18	60	7	7.3	35	5
1237	1	3.16	-1	4.94	-45	3.73	4.1	90	5
1239	1	3.36	1	0	-10	6.98	7.34	90	4
1241	1	4	-1	22.95	9	5.56	6.38	80	13
1243	1	3.6	1	0	8	5.97	6.35	73	19
1245	1	3.54	-1	1.47	-15	5.32	5.8	90	15
1246	1	3.7	-1	0.91	7	5.55	6.1	79	15
1247	1	3.9	1	0	-9	4.28	5	71	19
1248	1	3.8	1	0	-2	4.28	4.74	69	17
1250	1	3.8	1	0	-2	3.84	4.45	80	13
1251	1	3.5	2	0.84	-9	5.2	5.68	78	15
1258	1	3.8	-1	4.58	-2	7.01	7.59	76	18
1259	1	3.8	2	1.18	17	13.5	14.01	56	15
1260	1	3.64	2	0	-17	13.09	13.63	80	17
1261	1	3.09	2	0.65	-26	12.87	13.11	87	15
1264	1	3.43	-1	32.61	-14	5.36	5.77	73	52
1265	1	3.6	0	-999	-3	7.92	8.47	88	36
1266	1	3.5	0	-999	60	4.15	4.46	45	27

PEER REPORTS

PEER reports are available as a free PDF download from http://peer.berkeley.edu/publications/peer_reports_complete.html. Printed hard copies of PEER reports can be ordered directly from our printer by following the instructions at http://peer.berkeley.edu/publications/peer_reports.html. For other related questions about the PEER Report Series, contact the Pacific Earthquake Engineering Research Center, 325 Davis Hall mail code 1792, Berkeley, CA 94720. Tel.: (510) 642-3437; Fax: (510) 665-1655; Email: peer_editor@berkeley.edu

PEER 2013/04 *Update of the AS08 Ground-Motion Prediction Equations Based on the NGA-West2 Data Set.* Norman A. Abrahamson, Walter J. Silva, and Ronnie Kamai. May 2013.

PEER 2013/03 *PEER NGA-West2 Database.* Timothy D. Ancheta, Robert B. Darragh, Jonathan P. Stewart, Emel Seyhan, Walter J. Silva, Brian S.J. Chiou, Katie E. Wooddell, Robert W. Graves, Albert R. Kottke, David M. Boore, Tadahiro Kishida, and Jennifer L. Donahue. May 2013.

PEER 2013/02 *Hybrid Simulation of the Seismic Response of Squat Reinforced Concrete Shear Walls.* Catherine A. Whyte and Bozidar Stojadinovic. May 2013.

PEER 2013/01 *Housing Recovery in Chile: A Qualitative Mid-program Review.* Mary C. Comerio. February 2013.

PEER 2012/08 *Guidelines for Estimation of Shear Wave Velocity.* Bernard R. Wair, Jason T. DeJong, and Thomas Shantz. December 2012.

PEER 2012/07 *Earthquake Engineering for Resilient Communities: 2012 PEER Internship Program Research Report Collection.* Heidi Tremayne (Editor), Stephen A. Mahin (Editor), Collin Anderson, Dustin Cook, Michael Erceg, Carlos Esparza, Jose Jimenez, Dorian Krausz, Andrew Lo, Stephanie Lopez, Nicole McCurdy, Paul Shipman, Alexander Strum, Eduardo Vega. December 2012.

PEER 2012/06 *Fragilities for Precarious Rocks at Yucca Mountain.* Matthew D. Purvance, Rasool Anooshehpoor, and James N. Brune. December 2012.

PEER 2012/05 *Development of Simplified Analysis Procedure for Piles in Laterally Spreading Layered Soils.* Christopher R. McGann, Pedro Arduino, and Peter Mackenzie–Helnwein. December 2012.

PEER 2012/04 *Unbonded Pre-Tensioned Columns for Bridges in Seismic Regions.* Phillip M. Davis, Todd M. Janes, Marc O. Eberhard, and John F. Stanton. December 2012.

PEER 2012/03 *Experimental and Analytical Studies on Reinforced Concrete Buildings with Seismically Vulnerable Beam-Column Joints.* Sangjoon Park and Khalid M. Mosalam. October 2012.

PEER 2012/02 *Seismic Performance of Reinforced Concrete Bridges Allowed to Uplift during Multi-Directional Excitation.* Andres Oscar Espinoza and Stephen A. Mahin. July 2012.

PEER 2012/01 *Spectral Damping Scaling Factors for Shallow Crustal Earthquakes in Active Tectonic Regions.* Sanaz Rezaeian, Yousef Bozorgnia, I. M. Idriss, Kenneth Campbell, Norman Abrahamson, and Walter Silva. July 2012.

PEER 2011/10 *Earthquake Engineering for Resilient Communities: 2011 PEER Internship Program Research Report Collection.* Eds. Heidi Faison and Stephen A. Mahin. December 2011.

PEER 2011/09 *Calibration of Semi-Stochastic Procedure for Simulating High-Frequency Ground Motions.* Jonathan P. Stewart, Emel Seyhan, and Robert W. Graves. December 2011.

PEER 2011/08 *Water Supply in regard to Fire Following Earthquake.* Charles Scawthorn. November 2011.

PEER 2011/07 *Seismic Risk Management in Urban Areas. Proceedings of a U.S.-Iran-Turkey Seismic Workshop.* September 2011.

PEER 2011/06 *The Use of Base Isolation Systems to Achieve Complex Seismic Performance Objectives.* Troy A. Morgan and Stephen A. Mahin. July 2011.

PEER 2011/05 *Case Studies of the Seismic Performance of Tall Buildings Designed by Alternative Means.* Task 12 Report for the Tall Buildings Initiative. Jack Moehle, Yousef Bozorgnia, Nirmal Jayaram, Pierson Jones, Mohsen Rahnama, Nilesh Shome, Zeynep Tuna, John Wallace, Tony Yang, and Farzin Zareian. July 2011.

PEER 2011/04 *Recommended Design Practice for Pile Foundations in Laterally Spreading Ground.* Scott A. Ashford, Ross W. Boulanger, and Scott J. Brandenberg. June 2011.

PEER 2011/03 *New Ground Motion Selection Procedures and Selected Motions for the PEER Transportation Research Program.* Jack W. Baker, Ting Lin, Shrey K. Shahi, and Nirmal Jayaram. March 2011.

PEER 2011/02 *A Bayesian Network Methodology for Infrastructure Seismic Risk Assessment and Decision Support.* Michelle T. Bensi, Armen Der Kiureghian, and Daniel Straub. March 2011.

PEER 2011/01 *Demand Fragility Surfaces for Bridges in Liquefied and Laterally Spreading Ground.* Scott J. Brandenberg, Jian Zhang, Pirooz Kashighandi, Yili Huo, and Minxing Zhao. March 2011.

PEER 2010/05 *Guidelines for Performance-Based Seismic Design of Tall Buildings.* Developed by the Tall Buildings Initiative. November 2010.

PEER 2010/04 *Application Guide for the Design of Flexible and Rigid Bus Connections between Substation Equipment Subjected to Earthquakes.* Jean-Bernard Dastous and Armen Der Kiureghian. September 2010.

PEER 2010/03 *Shear Wave Velocity as a Statistical Function of Standard Penetration Test Resistance and Vertical Effective Stress at Caltrans Bridge Sites.* Scott J. Brandenberg, Naresh Bellana, and Thomas Shantz. June 2010.

PEER 2010/02 *Stochastic Modeling and Simulation of Ground Motions for Performance-Based Earthquake Engineering.* Sanaz Rezaeian and Armen Der Kiureghian. June 2010.

PEER 2010/01 *Structural Response and Cost Characterization of Bridge Construction Using Seismic Performance Enhancement Strategies.* Ady Aviram, Božidar Stojadinović, Gustavo J. Parra-Montesinos, and Kevin R. Mackie. March 2010.

PEER 2009/03 *The Integration of Experimental and Simulation Data in the Study of Reinforced Concrete Bridge Systems Including Soil-Foundation-Structure Interaction.* Matthew Dryden and Gregory L. Fenves. November 2009.

PEER 2009/02 *Improving Earthquake Mitigation through Innovations and Applications in Seismic Science, Engineering, Communication, and Response. Proceedings of a U.S.-Iran Seismic Workshop.* October 2009.

PEER 2009/01 *Evaluation of Ground Motion Selection and Modification Methods: Predicting Median Interstory Drift Response of Buildings.* Curt B. Haselton, Ed. June 2009.

PEER 2008/10 *Technical Manual for Strata.* Albert R. Kottke and Ellen M. Rathje. February 2009.

PEER 2008/09 *NGA Model for Average Horizontal Component of Peak Ground Motion and Response Spectra.* Brian S.-J. Chiou and Robert R. Youngs. November 2008.

PEER 2008/08 *Toward Earthquake-Resistant Design of Concentrically Braced Steel Structures.* Patxi Uriz and Stephen A. Mahin. November 2008.

PEER 2008/07 *Using OpenSees for Performance-Based Evaluation of Bridges on Liquefiable Soils.* Stephen L. Kramer, Pedro Arduino, and HyungSuk Shin. November 2008.

PEER 2008/06 *Shaking Table Tests and Numerical Investigation of Self-Centering Reinforced Concrete Bridge Columns.* Hyung IL Jeong, Junichi Sakai, and Stephen A. Mahin. September 2008.

PEER 2008/05 *Performance-Based Earthquake Engineering Design Evaluation Procedure for Bridge Foundations Undergoing Liquefaction-Induced Lateral Ground Displacement.* Christian A. Ledezma and Jonathan D. Bray. August 2008.

PEER 2008/04 *Benchmarking of Nonlinear Geotechnical Ground Response Analysis Procedures.* Jonathan P. Stewart, Annie On-Lei Kwok, Yousseff M. A. Hashash, Neven Matasovic, Robert Pyke, Zhiliang Wang, and Zhaohui Yang. August 2008.

PEER 2008/03 *Guidelines for Nonlinear Analysis of Bridge Structures in California.* Ady Aviram, Kevin R. Mackie, and Božidar Stojadinović. August 2008.

PEER 2008/02 *Treatment of Uncertainties in Seismic-Risk Analysis of Transportation Systems.* Evangelos Stergiou and Anne S. Kiremidjian. July 2008.

PEER 2008/01 *Seismic Performance Objectives for Tall Buildings.* William T. Holmes, Charles Kircher, William Petak, and Nabih Youssef. August 2008.

PEER 2007/12 *An Assessment to Benchmark the Seismic Performance of a Code-Conforming Reinforced Concrete Moment-Frame Building.* Curt Haselton, Christine A. Goulet, Judith Mitrani-Reiser, James L. Beck, Gregory G. Deierlein, Keith A. Porter, Jonathan P. Stewart, and Ertugrul Taciroglu. August 2008.

PEER 2007/11 *Bar Buckling in Reinforced Concrete Bridge Columns.* Wayne A. Brown, Dawn E. Lehman, and John F. Stanton. February 2008.

PEER 2007/10 *Computational Modeling of Progressive Collapse in Reinforced Concrete Frame Structures.* Mohamed M. Talaat and Khalid M. Mosalam. May 2008.

PEER 2007/09 *Integrated Probabilistic Performance-Based Evaluation of Benchmark Reinforced Concrete Bridges.* Kevin R. Mackie, John-Michael Wong, and Božidar Stojadinović. January 2008.

PEER 2007/08 *Assessing Seismic Collapse Safety of Modern Reinforced Concrete Moment-Frame Buildings.* Curt B. Haselton and Gregory G. Deierlein. February 2008.

PEER 2007/07 *Performance Modeling Strategies for Modern Reinforced Concrete Bridge Columns.* Michael P. Berry and Marc O. Eberhard. April 2008.

PEER 2007/06 *Development of Improved Procedures for Seismic Design of Buried and Partially Buried Structures.* Linda Al Atik and Nicholas Sitar. June 2007.

PEER 2007/05 *Uncertainty and Correlation in Seismic Risk Assessment of Transportation Systems.* Renee G. Lee and Anne S. Kiremidjian. July 2007.

PEER 2007/04 *Numerical Models for Analysis and Performance-Based Design of Shallow Foundations Subjected to Seismic Loading.* Sivapalan Gajan, Tara C. Hutchinson, Bruce L. Kutter, Prishati Raychowdhury, José A. Ugalde, and Jonathan P. Stewart. May 2008.

PEER 2007/03 *Beam-Column Element Model Calibrated for Predicting Flexural Response Leading to Global Collapse of RC Frame Buildings.* Curt B. Haselton, Abbie B. Liel, Sarah Taylor Lange, and Gregory G. Deierlein. May 2008.

PEER 2007/02 *Campbell-Bozorgnia NGA Ground Motion Relations for the Geometric Mean Horizontal Component of Peak and Spectral Ground Motion Parameters.* Kenneth W. Campbell and Yousef Bozorgnia. May 2007.

PEER 2007/01 *Boore-Atkinson NGA Ground Motion Relations for the Geometric Mean Horizontal Component of Peak and Spectral Ground Motion Parameters.* David M. Boore and Gail M. Atkinson. May. May 2007.

PEER 2006/12 *Societal Implications of Performance-Based Earthquake Engineering.* Peter J. May. May 2007.

PEER 2006/11 *Probabilistic Seismic Demand Analysis Using Advanced Ground Motion Intensity Measures, Attenuation Relationships, and Near-Fault Effects.* Polsak Tothong and C. Allin Cornell. March 2007.

PEER 2006/10 *Application of the PEER PBEE Methodology to the I-880 Viaduct.* Sashi Kunnath. February 2007.

PEER 2006/09 *Quantifying Economic Losses from Travel Forgone Following a Large Metropolitan Earthquake.* James Moore, Sungbin Cho, Yue Yue Fan, and Stuart Werner. November 2006.

PEER 2006/08 *Vector-Valued Ground Motion Intensity Measures for Probabilistic Seismic Demand Analysis.* Jack W. Baker and C. Allin Cornell. October 2006.

PEER 2006/07 *Analytical Modeling of Reinforced Concrete Walls for Predicting Flexural and Coupled–Shear-Flexural Responses.* Kutay Orakcal, Leonardo M. Massone, and John W. Wallace. October 2006.

PEER 2006/06 *Nonlinear Analysis of a Soil-Drilled Pier System under Static and Dynamic Axial Loading.* Gang Wang and Nicholas Sitar. November 2006.

PEER 2006/05 *Advanced Seismic Assessment Guidelines.* Paolo Bazzurro, C. Allin Cornell, Charles Menun, Maziar Motahari, and Nicolas Luco. September 2006.

PEER 2006/04 *Probabilistic Seismic Evaluation of Reinforced Concrete Structural Components and Systems.* Tae Hyung Lee and Khalid M. Mosalam. August 2006.

PEER 2006/03 *Performance of Lifelines Subjected to Lateral Spreading.* Scott A. Ashford and Teerawut Juirnarongrit. July 2006.

PEER 2006/02 *Pacific Earthquake Engineering Research Center Highway Demonstration Project.* Anne Kiremidjian, James Moore, Yue Yue Fan, Nesrin Basoz, Ozgur Yazali, and Meredith Williams. April 2006.

PEER 2006/01 *Bracing Berkeley. A Guide to Seismic Safety on the UC Berkeley Campus.* Mary C. Comerio, Stephen Tobriner, and Ariane Fehrenkamp. January 2006.

PEER 2005/16 *Seismic Response and Reliability of Electrical Substation Equipment and Systems.* Junho Song, Armen Der Kiureghian, and Jerome L. Sackman. April 2006.

PEER 2005/15 *CPT-Based Probabilistic Assessment of Seismic Soil Liquefaction Initiation.* R. E. S. Moss, R. B. Seed, R. E. Kayen, J. P. Stewart, and A. Der Kiureghian. April 2006.

PEER 2005/14 *Workshop on Modeling of Nonlinear Cyclic Load-Deformation Behavior of Shallow Foundations.* Bruce L. Kutter, Geoffrey Martin, Tara Hutchinson, Chad Harden, Sivapalan Gajan, and Justin Phalen. March 2006.

PEER 2005/13 *Stochastic Characterization and Decision Bases under Time-Dependent Aftershock Risk in Performance-Based Earthquake Engineering.* Gee Liek Yeo and C. Allin Cornell. July 2005.

PEER 2005/12 *PEER Testbed Study on a Laboratory Building: Exercising Seismic Performance Assessment.* Mary C. Comerio, editor. November 2005.

PEER 2005/11 *Van Nuys Hotel Building Testbed Report: Exercising Seismic Performance Assessment.* Helmut Krawinkler, editor. October 2005.

PEER 2005/10 *First NEES/E-Defense Workshop on Collapse Simulation of Reinforced Concrete Building Structures.* September 2005.

PEER 2005/09 *Test Applications of Advanced Seismic Assessment Guidelines.* Joe Maffei, Karl Telleen, Danya Mohr, William Holmes, and Yuki Nakayama. August 2006.

PEER 2005/08 *Damage Accumulation in Lightly Confined Reinforced Concrete Bridge Columns.* R. Tyler Ranf, Jared M. Nelson, Zach Price, Marc O. Eberhard, and John F. Stanton. April 2006.

PEER 2005/07 *Experimental and Analytical Studies on the Seismic Response of Freestanding and Anchored Laboratory Equipment.* Dimitrios Konstantinidis and Nicos Makris. January 2005.

PEER 2005/06 *Global Collapse of Frame Structures under Seismic Excitations*. Luis F. Ibarra and Helmut Krawinkler. September 2005.

PEER 2005//05 *Performance Characterization of Bench- and Shelf-Mounted Equipment.* Samit Ray Chaudhuri and Tara C. Hutchinson. May 2006.

PEER 2005/04 *Numerical Modeling of the Nonlinear Cyclic Response of Shallow Foundations.* Chad Harden, Tara Hutchinson, Geoffrey R. Martin, and Bruce L. Kutter. August 2005.

PEER 2005/03 *A Taxonomy of Building Components for Performance-Based Earthquake Engineering.* Keith A. Porter. September 2005.

PEER 2005/02 *Fragility Basis for California Highway Overpass Bridge Seismic Decision Making*. Kevin R. Mackie and Božidar Stojadinović. June 2005.

PEER 2005/01 *Empirical Characterization of Site Conditions on Strong Ground Motion.* Jonathan P. Stewart, Yoojoong Choi, and Robert W. Graves. June 2005.

PEER 2004/09 *Electrical Substation Equipment Interaction: Experimental Rigid Conductor Studies.* Christopher Stearns and André Filiatrault. February 2005.

PEER 2004/08 *Seismic Qualification and Fragility Testing of Line Break 550-kV Disconnect Switches.* Shakhzod M. Takhirov, Gregory L. Fenves, and Eric Fujisaki. January 2005.

PEER 2004/07 *Ground Motions for Earthquake Simulator Qualification of Electrical Substation Equipment.* Shakhzod M. Takhirov, Gregory L. Fenves, Eric Fujisaki, and Don Clyde. January 2005.

PEER 2004/06 *Performance-Based Regulation and Regulatory Regimes.* Peter J. May and Chris Koski. September 2004.

PEER 2004/05 *Performance-Based Seismic Design Concepts and Implementation: Proceedings of an International Workshop.* Peter Fajfar and Helmut Krawinkler, editors. September 2004.

PEER 2004/04 *Seismic Performance of an Instrumented Tilt-up Wall Building.* James C. Anderson and Vitelmo V. Bertero. July 2004.

PEER 2004/03 *Evaluation and Application of Concrete Tilt-up Assessment Methodologies.* Timothy Graf and James O. Malley. October 2004.

PEER 2004/02 *Analytical Investigations of New Methods for Reducing Residual Displacements of Reinforced Concrete Bridge Columns.* Junichi Sakai and Stephen A. Mahin. August 2004.

PEER 2004/01 *Seismic Performance of Masonry Buildings and Design Implications.* Kerri Anne Taeko Tokoro, James C. Anderson, and Vitelmo V. Bertero. February 2004.

PEER 2003/18 *Performance Models for Flexural Damage in Reinforced Concrete Columns.* Michael Berry and Marc Eberhard. August 2003.

PEER 2003/17 *Predicting Earthquake Damage in Older Reinforced Concrete Beam-Column Joints.* Catherine Pagni and Laura Lowes. October 2004.

PEER 2003/16 *Seismic Demands for Performance-Based Design of Bridges.* Kevin Mackie and Božidar Stojadinović. August 2003.

PEER 2003/15 *Seismic Demands for Nondeteriorating Frame Structures and Their Dependence on Ground Motions*. Ricardo Antonio Medina and Helmut Krawinkler. May 2004.

PEER 2003/14 *Finite Element Reliability and Sensitivity Methods for Performance-Based Earthquake Engineering.* Terje Haukaas and Armen Der Kiureghian. April 2004.

PEER 2003/13 *Effects of Connection Hysteretic Degradation on the Seismic Behavior of Steel Moment-Resisting Frames.* Janise E. Rodgers and Stephen A. Mahin. March 2004.

PEER 2003/12 *Implementation Manual for the Seismic Protection of Laboratory Contents: Format and Case Studies.* William T. Holmes and Mary C. Comerio. October 2003.

PEER 2003/11 *Fifth U.S.-Japan Workshop on Performance-Based Earthquake Engineering Methodology for Reinforced Concrete Building Structures.* February 2004.

PEER 2003/10 *A Beam-Column Joint Model for Simulating the Earthquake Response of Reinforced Concrete Frames.* Laura N. Lowes, Nilanjan Mitra, and Arash Altoontash. February 2004.

PEER 2003/09 *Sequencing Repairs after an Earthquake: An Economic Approach.* Marco Casari and Simon J. Wilkie. April 2004.

PEER 2003/08 *A Technical Framework for Probability-Based Demand and Capacity Factor Design (DCFD) Seismic Formats*. Fatemeh Jalayer and C. Allin Cornell. November 2003.

PEER 2003/07 *Uncertainty Specification and Propagation for Loss Estimation Using FOSM Methods.* Jack W. Baker and C. Allin Cornell. September 2003.

PEER 2003/06 *Performance of Circular Reinforced Concrete Bridge Columns under Bidirectional Earthquake Loading*. Mahmoud M. Hachem, Stephen A. Mahin, and Jack P. Moehle. February 2003.

PEER 2003/05 *Response Assessment for Building-Specific Loss Estimation.* Eduardo Miranda and Shahram Taghavi. September 2003.

PEER 2003/04 *Experimental Assessment of Columns with Short Lap Splices Subjected to Cyclic Loads*. Murat Melek, John W. Wallace, and Joel Conte. April 2003.

PEER 2003/03 *Probabilistic Response Assessment for Building-Specific Loss Estimation.* Eduardo Miranda and Hesameddin Aslani. September 2003.

PEER 2003/02 *Software Framework for Collaborative Development of Nonlinear Dynamic Analysis Program.* Jun Peng and Kincho H. Law. September 2003.

PEER 2003/01 *Shake Table Tests and Analytical Studies on the Gravity Load Collapse of Reinforced Concrete Frames.* Kenneth John Elwood and Jack P. Moehle. November 2003.

PEER 2002/24 *Performance of Beam to Column Bridge Joints Subjected to a Large Velocity Pulse.* Natalie Gibson, André Filiatrault, and Scott A. Ashford. April 2002.

PEER 2002/23 *Effects of Large Velocity Pulses on Reinforced Concrete Bridge Columns.* Greg L. Orozco and Scott A. Ashford. April 2002.

PEER 2002/22 *Characterization of Large Velocity Pulses for Laboratory Testing.* Kenneth E. Cox and Scott A. Ashford. April 2002.

PEER 2002/21 *Fourth U.S.-Japan Workshop on Performance-Based Earthquake Engineering Methodology for Reinforced Concrete Building Structures*. December 2002.

PEER 2002/20 *Barriers to Adoption and Implementation of PBEE Innovations.* Peter J. May. August 2002.

PEER 2002/19 *Economic-Engineered Integrated Models for Earthquakes: Socioeconomic Impacts.* Peter Gordon, James E. Moore II, and Harry W. Richardson. July 2002.

PEER 2002/18 *Assessment of Reinforced Concrete Building Exterior Joints with Substandard Details.* Chris P. Pantelides, Jon Hansen, Justin Nadauld, and Lawrence D. Reaveley. May 2002.

PEER 2002/17 *Structural Characterization and Seismic Response Analysis of a Highway Overcrossing Equipped with Elastomeric Bearings and Fluid Dampers: A Case Study.* Nicos Makris and Jian Zhang. November 2002.

PEER 2002/16 *Estimation of Uncertainty in Geotechnical Properties for Performance-Based Earthquake Engineering.* Allen L. Jones, Steven L. Kramer, and Pedro Arduino. December 2002.

PEER 2002/15 *Seismic Behavior of Bridge Columns Subjected to Various Loading Patterns.* Asadollah Esmaeily-Gh. and Yan Xiao. December 2002.

PEER 2002/14 *Inelastic Seismic Response of Extended Pile Shaft Supported Bridge Structures.* T.C. Hutchinson, R.W. Boulanger, Y.H. Chai, and I.M. Idriss. December 2002.

PEER 2002/13 *Probabilistic Models and Fragility Estimates for Bridge Components and Systems.* Paolo Gardoni, Armen Der Kiureghian, and Khalid M. Mosalam. June 2002.

PEER 2002/12 *Effects of Fault Dip and Slip Rake on Near-Source Ground Motions: Why Chi-Chi Was a Relatively Mild M7.6 Earthquake.* Brad T. Aagaard, John F. Hall, and Thomas H. Heaton. December 2002.

PEER 2002/11 *Analytical and Experimental Study of Fiber-Reinforced Strip Isolators*. James M. Kelly and Shakhzod M. Takhirov. September 2002.

PEER 2002/10 *Centrifuge Modeling of Settlement and Lateral Spreading with Comparisons to Numerical Analyses***.** Sivapalan Gajan and Bruce L. Kutter. January 2003.

PEER 2002/09 *Documentation and Analysis of Field Case Histories of Seismic Compression during the 1994 Northridge, California, Earthquake.* Jonathan P. Stewart, Patrick M. Smith, Daniel H. Whang, and Jonathan D. Bray. October 2002.

PEER 2002/08 *Component Testing, Stability Analysis and Characterization of Buckling-Restrained Unbonded Braces™.* Cameron Black, Nicos Makris, and Ian Aiken. September 2002.

PEER 2002/07 *Seismic Performance of Pile-Wharf Connections.* Charles W. Roeder, Robert Graff, Jennifer Soderstrom, and Jun Han Yoo. December 2001.

PEER 2002/06 *The Use of Benefit-Cost Analysis for Evaluation of Performance-Based Earthquake Engineering Decisions*. Richard O. Zerbe and Anthony Falit-Baiamonte. September 2001.

PEER 2002/05 *Guidelines, Specifications, and Seismic Performance Characterization of Nonstructural Building Components and Equipment*. André Filiatrault, Constantin Christopoulos, and Christopher Stearns. September 2001.

PEER 2002/04 *Consortium of Organizations for Strong-Motion Observation Systems and the Pacific Earthquake Engineering Research Center Lifelines Program: Invited Workshop on Archiving and Web Dissemination of Geotechnical Data, 4–5 October 2001*. September 2002.

PEER 2002/03 *Investigation of Sensitivity of Building Loss Estimates to Major Uncertain Variables for the Van Nuys Testbed.* Keith A. Porter, James L. Beck, and Rustem V. Shaikhutdinov. August 2002.

PEER 2002/02 *The Third U.S.-Japan Workshop on Performance-Based Earthquake Engineering Methodology for Reinforced Concrete Building Structures*. July 2002.

PEER 2002/01 *Nonstructural Loss Estimation: The UC Berkeley Case Study.* Mary C. Comerio and John C. Stallmeyer. December 2001.

PEER 2001/16 *Statistics of SDF-System Estimate of Roof Displacement for Pushover Analysis of Buildings.* Anil K. Chopra, Rakesh K. Goel, and Chatpan Chintanapakdee. December 2001.

PEER 2001/15 *Damage to Bridges during the 2001 Nisqually Earthquake.* R. Tyler Ranf, Marc O. Eberhard, and Michael P. Berry. November 2001.

PEER 2001/14 *Rocking Response of Equipment Anchored to a Base Foundation.* Nicos Makris and Cameron J. Black. September 2001.

PEER 2001/13 *Modeling Soil Liquefaction Hazards for Performance-Based Earthquake Engineering.* Steven L. Kramer and Ahmed-W. Elgamal. February 2001.

PEER 2001/12 *Development of Geotechnical Capabilities in OpenSees.* Boris Jeremić. September 2001.

PEER 2001/11 *Analytical and Experimental Study of Fiber-Reinforced Elastomeric Isolators*. James M. Kelly and Shakhzod M. Takhirov. September 2001.

PEER 2001/10 *Amplification Factors for Spectral Acceleration in Active Regions.* Jonathan P. Stewart, Andrew H. Liu, Yoojoong Choi, and Mehmet B. Baturay. December 2001.

PEER 2001/09 *Ground Motion Evaluation Procedures for Performance-Based Design.* Jonathan P. Stewart, Shyh-Jeng Chiou, Jonathan D. Bray, Robert W. Graves, Paul G. Somerville, and Norman A. Abrahamson. September 2001.

PEER 2001/08 *Experimental and Computational Evaluation of Reinforced Concrete Bridge Beam-Column Connections for Seismic Performance*. Clay J. Naito, Jack P. Moehle, and Khalid M. Mosalam. November 2001.

PEER 2001/07 *The Rocking Spectrum and the Shortcomings of Design Guidelines.* Nicos Makris and Dimitrios Konstantinidis. August 2001.

PEER 2001/06 *Development of an Electrical Substation Equipment Performance Database for Evaluation of Equipment Fragilities*. Thalia Agnanos. April 1999.

PEER 2001/05 *Stiffness Analysis of Fiber-Reinforced Elastomeric Isolators.* Hsiang-Chuan Tsai and James M. Kelly. May 2001.

PEER 2001/04 *Organizational and Societal Considerations for Performance-Based Earthquake Engineering.* Peter J. May. April 2001.

PEER 2001/03 *A Modal Pushover Analysis Procedure to Estimate Seismic Demands for Buildings: Theory and Preliminary Evaluation.* Anil K. Chopra and Rakesh K. Goel. January 2001.

PEER 2001/02 *Seismic Response Analysis of Highway Overcrossings Including Soil-Structure Interaction.* Jian Zhang and Nicos Makris. March 2001.

PEER 2001/01 *Experimental Study of Large Seismic Steel Beam-to-Column Connections.* Egor P. Popov and Shakhzod M. Takhirov. November 2000.

PEER 2000/10 *The Second U.S.-Japan Workshop on Performance-Based Earthquake Engineering Methodology for Reinforced Concrete Building Structures.* March 2000.

PEER 2000/09 *Structural Engineering Reconnaissance of the August 17, 1999 Earthquake: Kocaeli (Izmit), Turkey.* Halil Sezen, Kenneth J. Elwood, Andrew S. Whittaker, Khalid Mosalam, John J. Wallace, and John F. Stanton. December 2000.

PEER 2000/08 *Behavior of Reinforced Concrete Bridge Columns Having Varying Aspect Ratios and Varying Lengths of Confinement.* Anthony J. Calderone, Dawn E. Lehman, and Jack P. Moehle. January 2001.

PEER 2000/07 *Cover-Plate and Flange-Plate Reinforced Steel Moment-Resisting Connections.* Taejin Kim, Andrew S. Whittaker, Amir S. Gilani, Vitelmo V. Bertero, and Shakhzod M. Takhirov. September 2000.

PEER 2000/06 *Seismic Evaluation and Analysis of 230-kV Disconnect Switches.* Amir S. J. Gilani, Andrew S. Whittaker, Gregory L. Fenves, Chun-Hao Chen, Henry Ho, and Eric Fujisaki. July 2000.

PEER 2000/05 *Performance-Based Evaluation of Exterior Reinforced Concrete Building Joints for Seismic Excitation.* Chandra Clyde, Chris P. Pantelides, and Lawrence D. Reaveley. July 2000.

PEER 2000/04 *An Evaluation of Seismic Energy Demand: An Attenuation Approach.* Chung-Che Chou and Chia-Ming Uang. July 1999.

PEER 2000/03 *Framing Earthquake Retrofitting Decisions: The Case of Hillside Homes in Los Angeles.* Detlof von Winterfeldt, Nels Roselund, and Alicia Kitsuse. March 2000.

PEER 2000/02 *U.S.-Japan Workshop on the Effects of Near-Field Earthquake Shaking.* Andrew Whittaker, ed. July 2000.

PEER 2000/01 *Further Studies on Seismic Interaction in Interconnected Electrical Substation Equipment.* Armen Der Kiureghian, Kee-Jeung Hong, and Jerome L. Sackman. November 1999.

PEER 1999/14 *Seismic Evaluation and Retrofit of 230-kV Porcelain Transformer Bushings.* Amir S. Gilani, Andrew S. Whittaker, Gregory L. Fenves, and Eric Fujisaki. December 1999.

PEER 1999/13 *Building Vulnerability Studies: Modeling and Evaluation of Tilt-up and Steel Reinforced Concrete Buildings.* John W. Wallace, Jonathan P. Stewart, and Andrew S. Whittaker, editors. December 1999.

PEER 1999/12 *Rehabilitation of Nonductile RC Frame Building Using Encasement Plates and Energy-Dissipating Devices.* Mehrdad Sasani, Vitelmo V. Bertero, James C. Anderson. December 1999.

PEER 1999/11 *Performance Evaluation Database for Concrete Bridge Components and Systems under Simulated Seismic Loads.* Yael D. Hose and Frieder Seible. November 1999.

PEER 1999/10 *U.S.-Japan Workshop on Performance-Based Earthquake Engineering Methodology for Reinforced Concrete Building Structures.* December 1999.

PEER 1999/09 *Performance Improvement of Long Period Building Structures Subjected to Severe Pulse-Type Ground Motions.* James C. Anderson, Vitelmo V. Bertero, and Raul Bertero. October 1999.

PEER 1999/08 *Envelopes for Seismic Response Vectors.* Charles Menun and Armen Der Kiureghian. July 1999.

PEER 1999/07 *Documentation of Strengths and Weaknesses of Current Computer Analysis Methods for Seismic Performance of Reinforced Concrete Members.* William F. Cofer. November 1999.

PEER 1999/06 *Rocking Response and Overturning of Anchored Equipment under Seismic Excitations.* Nicos Makris and Jian Zhang. November 1999.

PEER 1999/05 *Seismic Evaluation of 550 kV Porcelain Transformer Bushings.* Amir S. Gilani, Andrew S. Whittaker, Gregory L. Fenves, and Eric Fujisaki. October 1999.

PEER 1999/04 *Adoption and Enforcement of Earthquake Risk-Reduction Measures.* Peter J. May, Raymond J. Burby, T. Jens Feeley, and Robert Wood.

PEER 1999/03 *Task 3 Characterization of Site Response General Site Categories.* Adrian Rodriguez-Marek, Jonathan D. Bray, and Norman Abrahamson. February 1999.

PEER 1999/02 *Capacity-Demand-Diagram Methods for Estimating Seismic Deformation of Inelastic Structures: SDF Systems.* Anil K. Chopra and Rakesh Goel. April 1999.

PEER 1999/01 *Interaction in Interconnected Electrical Substation Equipment Subjected to Earthquake Ground Motions.* Armen Der Kiureghian, Jerome L. Sackman, and Kee-Jeung Hong. February 1999.

PEER 1998/08 *Behavior and Failure Analysis of a Multiple-Frame Highway Bridge in the 1994 Northridge Earthquake.* Gregory L. Fenves and Michael Ellery. December 1998.

PEER 1998/07 *Empirical Evaluation of Inertial Soil-Structure Interaction Effects.* Jonathan P. Stewart, Raymond B. Seed, and Gregory L. Fenves. November 1998.

PEER 1998/06 *Effect of Damping Mechanisms on the Response of Seismic Isolated Structures.* Nicos Makris and Shih-Po Chang. November 1998.

PEER 1998/05 *Rocking Response and Overturning of Equipment under Horizontal Pulse-Type Motions.* Nicos Makris and Yiannis Roussos. October 1998.

PEER 1998/04 *Pacific Earthquake Engineering Research Invitational Workshop Proceedings, May 14–15, 1998: Defining the Links between Planning, Policy Analysis, Economics and Earthquake Engineering.* Mary Comerio and Peter Gordon. September 1998.

PEER 1998/03 *Repair/Upgrade Procedures for Welded Beam to Column Connections.* James C. Anderson and Xiaojing Duan. May 1998.

PEER 1998/02 *Seismic Evaluation of 196 kV Porcelain Transformer Bushings.* Amir S. Gilani, Juan W. Chavez, Gregory L. Fenves, and Andrew S. Whittaker. May 1998.

PEER 1998/01 *Seismic Performance of Well-Confined Concrete Bridge Columns.* Dawn E. Lehman and Jack P. Moehle. December 2000.

ONLINE PEER REPORTS

The following PEER reports are available by Internet only at http://peer.berkeley.edu/publications/peer_reports_complete.html.

PEER 2012/103 *Performance-Based Seismic Demand Assessment of Concentrically Braced Steel Frame Buildings.* Chui-Hsin Chen and Stephen A. Mahin. December 2012.

PEER 2012/102 *Procedure to Restart an Interrupted Hybrid Simulation: Addendum to PEER Report 2010/103.* Vesna Terzic and Bozidar Stojadinovic. October 2012.

PEER 2012/101 *Mechanics of Fiber Reinforced Bearings.* James M. Kelly and Andrea Calabrese. February 2012.

PEER 2011/107 *Nonlinear Site Response and Seismic Compression at Vertical Array Strongly Shaken by 2007 Niigata-ken Chuetsu-oki Earthquake.* Eric Yee, Jonathan P. Stewart, and Kohji Tokimatsu. December 2011.

PEER 2011/106 *Self Compacting Hybrid Fiber Reinforced Concrete Composites for Bridge Columns.* Pardeep Kumar, Gabriel Jen, William Trono, Marios Panagiotou, and Claudia Ostertag. September 2011.

PEER 2011/105 *Stochastic Dynamic Analysis of Bridges Subjected to Spacially Varying Ground Motions.* Katerina Konakli and Armen Der Kiureghian. August 2011.

PEER 2011/104 *Design and Instrumentation of the 2010 E-Defense Four-Story Reinforced Concrete and Post-Tensioned Concrete Buildings.* Takuya Nagae, Kenichi Tahara, Taizo Matsumori, Hitoshi Shiohara, Toshimi Kabeyasawa, Susumu Kono, Minehiro Nishiyama (Japanese Research Team) and John Wallace, Wassim Ghannoum, Jack Moehle, Richard Sause, Wesley Keller, Zeynep Tuna (U.S. Research Team). June 2011.

PEER 2011/103 *In-Situ Monitoring of the Force Output of Fluid Dampers: Experimental Investigation.* Dimitrios Konstantinidis, James M. Kelly, and Nicos Makris. April 2011.

PEER 2011/102 *Ground-motion prediction equations 1964 - 2010.* John Douglas. April 2011.

PEER 2011/101 *Report of the Eighth Planning Meeting of NEES/E-Defense Collaborative Research on Earthquake Engineering.* Convened by the Hyogo Earthquake Engineering Research Center (NIED), NEES Consortium, Inc. February 2011.

PEER 2010/111 *Modeling and Acceptance Criteria for Seismic Design and Analysis of Tall Buildings.* Task 7 Report for the Tall Buildings Initiative - Published jointly by the Applied Technology Council. October 2010.

PEER 2010/110 *Seismic Performance Assessment and Probabilistic Repair Cost Analysis of Precast Concrete Cladding Systems for Multistory Buildlings.* Jeffrey P. Hunt and Božidar Stojadinovic. November 2010.

PEER 2010/109 *Report of the Seventh Joint Planning Meeting of NEES/E-Defense Collaboration on Earthquake Engineering. Held at the E-Defense, Miki, and Shin-Kobe, Japan, September 18–19, 2009.* August 2010.

PEER 2010/108 *Probabilistic Tsunami Hazard in California.* Hong Kie Thio, Paul Somerville, and Jascha Polet, preparers. October 2010.

PEER 2010/107 *Performance and Reliability of Exposed Column Base Plate Connections for Steel Moment-Resisting Frames.* Ady Aviram, Božidar Stojadinovic, and Armen Der Kiureghian. August 2010.

PEER 2010/106 *Verification of Probabilistic Seismic Hazard Analysis Computer Programs.* Patricia Thomas, Ivan Wong, and Norman Abrahamson. May 2010.

PEER 2010/105 *Structural Engineering Reconnaissance of the April 6, 2009, Abruzzo, Italy, Earthquake, and Lessons Learned.* M. Selim Günay and Khalid M. Mosalam. April 2010.

PEER 2010/104 *Simulating the Inelastic Seismic Behavior of Steel Braced Frames, Including the Effects of Low-Cycle Fatigue.* Yuli Huang and Stephen A. Mahin. April 2010.

PEER 2010/103 *Post-Earthquake Traffic Capacity of Modern Bridges in California.* Vesna Terzic and Božidar Stojadinović. March 2010.

PEER 2010/102 *Analysis of Cumulative Absolute Velocity (CAV) and JMA Instrumental Seismic Intensity (I_{JMA}) Using the PEER–NGA Strong Motion Database.* Kenneth W. Campbell and Yousef Bozorgnia. February 2010.

PEER 2010/101 *Rocking Response of Bridges on Shallow Foundations.* Jose A. Ugalde, Bruce L. Kutter, and Boris Jeremic. April 2010.

PEER 2009/109 *Simulation and Performance-Based Earthquake Engineering Assessment of Self-Centering Post-Tensioned Concrete Bridge Systems.* Won K. Lee and Sarah L. Billington. December 2009.

PEER 2009/108 *PEER Lifelines Geotechnical Virtual Data Center.* J. Carl Stepp, Daniel J. Ponti, Loren L. Turner, Jennifer N. Swift, Sean Devlin, Yang Zhu, Jean Benoit, and John Bobbitt. September 2009.

PEER 2009/107 *Experimental and Computational Evaluation of Current and Innovative In-Span Hinge Details in Reinforced Concrete Box-Girder Bridges: Part 2: Post-Test Analysis and Design Recommendations.* Matias A. Hube and Khalid M. Mosalam. December 2009.

PEER 2009/106 *Shear Strength Models of Exterior Beam-Column Joints without Transverse Reinforcement.* Sangjoon Park and Khalid M. Mosalam. November 2009.

PEER 2009/105 *Reduced Uncertainty of Ground Motion Prediction Equations through Bayesian Variance Analysis.* Robb Eric S. Moss. November 2009.

PEER 2009/104 *Advanced Implementation of Hybrid Simulation.* Andreas H. Schellenberg, Stephen A. Mahin, Gregory L. Fenves. November 2009.

PEER 2009/103 *Performance Evaluation of Innovative Steel Braced Frames.* T. Y. Yang, Jack P. Moehle, and Božidar Stojadinovic. August 2009.

PEER 2009/102 *Reinvestigation of Liquefaction and Nonliquefaction Case Histories from the 1976 Tangshan Earthquake.* Robb Eric Moss, Robert E. Kayen, Liyuan Tong, Songyu Liu, Guojun Cai, and Jiaer Wu. August 2009.

PEER 2009/101 *Report of the First Joint Planning Meeting for the Second Phase of NEES/E-Defense Collaborative Research on Earthquake Engineering.* Stephen A. Mahin et al. July 2009.

PEER 2008/104 *Experimental and Analytical Study of the Seismic Performance of Retaining Structures.* Linda Al Atik and Nicholas Sitar. January 2009.

PEER 2008/103 *Experimental and Computational Evaluation of Current and Innovative In-Span Hinge Details in Reinforced Concrete Box-Girder Bridges. Part 1: Experimental Findings and Pre-Test Analysis.* Matias A. Hube and Khalid M. Mosalam. January 2009.

PEER 2008/102 *Modeling of Unreinforced Masonry Infill Walls Considering In-Plane and Out-of-Plane Interaction.* Stephen Kadysiewski and Khalid M. Mosalam. January 2009.

PEER 2008/101 *Seismic Performance Objectives for Tall Buildings.* William T. Holmes, Charles Kircher, William Petak, and Nabih Youssef. August 2008.

PEER 2007/101 *Generalized Hybrid Simulation Framework for Structural Systems Subjected to Seismic Loading.* Tarek Elkhoraibi and Khalid M. Mosalam. July 2007.

PEER 2007/100 *Seismic Evaluation of Reinforced Concrete Buildings Including Effects of Masonry Infill Walls.* Alidad Hashemi and Khalid M. Mosalam. July 2007.

The Pacific Earthquake Engineering Research Center (PEER) is a multi-institutional research and education center with headquarters at the University of California, Berkeley. Investigators from over 20 universities, several consulting companies, and researchers at various state and federal government agencies contribute to research programs focused on performance-based earthquake engineering.

These research programs aim to identify and reduce the risks from major earthquakes to life safety and to the economy by including research in a wide variety of disciplines including structural and geotechnical engineering, geology/seismology, lifelines, transportation, architecture, economics, risk management, and public policy.

PEER is supported by federal, state, local, and regional agencies, together with industry partners.

PEER Core Institutions:
University of California, Berkeley (Lead Institution)
California Institute of Technology
Oregon State University
Stanford University
University of California, Davis
University of California, Irvine
University of California, Los Angeles
University of California, San Diego
University of Southern California
University of Washington

PEER reports can be ordered at http://peer.berkeley.edu/publications/peer_reports.html or by contacting

Pacific Earthquake Engineering Research Center
University of California, Berkeley
325 Davis Hall, mail code 1792
Berkeley, CA 94720-1792
Tel: 510-642-3437
Fax: 510-642-1655
Email: peer_editor@berkeley.edu

ISSN 1547-0587X